UNIVERSITÀ
DEGLI STUDI
DI PADOVA

Administrative seat: Università degli Studi di Padova

Department of Chemical Sciences

Doctoral Course in Molecular Sciences

Curriculum: Chemical Sciences

Cycle: XXXVI

A THEORETICAL MECHANISTIC JOURNEY INTO ORGANOSELENIUM (BIO)CHEMISTRY: FROM ELEMENTARY MOLECULAR MODELS TO CATALYSIS

Coordinator: Prof. Dr. Stefano Corni

Supervisor: Prof. Dr. Laura Orian

Co-Supervisor: Prof. Dr. Massimo Bellanda

Ph.D. Candidate: Andrea Madabeni

A Theoretical Mechanistic Journey

into Organoselenium (Bio)Chemistry:

from Elementary Molecular Models to Catalysis

Andrea Madabeni

The limits of my language
mean the limits of my world

{Ludwig Wittgenstein,
Tractatus Logico-Philosophicus

Table of Contents

Abstract

In this Thesis, density functional theory (DFT) calculations have been employed to investigate various aspects of organoselenium chemistry. Organoselenium chemistry emerged in the past fifty years as a green approach to introduce and modify functional groups into organic molecular scaffolds. The various topics explored cover both biological and synthetic applications. Particularly, the inhibitory mechanism of ebselen, a popular organoselenide, against target proteins have been investigated, as well as the reasons explaining the selectivity of a recently designed specific probe for thioredoxin reductase, whose chemistry is based on a selenyl sulfide. Then, the reactivity of the glutathione peroxidase enzyme was explored in the presence of peroxynitrite. In the second part of the Thesis, various reactivity aspects of organoselenides with application in synthetic organic chemistry have been tackled. The chalcogenoxide elimination reaction has been investigated in detail, both in minimal and in realistic models. Then, the reduction mechanism of sulfoxides and selenoxides by thiols and selenols has been explored. In both cases, the factors responsible for the faster reactivity of organoselenides as compared to organosulfides have been pinpointed. Lastly, the mechanism of the organoselenium catalyzed oxidation of aniline to nitrobenzene has been extensively investigated, to obtain insight into the role of the oxidation state of selenium in the reaction. Overall, the mechanistic descriptions proposed and explored in this Thesis can assist in the rationalization of organoselenides reactivity and provide a theoretical picture of the factors responsible for their behavior.

VI

Preface

In 1818, Berzelius named selenium after the moon goddess Σεληνη (*Selene*). It is quite amusing that, like the moon, selenium was later found to be a two-faced element, i.e., with a face of a poison, well-known since its discovery, and another one of a vital micronutrient, which was observed only much later. In the same way, organic chemists learned that a smelly toxicant could also evolve into a green catalyst when cleverly used.

The questions surrounding the role of Se in biology are as old as the field of selenium enzymology itself: why was Se usage favored by evolution over S in some proteins, when the latter is so widely employed by living beings, can perform essentially the same functions, and is way more available on earth and less toxic? What properties does selenium possess that sulfur alone cannot emulate? While the consequences of these questions propagate in the realm of biology, they have their roots in the atomistic world of chemistry: the very same organoselenium chemistry that synthetic chemists have understood how to exploit and control in the past fifty years.

I must stop you before it is too late: this work does not provide an answer (if *one* answer exists) to these questions. In this regard, I am reassured by the fact that one alone cannot have the ambition of solving such a long-standing problem, but puzzles can be built one piece at a time by *standing on the shoulders of giants*. Thus, this Thesis will start with an historical introduction, focused on selected experiences from the early days of selenium biological and organic chemistry: it will work especially as a tribute to those that worked as pioneers in both fields. Every research

Chapter has a brief introduction focusing on the state-of-the-art of the topic under investigation. Thus, this historical background can be skipped altogether. However, this Introduction serves the purpose of unifying the Chapters of this dissertation under the banner of one community, giving the flavor, if not the meaning, to the investigation I carried out in the last three years.

In the span of these years, I had the occasion of exchanging ideas and opinions with many young colleagues as well as with experienced chemists and teachers, including a couple of the pioneers mentioned later in the Introduction. Some of them contributed, with perspectives or suggestions, to some of this work and I can say that without their contributions part of this Thesis would not exist in the form in which it does today. It was an uphill but beautiful journey into different areas, from the *empyreal* of theoretical organic chemistry to the perilous territory of enzymology. Of course, there were some debates. In retrospect, I like to see these debates as part of the journey: not as inconveniences, but as some of the beauties of the science landscape.

This landscape may as well be inextricable, but as a theoretician I believe it is my duty to try to find the connections between the intricacies of chemistry. In the worst cases, something old (and, perhaps, obvious) might get corroborated, but with luck something new might be highlighted. While it can be quite discouraging to (re)observe something that was already discussed fifty years ago, it is only through the process of sifting this sea of possible outcomes that the joy of new discoveries and interpretations can be experienced. Indeed, these are the only two possible outcomes in science. In the words commonly attributed to the Italian physicist Enrico Fermi:

> *"If the result confirms the hypothesis, then you've made a measurement.*
> *If the result is contrary to the hypothesis, then you've made a discovery."*

Along this excursion, I "measured" some old things, discovered some new things, and observed things whose definition is still pending: measurement, or discovery. Nevertheless, I believe in the end it was worth my while.

I will leave you to it.

1 Introduction

This thesis deals with topics revolving around organoselenium chemistry, selenium in biology and selenium in catalysis. Thus, the question comes unbidden: *why selenium*? Why should anyone bother with the large brother of the well-studied sulfur, leaving its safety to venture in the treacherous land of heavy chalcogens?

The emergence of selenium in organic synthesis dates back to the 70s,[1–3] and incidentally, the same years defined the rise of selenium enzymology in vertebrates, with the discovery that some enzymes require selenium to exert their catalytic activity.[4,5] After fifty years, much is still to know about the way in which Se takes part in catalytic mechanisms and, above all, why evolution preserved this heavy chalcogen in higher biological systems: this has been an open debate since the beginning of the field. Summarizing why selenium caught the attention of organic chemists and biologists is not an easy task, but this Introduction aims at giving some pills of *why selenium* still attracts the interest of a large community of researchers.

1.1 The Road of Selenium into Biology

Since its historical discovery by Berzelius in 1818, the only recognized biological "role" of selenium was as a poison. By the end of the 1930s it was considered a toxicant in foodstuff[6,7] and a potential industrial hazard.[8] Only in 1954, the first account on the necessity of Se in living beings was published, when Jane Pinsent observed that *E. Coli* produces the enzyme formate dehydrogenase only in the presence of selenite.[9] A couple of years later, the importance of low dietary doses

of selenium became clear also in vertebrates.[10–12] Despite this knowledge, the direct molecular link between selenium and vertebrate health remained in the dark for fifteen years. In fact, only in the 70s, the role of Se in living beings was bridged at the molecular level to its enzymatic importance, marking the true beginning of selenium enzymology.[4]

In 1973, after a rediscovered interest in the relationship between formate dehydrogenase and selenium,[13] two bacterial enzymes (glycine reductase and formate dehydrogenase)[14,15] and two mammalian enzymes (ovine and bovine glutathione peroxidases)[5,16] were proved to be selenoproteins, incorporating selenium within the protein architecture. However, at the time, for only one bacterial protein there was evidence of covalent binding between Se and the enzyme itself, and in all cases the form in which Se was incorporated in these selenoproteins was unknown.[17] Hypotheses were made already in the same year, but the experimental verification proved to be troublesome due to the instability of organoselenium species.[18] Luckily, this mystery was solved in 1976 by the group of Thressa Stadtman, when the *unknown selenium species* within glycine reductase was identified as a selenocysteine (Sec) residue integrated in the peptide chain,[1] i.e. a canonical cysteine (Cys), with the S atom replaced by the heavier Se.[19] Soon later, selenocysteine was discovered to be the form in which selenium was incorporated also in mammalian glutathione peroxidase[20] and, up to now, it proved to be the only form in which selenium is present in all "real" selenoproteins.[4]

At the beginning of the 2000s, thanks to the effort of Gladyshev and coworkers,[21,22] 25 genes were identified in humans coding for selenoproteins. Unluckily, as of today, only five enzyme classes have clearly defined functions in mammals, i.e., glutathione peroxidase (GPx), methionine sulfoxide reductase (Msr), thioredoxin reductase (TrxR), iodothyronine deiodinase (DIO) and selenophosphate synthetase (SPS2). (Figure 1.1)

---

[1] It is worth mentioning that *forty years* before the Stadtman group's discovery, the hypothesis that Se was accumulated into toxic crops in a form "very similar to cystine" (cysteine disulfide) was made by Franke and coworkers but went essentially unrecognized.[6] As reference, Stadtman 1976 research article and 1996 review have been cited more than 200 and 800 times respectively. Franke work has received less than 20 citations up to today (27/06/2023).
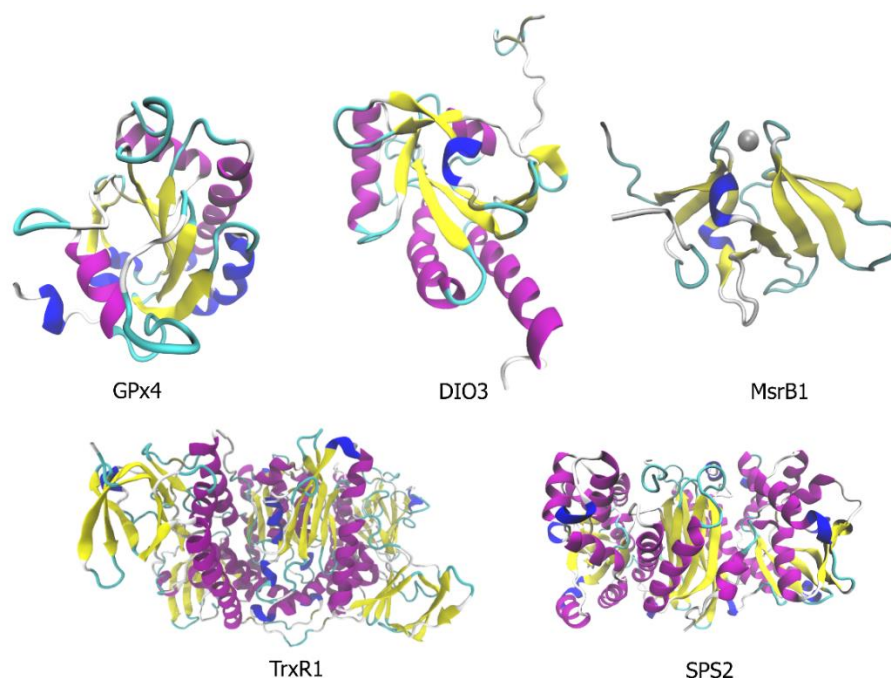
Figure 1.1 Representative structures of selenoenzymes with known function: monomeric glutathione peroxidase 4 (GPx4, #2OBI), catalytic domain of iodothyronine deiodinase 3 (DIO3, #4TR4), methionine sulfoxide reductase B1 (MsrB1, #3MAO), dimeric thioredoxin reductase 1 (TrxR1, #1H6V) and dimeric selenophosphate synthetase 2 (SPS2, #2ZOD).

In addition, selenoprotein P (SELENOP) constitutes the sixth selenoprotein with known function, i.e., Se transport, however it is still unclear if it has any enzymatic function; thus, here, it will not be considered as a selenoenzyme. These six classes account for roughly half of the human selenoproteome. The missing half is made of proteins known only by sequence. In bacteria, different selenoenzymes are present. In fact, mammals' selenoenzymes are usually present as Cys homologues in bacteria and *vice versa*.[4,23] (Figure 1.1)
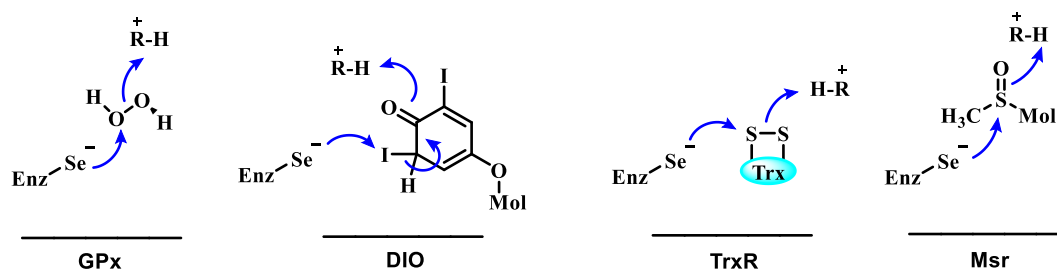
Scheme 1.1 Key reactive steps of glutathione peroxidase (GPx), iodothyronine deiodinase (DIO), thioredoxin reductase (TrxR) and methionine sulfoxide reductase (Msr). Enz stands for the enzyme, R for an enzyme residue and Mol for the rest of the substrate molecular structure.

While essentially all known vertebrate selenoenzymes belong to the broad group of oxidoreductases, they catalyze very different reactions on much different

substrates. (Scheme 1.1) Particularly, GPxs (of which eight isoforms have been isolated so far, five of them selenoproteins in humans) act as direct antioxidant enzymes,[2] by reducing harmful hydroperoxides to innocuous water or alcohols.[24,25] Among these, GPx4 is peculiar for its capacity of tackling non-soluble lipid hydroperoxides, thus acting as a *front-line* membrane antioxidant.[24,26] For true *glutathione* peroxidase, two equivalents of sacrificial glutathione (GSH) are oxidized to disulfide (GSSG) per peroxide reduced. Some GPxs, such as GPx4, can employ other thiols in place of GSH in a somewhat unspecific way, resulting however in the same overall reaction. More details on the catalytic cycle of this enzyme will be given in Chapter 1.5.

Msr and TrxR also take part in the antioxidant defenses of mammals, even if in different and somewhat opposite ways. Particularly, Msr catalyzes the reduction of sulfoxides to sulfides (thus, repairing oxidized residues) employing thioredoxins (Trx^R) as sacrificial reducing agents, which are oxidized to thioredoxin disulfides (Trx^{Ox}) to restore the ground state Msr.[27,28] On the other hand, TrxR reduces Trx^{Ox} to Trx^R, breaking the disulfide bond employing NADPH as the final reducing agent and is thus responsible for the upkeeping of the biological reducing environment.[29] In mammals, all these three families employ only one critical Sec residue as central redox "catalyst" to exert their antioxidant activity. DIO and SPS2 employ Sec to remove one iodine nucleus from iodothyronine, and to catalyze the formation of selenophosphate from Se and ATP, which is ultimately employed in the synthesis of Sec. Thus, they are key enzymes for the functioning of thyroid (DIO) and for the effective usage of Se by mammals (SPS2). However, their mechanisms are far less characterized and understood when compared to the other three selenoenzyme.[30,31]

1.2 Selenocysteine: the Catalytic Tool of Selenoenzymes

The discovery that vertebrates require low dietary doses of Se to survive, prompted the biochemical community to understand why it is so. Already in the 60s, long before the recognition of true selenoproteins existence, it had been observed that Se

---

[2] Not all GPxs are implicated in the direct antioxidant defenses; for some of them, a role as redox sensors have been hypothesized. However, at least for the first two GPxs discovered (today GPx1 and GPx4), the antioxidant function is well-established.

could attenuate the symptoms of vitamin E deficiency, a known peroxide scavenger. This preliminary knowledge favored the hypothesis that selenium role in biology was as an antioxidant, similarly to vitamin E.[4,32,33] This idea seemed supported in 1973 when the first mammal selenoenzyme was identified, i.e. GPx. In the words of its discoverer, L. Flohé,[5]:

> *"Most of the pathological conditions of selenium deficiency are related to peroxidation of unsaturated lipids in biological membranes. It is a well-established physiological function of GSH peroxidase to prevent lipid peroxidation. [...] Thus, the antioxidative effects of alimentary selenium could be well attributed to the fact that it functions as an integral component of GSH peroxidase."*

While Se integration in GPx accounts for the antioxidant effects of alimentary selenium, the whole picture is unluckily more complicated. [4,34] Indeed, while GPx, TrxR and Msr are deeply involved in the antioxidant (or antioxidant repair) defenses of mammals, supporting the antioxidant role of Sec, DIO and SPS2 have no (direct) connection to the biological antioxidant system. Moreover, selenium *per se* is not necessarily a good antioxidant. Inorganic selenium species such as selenates are stable and have no antioxidant potential (unless metabolized), while many fully reduced selenides can paradoxically display pro-oxidant activity (here comes the poison!).[4] Thus, the question remained only partly answered, and partly shifted to another and more general one: why has evolution preserved Sec?

The question surrounding the purpose of Se in biology is not a mere curiosity, but rather stems from a fundamental problem: Sec is not easily incorporated into proteins and thus its use by living beings comes at a high price. To insert Sec into the peptide architecture, a complicated genetic machinery is employed by animals, starting with an unusual way of reading the genome. Indeed, Sec is inserted co-translationally, but contrarily to the 20 "conventional" proteinogenic amino acids it lacks a fully dedicated codon. Instead, an in-frame TGA triplet, standardly a stop-codon, must be interpreted as a sense codon for Sec insertion. This process requires more than five additional enzymes to insert Sec in a protein, with respect to Cys, thus strongly increasing the energetic consumption.[35,36] Moreover, Se toxicity implies that all this machinery relies just on the proper dietary Se assumption: not too much, neither too little. This last point is even more critical, since Se is not

evenly distributed in the soil: its availability in some environments is so low as to become limiting for selenoprotein biosynthesis.[23]

Since selenoproteins are such a heterogenous group of proteins, the role of Se in biology lies probably not simply in the *end*, but also in the *means*: if evolution has preserved Sec up to vertebrates, Sec must provide some mechanistic advantages over the standard Cys.[35] Some answers came with the first mutations of selenoproteins to analogous "sulfur" proteins (via Sec to Cys mutation). In agreement with the useful nature of Sec, in most cases their catalytic power was greatly reduced after mutation.[37,38] However, it did not necessarily vanish. Focusing on the reduction of hydroperoxides by GPxs, the CysGPx4 mutant prepared by Maiorino and coworkers was three orders of magnitude less efficient than SecGPx4, but it could still reduce harmful hydroperoxides *ten thousand times* faster than Cys does alone.[39] Additionally, some natural occurring CysGPxs can reduce peroxides only one order of magnitude less efficiently than mammals SecGPxs.[40] These observations suggest that the protein architecture can tune Cys reactivity to work almost as good as a Sec, even if somehow Sec still holds the first place in term of catalytic efficiency, at least for what concerns hydroperoxide reduction. This first place has been attributed to different chemical reasons: particularly, Sec is more acidic and more nucleophilic than Cys. At the same time, selenides are more electrophilic than sulfides. Thus, expectedly, Sec can engage in a faster nucleophilic reactivity when Se acts either as the proton donor, the nucleophile, or the electrophile in a reaction.[35,41]

In a popular review of 2016 by Hondal and Reich, this asset of Sec over Cys was classified as the *rate advantage*.[35] Straightforward as it is, Sec does faster what Cys can do slowly. Recently, however, a second hypothesis emerged. Indeed, for Sec to be a good catalyst (and not simply a faster reactant) its reactions must be *fast and readily reversible*, that is, it must be possible for Se to cycle between its oxidation states without undergoing irreversible inactivation, as transition metal catalysts do.[35,42] Hondal and Reich classified this strength of Se over S as a *redox advantage* in the form of resistance toward overoxidation to (high) oxidation states that cannot be easily reduced back. Indeed, the reactions involving the lower oxidation states are fast and reversible for Se, but not always for S. Additionally, S is easily oxidized to its highest oxidation state, while the same process is quite slow

for Se, and unlikely to occur in biological conditions.[35,41][3]   The ease toward overoxidation (and inactivation) conferred by Cys rather than Sec in enzymes is well-documented for TrxR,[42,43] but was assessed also for Cys mutants of wild-type Sec Gpxs.[38,44]

While the rate advantage is rather general in nature, the redox advantage stems from both intrinsic properties (i.e., the well-known preference for low oxidation states increasing the atom weight along a group in the periodic table) and enzyme specific circumstances. A peculiar example is provided by naturally occurring SecGPx4, in which Sec can be protected by overoxidation forming an intramolecular Se–N bond with a backbone amide.[44–46] CysGPxs seem to not employ this trick,[44] even if intramolecular S–N bonds have been detected in other enzymes,[47] and instead are hypothesized to be stabilized against overoxidation by formation of an intramolecular disulfide bond.[44] Conversely, Cys mutants of wild-type SecGpxs, lacking an intramolecular partner to form a disulfide, easily react with hydroperoxides and overoxidation is reached by their catalytic Cys to sulfinic and sulfonic acids.[38,44]

Nevertheless, the whole picture regarding the role of Se in biology is still far from understood, and a unanimous agreement on the reasons which made Sec survive up to mammals is not reached, explaining why this molecular tool still attracts the interest of researchers fifty years after its discovery.[23]

---

[3] Recently a debate emerged about the extent of the generality of selenium resistance toward overoxidation to the highest oxidation state, +6. For a discussion on the topic, see Chapter 8.

1.3 The Early Days of Organoselenides Reactivity

It is perhaps by chance that the same years that saw the birth of selenium enzymology, also marked the beginning of the widespread use of Se in organic chemistry. It is interesting to point out that a careful understanding of this matter inevitably sheds some light also on biological problems, being selenoenzymes extremely sophisticated organoselenium catalysts.

Already in 1979, Hans Reich,[41] a pioneer in the use of organoselenium chemistry in organic synthesis, provided a nice introduction on the topic:

> *"The chemistry of sulfur and selenium is very closely related. The greater expense of selenium and the hazard resulting from its toxicity are justifiable only if there is some qualitative or quantitative chemical difference which allows introduction, modification, or removal of the organoselenium group under conditions not possible with sulfur."*

Thus, as previously discussed, for Se to hold a (useful) place in organic synthesis, it must display some advantageous properties S does not. In this scenario, the synthetic chemist took the place of evolution in selecting the conditions in which organoselenides were better than organosulfides. Particularly, as highlighted by Reich,[41] the weaker Se–C bond, as compared to S–C bond, the enhanced nucleophilicity of selenolates as compared to thiolates and the ease by which organoselenides undergo nucleophilic attack at Se, among other properties, represent some valuable assets upon which organoselenium chemistry can be built.

Nevertheless, before the 70s, the role of Se in organic synthesis was mainly limited to the use of the inorganic SeO_2 as a (sometimes catalytic) oxidant.[48–51] During such oxidations, variable quantities of organoselenides were known to form but at the time were considered unwanted side products and received little attention until the end of the 60s.[50] This does not mean that the *organic chemistry of selenium* was undeveloped. Quite the contrary, the birthday of the field can be traced back at least to 1847, when, according to Fredga, Wöhler wrote to Berzelius: "a small grandchild of yours has come into the world, a child of selenium, the selenomercaptan".[52] By the first half of the 1900, many classes of organoselenides had been synthesized, even if the references were scattered and the field was characterized by lack of systematicity.[53–55] In fact, even after the discovery of the

vital role of Se in living beings, organic chemists of the time were affected by a form of *selenophobia*,[56,57] not only due to the well-known toxicity of selenium, but also to the *infernal* smell which was historically associated to organoselenium work.[52,56] An instructive anecdote is provided in a 1972 communication by Arne Fredga,[52] where the unfortunate attempt of an organic chemist to synthesize some organoselenides at the beginning of the 20th century is remembered:

> *"He soon found that work indoors was impossible and pursued the experiments on the roof of the building, but the smell spread over defenceless Cambridge. It caused much commotion and partly spoiled the centenary celebrations of Charles Darwin's birth. The origin of the smell was soon discovered, and he had to assemble his equipment in an open field in the fens, far from human dwellings. Laboratory work in this place was of course not comfortable, and in addition he was pestered by herds of creeping and flying insects who found the smell attractive. At last, he resigned, and the project was abandoned."*

These inconveniences surely delayed the development of the field. Indeed, what was overall missing, before the 70s, was any real exploitation of *the reactivity of organoselenides*.[58] Huguet in 1967 was probably one of the first to focus on the organoselenides formed during the oxidation of alkenes with SeO_2, *inter alia* postulating for the first time a reaction step which would have been known in the future as selenoxide elimination.[50] (*Vide infra*) Still, organoselenides were regarded at best as reactive intermediates in reactions mediated by an inorganic selenium oxidant.[50,59]

Things changed with the recognition that organic selenoxides, i.e., organic species with a formal selenium=oxygen double bond, could rapidly undergo an intramolecular deselenylation reaction (the so-called *selenoxide elimination*) which leads to formation of alkenes at room temperature, under very mild conditions, thus providing an easily accessible route to olefine synthesis. (Scheme 1.2) The thermal instability of selenoxides had been known for decades at the time, but the decomposition pathway was somewhat uncharacterized and thus its synthetic potential remained unappreciated.[53,58]
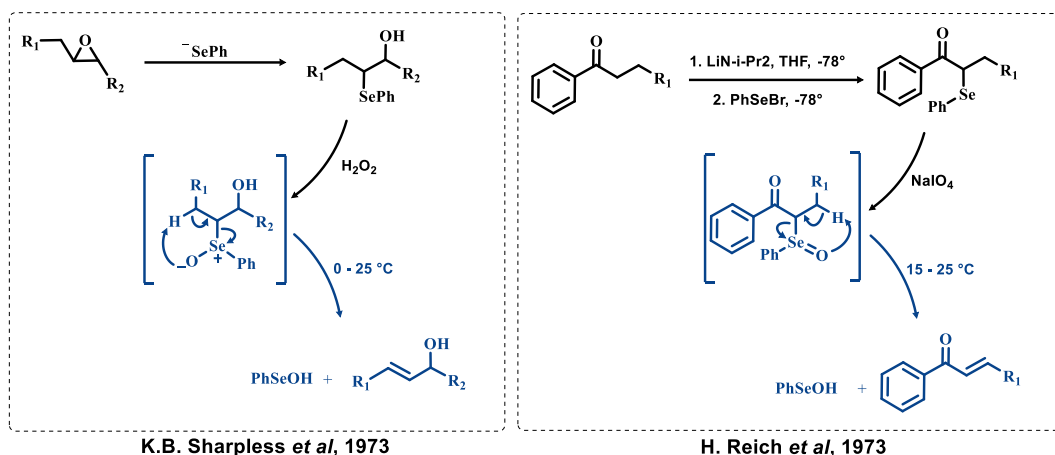
Scheme 1.2 First investigations and applications of the selenoxide elimination appeared in the literature by the groups of Sharpless and Reich for the synthesis of allylic alcohols and α,β unsaturated carbonyls, respectively.[2,60] The selenoxide elimination step is highlighted in blue. Differences in representation of the selenoxide bond (i.e., as a charge-separated Se–O single bond, or as a true Se=O double bond) are faithful to the choices of Sharpless and Reich, respectively.

After the first definitive observation at the very beginning of the 70s,[61,62] Sharpless,[1,60,63] Reich[2] and Clive[64] groups in 1973 were pioneers in popularizing the reaction by highlighting its synthetic usefulness. (Scheme 1.2) This reactivity has been widely exploited in the following years by various groups who confirmed the synthetic potential of the reaction by employing the selenoxide elimination in various synthetic protocols.[48,65–67] Even if other reactions of organoselenides were developed and characterized more or less in the same years (a few even a couple of years before),[3,68–74] the discovery of the selenoxide elimination is currently recognized to have been the breakthrough responsible for the "explosive" development of organoselenium chemistry.[48,57,75,76]

Another important step toward the development of modern organoselenium chemistry, was the awareness that as the inorganic SeO_2, also organoselenides could be employed for the practical oxidation of organic substrates. Particularly, the oxidizing power of seleninic anhydride was observed by the group of Barton[77–80] and then further explored separately by the group of Back,[81,82] expanding the scope of organoselenides with applications in organic synthesis. While these first rudiments of organoselenides reactivity required a stoichiometric amount of selenium, even before the end of the 70s the first organoselenium catalysts started to appear in the literature.

One of the first observation of the catalytic potential of organoselenides can be traced back to the pioneering work of Reich and coworkers in 1975. While working

on the selenoxide elimination, they found that selenides with β-hydrogens (a prerequisite for the elimination) were oxidized by H_2O_2 faster than selenides lacking such feature.[83] A plausible explanation was provided in terms of further oxidation of the released phenyl selenenic acid to phenyl seleninic acid,[60] which was hypothesized to lastly "activate" H_2O_2 in the form of a peroxyseleninic acid. This species was deemed capable of oxidizing the remaining selenide to selenoxide faster than H_2O_2 itself, thus triggering an autocatalytic reaction.[84] (Scheme 1.3)
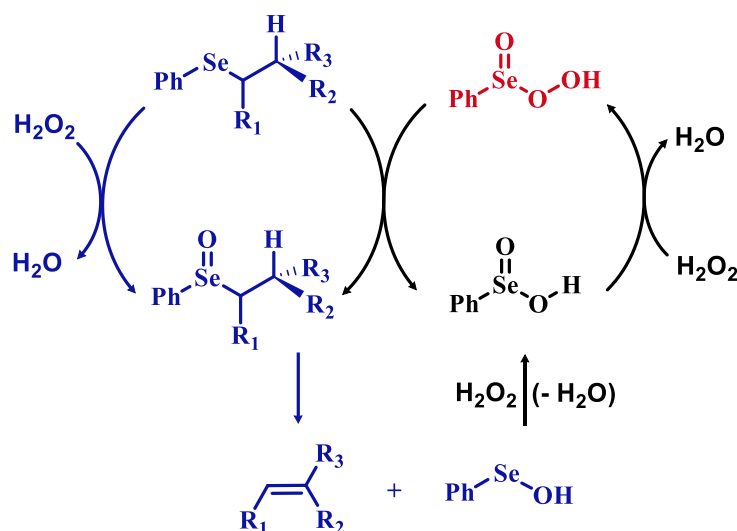
Scheme 1.3 Reich *et al* mechanistic hypothesis to rationalize the autocatalytic oxidation of β-eliminating organoselenides. The inductive step (i.e., prior to autocatalysis) is highlighted in blue, the peroxyseleninic acid is highlighted in red.

The oxidizing power of peroxyseleninic acid was soon found capable of epoxidizing alkenes, when peroxyseleninic acid was formed in a stoichiometric amount starting from phenyl seleninic acid and H_2O_2 by Grieco and coworkers.[85] It took less than one year to verify that the reaction could occur when only catalytic quantities of the phenyl seleninic acid were employed in the presence of H_2O_2 by Sharpless and Hori.[83,86] It was 1978, and the newly discovered catalytic potential of the phenylseleninic acid and H_2O_2 combination was about to become one of the key-ingredients of the modern organoselenium catalysis. Given the nature of seleninic acid as a precursor of a peroxyseleninic acid, Reich and coworkers foreseen its use also for other oxidations which were normally carried out with peroxycarboxylic acids, with the great advantage of the peroxyseleninic acid to be rapidly produced *in-situ* using H_2O_2 as sacrificial oxidant. The past forty years of research proved such foresight to be, indeed, quite right (Chapter 8).[57,87]

In just a couple of years these results provided evidence that organoselenium chemistry could be employed as a convenient way to alter or transfer selected functional groups,[66,88–90] thus leading to the development of new protocols for the synthesis of organoselenides[91] and to new routes to insert the organoselenium moiety into the desired molecular scaffold.[65,67,88,92] All this, despite Se well-known toxicity and ugly smell, which somewhat dissuaded organic chemists to pursue investigations in the area. The *selenophobia* which had afflicted many organic chemists[93] of the time was starting to fade away, and Se was evolving from a despicable element to a useful synthetic tool.[41,58]

1.4 The GPx Catalytic Cycle and GPx-like Catalysts

Since its recognition as a true selenoenzyme, GPx has been the face of selenium enzymology. It is by far the most studied and understood selenoenzyme: as of today,[4] searching for "glutathione peroxidase" on the Web of Science database returns about 37000 results only in the past twenty years. By comparison, searching for "thioredoxin reductase" the second most famous and studied selenoenzyme, returns about 5000 results. As briefly mentioned in Paragraph 1.1, at least eight different types of GPxs have been identified, not all of them selenoproteins in mammals:[24] GPxs 1 to 4 are selenoproteins, while GPx6 is a selenoprotein in humans only. Conversely, in mammals, GPx5, 7 and 8 contain Cys instead of Sec. Additionally, it is nowadays clear that only a minority of GPxs are actually selenoenzymes, since many insects and all land plants rely on CysGPxs instead, which can in some cases be almost as efficient as Sec analogues.[23,24]

Since its discovery by G. Mills in 1957, it had been clear that GPx catalyzes the oxidation of GSH to GSSG, accompanied by the reduction of hydroperoxides to the correspondent alcohol or water.[94] However, some GPxs can employ different thiols in place of GSH, while plant CysGPxs prefer thio- and glutaredoxins as cofactors.[24] A similar preference has been discussed for GPx3, which is mainly expressed in the extracellular environment, where GSH concentrations are in the μM range as compared to the mM range usually present in the cytosol. Thus, while GPx3 can in principle employ GSH, it is more likely to oxidize redoxins to redoxins disulfides.

---

[4] Last update June 19, 2023.

Additionally, while essentially all GPxs can reduce H_2O_2 (no data is available for GPx5 and 6), some of them accept small soluble lipid hydroperoxides as substrate, and GPx4 is unique in its capacity of reducing not only phospholipid peroxides but also cholesterol peroxide firmly embedded in a cell membrane.[24–26]

Despite this great variety, all GPxs are hypothesized to exert their peroxidase activity thorough similar chemical mechanisms, with some remarkable distinctions between Cys and SecGPxs.[24,25] The investigation of the catalytic cycle of GPxs began with the pioneering work of Flohé and coworkers on GPx1 in 1972, before its recognition as a true selenoenzyme.[95,96] The full characterization of the kinetic pattern of bovine GPx1 proved to be inconsistent with a canonical Michaelis-Menten hypothesis. Particularly, GPxs are characterized by a ping-pong kinetics, with an infinite K_M and v_{max} regardless of the peroxide. These results were found compatible with three independent substitution reactions.[18,96] (Scheme 1.4a)
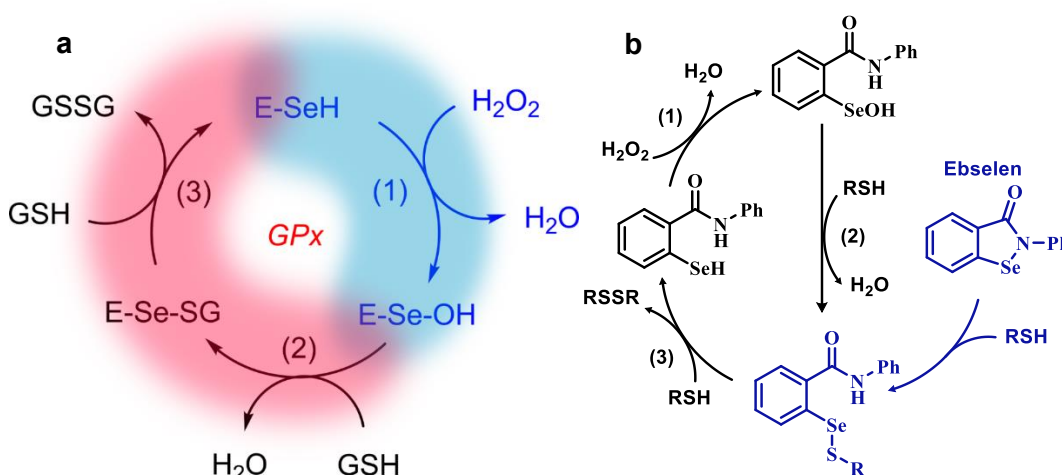
Scheme 1.4a Catalytic mechanism of SecGPx. E = Enzyme. G = Glutathione. The peroxidatic part of the catalytic cycle is highlighted in blue and the reductive part in red. **b** GPx-like catalytic cycle for Ebselen. In the first step (highlighted in blue) the selenyl amide bond is broken and the selenyl sulfide bond is integrated in the canonical GPx catalytic mechanism. Steps are numbered in analogy with the GPx catalytic cycle in scheme 1.4a.

In the first part of the catalytic mechanism (1), the selenol function of Sec undergoes deprotonation to a selenolate and then oxidation to selenenic acid, thus reducing the peroxide (H_2O_2 in Scheme 1.4). Later on, two equivalents of GSH reduce the enzyme active site back to the selenol function in a stepwise manner, *via* two independent S_N2 reactions: firstly reducing the selenenic acid to a selenyl sulfide intermediate (2) and lastly regenerating the fully reduced enzyme (3).[24,25,44] Importantly, the selenenic acid is so unstable that it has never been observed directly

within the actual enzyme, and only a couple of stable molecular analogues have been synthesized in confined environment to suppress their further reactivity.[97,98] Particularly, the Sec selenenic acid was isolated only in 2021, protected by a molecular cradle.[46]

For SecGPx, the kinetic constant associated with the peroxidatic part of the mechanism is larger than $10^7 \text{ M}^{-1} \text{ s}^{-1}$, while the one associated with the (overall) reductive part is 2 to 3 orders of magnitude smaller. However, since *in vivo* GSH reaches mM concentrations and the physiological steady state of H_2O_2 is *sub*-μM, the enzyme is physiologically kept in its reduced state and the overall velocity is independent on the concentration of GSH.[24] Naturally occurring CysGPx exploits a similar chemical mechanism, with S instead of Se. However, differently from SecGPx, the role of the first GSH in Scheme 1.4 is taken on by another GPx Cys, the so called resolving Cys. Thus, step (2) in Scheme 1.4 leads to an intramolecular disulfide, which is lastly reduced by a thioredoxin, making these enzymes functionally *thioredoxin peroxidases*.[24,26]

Given the detailed knowledge about the reaction mechanism of GPx and its deep involvement in the human antioxidant defenses, organic and medicinal chemists have been tempted by the idea of capturing the enzyme activity and transferring it to a small, drug-like molecule which can sustain the same, or a similar, catalytic cycle. Organoselenides had, obviously, a privileged role in this field given the importance of Sec in GPx catalysis. Several reviews can be consulted on the topic, in which detailed perspectives on their structure, mechanism and medicinal potential is provided.[99–102] The most famous case is without doubt ebselen, a selenyl amide which reached several clinical trials.[103] (Scheme 1.4b)

Unfortunately, the GPx-like antioxidant activity of biomimetic organoselenides proved to be somewhat difficult to control, since the exposed Se nucleus can engage in an unspecific reactivity with redox-sensitive thiols within the biological environment, hampering organoselenides catalytic potential and triggering toxic effects.[99] For ebselen, this was found to be particularly troublesome for step (3) in Scheme 1.4b. Indeed, the enhanced electrophilicity of Se preferentially directs the attack of a second thiol towards itself rather than towards the sulfur atom, thus the regeneration of the reduced organoselenide is hampered and the catalytic cycle remains stuck in the selenyl sulfide intermediate, which undergoes detrimental thiol

exchange side reactions.[101,104,105] This phenomenon does not occur, or is strongly suppressed, when the reaction takes place in the enzyme, explaining the relatively poor catalytic activities of many GPx-like organoselenides.[101] Strategies to suppress thiol exchange reactions also in organoselenides were pursued, with the best results being obtained replacing the amide function with a *sec*-amine and with the further addition of a methoxy function in *ortho* to the selenol.[101] Despite the success in the field, their employment as antioxidant GPx-like *drugs* remains unlikely due to the lack of substrate specificity,[99] and drug repurposing strategies have been envisioned to find alternative pharmaceutical applications to organoselenides.[102,106,107]

1.6 Last Remarks and Some Words of Caution

The aim of this Introduction was to show how the modern "organoselenium community" emerged across different fields, among which biochemistry and organic chemistry are two active representative areas. Many aspects were not covered, e.g. the use of organoselenides as ligands for metal catalysts,[57,108] many pharmaceutical aspects of organoselenides[109] as well as their toxicological aspects.[100,102] The vast area of organoselenium catalysis related to selenylation–deselenylation reactions was also not covered.[57,87,110,111] In this wide panorama, this Thesis wants to provide a theoretical chemist perspective on some topics spanning chemical and biochemical questions. Particularly, in Chapter 2, a brief description of the employed theoretical methods will be provided. Chapters 3 to 5 will mainly tackle topics surrounding the biological chemistry of organoselenides, i.e., the formation of a Se–S bond between target proteins and ebselen, the formation and disruption of the Se–S bond in models and in organoselenides with biological applications and the interaction of GPx with the peroxynitrite oxidant. Then, Chapters 6 to 8 will discuss mechanistic aspects of organoselenium chemistry mainly related to organic reactivity and synthesis, i.e., the chalcogenoxide elimination reaction, the reduction mechanism of sulfoxides and selenoxides by thiols and selenols, and the role of selenium oxidation state in organoselenium catalyzed oxygen-transfer reactions, respectively.

One thing should be kept in mind: there are a multitude of phenomena occurring all at once in any biological or chemical process. Quite the opposite, computational chemistry is a science of simplification: to bring down the complexity occurring inside of a round bottom flask to a couple of computer processable equations, some aspects must be wisely sacrificed.[112] Thus, do not be unsettled by somewhat large activation energies, minimalistic descriptions, *in vacuo* investigations or enzymes shattered down to pieces: these are just models of a much more vast and complicated reality. As such, they have a meaning in the measure they are helpful, not in the measure they are true. In the words of the Italian physicist Evangelista Torricelli:

> *"That the (Galilean) principles of movement are true or false, I care very little. Because, if they are not true, pretend them to be. [...] I pretend or hypothesize that a body or a point will move up and down following the known proposition, and horizontally in the same way (without friction). If this complies with observation, I will say that body follows what I said, and Galileo said before me. If then, lead, iron and stone balls do not obey to this hypothesis, such a shame, we will say we are not talking of them."*[5]

I tried to keep my models as close to reality as sensible, but approximations were made (see, e.g., Chapter 2). Even so, I believe these models were able to capture the essence of the organoselenium chemistry under investigation. If they indeed did so, despite the simplifications made in the process, they will have fulfilled their purpose.

---

[5]Evangelista Torricelli a Michelangelo Ricci, Firenze, 10 Febbraio 1646. Opere dei Discepoli di Galileo. Freely translated from Italian by the author of the thesis. This instructive piece of science history was brought to my attention by the 2021 Nobel Prize in Physics Giorgio Parisi, who quoted this paragraph in his *lectio magistralis* at Università degli Studi di Padova.

References

[1]   K. B. Sharpless, M. W. Young, R. F. Lauer, *Tetrahedron Lett.* **1973**, *14*, 1979–1982.

[2]   H. J. Reich, I. L. Reich, J. M. Renga, *J. Am. Chem. Soc.* **1973**, *95*, 5813–5815.

[3]   K. . Sharpless, K. M. Gordon, R. F. Lauer, D. W. Patrick, S. P. Singer, M. W. Young, *Chem. Scr.* **1975**, *8A*, 9.

[4]   L. Flohé, M. Maiorino, F. Ursini, *Free Radic. Biol. Med.* **2022**, *183*, 104–105.

[5]   L. Flohe, W. A. Günzler, H. H. Schock, *FEBS Lett.* **1973**, *32*, 132–134.

[6]   E. P. Painter, K. W. Franke, *J. Biol. Chem.* **1935**, *111*, 643–651.

[7]   K. W. Franke, *J. Nutr.* **1934**, *8*, 597–608.

[8]   H. C. Dudley, *Public Heal. Reports* **1938**, *53*, 281.

[9]   J. Pinsent, *Biochem. J.* **1954**, *57*, 10–16.

[10] K. Schwarz, J. G. Bieri, G. M. Briggs, M. L. Scott, *Exp. Biol. Med.* **1957**, *95*, 621–625.

[11] E. L. Patterson, R. Milstrey, E. L. R. Stokstad, *Exp. Biol. Med.* **1957**, *95*, 617–620.

[12] K. Schwarz, C. M. Foltz, *J. Biol. Chem.* **1958**, *233*, 245–251.

[13] A. C. Shum, J. C. Murphy, *J. Bacteriol.* **1972**, *110*, 447–449.

[14] D. C. Turner, T. C. Stadtman, *Arch. Biochem. Biophys.* **1973**, *154*, 366–381.

[15] J. R. Andreesen, L. G. Ljungdahl, *J. Bacteriol.* **1973**, *116*, 867–873.

[16] J. T. Rotruck, A. L. Pope, H. E. Ganther, A. B. Swanson, D. G. Hafeman, W. G. Hoekstra, *Science (80-.).* **1973**, *179*, 588–590.

[17] T. C. Stadtman, *Science (80-.).* **1974**, *183*, 915–922.

[18] L. Flohé, *Biochim. Biophys. Acta - Gen. Subj.* **2009**, *1790*, 1389–1403.

[19] J. E. Cone, R. Martin Del Rio, J. N. Davis, T. C. Stadtman, *Proc. Natl. Acad. Sci. U. S. A.* **1976**, *73*, 2659–2663.

[20] J. W. Forstrom, J. J. Zakowski, A. L. Tappel, *Biochemistry* **1978**, *17*, 2639–2644.

[21] G. V. Kryukov, S. Castellano, S. V. Novoselov, A. V. Lobanov, O. Zehtab, R. Guigó, V. N. Gladyshev, *Science (80-.).* **2003**, *300*, 1439–1443.

[22] V. N. Gladyshev, G. V. Kryukov, *BioFactors* **2001**, *14*, 87–92.

[23] M. Mariotti, V. N. Gladyshev, *Selenocysteine-Containing Proteins*, Elsevier Inc., **2022**.

[24] R. Brigelius-Flohé, M. Maiorino, *Biochim. Biophys. Acta - Gen. Subj.* **2013**, *1830*, 3289–3303.

[25] L. Flohé, S. Toppo, L. Orian, *Free Radic. Biol. Med.* **2022**, *187*, 113–122.

[26] M. Trujillo, C. A. Tairum, M. A. de Oliveira, L. E. S. Netto, *Thiol- and Selenol-Based Peroxidases: Structure and Catalytic Properties*, Elsevier Inc., **2022**.

[27] L. Tarrago, A. Kaya, H.-Y. Kim, B. Manta, B.-C. Lee, V. N. Gladyshev, *Free Radic. Biol. Med.* **2022**, *191*, 228–240.

[28] W. T. Lowther, N. Brot, H. Weissbach, B. W. Matthews, *Biochemistry* **2000**, *39*, 13307–13312.

[29] E. S. J. Arnér, *Biochim. Biophys. Acta - Gen. Subj.* **2009**, *1790*, 495–526.

[30] B. Manta, N. E. Makarova, M. Mariotti, *Free Radic. Biol. Med.* **2022**, *192*, 63–76.

[31] J. Köhrle, C. Frädrich, *Free Radic. Biol. Med.* **2022**, *193*, 59–79.

[32] A. L. Tappel, *Vitam. Horm.* **1962**, *20*, 493–510.

[33] J. G. Bieri, **1961**, 247–266.

[34] L. Flohé, J. R. Andreesen, R. Brigelius-Flohé, M. Maiorino, F. Ursini, *IUBMB Life* **2000**, *49*, 411–420.

[35] H. J. Reich, R. J. Hondal, *ACS Chem. Biol.* **2016**, *11*, 821–841.

[36] J. E. Squires, M. J. Berry, *IUBMB Life* **2008**, *60*, 232–235.

[37] M. J. Axley, A. Böck, T. C. Stadtman, *Proc. Natl. Acad. Sci.* **1991**, *88*, 8450–8454.

[38] C. ROCHER, J. -L LALANNE, J. CHAUDIÈRE, *Eur. J. Biochem.* **1992**, *205*, 955–960.

[39] M. Maiorino, K. D. Aumann, R. Brigelius-Flohe, F. Ursini, J. van den

Heuvel, J. McCarthy, L. Flohé, *Biol. Chem. Hoppe. Seyler.* **1995**, *376*, 651–660.

[40] S. Toppo, L. Flohé, F. Ursini, S. Vanin, M. Maiorino, *Biochim. Biophys. Acta - Gen. Subj.* **2009**, *1790*, 1486–1500.

[41] H. J. Reich, *Acc. Chem. Res.* **1979**, *12*, 22–30.

[42] R. J. Hondal, E. L. Ruggles, *Amino Acids* **2011**, *41*, 73–89.

[43] G. W. Snider, E. Ruggles, N. Khan, R. J. Hondal, *Biochemistry* **2013**, *52*, 5472–5481.

[44] L. Orian, P. Mauri, A. Roveri, S. Toppo, L. Benazzi, V. Bosello-Travain, A. De Palma, M. Maiorino, G. Miotto, M. Zaccarin, A. Polimeno, L. Flohé, F. Ursini, *Free Radic. Biol. Med.* **2015**, *87*, 1–14.

[45] H. J. Reich, C. P. Jasperse, *J. Am. Chem. Soc.* **1987**, *109*, 5549–5551.

[46] R. Masuda, R. Kimura, T. Karasaki, S. Sase, K. Goto, *J. Am. Chem. Soc.* **2021**, *143*, 6345–6350.

[47] B. K. Sarma, G. Mugesh, *J. Am. Chem. Soc.* **2007**, *129*, 8872–8881.

[48] D. Liotta, R. Monahan, *Science (80-.).* **1986**, *231*, 356–361.

[49] N. Sonoda, S. Tsutsumi, *Bull. Chem. Soc. Jpn.* **1965**, *38*, 958–961.

[50] J. L. Huguet, in *Oxid. Org. Compd.*, **1967**, pp. 345–351.

[51] C. W. Wilson, P. E. Shaw, *J. Org. Chem.* **1973**, *38*, 1684–1687.

[52] A. Fredga, *Ann. N. Y. Acad. Sci.* **1972**, *192*, 1–9.

[53] T. O. D. W. Campbell, H. G. Walker, G. M. Coppinger, A. Selenocyanates, B. Selenols, **1951**.

[54] J. Gosselck, *Angew. Chemie Int. Ed. English* **1963**, *2*, 660–669.

[55] D. De Filippo, F. Momicchioli, *Tetrahedron* **1969**, *25*, 5733–5744.

[56] D. V. Frost, O. E. Olson, *CRC Crit. Rev. Toxicol.* **1972**, *1*, 467–514.

[57] S. Santoro, J. B. Azeredo, V. Nascimento, L. Sancineto, A. L. Braga, C. Santi, *RSC Adv.* **2014**, *4*, 31521–31535.

[58] D. L. J. Clive, *Tetrahedron* **1978**, *34*, 1049–1132.

[59] J. P. Schaefer, B. Horvath, H. P. Klein, *J. Org. Chem.* **1968**, *33*, 2647–2655.

[60] K. B. Sharpless, R. F. Lauer, *J. Am. Chem. Soc.* **1973**, *95*, 2697–2699.

[61] R. Walter, J. Roy, *J. Org. Chem.* **1971**, *36*, 2561–2563.

[62] D. N. Jones, D. Mundy, R. D. Whitehouse, *J. Chem. Soc. D Chem. Commun.* **1970**, 86–87.

[63] K. B. Sharpless, R. F. Lauer, A. Y. Teranishi, *J. Am. Chem. Soc.* **1973**, *95*, 6137–6139.

[64] D. L. J. Clive, *J. Chem. Soc. Chem. Commun.* **1973**, 695–696.

[65] P. A. Grieco, S. Gilman, M. Nishizawa, *J. Org. Chem.* **1976**, *41*, 1485–1486.

[66] K. C. Nicolaou, Z. Lysenko, *Tetrahedron Lett.* **1977**, *18*, 1257–1260.

[67] D. Liotta, G. Zima, *Tetrahedron Lett.* **1978**, *19*, 4977–4980.

[68] K. B. Sharpless, R. F. Lauer, *J. Am. Chem. Soc.* **1972**, *94*, 7154–7155.

[69] H. J. Reich, F. Chow, *J. Chem. Soc. Chem. Commun.* **1975**, 790–791.

[70] J. Rémion, W. Dumont, A. Krief, *Tetrahedron Lett.* **1976**, *17*, 1385–1388.

[71] K. B. Sharpless, R. F. Lauer, *J. Org. Chem.* **1974**, *39*, 429–430.

[72] D. L. J. Clive, C. V. Denyer, *J. Chem. Soc. Chem. Commun.* **1973**, 253a.

[73] K. BALENOVIĆ, N. BREGANT, I. PERINA, *Synthesis (Stuttg).* **1973**, *1973*, 172–172.

[74] N. Miyoshi, S. Furui, S. Murai, N. Sonoda, *J. Chem. Soc. Chem. Commun.* **1975**, *2*, 293a.

[75] T. Wirth, *Angew. Chemie - Int. Ed.* **2000**, *39*, 3740–3749.

[76] T. Wirth, *Tetrahedron* **1999**, *55*, 1–28.

[77] D. H. R. Barton, A. G. Brewster, S. V. Ley, M. N. Rosenfeld, *J. Chem. Soc. Chem. Commun.* **1976**, 985.

[78] D. H. R. Barton, D. J. Lester, S. V. Ley, *J. Chem. Soc. Chem. Commun.* **1978**, 130.

[79] D. H. R. Barton, P. D. Magnus, M. N. Rosenfeld, *J. Chem. Soc. Chem. Commun.* **1975**, 301.

[80] D. H. R. Barton, D. J. Lester, S. V. Ley, *J. Chem. Soc. Chem. Commun.* **1978**, 276.

[81] D. H. R. Barton, A. G. Brewster, R. A. H. F. Hui, D. J. Lester, S. V. Ley, T. G. Back, *J. Chem. Soc. Chem. Commun.* **1978**, 952.

[82] T. G. Back, N. Ibrahim, *Tetrahedron Lett.* **1979**, *20*, 4931–4934.

[83] H. J. REICH, F. CHOW, S. L. PEAKE, *Synthesis (Stuttg).* **1978**, *1978*, 299–301.

[84] H. J. Reich, J. M. Renga, I. L. Reich, *J. Am. Chem. Soc.* **1975**, *97*, 5434–5447.

[85] P. A. Grieco, Y. Yokoyama, S. Gilman, M. Nishizawa, *J. Org. Chem.* **1977**, *42*, 2034–2036.

[86] T. Hori, K. B. Sharpless, *J. Org. Chem.* **1978**, *43*, 1689–1697.

[87] D. M. Freudendahl, S. Santoro, S. A. Shahzad, C. Santi, T. Wirth, *Angew. Chemie - Int. Ed.* **2009**, *48*, 8409–8411.

[88] D. L. J. Clive, G. Chittattu, N. J. Curtis, W. A. Kiel, C. K. Wong, *J. Chem. Soc. Chem. Commun.* **1977**, 725.

[89] T. G. Back, D. H. R. Barton, M. R. Britten-Kelly, F. S. Guziec, *J. Chem. Soc. Perkin Trans. 1* **1976**, 2079.

[90] A. P. Kozikowski, A. Ames, *J. Org. Chem.* **1978**, *43*, 2735–2737.

[91] J. A. Gladysz, J. L. Hornby, J. E. Garbe, *J. Org. Chem.* **1978**, *43*, 1204–1208.

[92] D. Liotta, H. Santiesteban, *Tetrahedron Lett.* **1977**, *18*, 4369–4372.

[93] M. A. Umbreit, K. B. Sharpless, *J. Am. Chem. Soc.* **1977**, *99*, 5526–5528.

[94] G. C. Mills, *J. Biol. Chem.* **1957**, *229*, 189–197.

[95] L. Flohe, W. A. Gimzler, E. Eichele, *Hoppe Seylers Z Physiol Chem .* **1972**, 987–999.

[96] L. Flohé, S. Toppo, L. Orian, *Free Radic. Biol. Med.* **2022**, *187*, 113–122.

[97] T. Saiki, K. Goto, R. Okazaki, *Angew. Chemie Int. Ed. English* **1997**, *36*, 2223–2224.

[98] K. Goto, M. Nagahama, T. Mizushima, K. Shimada, T. Kawashima, R. Okazaki, *Org. Lett.* **2001**, *3*, 3569–3572.

[99] L. Orian, S. Toppo, *Free Radic. Biol. Med.* **2014**, *66*, 65–74.

[100] C. W. Nogueira, J. B. T. Rocha, **2011**, 1313–1359.

[101] K. P. Bhabak, G. Mugesh, *Acc. Chem. Res.* **2010**, *43*, 1408–1419.

[102] C. W. Nogueira, N. V. Barbosa, J. B. T. Rocha, *Arch. Toxicol.* **2021**, *95*, 1179–1226.

[103] P. A. Nogara, M. E. Pereira, C. S. Oliveira, L. Orian, J. B. T. da Rocha, in *Chalcogen Chem. Fundam. Appl.*, The Royal Society Of Chemistry, **2023**, pp. 567–591.

[104] B. K. Sarma, G. Mugesh, *J. Am. Chem. Soc.* **2005**, *127*, 11477–11485.

[105] M. Bortoli, L. P. Wolters, L. Orian, F. M. Bickelhaupt, *J. Chem. Theory Comput.* **2016**, *12*, 2752–2761.

[106] N. Singh, A. C. Halliday, J. M. Thomas, O. V Kuznetsova, R. Baldwin, E. C. Y. Woon, P. K. Aley, I. Antoniadou, T. Sharp, S. R. Vasudevan, G. C. Churchill, *Nat. Commun.* **2013**, *4*, 1332.

[107] Z. Jin, X. Du, Y. Xu, Y. Deng, M. Liu, Y. Zhao, B. Zhang, X. Li, L. Zhang, C. Peng, Y. Duan, J. Yu, L. Wang, K. Yang, F. Liu, R. Jiang, X. Yang, T. You, X. Liu, X. Yang, F. Bai, H. Liu, X. Liu, L. W. Guddat, W. Xu, G. Xiao, C. Qin, Z. Shi, H. Jiang, Z. Rao, H. Yang, *Nature* **2020**, *582*, 289–293.

[108] F. V. Singh, T. Wirth, in *Organoselenium Chem.*, Wiley, **2011**, pp. 321–360.

[109] P. A. Nogara, C. S. Oliveira, M. E. Pereira, M. Bortoli, L. Orian, M. Aschner, J. B. T. Rocha, in *Redox Chem. Biol. Thiols*, Elsevier, **2022**, pp. 643–677.

[110] S. Ortgies, A. Breder, *ACS Catal.* **2017**, *7*, 5828–5840.

[111] F. V. Singh, T. Wirth, in *Encycl. Inorg. Bioinorg. Chem.*, Wiley, **2018**, pp. 1–32.

[112] O. Eisenstein, G. Ujaque, A. Lledós, *Top. Organomet. Chem.* **2020**, *67*, 1–38.

2 Theory and Methods

This Thesis is a computational research work. As such, the bulk of the results presented herein were obtained by the computational implementation of some equations, whose theoretical framework can describe (with some degree of approximation) the physics of chemical reactions. In contemporary mechanistic investigations, the workhorse of computational chemistry is Density Functional Theory (DFT).[1,2] In this Chapter, a brief but precise overview is given over the basic concepts behind this theory, with an emphasis on the reasons explaining its popularity, and over the theoretical methods which can be used to extract further information from computational results.

2.1 Density Functional Theory and the Kohn-Sham Approach

Due to the quantum nature of matter and bonding, the physics behind bond breaking and formation events must be described at the quantum mechanical level, that is, by obtaining and working with the wave function Ψ of the system. This implies writing a time-independent Schrödinger equation, $\hat{H}\Psi = E\Psi$, by defining the Hamiltonian $\hat{H}$ of the molecular system and obtaining the energy E and the wave function Ψ by the solution of the corresponding eigenvalue problem.[3,4] The inherent complication in the wave mechanics approach is that only one-electron problems have analytical solution. Thus, all of chemistry resides in equations which are too complicated to be solved analytically. While numerically exact solutions can in

principle be obtained, by the combination of the (single-particle) Hartree-Fock and (correlated) post Hartree-Fock methods, the procedures required to reach sufficient levels of accuracy are computationally too demanding to be applied to any system larger than a couple of atoms, especially when extensive investigation are envisioned. This problem was already foreseen by the founding father of Relativistic Quantum Mechanics, Paul Dirac, in 1929:[5]

> *"The general theory of quantum mechanics is now almost complete, the imperfections that still remain being in connection with the exact fitting in of the theory with relativity ideas. [...] The underlying physical laws necessary for the mathematical theory of a large part of physics and the whole of chemistry are thus completely known, and the difficulty is only that the exact application of these laws leads to equations much too complicated to be soluble. It therefore becomes desirable that approximate practical methods of applying quantum mechanics should be developed, which can lead to an explanation of the main features of complex atomic systems without too much computation."*

The computationally unfavourable scaling factor of the wave mechanics approach is partly intrinsic in the mathematical form of its central object, Ψ, which is a function of three spatial coordinates and one spin coordinate *for each electron.* Thus, many electron problems naturally become untreatable fast with the increasing size of the system. Density Functional Theory (DFT) promised a way around this problem.[4]

Conceptually, DFT is an approach to treat a system of N *interacting* electrons,[6] not differently from post Hartree-Fock methods. Conversely, the whole theory is based on the investigation of the electron density ρ, rather than of Ψ. Differently from Ψ, in fact, ρ has only four degrees of freedom (three spatial coordinates, *r*, and one spin coordinate, *s*) regardless of the number of electrons.[6] Thus its mathematical complexity is independent on the size of the system. Here is the catch: while the mechanics of Ψ is well-known, and equations to obtain energies and other properties from it are available since the development of the quantum theory, the same is not true for ρ.

Only in 1964, Hohenberg and Kohn (HK) proved two theorems which became the true theoretical foundation of DFT.[4,7] The two theorems are known as the

existence theorem and the *variational theorem*. The first one states that *the ground state properties of a N-electron system are determined by the corresponding electron density.* Particularly, referring to energy, this means that the ground state energy of a system is a unique functional of the electronic density.

$$E = E[\rho(\boldsymbol{r}, s)] \qquad (2.1)$$

The HK *variational theorem* extends the wave function variational theorem also to $E[\rho(\boldsymbol{r}, s)]$, by proving that *for a well-behaved trial density ρ the energy functional yields an energy that is higher than or equal to that belonging to the exact ground state density ρ_0:*

$$E[\rho] \geq E[\rho_0] \qquad (2.2)$$

That is, all the information (particularly, the energy) which can be extracted from Ψ can be extracted also from ρ.[6] Unluckily, while the relationship between the energy and the wave function is well-known, the HK theorems just state the existence of such correspondence for the electronic density, but no means of obtaining an analytical expression of $E[\rho]$ are provided.

One year later, in 1965, Kohn and Sham (KS) provided a way around this problem, with the development of a self-consistent field (SCF) procedure.[8] Their idea is rather simple in philosophy, and can be summarized as follows: even if $E[\rho]$ is unknown, it can be expressed as the sum of a kinetic $T[\rho]$ energy term, and two potential energy terms, related to electron-electron and electron-nuclei interactions, $V_{ee}[\rho]$ and $V_{Ne}[\rho]$ respectively:

$$E[\rho] = T[\rho] + V_{ee}[\rho] + V_{Ne}[\rho] \qquad (2.3)$$

Among these three terms, only the last one has a quantum mechanically sound expression, while the $V_{ee}[\rho]$ can be written as a classical approximation, $J[\rho]$. The key to KS theory is then to work under the *non-interacting* particles hypothesis. In fact, the kinetic energy term can be evaluated exactly as a functional of the molecular orbitals for a *non-interacting* electron system, Ts. By summing and subtracting the two approximate, $J[\rho]$ and Ts, terms to Equation (2.3), we obtain:

$$E[\rho] = \text{Ts} + V_{Ne}[\rho] + J[\rho] +$$
$$+ (T[\rho] - \text{Ts}) + (V_{ee}[\rho] - J[\rho].) \qquad (2.4)$$

In which the first line can be evaluated explicitly, but provides only an approximation to the total energy, and the second line represents the difference

between the unknown density functionals and the known, approximated, kinetic, and potential energy terms. This difference, by definition, includes all the correlation and exchange effects which are not captured by the other terms, and is thus named *exchange-correlation functional, Exc*.[3] Thus, the overall energy density functional can be rewritten as a sum of three known terms, plus a small unknown term accounting only for a minor (albeit important) part of the energy.

The ansatz (so far unproved) at the core of KS-SCF theory is that a local potential $u_s(r)$ (with an explicit dependence on Exc) exists for which the density of the *non-interacting electron system* invoked in the definition of Ts is exactly identical to the density of the *interacting electron system* moving in an external local potential.[6] If this holds true, the whole interacting electrons problem is reduced to a one-electron formalism that can be solved iteratively if one chooses a suitable model for Exc. Thus, eigenvalue equations can be written (Equation 2.5), the so-called KS equations, whose solutions are KS orbitals χ_i of energy ε_i:

$$\left(-\frac{\hbar}{2m}\nabla^2 + u_s(r)\right)\chi_i(r) = \varepsilon_i\,\chi_i(r) \tag{2.5}$$

In which u_s, the KS local potential contains not only the classical electron-electron, electron-nuclei interactions, but also all the exchange and correlation effects ("folded" into Exc).[6] Lastly, the density of the system can be evaluated by summing over the square modules of all N occupied KS molecular orbitals according to Equation 2.6:

$$\rho(r) = \sum_i^N |\chi_i(r)|^2 \tag{2.6}$$

By plugging this density into Equation 2.4, the energy of the system can be evaluated until self-consistence.[4]

Incidentally, Equation 2.5 shares remarkable similarity with the Hartree-Fock equations, which are instead the result of an approximated theory exactly solved. In developing their theory, KS had to abandon the idea of the mathematical simplification which should have come by dealing with ρ, since molecular orbitals χ_i are once again introduced into the theory. However, since the energy which is minimized in the KS approach is the correlated energy, but the KS equations are mathematically similar to the Hartree-Fock equations, the KS-SCF procedure has

the potential to obtain results comparable in accuracy to post Hartree-Fock methods (in fact, exact results in the limit of the true Exc), but with a computational cost similar to that of the Hartree-Fock approach. For the price of a non-correlated approach, correlated results can be obtained.[4]

Unfortunately, the simplification of the KS approach is, up to today, merely formal: no explicit functional form of Exc is known, and thus all the complexity of the wave mechanics approach is simply hidden in an unknown term.[6,9] Thus, a plethora of density functionals have been developed to approximate Exc, with very different performances when used to tackle chemical problems. Even if such approximations are not systematically improvable, a sort of Jacob's latter was developed, each step of which represent an "improvement" over the previous one.[1,10,11] The first step is the Local Density Approximation (LDA) approach, in which the value of the functional at any position **r** is computed exclusively from the value of ρ at the same position.[4] Due to the lack of uniformness of ρ in molecular systems, its application to molecular properties is rather limited. The natural evolution is represented by Generalized Gradient Approximation (GGA) functionals, which also have an explicit dependence on the gradient of the density. This approach can be in theory pursued to higher orders leading to meta-GGA functionals. An even higher improvement of DFT performances can be obtained by including in Exc a certain percentage of the exact Hartree-Fock exchange. Such functionals are named as hybrids, and the combination of the last two approaches leads to functionals named meta-Hybrids. While each new step tends to perform in average better than the previous one, for specific tasks GGA functionals can perform as good as hybrid functionals.[1,10]

Despite such plethora of methods, DFT can still display some pitfalls. As a crucial example, when Exc is not parametrized to do so, essentially all density functional approximations fail to properly describe dispersive interactions. Since dispersion can be described as the interaction between fluctuating densities, which depend on "excitations" on the two interacting fragments and no information about the virtual orbitals is contained in standard KS-DFT methods, their failure is expected.[12] The most common solution to this problem is to introduce a semi-empirical dispersion correction that can be added to the functional, the most popular being the approach by Grimme and coworkers.[12–14]

2.2 The Activation Strain Model of Chemical Reactivity and the Energy Decomposition Analysis

The power of any computational method does not rely only on the ability to calculate energies, and, in doing so, to obtain the potential energy surface onto which reactions occur, but also on the possibility to rationalize the reactivity at an atomistic level. In the words of Peter Atkins:[15]

> *"Now we come to the heart of chemistry. If we can understand the forces that hold atoms together in molecules we may also start to understand why, under certain conditions, initial arrangements of atoms change into new ones in the course of the events we call 'chemical reactions'."*

While electronic-structure methods can provide *numerical* insight into a reaction, the wave function is not an easily interpretable object. It is the interest of the computational chemist not only to obtain numbers, which can quantify how fast and how well a reaction will go, but also to gain qualitative insight into the behaviour of matter.[16] That is, understood that one reaction proceeds and another one does not, which intrinsic properties of the reactants lead to this outcome?

The Activation Strain Model (ASM) of chemical reactivity, sometimes referred to as Activation Strain Analysis (ASA) was designed precisely with this philosophy in mind.[17,18] The ASM is a fragment-based approach that can be used to understand which factors influence the height of the activation barrier in a reaction, relating the properties of any molecular geometry (e.g. the transition state) to those of a reference state (e.g. the reactants of the reaction under investigation).[18] In this model, once two chemically meaningful fragments have been chosen, the energy of any point along a useful reaction coordinate (ζ) is split into two different contributions: *strain* ΔE_{strain} and *interaction* ΔE_{int} according to Equation 2.7:

$$\Delta E(\zeta) = \Delta E_{strain}(\zeta) + \Delta E_{int}(\zeta) \tag{2.7}$$

where the ΔE_{strain} is the energy difference between the structure the fragments have at the investigated point ζ with respect to their free fully optimized geometry, and ΔE_{int} is the instantaneous interaction energy between the distorted fragments According to this definition, the strain contribution is usually positive (i.e.

destabilizing), while the interaction energy is usually negative (i.e. stabilizing).[17] (Figure 2.1)
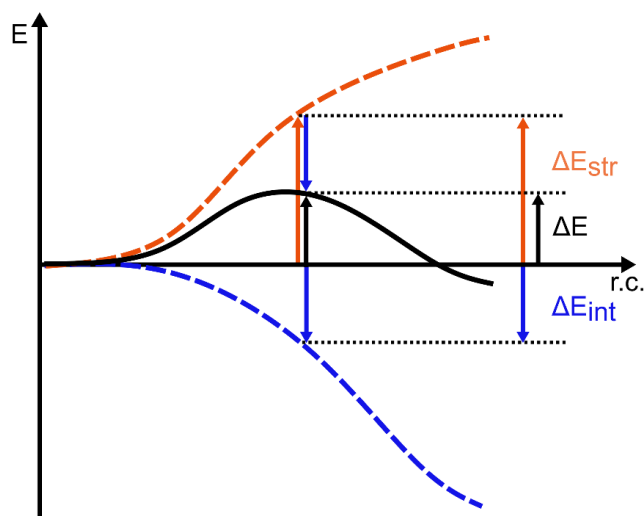
Figure 2.1. Schematic representation of the ASA applied along a generic reaction coordinate (r.c.)

While the strain energy refers to the geometrical modification the reactants must undergo to transform into the products, the interaction energy accounts for all the chemical interactions that arise when two distorted fragments are brought in proximity. By means of an Energy Decomposition Analysis procedure (EDA), it is possible to separate $\Delta E_{int}(\zeta)$ into chemically meaningful terms e.g., electrostatic interaction, orbital interaction, and steric repulsion. It is important to stress that no univocal approach exists to perform such decomposition, because while the total energy of a system is an observable, the decomposed energies are not. The approach used in this work has been explored in the KS-DFT framework by Baerends and Bickelhaupt[6] starting from the decomposition schemes of Ziegler, Morokuma and Rauk.[19–21] Thus, $\Delta E_{int}(\zeta)$ can be partitioned according to Equation 2.8:

$$\Delta E_{int}(\zeta) = \Delta V_{elstat}(\zeta) + \Delta E_{Pauli}(\zeta) + \Delta E_{OI}(\zeta) + \Delta E_{disp}(\zeta) \qquad (2.8)$$

in which $\Delta V_{elstat}(\zeta)$ is the *electrostatic interaction* between the unperturbed electron densities of the distorted fragments; $\Delta E_{Pauli}(\zeta)$ is interpreted as the (steric) repulsion occurring between occupied orbitals localized on the two fragments and is labelled as *Pauli repulsion*; $\Delta E_{OI}(\zeta)$ quantifies all the occupied-empty *orbital interactions*, such as the HOMO-LUMO interaction. Finally, $\Delta E_{disp}(\zeta)$ quantifies

dispersion interactions within the model of dispersion used in the calculation. While electrostatic and orbital interactions are usually stabilizing terms, Pauli repulsion is a destabilizing part of the interaction energy and gives rise to the barrier together with the strain contribution.

By defining two (molecular) fragments, A and B, with their appropriate (i.e., normalized and antisymmetrized) wave functions ψ_A and ψ_B and related densities ρ_A and ρ_B, it is possible to evaluate the electrostatic interaction $\Delta V_{elstat}(\zeta)$ between the two undistorted densities in a semi-classical fashion, according to Equation 2.9 (in atomic units):

$$\Delta V_{elstat} = \sum_{\substack{\alpha \in A \\ \beta \in b}} \frac{Z_\alpha Z_\beta}{R_{\alpha\beta}}$$

$$+ \int V_A(r)\rho_B(r)dr + \int V_B(r)\rho_A(r)dr \qquad (2.9)$$

$$+ \int \frac{\rho_A(r_1)\rho_B(r_2)}{r_{12}} dr_1 dr_2$$

in which Z_α and Z_β are the nuclear charges belonging to the nuclei of fragments A and B, and $V_{A/B}$ is the classical electrostatic potential due to nuclear charges $Z_{\alpha/\beta}$. While the first and the last term in Equation 2.7 are repulsive, being respectively the nuclear–nuclear repulsion and the electron density–electron density repulsion, the middle terms are the attractive interactions between the nuclear charges of one fragment and the electron density of the other, and *vice versa*. Within this EDA approach, this is the only term which needs to be evaluated explicitly. In fact, by defining as intermediate state for total wave function of the system (AB) the Hartree-product-like wave function $\psi_A\psi_B$, the energy change which occurs upon its antisymmetrization and renormalization can be defined to be equal to $\Delta V_{elstat}(\zeta) + \Delta E_{Pauli}(\zeta)$. Thus, Pauli repulsion can be obtained by difference, once $\Delta V_{elstat}(\zeta)$ is evaluated. Lastly, allowing for further mixing of the molecular orbitals, which are employed to build the Slater determinants ψ_A and ψ_B, to reach the molecular orbitals of the optimized total wave function ψ_{AB}, leads to a further stabilization, namely $\Delta E_{OI}(\zeta)$. Nevertheless, this term can be evaluated also by difference from the total $\Delta E_{int}(\zeta)$, since $\Delta E_{disp}(\zeta)$, if present, is computed in a semi-empirical fashion according to the dispersion correction employed.

While these terms are not observables and are constructed by means of "unphysical" intermediate states (e.g., the Hartree-product-like wave function $\psi_A\psi_B$ does not obey the Pauli principle), they provide a bridge between the total (complicated) energy and chemically intuitive concepts. The use of non-observable quantities is indeed a staple of chemistry:[22] and while their lack of uniqueness can be bothersome,[23] it does not undermine their usefulness as long as the model is not overinterpreted by its blind application, forgetting the way in which each term is evaluated. Indeed, the great advantage of the EDA scheme, in this context, does not lay in the absolute energy values obtained with the partitioning procedure, but in its use as a "theoretical probe": by employing the same EDA scheme to compare similar reactions, one can quantify how each of the energetic terms changes upon changing one factor (e.g., one reactant) in the reaction. Once the main term(s) affecting the reactivity has been individuated, chemical insight can be obtained by inspection of the electronic structure (if Pauli repulsion or orbital interaction define the observed phenomena) or analysing partial charges and electrostatic potentials (if the electrostatic interaction is the leading factor).[24]

Additionally, a deeper analysis of the orbital interaction term can be reached by combining the canonical EDA above described, with the Natural Orbitals for Chemical Valence (NOCV) method. The NOCV are the eigenvectors of the one-electron deformation density matrix $\Delta\boldsymbol{P}$, i.e., the difference between the one-electron density matrix of the full system (AB), and the one-electron density matrix obtained from the orbitals of the two separated fragments, A and B, orthogonalized with respect to each other and renormalized: a fictitious system usually referred to as "promolecule".[25] An interesting feature of the NOCV is to be always coupled in complementary pairs $(\varphi_{\pm k})$ associated to eigenvalues equal in absolute value but with opposed sign $(\pm v_k)$.[26]

These properties can be used to define the deformation density $\Delta\rho$, i.e., the difference in the electron density between the real system and the promolecule, as a sum over pairs of NOCV.[25–27] (Equation 2.10)

$$\Delta\rho = \sum_k \Delta\rho_k = \sum_k v_k \left(|\varphi_k|^2 - |\varphi_{-k}|^2\right) \qquad (2.10)$$

Equation 2.10 also sheds light on the physical meaning of NOCVs: the eigenvalue v_k can be interpreted as the fraction of electrons which is transferred from φ_{-k} to

φ_k, after bond formation, i.e., after the orbitals of fragment A are allowed to mix with the orbitals of fragment B.

One of the advantages of this formalism, is that employing the NOCVs the total ΔE_{OI} of Equation 2.8 can be rewritten as a sum of pairwise interactions, $\Delta E_{OI}{}^k$, each associated to a $\Delta \rho_k$, and thus to a pair of NOCV.[25,28] (Equation 2.11)

$$\Delta E_{OI} = \sum_k \Delta E_{OI}{}^k \qquad (2.11)$$

This partitioning is commonly referred to as EDA-NOCV.[29] It has been observed that while the total ΔE_{OI} is the result of many orbital interactions between the two fragments, in the NOCV formalism only a small number of $\Delta E_{OI}{}^k$ gives a significant contribution to the overall ΔE_{OI}. Thus, *via* the EDA-NOCV, the most important orbital interactions can be directly quantified, and the deformation density $\Delta \rho_k$ associated to each interaction $\Delta E_{OI}{}^k$ can be visualized for qualitative insight into the electronic redistribution which occurs during bond formation and breaking.[25–27]

2.3 TOF Calculations and the Energetic Span Model

In the description of catalytic reactions, the turnover frequency (TOF) is a useful index of the performance of a catalyst and of its correspondent catalytic cycle. The TOF can be defined as the *derivative* of the number of turnovers with respect to time.[30] A pioneering mathematical description of the TOF in terms of the rate constants k of all steps in the cycle was provided already in 1953 by Christiansen, under the steady state approximation.[31] However such expression for the TOF, obtained in the k-representation, led to algebraically obnoxious equations whose intuitive meaning is too complex to grasp.[32,33]

Moreover, while the k-representation is certainly useful and intuitive for experimentalists, theoreticians are more accustomed to the E-representation of chemical reactions, that is, the energetic description of all transition states and intermediates. Kozuch and Shaik,[32] who elaborated previous ideas of Jutand and Amatore,[34] provided a bridge between the two representations: the Energetic Span Model (ESM). Additionally, they proved that not only the definition of the TOF in the E-representation allows for the use of computational data, but it can also bring

new insight into catalytic reactions. By combining Christiansen's approach with the Eyring equation of transition state theory, the following relationship can be obtained:

$$\text{TOF} = \frac{k_B T}{h} \frac{1 - e^{\frac{\Delta G_r}{RT}}}{\sum_{i,j=1}^{N} e^{(T_i - I_j + \delta G_{ij})/RT}} = \frac{\Delta}{M} \tag{2.12}$$

in which ΔG_r is the Gibbs free energy of the overall cycle, T_i and I_j are the energies of the ith and jth transition state and intermediate respectively, k_B, h and R are the Boltzmann, Planck, and universal gas constant respectively, and T is the temperature. Lastly, δG_{ij} equals ΔG_r if the transition state i comes before the intermediate j, or zero otherwise.

This equation bears some analogies to the Ohm law of electric circuits, in that the TOF can be interpreted as a catalytic "current". In this context, the numerator (Δ) of Equation 2.12, dependent only on the thermodynamic driving force of the reaction, can be interpreted as a catalytic "potential", while the denominator (M), can be interpreted as the catalytic "resistance". Indeed, in the *E*-representation, M has a clear physical meaning: it describes how difficult it is to climb from each intermediate j to each transition state i, as if each energy difference was a serial resistor in an electric circuit.[35]

Since a difference of only ca. three 3 kcal mol^{-1} in the exponential terms leads to a difference of ca. 99% in their relative importance in the summation of M, many times Equation 2.12 can be simplified by neglecting all but one exponential in the denominator.[32] When this approximation can be made, Equation 2.12 can be reduced to:

$$TOF = \frac{k_B T}{h} e^{-\frac{\delta E}{RT}} \tag{2.13}$$

in which the so-called energetic span δE appears:

$$\delta E = \max_{i,j} \left(T_i - I_j + \delta G_{ij} \right)$$
$$= T_{TDTS} - I_{TDI} + \delta G_{TDTS,TDI} \tag{2.14}$$

δE is defined by the energies of the so-called TOF determining transition state (TDTS) and of the TOF determining intermediate (TDI). The meaning of these two

states is rather intuitive, being the two states with the greatest impact on the TOF value, based on their relative importance in the denominator of Equation 2.12.

The meaning of Equation 2.14 is also rather intuitive: it shows that, in the *E*-representation, it makes sense to treat the catalytic cycle as a single reactive step operating under the transition state theory, in which the energetic span δE assumes the meaning of the apparent activation energy of the whole process.[35] While it is easy to see some kind of analogy between the TDI and TDTS and the concept of rate determining step (in the *k*-representation), no *a-priori* constraints exist over such states, which can even be not consecutive. When this is indeed the case, all the steps between the TDI and the TDTS, hence the rate determining states, can be considered a rate determining zone. For these reasons, the concept of TDI and TDTS was proved to be more general and flexible than the old rate determining *step.*[35,36]

Thus, the identification of the TDI and the TDTS clearly offers two important advantages: (1) it simplifies the somewhat complex Equation 2.12 into the chemically intuitive Eyring-like Equation 2.13 and (2) it allows the identification of the states which mostly affect the catalyst performance, thus providing not only a quantitative but also qualitative insight into the reaction.

Within the ESM approach, it is possible to define a degree of TOF control (Equation 2.15), that is, a quantitative index of how much each single intermediate and transition state affects the overall TOF value:

$$X_{TOF,i} = \left| \frac{1}{TOF} \frac{\partial TOF}{\partial E_i} \right| \tag{2.15}$$

Having in hand the analytical expression of TOF in the *E*-representation (Equation 2.12), it is possible to derive explicit equations for the degree of TOF control for all intermediates I_j and for all transition states T_i:

$$X_{TOF,I_j} = \frac{\sum_{i=1}^{N} e^{(T_i - I_j + \delta G_{ij})/RT}}{\sum_{i,j=1}^{N} e^{(T_i - I_j + \delta G_{ij})/RT}}$$

$$\tag{2.16}$$

$$X_{TOF,T_i} = \frac{\sum_{j=1}^{N} e^{(T_i - I_j + \delta G_{ij})/RT}}{\sum_{i,j=1}^{N} e^{(T_i - I_j + \delta G_{ij})/RT}}$$

Being normalized with respect to the overall TOF, the sum of all $X_{TOF,i}$ equals 1, thus allowing the precise identification of the TDI and TDTS as the states for which

$X_{TOF,i}$ is the closest to 1. When only one TDI and TDTS can be identified per catalytic cycle, Equation 2.13 with the intuitive energetic span quantitatively describes the TOF.

It is useful to remember that the whole ESM is valid under three assumptions,[33] which are implicit in the derivation of the key equation of the model, i.e. Equation 2.12, and thus in all following derivations:

(i) Eyring transition state theory must be valid.

(ii) Steady state regime is enforced.

(iii) All intermediates undergo fast relaxation.

In addition, once must remember that Equations 2.12–2.16 require in principle Gibbs free energies, which can be routinely obtained by computational methods only under strong approximations (e.g., perfect gas assumption). Even if a fair estimate of Gibbs free energies were possible, also the true electronic energy of the system would remain out of reach, since approximations must be made to make the calculations feasible (e.g., choice of a density functional in DFT, finite basis set, relativistic approximations and so on). Thus, even if the three conditions required for the validity of the ESM were satisfied, the accurate absolute value of the TOF would still be unattainable computationally. However, when the most interesting comparison is between two catalysts or between two different catalytic cycles, the TOF ratio can be quantitatively useful in predicting their relative performance due to error compensation.[33]

2.4 Continuum Solvation Models

Quantum mechanical calculations provide energies and structures for molecules considered as isolated systems in a void environment, which can accurately describe gas phase reactions but provide only a first approximation to reactions occurring in solution. While the inclusion of explicit solvent molecules is possible in order to introduce directly the effect of the solvent in the quantum mechanical model, treating explicitly a huge number of solvent molecules prohibitively increases the computational time required for the calculations. Thus, methods have been developed to account for solvation effects in a simplified way, which mimics the solvent environment. The most applied approach is based on *continuum solvation*

models,[37] which describe the solvent as a uniform polarizable medium characterized by the dielectric constant ε, in which the solute is placed inside a suitably shaped cavity. This family of models well describes average electrostatic interactions between the solvent and the solute but neglects directional solute–solvent interactions. Considering the different interactions arising when a solute molecule is placed into the solvent, the solvation (free) energy can be written as:

$$\Delta G_{solv} = \Delta G_{cav} + \Delta G_{disp} + \Delta G_{elstat} \qquad (2.17)$$

where ΔG_{cav} is the energy required to accommodate a solute molecule into the solvent (i.e. the energy required to create the cavity where the solute stays), ΔG_{disp} is the dispersive interaction between solute and solvent and ΔG_{elstat} is the electrostatic interaction between solute and solvent. The plethora of methods that exist to calculate solvation energies differ in the way one or more of these terms are approximated. Particularly, a common approach to the calculation of the electrostatic term relies on the definition of $\sigma(s)$, the *apparent surface charge* (ASC) spread over the cavity surface s, and thus on the definition of a cavity shape. This ASC will interact with the nuclei and with the electron density of the solute, as well as with itself.[38] Methods can differ in how the cavity is defined and in how the ASC is computed.[3,37]

The COnductor-like Screening MOdel (COSMO),[39,40] which has been mostly used in this Thesis work, assumes a value of ε = ∞ for the solvent, thus approximating a conductor-like behaviour. This assumption simplify the ASCs calculation.[37] In order to recover the non-infinite behaviour of the dielectric constant, a scaling function is included in the formulation of the "realistic" ASC in the semi-empirical form:

$$\sigma(s) = \frac{\varepsilon - 1}{\varepsilon + k} \sigma^*(s) \qquad (2.18)$$

where $\sigma(s)$ is the "realistic" ACS on the surface *s*, k is an empirical adjustable scaling factor and $\sigma^*(s)$ is the ASC calculated in the conductor-like approximation and ε is the dielectric constant of the solvent.

By definition, the solute–solvent interaction is included in the energy of the system directly as the Gibbs free energy of solvation, i.e., ΔG_{solv}. Conversely, the energy computed with the KS approach is the electronic energy of the (isolated) system, and the related Gibbs free energy is obtained under perfect gas

approximation, G_{gas}. Since the standard state for gases and condensed phases differs, this would lead to inconsistencies when summing ΔG_{solv} to G_{gas} to provide the total Gibbs free energy of the system in solution, G_{soln}. Thus, when the evaluation of G_{soln} is required, a correction must be made to convert from the gas phase standard state (1 bar) to the solution standard state (1 M) according to Equation 2.19:

$$G_{soln} = G_{gas} + \Delta G_{solv} + RT \ln\left(\frac{RT}{P}\right) \qquad (2.19)$$

In the last term, R is the universal gas constant, T the temperature and P the pressure of the gas. Thus, the argument of the logarithm corresponds to the molar volume of a perfect gas at fixed T and P values.[41,42] At 298.15 K, this correction effectively raises all G values by ca. 1.90 kcal mol^{-1} with respect to the uncorrected G. However, since the correction does not depend on the nature of the chemical species, when reactions of the same molecularity are compared, this term can only lead to a systematic shift of activation energies, leaving the relative trends unaffected.

References

[1]   L. Goerigk, A. Hansen, C. Bauer, S. Ehrlich, A. Najibi, S. Grimme, *Phys. Chem. Chem. Phys.* **2017**, *19*, 32184–32215.

[2]   O. Eisenstein, G. Ujaque, A. Lledós, *Top. Organomet. Chem.* **2020**, *67*, 1–38.

[3]   F. Jensen, *Introduction to Computational Chemistry*, Wiley, **2007**.

[4]   C. J. Cramer, *Essentials of Computational Chemistry Theories and Models*, **2004**.

[5]   P. A. M. Dirac, , *Proc. R. Soc. Lond. Ser. Contain. Pap. Math. Phys. Character* **1929**, *123*, 714–733.

[6]   F. M. Bickelhaupt, E. J. Baerends, in *Rev. Comput. Chem.*, **2007**, pp. 1–86.

[7]   P. Hohenberg, W. Kohn, *Phys. Rev.* **1964**, *136*, B864–B871.

[8]   W. Kohn, L. J. Sham, *Phys. Rev. A* **1965**, *140*, 1133.

[9]   W. Koch, M. C. Holthausen, *A Chemist's Guide to Density Functional Theory*, Wiley, **2001**.

[10]   N. Mardirossian, M. Head-Gordon, *Mol. Phys.* **2017**, *115*, 2315–2372.

[11]   J. P. Perdew, A. Ruzsinszky, J. Tao, V. N. Staroverov, G. E. Scuseria, G. I. Csonka, *J. Chem. Phys.* **2005**, *123*, 062201.

[12]   S. Grimme, *Wiley Interdiscip. Rev. Comput. Mol. Sci.* **2011**, *1*, 211–228.

[13]   S. Grimme, J. Antony, S. Ehrlich, H. Krieg, *J. Chem. Phys.* **2010**, *132*, 154104.

[14]   S. Grimme, J. Antony, T. Schwabe, C. Mück-Lichtenfeld, *Org. Biomol. Chem.* **2007**, *5*, 741–758.

[15]   P. Atkins, F. Friedman, *Molecular Quantum Mechanics*, 4[th]ed, Oxford University Press, Oxford, 2005, p249.

[16]   F. Neese, M. Atanasov, G. Bistoni, D. Maganas, S. Ye, *J. Am. Chem. Soc.* **2019**, DOI 10.1021/jacs.8b13313.

[17]   F. M. Bickelhaupt, K. N. Houk, *Angew. Chemie - Int. Ed.* **2017**, *56*, 10070–10086.

[18] L. P. Wolters, F. M. Bickelhaupt, *Wiley Interdiscip. Rev. Comput. Mol. Sci.* **2015**, *5*, 324–343.

[19] T. Ziegler, A. Rauk, *Inorg. Chem.* **1979**, *18*, 1558–1565.

[20] K. Kitaura, K. Morokuma, *Int. J. Quantum Chem.* **1976**, *10*, 325–340.

[21] K. Morokuma, *Acc. Chem. Res.* **1977**, *10*, 294–300.

[22] G. Frenking, A. Krapp, *J. Comput. Chem.* **2007**, *28*, 15–24.

[23] R. F. W. Bader, *Chem. - A Eur. J.* **2006**, *12*, 2896–2901.

[24] P. Vermeeren, S. C. C. van der Lubbe, C. Fonseca Guerra, F. M. Bickelhaupt, T. A. Hamlin, *Nat. Protoc.* **2020**, *15*, 649–667.

[25] L. Zhao, M. Hermann, W. H. E. Schwarz, G. Frenking, *Nat. Rev. Chem.* **2019**, *3*, 48–63.

[26] G. Bistoni, S. Rampino, F. Tarantelli, L. Belpassi, *J. Chem. Phys.* **2015**, *142*, DOI 10.1063/1.4908537.

[27] A. Michalak, M. Mitoraj, T. Ziegler, *J. Phys. Chem. A* **2008**, *112*, 1933–1939.

[28] M. P. Mitoraj, A. Michalak, T. Ziegler, *J. Chem. Theory Comput.* **2009**, *5*, 962–975.

[29] F. M. Bickelhaupt, C. Fonseca Guerra, M. Mitoraj, F. Sagan, A. Michalak, S. Pan, G. Frenking, *Phys. Chem. Chem. Phys.* **2022**, *24*, 15726–15735.

[30] S. Kozuch, J. M. L. Martin, *ACS Catal.* **2012**, *2*, 2787–2794.

[31] J. A. Christiansen, in *Adv. Catal.*, **1953**, pp. 311–353.

[32] S. Kozuch, S. Shaik, *J. Am. Chem. Soc.* **2006**, *128*, 3355–3365.

[33] S. Kozuch, S. Shaik, *Acc. Chem. Res.* **2011**, *44*, 101–110.

[34] C. Amatore, A. Jutand, *J. Organomet. Chem.* **1999**, *576*, 254–278.

[35] E. Solel, N. Tarannam, S. Kozuch, *Chem. Commun.* **2019**, *55*, 5306–5322.

[36] S. Kozuch, J. M. L. Martin, *ChemPhysChem* **2011**, *12*, 1413–1418.

[37] J. Tomasi, B. Mennucci, R. Cammi, *Chem. Rev.* **2005**, *105*, 2999–3093.

[38] C. C. Pye, T. Ziegler, *Theor. Chem. Acc.* **1999**, *101*, 396–408.

[39] A. Klamt, *J. Phys. Chem.* **1995**, *99*, 2224–2235.

[40] A. Klamt, G. Schüürmann, *J. Chem. Soc. Perkin Trans. 2* **1993**, 799–805.

[41]   J. Ho, A. Klamt, M. L. Coote, *J. Phys. Chem. A* **2010**, *114*, 13442–13444.

[42]   J. H. Jensen, *Phys. Chem. Chem. Phys.* **2015**, *17*, 12441–12451.

3 Se–S Bond Formation Between Ebselen and Target Proteins

Adapted From

A. Madabeni, P.A. Nogara, F.B. Omage, J.B.T. Rocha, L.Orian

Appl. Sci. **2021**, 11(14), 6291

And partially reprinted from

G. Ribaudo, A. Madabeni, P. A. Nogara, C. Pavan, M. Bortoli, J.B.T. Rocha, L. Orian

Curr. Org. Chem. **2022,** *26(16), 1503-1511*

with permission from Bentham.

3.1 Introduction

Ebselen (EbSe, Scheme 3.1) is a cyclic selenenyl amide and it is among the oldest and most popular small-molecules investigated as glutathione peroxidase (GPx) mimics (see Chapter 1).[1–4] Starting from the first synthesis in 1924, several synthetic methodologies were developed to design EbSe and EbSe-like scaffolds making the compound one of the most famous organoselenides, even reaching commercial availability. Nevertheless, EbSe suffers of various drawbacks as a GPx-mimic, since the enhanced electrophilicity of Se prevents the full attainment of its catalytic potential, due to unwanted side reactions, especially in the thiol-rich biological environment.[5]
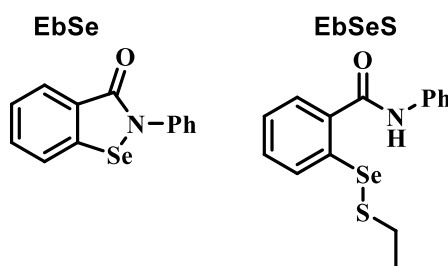
Scheme 3.1 Ebselen (EbSe) and ebselen ethanthiolate (EbSeS)

However, in the field of "drug rediscovery" and drug repurposing, EbSe is an outstanding example. In fact, this compound is currently being investigated as a multi-target antiviral agent,[6–10] for the prevention of noise-induced hearing loss and as a novel tool against neurodegeneration.[11–13] More specifically, the safety and pharmacokinetic profile of EbSe have been recently reviewed by Mengist *et al.* in their study focused on drug repurposing,[14] while an update on the toxicity of EbSe and organoselenium compounds was proposed by Rocha and coworkers.[15] In particular, it has been reported that EbSe has low toxicity in rats and was proven to be safe in humans during clinical trials[11,16,17] Moreover, absorption, distribution, metabolism, and excretion (ADME) profiles have been widely investigated throughout the years.[14,18]

The activity of EbSe in targeting different pathologies is usually related to its capacity of binding to critical Cys residues, disrupting protein function. In the following, EbSe binding mechanism to two different proteins will be discussed: (Paragraph 3.2) EbSe binding to SARS-CoV-2 main protease M^{pro} and (Paragraph 3.3) EbSe binding to inositol monophosphatase (IMPase).

3.2 SARS-CoV-2 M^{pro} Inhibition

The main protease (M^{pro}) and papain-like protease (PL^{pro}) of SARS-CoV-2 are suitable targets for the pharmacological action against its viral replication.[19] Both enzymes are cysteine (Cys) proteases,[20,21] and in the case of M^{pro}, the mechanism closely resembles the well-studied mechanism of serine protease. M^{pro} works via a catalytic dyad formed by a nucleophilic cysteine (Cys145) activated by a histidine (His41) residue. After a preliminary proton transfer from Cys145 to His41, through which the nucleophilic strength of the former residue is strongly enhanced, M^{pro} preferentially attacks peptide bonds after a glutamine residue,[22] leading to a tetrahedral intermediate from which the actual peptide bond cleavage occurs thanks to the back-proton-transfer from His45 leading to a thioester. (Scheme 3.2a) After that, the thioester is hydrolysed regenerating the active enzyme.

In early 2020, a high throughput screening discovered that EbSe is a potent inhibitor of SARS-CoV-2 M^{pro} (IC$_{50}$ = 0.67 μM).[6] EbSe is known to interact with

a plethora of biologically relevant cysteines[23–25] implying both pharmacological interest and toxicological concern. However, the low toxicity of EbSe, assessed in different experimental and clinical trials, makes it an interesting scaffold to design multipurpose drugs.[11,26]
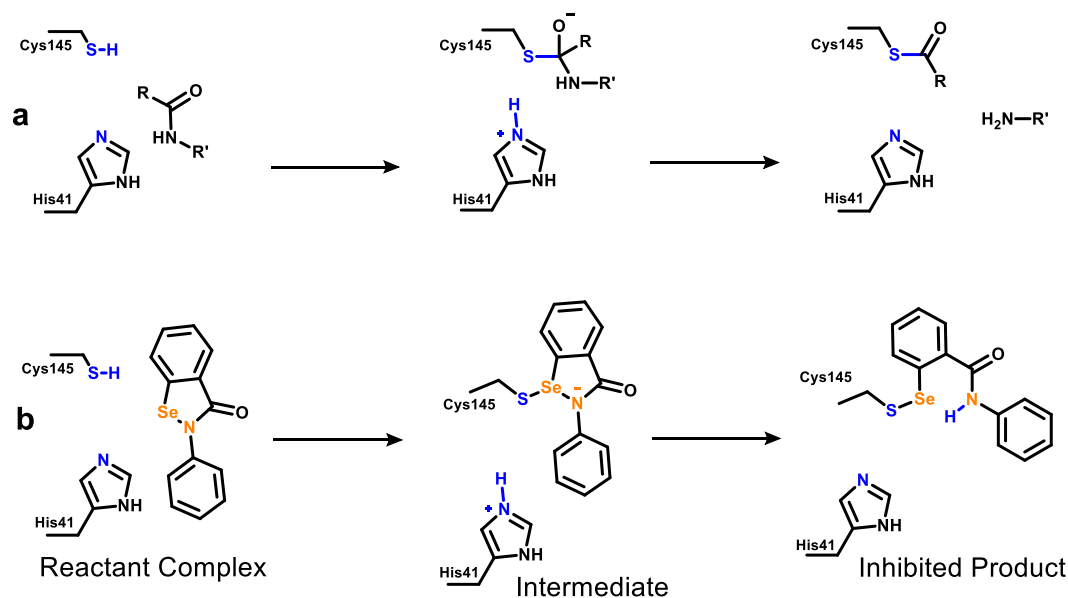
Scheme 3.2 (a) Acylation step of the proteolysis catalysed by SARS-CoV-2 M[pro]. **(b)** Predicted mechanism of the inhibition of SARS-CoV-2 M[pro] by ebselen as investigated in this study.

In a 2020 preprint, Sancineto *et al.*[27] reported interesting results indicating that the inhibitory capacity of organoselenium compounds towards M[pro] is greatly reduced upon dimerization to diselenides, and Ma *et al*. demonstrated that under reducing conditions, i.e., in presence of 1,4-dithiothreitol (DTT) and/or glutathione (GSH), EbSe is not able to effectively inhibit SARS-CoV-2 M[pro] as well as a panel of other Cys proteases.[28,29] Particularly, all the ebselen-like scaffolds investigated by Sancineto *et al.* were 1-2 orders of magnitude less efficient at inhibiting M[pro] after dimerization to diselenides. Moreover, the decrease in the inhibitory potency of EbSe in the presence of DTT and GSH raises the problem of formation of ebselen-low-molecular mass thiol adducts *in vivo* (i.e., adducts with free Cys and GSH). Further investigation is thus important to understand the true antiviral potential of organoselenium compounds starting from the chemical mechanism to move afterwards progressively to realistic biological conditions. For this reason, the chemical mechanism of Se–S bond formation between EbSe and Cys145, which is at the basis of the protease inhibition, was thoroughly analysed *in silico*.

Additionally, the analysis was extended to the Se–S bond formation starting from ebselen ethanthiolate (EbSeS) (Scheme 3.1) as a model of the adduct of EbSe with endogenous thiol molecules. In fact, since it is unlikely that the reactive N–Se bond of EbSe reaches M^{pro} unmodified, EbSeS was considered a general model of ebselen thiolates, which are expected to be present in the biological environment. Actually, EbSe travels through the plasma bonded to the free Cys of albumin and/or other low-molecular-containing thiol molecules (Cys and GSH).[30,31] Thus, EbSe is suitable to describe *in vitro* inhibition and EbSeS is a simplified model for the description of *in vivo* inhibition of M^{pro}.

A joint molecular docking and DFT approach was used, in which the speed of docking is exploited to provide a reasonable guess of the non-covalent complex between EbSe/EbSeS and M^{pro}, and DFT is used to investigate bond breaking and formation phenomena. Lastly, the thermodynamics of a possible evolution of the Se–S adduct is discussed based on X-ray structures and mass spectrometry data discussed in a recent study by Amporndanai *et al.*[10] The authors experimentally observed the breaking of the Se–C bond of EbSe in M^{pro}, with subsequent release of the EbSe scaffold in the form of a salicylanilide (IUPAC: 2-hydroxy-N-phenylbenzamide). (Scheme 3.3)
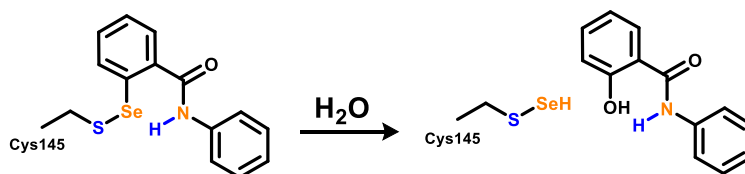
Scheme 3.3 Proposed hydrolysis (Amporndanai *et al.*) of Se-S adduct leading to salicylanilide release.

3.2.1 Computational Methods

Docking methodologies have been used to estimate a reasonable guess for the adduct between EbSe and M^{pro}. The mechanism was investigated employing the so-called cluster approach,[32] that is the fully quantum investigation of the enzyme reactivity using only selected residues that reproduce the chemical features of the catalytic pocket. Such method has been largely applied to the reactivity of much different

enzymes, spanning oxidoreductase,[33] lyase[34] and serine[35] or metalloprotease[36] enzymes.

Molecular docking was carried out to simulate the binding pose of EbSe with M^pro from SARS-CoV-2 (PDB ID 6LU7 [6]). AutoDock Vina software[37], which has a high accuracy for binding mode predictions, was used.[38] For the M^pro structure preparation, the waters, ions, ligands, and other molecules were removed, while the hydrogens atoms were added using the CHIMERA program, followed by 100 steps of energy minimization (amberff99SB).[39] The catalytic dyad (Cys145 and His41) was considered neutral, as highlighted in previous studies.[40,41] An adduct between EbSe and cysteine (EbSe-Cys) was used in the docking simulations to mimic the putative metabolites of EbSe.[42–44] The tridimensional model of the ligands (EbSe and EbSe-Cys) were created with Avogadro and MOPAC (PM6 method).[45,46] The files were prepared for the docking, using the AutoDock Tools 4.2,[37] with the ligands flexible. To consider the protein induced-fit effect and to improve the interactions between ligands and M^pro, the flexible-flexible docking method was applied, where EbSe, EbSe-Cys, and the side chain of His41, Met49, Asn142, Cys145, Met165, Glu166, and Gln189 residues (from the active site) were considered flexible during the simulations. The grid box was centered on the coordinates x = -14.04, y = 17.44, and z = 66.22 (size = 25 x 25 x 25 Å), and an exhaustiveness of 50 was used. The complex ligand-receptor with the most favorable binding free energy and with the best Se⋯S(Cys145) orientation was selected as a model of the binding pose and was used to build the M^pro pocket cluster for the DFT study.

After the docking, taking into account the closest M^pro residues (at 4.0 Å) from EbSe and EbSeS, His41, Met49, Cys145, and Met165 were selected and removed from the M^pro pocket, and the CH_3CO and CH_3NH groups were added to the N- and C-terminal regions, respectively, to mimic the backbone peptide bonds. In fact, the His41, Met49, Cys145, and Met165 residues were involved in many interactions with small molecules.[47] As a general model of ebselen thiolates, the carboxyl and amino moieties of EbSe-Cys were replaced with H atoms to create the ebselen ethanethiolate (EbSeS).

All density functional theory calculations were performed employing Gaussian16.[48] The level of theory employed was based on previous mechanistic

investigations in enzyme whose catalysis is based on reactive Cys or Sec residues.[49,50] Thus, the B3LYP hybrid functional[51,52] in combination with Grimme D3 dispersion correction and the Becke-Johnson damping function[53,54] was used. All first and second period atoms were described with 6-311G(d,p) basis set, while for sulfur and selenium, Dunning's correlation consistent cc-pVTZ basis set was used. All structures were optimized in gas phase and further solvation correction was taken into account as single point employing the SMD solvation model at SMD-B3LYP-D3(BJ)/6-311G(d,p), cc-pVTZ// B3LYP-D3(BJ)/6-311G(d,p), cc-pVTZ level of theory.[55] Diethyl ether was used to mimic the low dielectric constant of the enzymatic environment, as described in the literature.[56] Thermodynamics corrections at 298.15 K and 1 atm were computed by means of standard statistical mechanics relationship based on electronic energies and gas phase frequency calculations, as implemented in the Gaussian software. The atoms from the backbone were kept constrained during all geometry optimizations. Frequency calculations were performed to assess the nature of the optimized geometries: all transition states have one imaginary frequency related to the normal mode connecting reactants to products; all minima have no imaginary frequencies. For EbSe, starting from TS1 and TS2, an intrinsic reaction coordinate (IRC) calculation was done to verify that the correct transition state was located. [57]

3.2.2 Results and Discussion

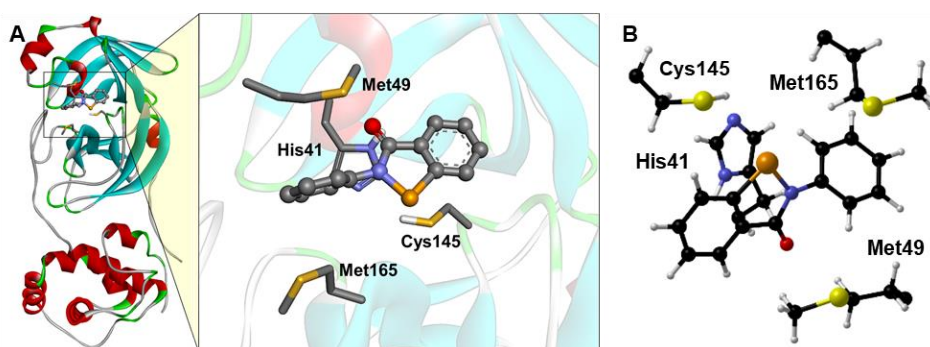**Figure 3.1** (**A**) Docking simulations between M^{pro} and EbSe. For better visualization, only the side chain of the main residues is shown. (**B**) Optimized M^{pro} cluster, with EbSe docked inside. For clarity, only C$^{\alpha}$, H$^{\alpha}$ and amino acids side chains are displayed, and it is oriented for optimal view. Level of theory: B3LYP-D3(BJ)/6-311G(d,p), cc-pVTZ.

The starting point of the mechanistic investigation for both EbSe and EbSeS was considered the reactant complex (RC) obtained after DFT optimization of the docking binding pose. (Figure 3.1, B)

As modelled, (Scheme 3.2B and Figure 3.2) the overall inhibition mechanism closely resembles the acylation step of the fully functional M^{pro} shown in Scheme 3.2A. The presence of EbSe does not impair the activation of Cys145, which is effectively deprotonated by His41 with an activation energy of about 15.16 kcal mol^{-1} (TS1), a value close to that previously reported for this step in a computational study on the functional enzyme (19.9 kcal mol^{-1}).[58] (Figure 3.2)
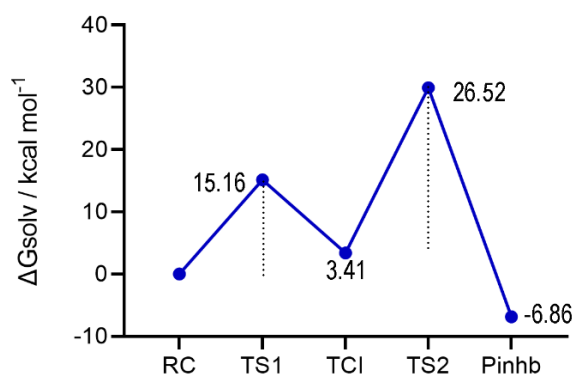
Figure 3.2 Energy profile for the inhibition mechanism of M^{pro} by EbSe. Activation energies of TS1 and TS2 are relative to the RC and TCI, respectively. Level of theory: SMD-B3LYP-D3(BJ)/6-311G(d,p), cc-pVTZ//B3LYP-D3(BJ)/6-311G(d,p), cc-pVTZ.

Notably, an Ion Pair (IP) between deprotonated cysteine (Cys$^-$) and protonated Histidine (HIP) was not located on the potential energy surface (PES), and, after the proton transfer, the cysteinate residue efficiently attacks the Se atom of EbSe, leading to an adduct with an almost linear N-Se-S bond (three centres intermediate, TCI). While conformational freedom of the backbone might help stabilizing an Ion Pair, which was located in another M^{pro} mechanistic investigation,[59] these results suggest that the cysteinate attack to the Se–N bond occurs with a very low, if any, activation energy.

The TCI lays 3.41 kcal mol^{-1} above the RC; thus, the step is weakly endergonic. After the formation of the TCI, full covalent inhibition is reached with the back proton transfer from HIP to the N atom of EbSe, leading to the N–Se bond cleavage and to the complete formation of the S–Se bond between Cys145 and EbSe. Such

step is exergonic; the inhibited product (Pinhb) is almost 7 kcal mol^{-1} more stable than the RC. While the back-proton transfer is predicted to have an activation energy of about 26 kcal mol^{-1}, thus being rate determining for the whole process, the geometrical features of the transition state (TS2) appear slightly distorted, likely due to the constraints imposed to His41 backbone. So, the activation energy of this process is expected to be overestimated in the model because of the limited flexibility of the catalytic pocket.[1] Indeed, in the acylation step of the functional M[pro], the analogous step occurs with a definitively lower activation energy.[58]

Using the same approach, the inhibition mechanism by EbSeS has been explored. (Figure 3.3) As seen for EbSe, also in this case the inhibitor does not impair Cys145 activation, which occurs with an even lower activation energy of 8.83 kcal mol^{-1} (TS1). However, this is almost certainly related to the closer proximity of Cys145 and His41 residues in the cluster (the distance between S and N atoms is 3.46 Å; conversely, in the cluster docked with EbSe, the corresponding distance is 4.61 Å).
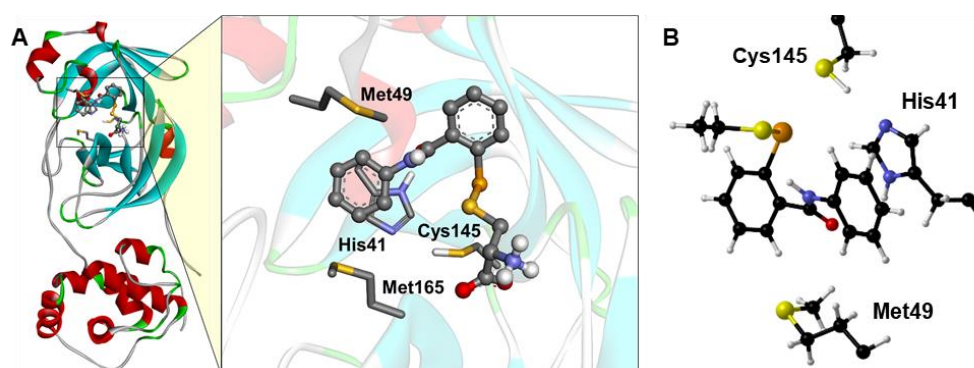
Figure 3.3 (**A**) Docking simulations between M[pro] and EbSeS. The carboxyl and amino moieties of EbSe-Cys were replaced with H atoms to create the ethanthiolate (EbSeS), as a general model of EbSe-thiol adduct/metabolite. For better visualization, only the side chain of the main residues is shown. (**B**) DFT optimized M[pro] cluster, with EbSeS docked inside. For clarity, only C[α], H[α] and amino acid side chains are displayed, Met165 is not represented and the cluster is oriented for optimal view. Level of theory: B3LYP-D3(BJ)/6-311G(d,p), cc-pVTZ.

After TS1, the mechanism of EbSeS displays important differences with respect to that of EbSe. Particularly, a strongly destabilized IP (9.62 kcal mol^{-1}) has been

---

[1] Interestingly, some months after our investigation, a similar study was published in which a larger cluster was used, together with a solvent-assisted mechanism. While some features of the two mechanisms differ (and, as expected, the energetics associated to the larger cluster was found to be lower compared to our reduced one), the two studies nicely agree in that the activation part of the mechanism has a lower activation energy than the actual inhibition step. (*Int. J. Mol. Sci.* **2021**, *22*, 9792)

located on the PES, from which the proton dislocated on HIP might be shuttled to Cys145, leading back to the RC. In addition, different pathways might be suitable for the nucleophilic Cys⁻ attack to the Se atom of EbSeS. First, the deprotonated Cys might attack the Se–S bond of EbSeS, leading to a TCI which has been previously identified in vacuo and in water in model molecular systems.[60] In this case, the TCI is located only 1.25 kcal mol⁻¹ above the RC. Further re-optimization of the TCI in diethyl ether (see Computational Methods) does not significantly affect the geometry, confirming the stability of such intermediate also in a non-polar environment like the enzymatic pocket.

Such structure might spontaneously loose ethanethiolate (EtS⁻), leading to the desired thiolate exchange and the EbSe-S-Cys(M^pro) adduct. However, this process is computed to be endergonic (+5.20 kcal mol⁻¹ with respect to the RC) and the back proton transfer from HIP to EtS⁻ is required for the overall inhibition process to become exergonic (-1.78 kcal mol⁻¹ with respect to the RC). Whether such back proton transfer happens directly from the IP (thus leading to the concerted breaking of the EbSeS Se-S bond and to the formation of Cys-Se bond, bypassing the formation of a TCI) or at a later mechanistic stage (e.g. at the TCI itself) was not investigated, since such analysis is expected to be strongly influenced by the nature of the thiolate, by cavity rearrangements and by the presence of explicit water molecules, which can assist the thiol exchange mechanism. Further investigation employing molecular dynamics simulation are thus prompted, to understand how the evolution of the binding site can affect ebselen inhibition. However, the overall thermodynamic feasibility of the inhibition process seems to be less favourite with respect to the same process for EbSe (-1.78 and -6.86 kcal mol⁻¹ respectively). Since the chalcogenolate exchange between a thiolate and a diselenide was previously computed to be less thermodynamically favourite (in condensed phase) with respect to the thiolate exchange between a thiolate and a selenyl sulfide,[60] the same trend in thermodynamics can be expected to hold true also when comparing EbSe to its diselenide, in agreement with Sancineto et al.[27] findings. For a dedicated discussion on Se–S and Se–Se bond breaking, see also Chapter 4.

Lastly, starting from the Pinhb obtained from EbSe, the mechanistic hypothesis of Se–C bond-breaking depicted in Scheme 3.3 was investigated. The reaction appears to proceed as an aromatic nucleophilic substitution (S_NAr), but no

Meisenheimer intermediate was located, and all attempted optimizations led back to either the reactants or to the products, both in gas and condensed phase. Thus, in agreement with previous studies on molecular models, the soft chalcogen-leaving group and the weakly activated aromatic ring seem to favor a concerted S_NAr mechanism.[61] Beside the level of theory used throughout this work, some other density functionals (i.e., M06-2X,[62] M11[63] and B3LYP without Grimme dispersion) were tested to assess the non-existence of a Meisenheimer intermediate, as was done for model compounds in ref. 61. In all cases, the guess intermediate broke down.

Interestingly, the step described in Scheme 3.3 appears to be energetically favorite, leading to products (i.e., Cys-SSeH and salicylanilide) which are located on the PES 4.56 kcal mol^{-1} below the Pinhb with the addition of one water molecule. However, the mechanistic details of the Se–C bond-breaking of EbSe should be carefully investigated to assess the kinetic feasibility of such a pathway and the role of the catalytic pocket residues, especially since no evidence suggests the occurrence of a similar reaction in solution. Such an extensive investigation is beyond the scope of this investigation, which revolves around the preliminary Se–S bond formation. However, the preliminary computation of one of the possible transition states involved in the process has been carried out i.e., for the attack of OH$^-$ to the aromatic ring, with the other water proton located on His41 (HIP). Such transition state lies at a prohibitively high energy on the PES (+57.14 with respect to the Pinhb with the addition of a water molecule). This suggests that it is unlikely that such reaction proceeds in a biological environment without the active participation of other nearby residues which can activate water so that it takes part in the S_NAr reactivity in a more efficient way.

3.3 Inositol Monophosphatase Inhibition

Inositol Monophosphatase (IMPase) is considered to be the main target of lithium, being responsible for its pharmacological activity against bipolar disorder. Despite its narrow therapeutic index and the toxicity issues related to renal injuries, lithium is still a first-line choice for the treatment of mania and for preventing recurrences in bipolar disorder. Nevertheless, side effects and limited efficacy in some of the

cases push the search for novel tools to ameliorate these conditions, which still represent a social burden, and great efforts are being made towards the identification of alternative therapeutic options.

In 2013, EbSe was identified as a non-competitive, irreversible IMPase inhibitor (IC_{50} = 1.5 μM),[64] thus suggesting its possible use in the treatment of bipolar disorder as an alternative to lithium.

Singh *et al*. detected a 1:1 covalent binding of ebselen to the IMPase monomer. Based on mutagenesis studies, among the seven Cys residues in IMPase, the authors postulated that Cys218 could have been the ligand interaction residue.[64,65] Nevertheless, even if Cys218 is located in proximity to the enzymatic active site, it is not easily accessible as it is buried in the protein. Moreover, the crystallographic structure that was recently made available indicates that EbSe binds Cys141 (PDB ID 6zk0). This residue is known to be reactive and conserved in mammals[64,65] and, to a certain extent, in *Staphylococcus aureus* (Cys138).[66] These elements suggest a critical role for this residue, even if its exact function has not been fully determined yet.[67] In fact, even if Cys141 may not participate directly in the chemical catalysis, it cannot be ruled out that its inactivation could disrupt the normal interaction of substrates with the catalytic site.

Here, a molecular mechanism leading to the formation of the Se-S bond between Cys141 and EbSe is proposed in analogy with the previous Paragraph.

3.3.1 Computational Details

For consistency with the study reported in Paragraph 3.2, the same protocol has been adopted. Initially, docking experiments were performed to simulate the starting conformation adopted by ebselen when approaching Cys141. The structure of the macromolecular target was obtained from the RCSB Protein Data Bank (www.rcsb.org, PDB ID 6zk0) and the docking grid was centered on Cys141 (X: 32.3821, Y: 4.5928, Z: 175.5843) with a size of 15 x 15 x 15 Å. A binding energy of -3.9 kcal/mol was calculated for EbSe in the considered pose.

The enzyme cluster was prepared by selecting the residues included in a 5 Å spherical volume centered on EbSe (Ile68, Val73, Ser79, Ile80, Leu81, Thr86, Ile88,

His217, Cys218, Trp219, Leu245, Met246, Asp274, Asp275), linking close lying residues (less than two positions apart) with a Gly residue and capping the terminal amino acids with C(O)CH$_3$ (ACE) and N(H)CH$_3$ (NME) to mimic the peptide bond. All DFT calculations are at the same level of theory described in Paragraph 3.2.1.

3.3.2 Results and Discussion

As previously discussed for SARS-Cov-2 M^{pro}, for Cys to be an effective nucleophile, the residue must be deprotonated. In the selected protein cluster, a close lysine residue (Lys129) can behave as a general base, leading to a water-mediated proton abstraction from Cys. Indeed, such proton transfer proceeds with a low activation energy, comparable to the one discussed in 3.2.2. Such proton transfer leads to a cysteinate (Cys-S$^-$) and to a lysinium (Lys-NH$_3^+$) ion pair (IP), located about 5 kcal/mol above the initial adduct. The IP can attack the N-Se bond of EbSe (TS2), leading to the ring opening of the ebselen selenenyl amide ring, and to S–Se bond formation. Despite the nucleophilicity of Cys-S$^-$, the activation energy for the process is computed to be 29 kcal/mol. The magnitude of the barrier stems from the geometrical arrangement of EbSe within the catalytic pocket since the N–Se–C plane lies almost perpendicularly to the S–Se internuclear axis, a spatial disposition which does not favour an S$_N$2-like process, usually occurring with the interacting atoms almost aligned.

In this model, such orientation was chosen according to its resemblance to the crystallography binding pose, where the covalent S–Se bond is, however, already formed. By analogy with the discussion on Sars-Cov-2 M^{pro}, it seems reasonable to hypothesize that if the surrounding of Cys141 is flexible enough to accommodate EbSe with an almost linear arrangement of the S–Se–N atoms, the activation energy for S–Se bond formation will be much lower. The S–Se adduct (product complex, PC) is thermodynamically unstable with respect to both the RC and IP, being almost 10 kcal mol^{-1} higher in energy than the latter. Such structure presents a fully formed S-Se bond and a fully broken N–Se bond, with a deprotonated amide function. Indeed, Lys-NH$_3^+$ back-proton transfer to the amide function of EbSe is essential for the overall inhibition process to become thermodynamically favoured, as previously observed for the inhibition of M^{pro}. Such water-mediated back proton transfer (TS3)

occurs with a low activation energy, even lower than the Cys to Lys proton transfer (about 4 kcal mol^{-1}) and leads to an inhibited product (Pinhb) lying at around 3 kcal mol^{-1} below the initial RC and more than 16 kcal mol^{-1} below the PC (Figure 3.4). The thermodynamic feasibility of the overall inhibition process resembles that of the analogous process between EbSe and SARS-CoV-2 M[pro] Cys145, with differences in the mechanistic process likely to be due to the different orientation of EbSe with respect to the target Cys.
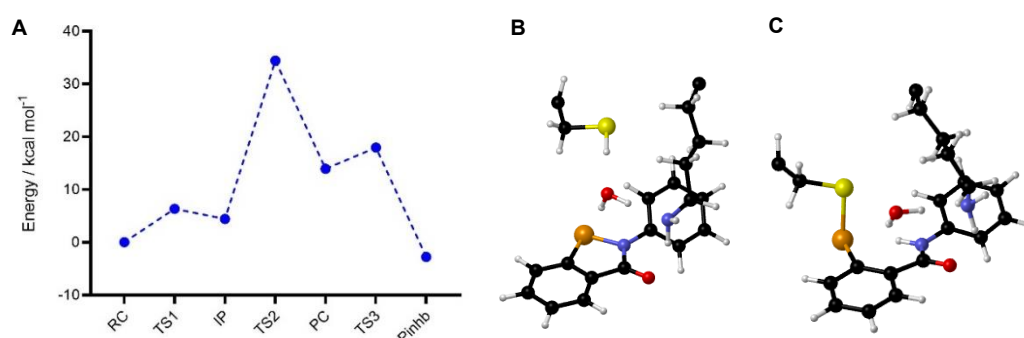
Figure 3.4. A) Stationary points and energy profile for the mechanism of ebselen binding to Cys141 of IMPase; B) RC and C) Pinhb of the reaction. Only two residues directly participating in the binding event are represented. For clarity, only C$^\alpha$, H$^\alpha$, and the amino acid side chains are displayed. Level of theory: SMD-B3LYP-D3(BJ)/6-311G(d,p), cc-pVTZ // B3LYP-D3(BJ)/6-311G(d,p), cc-pVTZ.

While for this protein the inhibitory potency of EbSeS was not evaluated, the same discussion above present should be readily extendable also to IMPase, since it is rooted in the thermodynamics of N–Se, S–Se or Se–Se bond breaking, which is expected to make EbSeS and EbSe diselenide less active than the parent compound.

3.4 Conclusions

The mechanistic details of S–Se bond formation between EbSe and the catalytic Cys145 of M[pro] and Cys141 of IMPase were investigated. Similar mechanisms were proposed, and the overall thermodynamics of binding were computed. An important effect on the energetics of the reaction was observed due to the geometrical arrangement of EbSe within the binding site. Particularly, while for M[pro] Cys attack to Se–N bond occurs without any appreciable activation energy, the correspondent process in our IMPase model is activated. These two views might be reconciled by taking into account the enzyme dynamics, to evaluate the effect of the conformational freedom of EbSe within the enzyme pocket on its reactivity: indeed, it seems reasonable to hypothesize that if EbSe reaches IMPase with a linear

S–Se–N arrangement, IMPase Cys141 will attack the Se nucleus with an activation energy similar to that of M^{pro} Cys145.

For M^{pro}, a comparison was made between EbSe and EbSeS binding. To the best of our knowledge, our investigation provides for the first time the stationary points for the covalent binding mechanism of EbSe and one of its possible metabolites to an enzymatic Cys, i.e., M^{pro} Cys145. Overall, the energetics computed for the metabolite suggests its weaker inhibition potential with respect to EbSe, in agreement with the recent studies on the activity of EbSe upon reduction to diselenide or in the presence of DTT/GSH. However, the nature of the leaving thiol might exert an important effect on the thermodynamics of the whole reaction, especially since EbSe might reach the M^{pro} bonded to an extremely bulky group such as a whole protein. Moreover thermodynamic support to the hypothesis of Se–C bond breaking within M^{pro} is provided,[10] and a detailed mechanistic investigation is prompted to understand if and how the direct participation of other residues of the catalytic pocket lowers the activation energy of the process.

Notably, since SARS-CoV-2 PL^{pro} employs a catalytic triad that includes reactive Cys and His residues too, a similar mechanism is readily extendable to this and other viral Cys proteases, both for EbSe and EbSeS. Thus, efforts should be prompted to design selenium-based systems capable to reach the target protein with the N–Se bond still intact, to prevent the loss of potency computationally predicted when the selenyl sulfide intermediate of EbSe (EbSeS in our model) reaches the protein.

References

[1] A. Wendel, M. Fausel, H. Safayhi, G. Tiegs, R. Otter, **1984**, *33*, 3241–3245.

[2] A. Müller, E. Cadenas, P. Graf, H. Sies, *Biochem. Pharmacol.* **1984**, *33*, 3235–3239.

[3] L. Orian, S. Toppo, *Free Radic. Biol. Med.* **2014**, *66*, 65–74.

[4] P. A. Nogara, C. S. Oliveira, M. E. Pereira, M. Bortoli, L. Orian, M. Aschner, J. B. T. Rocha, in *Redox Chem. Biol. Thiols*, Elsevier, **2022**, pp. 643–677.

[5] B. K. Sarma, G. Mugesh, *J. Am. Chem. Soc.* **2005**, *127*, 11477–11485.

[6] Z. Jin, X. Du, Y. Xu, Y. Deng, M. Liu, Y. Zhao, B. Zhang, X. Li, L. Zhang, C. Peng, Y. Duan, J. Yu, L. Wang, K. Yang, F. Liu, R. Jiang, X. Yang, T. You, X. Liu, X. Yang, F. Bai, H. Liu, X. Liu, L. W. Guddat, W. Xu, G. Xiao, C. Qin, Z. Shi, H. Jiang, Z. Rao, H. Yang, *Nature* **2020**, *582*, 289–293.

[7] A. Madabeni, P. A. Nogara, F. B. Omage, J. B. T. Rocha, L. Orian, *Appl. Sci.* **2021**, *11*, 6291.

[8] C. V. Haritha, K. Sharun, B. Jose, *Int. J. Surg.* **2020**, *84*, 53–56.

[9] P. A. Nogara, F. B. Omage, G. R. Bolzan, C. P. Delgado, M. Aschner, L. Orian, J. B. Teixeira Rocha, *Mol. Inform.* **2021**, *40*, 1–13.

[10] K. Amporndanai, X. Meng, W. Shang, Z. Jin, M. Rogers, Y. Zhao, Z. Rao, Z.-J. Liu, H. Yang, L. Zhang, P. M. O'Neill, S. Samar Hasnain, *Nat. Commun.* **2021**, *12*, 3061.

[11] J. Kil, E. Lobarinas, C. Spankovich, S. K. Griffiths, P. J. Antonelli, E. D. Lynch, C. G. Le Prell, *Lancet* **2017**, *390*, 969–979.

[12] M. Bortoli, A. Madabeni, P. Nogara, F. Omage, G. Ribaudo, D. Zeppilli, J. Rocha, L. Orian, **2020**, *11*, 7589.

[13] A. D. Landgraf, A. S. Alsegiani, S. Alaqel, S. Thanna, Z. A. Shah, S. J. Sucheck, *ACS Chem. Neurosci.* **2020**, *11*, 3008–3016.

[14] H. M. Mengist, D. Mekonnen, A. Mohammed, R. Shi, T. Jin, *Front. Pharmacol.* **2021**, *11*, 1–8.

[15] C. W. Nogueira, N. V. Barbosa, J. B. T. Rocha, *Arch. Toxicol.* **2021**, *95*, 1179–1226.

[16] E. Lynch, J. Kil, *Semin. Hear.* **2009**, *30*, 047–055.

[17] C. Masaki, A. L. Sharpley, B. R. Godlewska, A. Berrington, T. Hashimoto, N. Singh, S. R. Vasudevan, U. E. Emir, G. C. Churchill, P. J. Cowen, *Psychopharmacology (Berl).* **2016**, *233*, 1097–1104.

[18] K. Loeschner, N. Hadrup, M. Hansen, S. A. Pereira, B. Gammelgaard, L. H.

Møller, A. Mortensen, H. R. Lam, E. H. Larsen, *Metallomics* **2014**, *6*, 330.

[19] A. Francés-Monerris, C. Hognon, T. Miclot, C. García-Iriepa, I. Iriepa, A. Terenzi, S. Grandemange, G. Barone, M. Marazzi, A. Monari, *J. Proteome Res.* **2020**, *19*, 4291–4315.

[20] Y. Zhang, L. V. Tang, *J. Proteome Res.* **2021**, *20*, 49–59.

[21] R. Cannalire, C. Cerchia, A. R. Beccari, F. S. Di Leva, V. Summa, *J. Med. Chem.* **2020**, DOI 10.1021/acs.jmedchem.0c01140.

[22] S. Ullrich, C. Nitsche, *Bioorganic Med. Chem. Lett.* **2020**, *30*, 127377.

[23] L. Favrot, A. E. Grzegorzewicz, D. H. Lajiness, R. K. Marvin, J. Boucau, D. Isailovic, M. Jackson, D. R. Ronning, *Nat. Commun.* **2013**, *4*, 1–10.

[24] J. Chiou, S. Wan, K. F. Chan, P. K. So, D. He, E. W. C. Chan, T. H. Chan, K. Y. Wong, J. Tao, S. Chen, *Chem. Commun.* **2015**, *51*, 9543–9546.

[25] H. Sies, M. J. Parnham, *Free Radic. Biol. Med.* **2020**, *156*, 107–112.

[26] M. J. Parnham, H. Sies, *Biochem. Pharmacol.* **2013**, *86*, 1248–1253.

[27] L. Sancineto, F. Mangiavacchi, A. Dabrowska, A. Pacuła, M. Obieziurska-Fabisiak, C. Scimmi, Y. Lei, J. Kong, Y. Zhao, K. dos Santos Machado, A. V. Werhli, G. Ciancaleoni, V. Nascimento, A. Kula-Pacurar, E. J. Lenardao, H. Yang, J. Ścianowski, K. Pyrc, C. Santi, *ChemRxiv* **2020**, DOI 10.26434/chemrxiv.12994250.v1.

[28] C. Ma, Y. Hu, J. A. Townsend, P. I. Lagarias, M. T. Marty, A. Kolocouris, J. Wang, *ACS Pharmacol. Transl. Sci.* **2020**, *3*, 1265–1277.

[29] L. Y. Sun, C. Chen, J. Su, J. Q. Li, Z. Jiang, H. Gao, J. Z. Chigan, H. H. Ding, L. Zhai, K. W. Yang, *Bioorg. Chem.* **2021**, *112*, 104889.

[30] V. Ullrich, P. Weber, F. Meisch, F. Von Appen, *Biochem. Pharmacol.* **1996**, *52*, 15–19.

[31] G. Wagner, G. Schuch, T. P. M. Akerboom, H. Sies, *Biochem. Pharmacol.* **1994**, *48*, 1137–1144.

[32] P. E. M. Siegbahn, F. Himo, *J. Biol. Inorg. Chem.* **2009**, *14*, 643–651.

[33] R. Prabhakar, T. Vreven, K. Morokuma, D. G. Musaev, *Biochemistry* **2005**, *44*, 11864–11871.

[34] J. M. Parks, H. Guo, C. Momany, L. Liang, S. M. Miller, A. O. Summers, J. C. Smith, *J. Am. Chem. Soc.* **2009**, *131*, 13278–13285.

[35] P. D. Ngo, S. O. Mansoorabadi, P. A. Frey, *J. Phys. Chem. B* **2016**, *120*, 7353–7359.

[36] Q. Hu, V. M. Jayasinghe-Arachchige, R. Prabhakar, *J. Chem. Inf. Model.* **2021**, *61*, 764–776.

[37] A. Allouche, *J. Comput. Chem.* **2012**, *32*, 174–182.

[38] T. Gaillard, *J. Chem. Inf. Model.* **2018**, *58*, 1697–1706.

[39] E. F. Pettersen, T. D. Goddard, C. C. Huang, G. S. Couch, D. M. Greenblatt, E. C. Meng, T. E. Ferrin, *J. Comput. Chem.* **2004**, *25*, 1605–1612.

[40] E. Awoonor-Williams, A. A. A. A. Abu-Saleh, *Phys. Chem. Chem. Phys.* **2021**, *23*, 6746–6757.

[41] D. Suárez, N. Díaz, *J. Chem. Inf. Model.* **2020**, *60*, 5815–5831.

[42] H. Sies, *Free Radic. Biol. Med.* **1993**, *14*, 313–323.

[43] T. Schewe, *Gen. Pharmacol.* **1995**, *26*, 1153–1169.

[44] G. R. M. M. Haenen, B. M. De Rooij, N. P. E. Vermeulen, A. Bast, *Mol. Pharmacol.* **1990**, *37*, 412–422.

[45] J. J. P. Stewart, *J. Mol. Model.* **2007**, *13*, 1173–1213.

[46] M. D. Hanwell, D. E. Curtis, D. C. Lonie, T. Vandermeersch, E. Zurek, G. R. Hutchison, *J. Cheminform.* **2012**, *4*, 1–17.

[47] N. Sepay, P. C. Saha, Z. Shahzadi, A. Chakraborty, U. C. Halder, *Phys. Chem. Chem. Phys.* **2021**, *23*, 7261–7270.

[48] **N.d.**

[49] M. Dalla Tiezza, F. M. Bickelhaupt, L. Flohé, M. Maiorino, F. Ursini, L. Orian, *Redox Biol.* **2020**, *34*, 101540.

[50] M. Bortoli, M. Torsello, F. M. Bickelhaupt, L. Orian, *ChemPhysChem* **2017**, *18*, 2990–2998.

[51] A. D. Becke, *J. Chem. Phys.* **1993**, *98*, 5648–5652.

[52] K. Raghavachari, *Theor. Chem. Acc.* **2000**, *103*, 361–363.

[53] S. Grimme, *Wiley Interdiscip. Rev. Comput. Mol. Sci.* **2011**, *1*, 211–228.

[54] A. D. Becke, E. R. Johnson, *J. Chem. Phys.* **2005**, *123*, 154101.

[55] A. V. Marenich, C. J. Cramer, D. G. Truhlar, *J. Phys. Chem. B* **2009**, *113*, 6378–6396.

[56] L. Li, C. Li, Z. Zhang, E. Alexov, *J. Chem. Theory Comput.* **2013**, *9*, 2126–2136.

[57] R. L. Kenyon, *Chem. Eng. News* **1968**, *46*, 5.

[58] K. Świderek, V. Moliner, *Chem. Sci.* **2020**, *11*, 10626–10630.

[59] C. A. Ramos-Guzmán, J. J. Ruiz-Pernía, I. Tuñón, *ACS Catal.* **2020**, *10*, 12544–12554.

[60] M. Bortoli, L. P. Wolters, L. Orian, F. M. Bickelhaupt, *J. Chem. Theory Comput.* **2016**, *12*, 2752–2761.

[61] S. Rohrbach, J. A. Murphy, T. Tuttle, *J. Am. Chem. Soc.* **2020**, *142*, 14871–14876.

[62] Y. Zhao, D. G. Truhlar, *Theor. Chem. Acc.* **2008**, *120*, 215–241.

[63] R. Peverati, D. G. Truhlar, *J. Phys. Chem. Lett.* **2011**, *2*, 2810–2817.

[64] N. Singh, A. C. Halliday, J. M. Thomas, O. V Kuznetsova, R. Baldwin, E. C. Y. Woon, P. K. Aley, I. Antoniadou, T. Sharp, S. R. Vasudevan, G. C. Churchill, *Nat. Commun.* **2013**, *4*, 1332.

[65] M. R. Knowles, N. Gee, G. McAllister, C. I. Ragan, P. J. Greasley, M. G. Gore, *Biochem. J.* **1992**, *285*, 461–468.

[66] A. Dutta, S. Bhattacharyya, D. Dutta, A. K. Das, *FEBS J.* **2014**, *281*, 5309–5324.

[67] G. D. Fenn, H. Waller-Evans, J. R. Atack, B. D. Bax, *Acta Crystallogr. Sect. F Struct. Biol. Commun.* **2020**, *76*, 469–476.

4 Se–S Bond Reactivity: Model Dichalcogenides and TrxR Probes

In Chapter 3, Se–S bond formation was investigated as a key-step in the inhibition mechanism of different proteins by EbSe. Particularly, when EbSe reaches the protein as a selenyl sulfide metabolite, the inhibition mechanism implies a thiol exchange reaction. While these thiol-dichalcogenide exchanges are recognized to be responsible for the relatively low catalytic performance of EbSe as a GPx mimic (see Chapter 1, Paragraph 1.5), and, in Chapter 3, it was described how they are responsible for the lowering of the inhibitory potential of EbSe, they can also be exploited to design functional molecules (*vide infra*). Thus, they deserve a deeper scrutiny.

4.1 Introduction

Thiolate-disulfide exchange reactions are well-known S_N2 reactions, occurring in solution in a single concerted step in which the incoming S nucleus of the thiolate attacks an S central atom, leading to the expulsion of a thiolate leaving group. (Scheme 4.1, X=X'=X'')

X, X', X''=S, Se
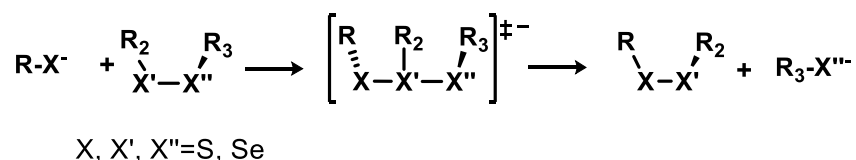
Scheme 4.1 General scheme for a chalcogenolate-dichalcogenide exchange in solution.

While disulfide exchanges have been intensively studied, both experimentally and computationally, somewhat less attention was devoted to the analogous reactions for selenyl sulfides.

Experiments on nucleophilic substitution at dichalcogenides involving the heavier Se started as early as 1989, when Rabenstein and coworkers observed that the symmetrical substitution of diselenides occurred 7 orders of magnitude faster than the corresponding one of disulfides.[1] Nevertheless, a complete investigation comparing thiolates and selenolates as nucleophiles and selenyl sulfides as dichalcogenides, was published only in 2010 by Koppenol and coworkers.[2] Among other results, it was observed that selenium acts both as a better nucleophile and as a better electrophile, but at neutral pH it did not provide any particular advantage (in terms of rate constants) as a leaving group instead of sulfur. While some of these observations were made somewhat earlier[3], Koppenol study provided a systematic experimental perspective, which is still a reference point for research on this topic.

From the computational point of view, the history of nucleophilic substitutions at selenium started at the beginning of the 2000s with the seminal studies of Bachrach and coworkers[4,5] who probed the gas phase mechanistic features of the potential energy surface (PES) and compared them to previous analysis on nucleophilic substitutions at the lighter sulfur,[6] providing evidence that the gas phase reactions occur with an addition-elimination (A-E) mechanism passing through a stable S–X–S, three-center intermediate (TCI), both when the attack occurs at the S or Se nucleus. (Figure 4.1)
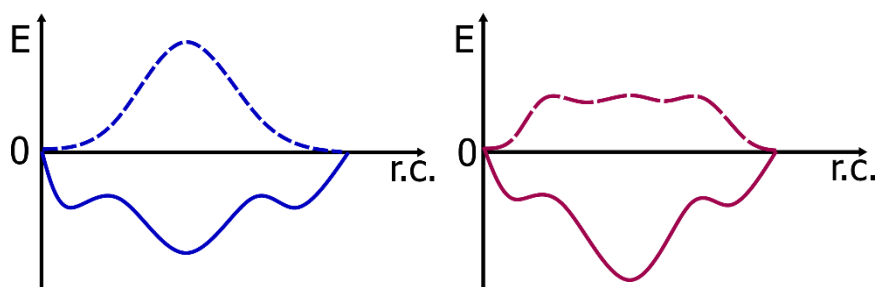
Figure 4.1 Schematic representation of the PES of nucleophilic substitution @S (blue) and @Se (red), in gas phase (solid line) and in water (dashed line), according to Bortoli *et al.*[7]

Conversely, for sulfur, when the central atom bears a methyl (i.e., organic) group, the reaction was found to occur in solution as a concerted $S_N2@S$.[6] The situation in solution remained unclear for the selenium central atom.

The S_N2 vs A-E picture was unified in 2016, in the study by Bortoli *et al*, showing that, while gas phase substitutions at selenium occur with the formation of a stable intermediate, the presence of a polar solvent destabilizes the central portion of the PES into a broad *plateau* upon which various transition states and intermediates are located at similar energy values (and geometries).[7] For the lighter sulfur central atom, polar (implicit) solvation is enough to turn the gas phase addition-elimination PES into a unimodal S_N2 PES. (Figure 4.1) Thus, while thiol-disulfide exchanges are conventional $S_N2@S$ in solution, nucleophilic substitutions at selenium are predicted to occur in a transitional regime in which the PES resembles a mechanism in-between A-E and S_N2. The presence of an intermediate on the PES is moreover expected to be influenced by the nature of the substituent on the central atom Se, as previously observed for other nucleophilic substitutions at heavy atoms.[8]
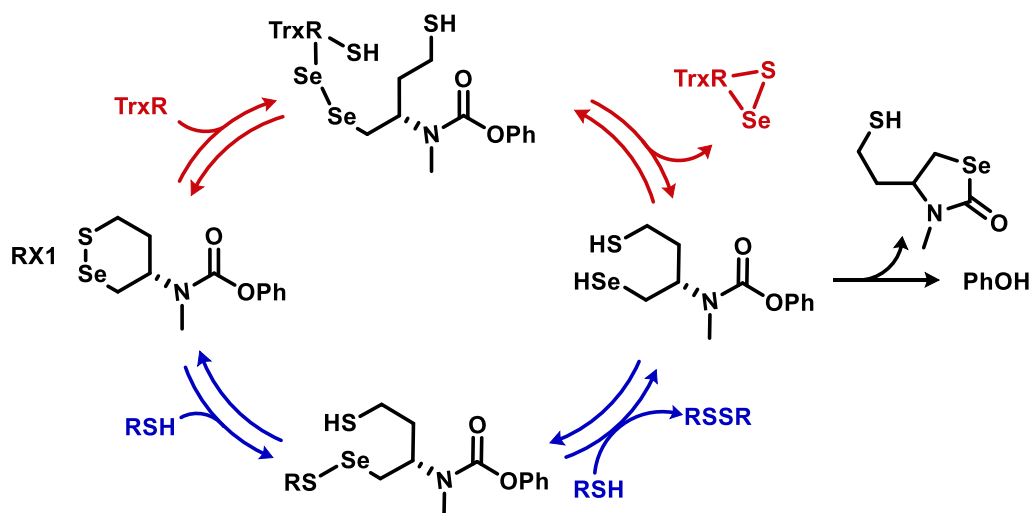
Figure 4.2 Schematic representation of RX1 interaction with TrxR (favored path: red) and with monothiols (disfavored path: blue) according to Zeisel *et al*.[9] PhOH is the fluorogenic cargo.

Beside this seminal mechanistic interest, a deep understanding of $S_N2@S$ and @Se is fundamental to grasp the behavior of dichalcogenides' evolution in the biological environment. Indeed, in 2021, Zeisel *et al* published a detailed account

on the design of RX1, a TrxR specific probe based on a cyclic selenyl sulfide. (Figure 4.2).

RX1 was designed in a way by which both the enhanced nucleophilicity of Sec (in TrxR) and the enhanced electrophilicity of Se (in RX1) are exploited to obtain a probe which releases a fluorogenic cargo (PhOH) *only* after interaction with TrxR, *via* nucleophilic substitutions at selenium. (Figure 4.2, red pathway) in fact, PhOH can be released only when the selenol moiety of RX1 is generated and can thus attack the carbonyl function by a fast nucleophilic acyl substitution (*5-exo-trig* cyclization) leading to a five-membered cycle. Most importantly, the design of RX1 grants it resistance towards cargo release even at high monothiols concentrations, which might be expected to complicate RX1 reactivity in the biological environment, in which thiols are indeed abundant.[9] (Figure 4.2, blue pathway)

In the following discussion, chalcogenol-dichalcogenide exchanges reactions will be investigated in two different systems: (1) An elementary model system in which the nucleophile is a methyl chalcogenol and the electrophile a diethyl dichalcogenide. This model reaction will be investigated for all combinations of S and Se on both the chalcogenol and dichalcogenide, to provide a comprehensive discussion on the topic; (2) Using the information obtained at the previous point, the chemistry of RX1 will be investigated, focusing on the specific reasons of its specificity for TrxR and its resistance against monothiols.

4.2 Computational methods

All DFT calculations were performed with the 2019.307 version of the Amsterdam Density Functional (ADF) software.[10,11] The OLYP[12,13] density functional has been used in combination with the TZ2P basis set, combined with a small frozen core approximation. Scalar relativistic effects were included by means of the Zeroth Order Regular Approximation (ZORA).[14] This level of theory was previously benchmarked[15] and applied[7,16] to the study of structure and reactivity of dichalcogenides. The Grimme D3 dispersion correction[17,18] with the Becke-Johnson damping factor[19,20] was included to facilitate the building of the adduct with two water molecules for the solvent-assisted mechanism (see Paragraph 4.3).

This level of theory is denoted as ZORA-OLYP-D3(BJ)/TZ2P. Frequency calculations were carried out to assess the nature of each optimized geometry. All minima have only positive frequencies, while transition states have one imaginary frequency associated to the atomic motion connecting reactants to products. For selected reactions, an intrinsic reaction coordinate (IRC) profile has been computed to verify that the correct transition state was indeed located on the PES.[21]

Thermodynamic corrections were calculated by means of standard statistical thermodynamics relationship at 1 atm and 298.15 K under perfect gas approximation. The effect of solvation (water) was included in a single-point calculation on the gas phase optimized geometry employing the COSMO model of solvation as implemented in ADF, with the default parameters for dielectric constant, atomic radii and empirical scaling function.[22,23] All energies discussed in the main text are Gibbs free energies in water, unless differently specified.

For the RX1 system, the molecular scaffold was built starting from available crystal structures of similar compounds. For intermediates which undergoes further evolution (RX1-SeSe and RX1-SeS, see Paragraph 4.3.2), a conformational search by means of the semiempirical GFN2-xTB method by Grimme and coworkers[24] combined with the CREST routine was carried out.[25] The minimum located by this approach was then reoptimized at ZORA-OLYP-D3(BJ)/TZ2P level of theory.

4.3 Results and discussion

In the chalcogenol-dichalcogenide exchange reactions, the thiolate / selenolate anion is recognized as the active nucleophile[2] which attacks the dichalcogenide bond. (Scheme 4.1) Nevertheless, around neutral pH (at which biological exchanges occur), the selenol moiety is expected to be completely deprotonated, while thiols will be in equilibrium with the correspondent thiolate (the pKa of Cys is ca. 8 while that of Sec is ca. 5)[26]1. At pH = 7, this results in selenols being 2–3 orders of magnitude more nucleophilic than thiols. At basic pH, where both thiols and selenols are completely deprotonated, the thiolate is still less nucleophilic than the selenolate,

---

[1] In proteins, the precise values depend on the local protein environment; nevertheless, selenols will be more acidic than analogous thiols.

but the reactivity difference is reduced to 1–2 orders of magnitude.[2] To take into account the effect of chalcogenol acidity on the nucleophilicity, all the nucleophilic substitutions at sulfur and at selenium have been modelled employing a solvent-assisted proton exchange (SAPE) mechanism, in which the nucleophile is considered to be protonated, but deprotonation occurs at the transition state *via* the mediation of explicit water molecules which drive the transfer of the proton from the nucleophile to the leaving group. This approach has been extensively used in the past fifteen years in organochalcogen chemistry, mainly by the group of Bayse.[27–29] Within the SAPE approach, all the substitutions occur in a concerted fashion, even for heavier Se central atoms in gas phase: thus, no information about the existence of TCIs on the PES can be obtained. Nevertheless, these species, even if they are present, are expected to be extremely labile and almost isoenergetic with the nearby TSs. Thus, their study should not bring any qualitative nor quantitative insight into dichalcogenide exchange reactivity.[7]

First (Paragraph 4.3.1), results about the model dichalcogenides will be presented. Later (Paragraph 4.3.2), the discussion will be extended to the RX1 TrxR probe, using the model dichalcogenides results as reference.

4.3.1 Model dichalcogenides reactivity

$$CH_3XH + \langle X'{-}X'' \rangle \longrightarrow \langle X{-}X' \rangle + HX''$$

X, X', X''=S, Se
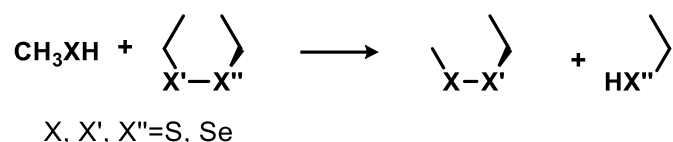
Scheme 4.2 Model reaction for the chalcogenol exchange between a methyl chalcogenol and a diethyl dichalcogenide. The proton transfer is mediated by two water molecules transferring the proton from CH_3XH to EtX''H.

With the aim in mind to understand the biological fate of RX1 and to provide a comprehensive picture of the dichalcogenides' reactivity, an oversimplified system was firstly employed. The dichalcogenides were modelled as diethyl dichalcogenides (disulfides, diselenides and selenyl sulfides) while the nucleophile was modelled as a simplified methyl chalcogenol (thiol or selenol). To simplify the discussion, a simple notation will be used omitting all methyl and ethyl groups, thus the thiol exchange on a disulfide will be labelled as SH + SS, while the same reaction occurring at the Se atom of a selenyl sulfide will be labelled as SH + SeS. (Scheme

4.2) By permutation of all possible X, X' and X'' = S, Se in Scheme 4.2, a total of eight reactions were studied. Gibbs free activation and reaction energies are collected in Table 4.1.

Table 4.1 Activation ($\Delta G^{\ddagger}$) and reaction (ΔG_r) energies (kcal mol^{-1}) for the eight model reactions in Scheme 4.2.[a]

		$\Delta G^{\ddagger}$	ΔG_r
1	SH + SS	38.63	-1.58
2	SeH + SS	33.97	-5.78
3	SH + SSe	38.45	2.84
4	SH+ SeS	32.50	-1.23
5	SeH + SSe	33.36	-1.35
6	SeH + SeS	27.89	-6.37
7	SH + SeSe	33.17	4.04
8	SeH + SeSe	28.04	-1.10

[a]The dichalcogenide is always written with the chalcogen to which the attack is occurring on the left.

As anticipated, all reactions occur in a single step in which the proton is transferred from the nucleophile to the leaving group, leading to the concerted formation of the X–X' bond and to the breaking of the X'–X'' bond. (Figure 4.3) While weakly bonded adducts (reactant complexes) can be located on the PES of these reactions, the solvation effect and, especially, the inclusion of thermodynamics correction make these species destabilized with respect to the free reactants. Thus, all activation energies are given with respect to the isolated reactants.
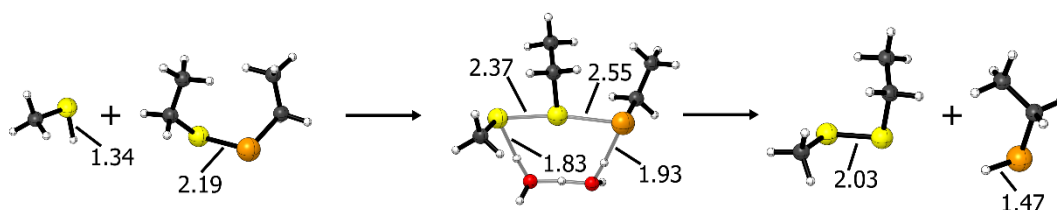
Figure 4.3 Optimized reactants, transition state and products (from left to right) for the reaction SH + SSe. Relevant bond lengths (in Å) are represented near the structure. Geometries are oriented for optimal visualization.

Focusing on the effect of the nucleophile, changing SH with SeH systematically lowers the activation energy of ca. 4.5–5 kcal mol^{-1}, regardless of the substrate and of the chalcogen at which the nucleophilic attack occurs. Taking as example SeS as electrophile, SH+SeS has an activation energy of 32.50 kcal mol^{-1}, while the analogous reaction with SeH has an activation energy of ca. 28 kcal mol^{-1}. Similarly,

all reaction energies are systematically thermodynamically more favorable by ca. 4–5 kcal mol^{-1} when SeH acts as the nucleophile in place of SH. Conversely, the leaving group effect on the activation energy of the reaction is rather weak in essentially all investigated reactions: changing the leaving group from SH to SeH affects the activation energy of the reaction by fractions (0.2 – 0.6) of kcal mol^{-1}. Nevertheless, a significant effect on the reaction energy can be observed, which rules in favor of the thiol as a leaving group. Indeed, while the S–Se bond is intrinsically weaker than the S–S bond (electronic bond dissociation energy (BDE) of 63.62 and of 68.58, respectively, both computed at ZORA-OLYP-D3(BJ)/TZ2P level), and thus easier to break, the released selenol is also a better nucleophile than the thiol, thus the backward reaction is favored. In addition, as observed by Koppenol *et al,*[2] the weaker S–Se bond does not affect much the kinetic of the process when SeH is the laving group compared to SH.

Lastly, a comparison between S and Se as central atoms (i.e., the electrophiles) in the reaction was made. As expected (see Paragraphs 1.5 and 4.1), Se behaves as a better electrophile, and all reactions occurring at Se have a $\Delta G^{\ddagger}$ of 5–6 kcal mol^{-1} lower than the corresponding ones occurring at S. Focusing on the thiol attack at a selenyl sulfide (SH + SSe and SH + SeS), the attack at the Se end of the Se–S bond occurs with an activation energy almost 6 kcal mol^{-1} lower than the attack at the S end. Moreover, attack at Se is favored thermodynamically when compared to the correspondent attack at S.

An interesting comparison can be made observing the reaction of the diselenide and the correspondent disulfide (on which both the central atom and the leaving groups are switched from S to Se). In this case, thermodynamics and kinetics follow different, i.e., opposite trends. The central Se nucleus favors the attack, as observed in the other cases, since it acts as a more electrophilic central atom in the S_N2 process. Thus, methyl thiol attack to diethyl diselenide (SH+SeSe) occurs with an activation energy more than 5 kcal mol^{-1} lower than the correspondent attack at the correspondent disulfide (SH+SS). However, the reaction is less favored thermodynamically. While the disulfide exchange has a weakly negative, almost thermoneutral reaction energy, thiol attack at the diselenide has a positive reaction energy (the most positive reaction energy observed in the eight reactions under

investigation) implying that the diselenide bond is somewhat less reactive as previously observed in experimental studies.[30]

It must always be kept in mind that while selenols are completely deprotonated at neutral pH, thiols will mostly be in equilibrium between their protonated and deprotonated form, and this might affect the stabilization of reactants and products based on the way in which the solvent stabilizes the charged species. Nevertheless, for various reactions under investigation, qualitatively similar results were obtained by Bortoli *et al* considering both the selenolate and the thiolate as completely deprotonated.[7] For example, the comparison of SeH+SeS vs SeH + SeSe provides the same qualitative effect of the leaving group. However, for some of the investigated reactions, different trends were observed with respect to the fully deprotonated species. Notably, Bortoli *et al,* predicted the selenolate to be a better leaving group, from the thermodynamic point of view, then the thiolate in the SH+SX reaction (X=S, Se). However, the energy difference between the two reactions was, of only 0.2 kcal mol^{-1}, and both reactions appeared to be essentially thermoneutral.

Considering these aspects all together, the two analyses provide mostly the same overall picture of the title reactivity, with some differences naturally arising due to the protonation state of either reactants or products.

4.3.2 RX1 reactivity with thiols and selenols

Building upon the knowledge obtained for the model dichalcogenides (Paragraph 4.3.1), we moved our attention to the modelling of Se–S bond formation and disruption in the recently patented and published TrxR probe RX1. (Figure 4.2)

The fluorogenic cargo (PhOH) is released only when the selenol moiety is generated on the RX1 probe. The specificity of RX1 for TrxR and its resistance against monothiols are based, according to Zeisel *et al,*[9] on different *design factors* (Figure 4.2):

(1) Since selenols are better nucleophiles than thiols, selenoproteins, bearing a Sec residue, will react faster with RX1 than biological Cys.

(2) The Se electrophilicity in the selenyl sulfide directs the incoming chalcogenol attack preferentially at Se, rather than at S, thus preventing direct selenol generation and consequent cargo release.

(3) Even if random thiols interact with RX1 through attack at the Se nucleus, cargo release requires a second intermolecular S_N2 process, in which another thiol attacks the unfavored S end of the newly formed selenyl sulfides. Thiol exchanges can be expected to dominate the reactivity, thus preventing non-specific cargo release.

(4) Since TrxR has got a catalytic pocket with two sequential Sec and Cys residues, pre-organized to form an intramolecular S–Se bond,[31,32] the second S_N2 process (leading to selenol generation on RX1) is intramolecular when TrxR reacts with the probe, and is expected to occur on the Se atom of TrxR Sec. Being an *intramolecular* S_N2@Se, it can be envisioned to be far more productive than the correspondent *intermolecular* S_N2@S atom described in (3).

Lastly, **(5)** Once the selenol is generated on RX1, it will rapidly cyclize, releasing the signal-generating cargo.

The results presented by Zeisel and coworkers prove that this line of reasoning is effective, given the excellent performance of RX1 in targeting TrxR1.[9] Nevertheless, a consistent mechanistic picture would allow a more physical description of RX1 reactivity and of its evolution in the biological environment. Thus, prompted by a request from Zeisel and coworkers, the aim of this Chapter is to provide theoretical mechanistic data to discuss in a quantitative manner the design points (1) – (4) of Zeisel *et al* study, which are deeply rooted in the properties of dichalcogenide exchange reactions.

RX1 was modelled by replacing the fluorogenic cargo with a methyl group, while methyl thiol and selenol were chosen as chalcogenols. The other amide substituent was modelled as a simple methyl function. (Scheme 4.4) Additionally, to provide a more simplified picture to be compared with the results in 4.3.1, the blue structure in Scheme 4.4 was replaced by –H for some reactions. (RX1-H). In all cases, the SAPE approach described in Paragraph 4.3.1 (two water molecules) was employed.
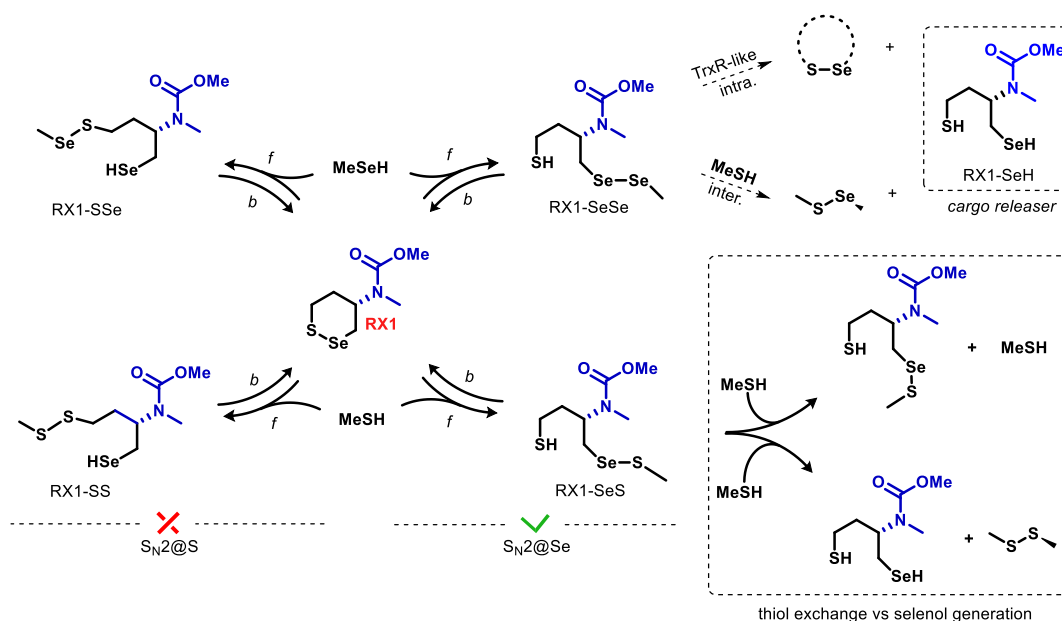
Scheme 4.4 Representation of RX1 chemistry as modelled in this study. All processes were mediated by two water molecules (not represented). *f* stands for forward and *b* for backward processes. The blue part was replaced by H in RX1-H.

Table 4.2 Activation energy and reaction energy (kcal mol^{-1}) for the forward ($\Delta G_F^{\ddagger}$) and backward ($\Delta G_B^{\ddagger}$) nucleophilic attack of methyl thiol (SH) and selenol (SeH) to RX1 and the simplified cyclic selenyl sulfide (RX1-H).

		$S_N2@S$		$S_N2@Se$	
		SH	SeH	SH	SeH
	$\Delta G_F^{\ddagger}$	38.82	35.15	34.50	31.07
RX1	$\Delta G_B^{\ddagger}$	26.66	27.32	26.80	27.16
	ΔG_r	12.16	7.83	7.70[a]	3.91[a]
	$\Delta G_F^{\ddagger}$	39.05	34.00	33.62	28.94
RX1-H	$\Delta G_B^{\ddagger}$	27.11	26.28	26.42	26.76
	ΔG_r	11.94	7.72	7.20	2.18

[a]The ΔG_r of the process is computed with the product in a reactant-like conformation, i.e., it is optimized in the structure in which it falls immediately after the transition state. For SH and SeH reaction @Se, since the adduct undergoes further evolution, a conformational search has been conducted (see computational methods). The absolute minima identified are 3.84 kcal mol^{-1} and 5.10 kcal mol^{-1} more stable for SH and SeH respectively. Thus, the reaction of RX1 with thiols remains endergonic, while the correspondent reaction with selenols appears to be weakly exergonic, with an overall ΔG_r of 3.86 and of -1.18 kcal mol^{-1} respectively. The overall discussion does not change.

All results for the first chalcogenol attack at RX1 are presented in Table 4.2. Very small qualitative differences can be seen between RX1 reactivity and RX1-H, suggesting that the carbamate function does not dramatically perturb the Se–S bond reactivity. Most of the conclusions drawn in Paragraph 4.3.1 apply also to RX1 and RX1-H reactivity, that is, as expected, SeH behaves as a better nucleophile, leading to S_N2@S and @Se which are between 3.5 and 5 kcal mol^{-1} more favored from the kinetic point of view than the correspondent reaction with the lighter SH. Thus, selenoproteins can be reasonably considered the preferential intrinsic target of RX1. (**Evidence in favor of Point 1**)

Moreover, thanks to the increased electrophilicity of Se as central atom, S_N2@Se occurs with a systematically lower activation energy (ca. 4–5 kcal mol^{-1}). Thus, the first S_N2 process which RX1 will undergo in the biological environment likely occurs at Se rather than at S nucleus. (**Evidence in favor of Point 2**) This implies that the whole leftmost part of Scheme 4.4 will be disfavored, and nor RX1-SSe or RX1-SS are expected to be produced: thus, our model rules in favor of the hypothesis that direct cargo release is prevented by Se electrophilicity, which pushes the reactivity towards the rightmost part of Scheme 4.4. The combination of the SeH nucleophilicity and Se electrophilicity as central atom results in a difference in activation energy between the desired interaction of RX1 with selenoproteins at the Se nucleus and the undesired interaction of RX1 with monothiols at the S nucleus of about 8 kcal mol^{-1}, at the current level of theory. Similarly, RX1-SeSe is thermodynamically favored by ca. 8 kcal mol^{-1} over the undesired RX1-SS. (Scheme 4.4 and Table 4.2)

All reactions are thermodynamically less favored with respect to the analogous ones in in Paragraph 4.3.1, due to the entropic penalty associated to the formation of an addition product. The most endergonic reaction, leading to RX1-SS, has a ΔG_r well above 10 kcal mol^{-1} in our model. This reaction corresponds to the undesired thiol S_N2@S reaction, which would lead to non-specific cargo release due to immediate selenol generation on RX1. Since the reaction is highly unfavored thermodynamically, the backward reaction is obviously way more favored kinetically. Indeed, it occurs with a $\Delta G_B^{\ddagger}$ of ca. 27 kcal mol^{-1}, thanks to the combined nucleophilicity of the selenol (which is released in the forward step and is free to react in RX1-SS), and to its nature of intramolecular reaction, which makes the

overall process more favored than the correspondent one for the model system (see Table 4.1, entry 2).

The process is close to thermoneutrality also for the desired attack of the selenol to the Se nucleus of RX1; however, the combined effect of SeH nucleophilicity and Se electrophilicity in the Se–S bond makes the process the most favored among the four possibilities (Table 4.1). Moreover, when TrxR binds to RX1 Se atom, a second thiol attack is expected to occur intramolecularly on the Se of the first selenol bound to RX1. While this step was not explicitly investigated for TrxR, it corresponds to an intramolecular attack of a thiol to a Se central atom. Thus, it is expected to occur with an activation energy comparable to the other $\Delta G_B^{\ddagger}$. This process leads to the release of the selenol moiety of RX1, which can lastly release the cargo. To provide at least an estimate of the energetics of the process, this intramolecular step was modelled using a 1-thiol 4-selenol butane model system, already bonded (and pre-organized) to RX1 with a diselenide moiety. (Figure 4.3)
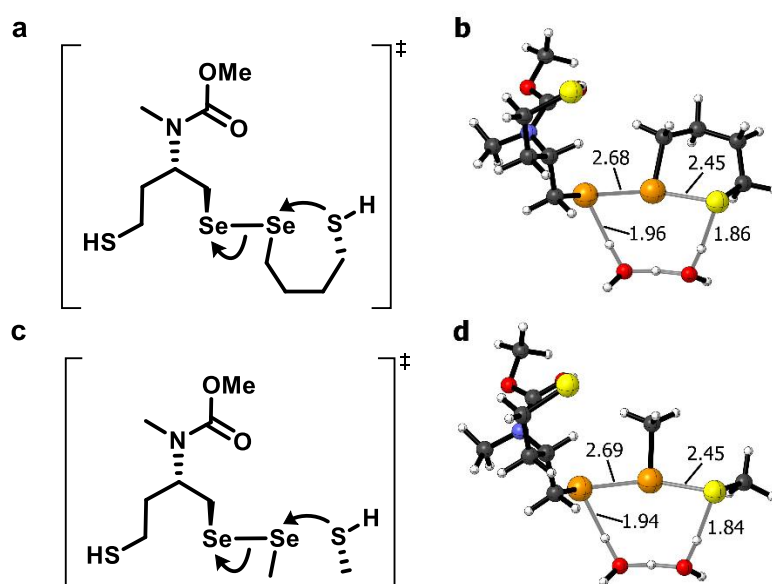
Figure 4.3 (a) Schematic representation of the transition state of the intramolecular, TrxR-like step leading to selenol generation and (**c**) correspondent intermolecular process (water molecules are excluded for clarity). (**b**) Optimized transition state for the TrxR-like process with explicit water molecules mediating the proton transfer from the thiol to the selenol moiety. (**d**) Correspondent optimized transition state for the intermolecular process. The TSs are oriented for optimal visualization.

As envisioned, the step occurs with an activation energy of 27.66 kcal mol^{-1}, similarly to the backward processes. Even if the diselenide bond breaking is the least thermodynamically favored process (Table 4.1), the intramolecular nature of the

reaction makes this step thermodynamically favored, occurring with a ΔG_r of -3.18 kcal mol^{-1}. (**Evidence in favor Point 4**) It should be mentioned that this ΔG_r must be considered with particular caution, because a six-membered ring is formed in our model reaction: the situation will clearly be different in TrxR, where if the two consecutive Cys and Sec residues interact with RX1, an eight-membered ring is formed, whose structure and stability can be expected to be influenced by the protein backbone constraints. Indeed, the formation of this cyclic intermediate is an integral part of the canonical catalytic mechanism of TrxR. Thus, the same reaction in TrxR might be even more favored than in the simplified model. Nevertheless, our results provide at least a qualitative insight into the productive selenol generation step of RX1 mechanism through intramolecular ring closure.

By comparison, the corresponding intermolecular process (Scheme 4.4, RX1-SeSe evolution with MeSH and Figure 4.3c,d) occurs with a higher activation energy (35.00 kcal mol^{-1}) and is thermodynamically unfavored (ΔG_r of 5.24), due to the resistance of the Se–Se bond against bond breaking by thiols, in line with the discussion presented in Paragraph 4.3.1. Thus, while for TrxR RX1-SeH generation benefits from the favor of intramolecular ring closure (in the enzyme), the same process in selenoproteins lacking a Cys close to the Sec residue occurs in line with the data of Table 4.1. and is, indeed, unfavored.

Table 4.3 Activation and reaction energies (kcal mol^{-1}) for thiol exchange ($S_N2@Se$) and selenol generation ($S_N2@S$) occurring to the product of the thiol addition to RX1 and to the simplified cyclic selenyl sulfide (RX1-H).

		Selenol generation	Thiol exchange
RX1	$\Delta G^{\ddagger}$	40.28	34.46
	ΔG_r	4.23	0.02
RX1-H	$\Delta G^{\ddagger}$	41.19	34.35
	ΔG_r	4.32	0.45

Most importantly, selenol generation cannot occur with monothiols, since for this step to be productive, a second thiol equivalent should attack the S end of the selenyl sulfide ($S_N2@S$) produced by addition of one thiol to RX1. Not only this step has an activation energy roughly 13 kcal mol^{-1} higher than the intramolecular diselenide bond breaking, but the competitive thiol exchange reaction ($S_N2@Se$) is

kinetically more favored by roughly 6 kcal mol^{-1}, and it is 4 kcal mol^{-1} more favored from the thermodynamic point of view. (Table 4.3) Thus, if any RX1-SeS is produced, thiol exchange reactions can act as a protective mechanism, preventing the selenol generation (and thus, the unspecific cargo release) in the thiol rich biological environment. (**Evidence in favor of Point 3**) Nevertheless, because RX1-SeS formation is endergonic, the backward process occurring at RX1-SeS is kinetically and thermodynamically favored over the thiol exchange process. Both are S$_N$2@Se processes, with SH as nucleophile, but while the former occurs intramolecularly, the latter is an intermolecular step. Thus, the restoration of the closed-ring form of RX1 is in our model a more effective protective mechanism than thiol exchange reactions, thanks to the endergonicity of RX1-SeS formation which drags the reaction back to the cyclic selenyl sulfide, RX1.

A final important aspect to be stressed is that, even if some RX1-SeS were indeed produced (e.g., due to high enough thiol concentration), and thus some RX1 reached TrxR as the open-ring RX1-SeS, TrxR selenol attack at the Se nucleus to form the diselenide RX1-SeSe would result in thiol freeing. While this specific step was not modelled, the process would not be entropically penalized anymore (as compared to RX1-SeSe formation from RX1 directly) and should occur with similar energetics to reaction 6 in Table 4.1, which is indeed thermodynamically favored, suggesting that even if some RX1-SeS is produced, it can remain active in targeting TrxR.

4.4 Conclusions

In this Chapter, a systematic perspective is offered over nucleophilic substitution at sulfur and selenium atoms. Firstly, eight model reactions are investigated, taking into account all possible substitutions in which both sulfur and selenium participates either as nucleophile, central electrophilic atom, or leaving group. Our results agree well with previous computational studies, performed considering the fully deprotonated thiolate and selenolate as nucleophiles. Additionally, the results match to the experimental conclusions by Koppenol and coworkers: selenols are better nucleophiles than thiols, the selenium end of selenyl sulfides is a better electrophilic

center for the reaction to occur, but from the kinetic point of view both the selenols and the thiols perform similarly as leaving groups.

Additionally, the energetics of these reactions have been used as reference point for the investigation of the more complex biological reactivity of RX1, a selenyl sulfide selective probe for the enzyme TrxR1. All reactive steps of RX1 with thiols and selenols comply well with the systematic investigation performed on model systems, with the additional variant in reactivity due to the occurrence of both intramolecular (favored) and intermolecular (disfavored) paths of the forementioned reactions. All key reactive steps of RX1 with thiols and selenols, which lead to the release of the fully reduced RX1-SeH species have been modelled and compared, providing a quantitative theoretical rationale to the design principles of Zeisel *et al* and obtaining, *inter alia*, a representative picture of RX1 chemistry in the thiol rich biological environment.

Importantly, we can conclude that the main protective mechanism of RX1 against monothiol non-selective cargo release is the backward $S_N2@Se$, which restores the ground state, closed-ring, RX1 scaffold. Even if some RX1 were opened non-selectively, intermolecular thiol exchanges at the Se nucleus are predicted to be effective in protecting the system against selenol generation. In this latter case, indeed, direct cargo release is additionally prevented by Se electrophilicity, which traps the Se nucleus in a selenylsulfide bond. The RX1 scaffold can be lastly transferred to TrxR1 by the selenol $S_N2@Se$ reaction. This pathway, leading in the end to selenol freeing, is indeed the most favored explored in this study, in agreement with RX1 performances in targeting TrxR1.

The same mechanistic analysis has been conducted to other selenylsulfides, based on structurally modified versions of RX1 proposed by Zeisel and coworkers, to obtain insight into the performances of other plausible TrxR probes.

References

[1]   J. C. Pleasants, W. Guo, D. L. Rabenstein, *J. Am. Chem. Soc.* **1989**, *111*, 6553–6558.

[2]   D. Steinmann, T. Nauser, W. H. Koppenol, *J. Org. Chem.* **2010**, *75*, 6696–6699.

[3]   R. Singh, L. Kats, *Anal. Biochem.* **1995**, *232*, 86–91.

[4]   S. M. Bachrach, D. W. Demoin, M. Luk, J. V. Miller, *J. Phys. Chem. A* **2004**, *108*, 4040–4046.

[5]   S. M. Bachrach, C. J. Walker, F. Lee, S. Royce, *J. Org. Chem.* **2007**, *72*, 5174–5182.

[6]   J. M. Hayes, S. M. Bachrach, *J. Phys. Chem. A* **2003**, *107*, 7952–7961.

[7]   M. Bortoli, L. P. Wolters, L. Orian, F. M. Bickelhaupt, *J. Chem. Theory Comput.* **2016**, *12*, 2752–2761.

[8]   T. A. Hamlin, M. Swart, F. M. Bickelhaupt, *ChemPhysChem* **2018**, *19*, 1315–1330.

[9]   L. Zeisel, J. G. Felber, K. C. Scholzen, L. Poczka, D. Cheff, M. S. Maier, Q. Cheng, M. Shen, M. D. Hall, E. S. J. Arnér, J. Thorn-Seshold, O. Thorn-Seshold, *Chem* **2022**, *8*, 1493–1517.

[10]   **N.d.**

[11]   G. te Velde, F. M. Bickelhaupt, E. J. Baerends, C. Fonseca Guerra, S. J. A. van Gisbergen, J. G. Snijders, T. Ziegler, *J. Comput. Chem.* **2001**, *22*, 931–967.

[12]   N. C. Handy, A. J. Cohen, *Mol. Phys.* **2001**, *99*, 403–412.

[13]   C. Lee, W. Yang, R. G. Parr, *Phys. Rev. B* **1988**, *37*, 785–789.

[14]   E. Van Lenthe, E. J. Baerends, J. G. Snijders, *J. Chem. Phys.* **1994**, *101*, 9783–9792.

[15]   F. Zaccaria, L. P. Wolters, C. Fonseca Guerra, L. Orian, *J. Comput. Chem.* **2016**, *37*, 1672–1680.

[16]   M. Bortoli, F. Zaccaria, M. D. Tiezza, M. Bruschi, C. F. Guerra, F. Matthias Bickelhaupt, L. Orian, *Phys. Chem. Chem. Phys.* **2018**, *20*, 20874–20885.

[17]   S. Grimme, J. Antony, T. Schwabe, C. Mück-Lichtenfeld, *Org. Biomol. Chem.* **2007**, *5*, 741–758.

[18]   S. Grimme, *Wiley Interdiscip. Rev. Comput. Mol. Sci.* **2011**, *1*, 211–228.

[19]   A. D. Becke, E. R. Johnson, *J. Chem. Phys.* **2005**, *123*, 154101.

[20]   E. R. Johnson, I. D. Mackie, G. A. DiLabio, *J. Phys. Org. Chem.* **2009**, *22*, 1127–1135.

[21]   L. Deng, T. Ziegler, *Int. J. Quantum Chem.* **1994**, *52*, 731–765.

[22]   A. Klamt, G. Schüürmann, *J. Chem. Soc. Perkin Trans. 2* **1993**, 799–805.

[23]   C. C. Pye, T. Ziegler, *Theor. Chem. Acc.* **1999**, *101*, 396–408.

[24]   S. Grimme, C. Bannwarth, P. Shushkov, *J. Chem. Theory Comput.* **2017**, *13*, 1989–2009.

[25]   P. Pracht, F. Bohle, S. Grimme, *Phys. Chem. Chem. Phys.* **2020**, *22*, 7169–7192.

[26]   R. E. Huber, R. S. Criddle, *Arch. Biochem. Biophys.* **1967**, *122*, 164–173.

[27]   C. A. Bayse, K. N. Ortwine, *Eur. J. Inorg. Chem.* **2013**, 3680–3688.

[28]   S. Antony, C. A. Bayse, *Inorg. Chem.* **2011**, *50*, 12075–12084.

[29]   C. A. Bayse, *J. Phys. Chem. A* **2007**, *111*, 9070–9075.

[30]   L. Sancineto, F. Mangiavacchi, A. Dabrowska, A. Pacuła, M. Obieziurska-Fabisiak, C. Scimmi, Y. Lei, J. Kong, Y. Zhao, K. dos Santos Machado, A. V. Werhli, G. Ciancaleoni, V. Nascimento, A. Kula-Pacurar, E. J. Lenardao, H. Yang, J. Ścianowski, K. Pyrc, C. Santi, *ChemRxiv* **2020**, DOI 10.26434/chemrxiv.12994250.v1.

[31]   H. J. Reich, R. J. Hondal, *ACS Chem. Biol.* **2016**, *11*, 821–841.

[32]   R. J. Hondal, E. L. Ruggles, *Amino Acids* **2011**, *41*, 73–89.

5 The Oxidative Step of Glutathione Peroxidase with Peroxynitrite

5.1 Introduction

The glutathione peroxidase (GPx) family of enzymes is one of the main groups of endogenous antioxidants. They exert their defensive action by reducing hydroperoxides to water or alcohols. (see Chapter 1) In the oxidative step of the catalytic mechanism, i.e., the actual peroxide reduction, GPxs are currently believed to break the peroxide bond by means of a stepwise process, in which firstly an unstable charge-separated intermediate is formed by proton shuttling from the catalytic Sec (or Cys, for CysGPxs) to a conserved residue of the catalytic pocket which can act as a labile proton acceptor, e.g. tryptophane. Secondly, the deprotonated selenolate (or thiolate) nucleophilically attacks one end of the peroxide bond, while a back-proton transfer from the protonated Trp leads to an electrophilic attack to the dislocated proton by the second oxygen of the peroxide bond.[1–4] (Scheme 5.1)
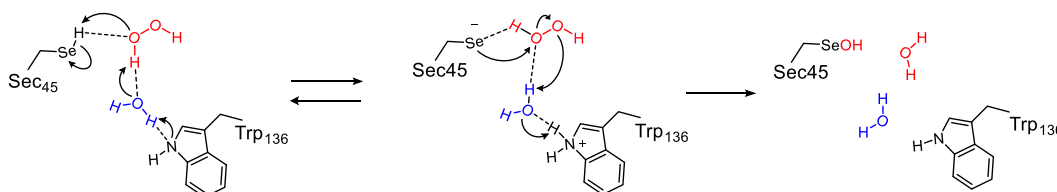
Scheme 5.1 Stepwise peroxide bond breaking as it is predicted to occur in GPx4.

This mechanism was proposed to account for the fast reactivity of SecGPxs in hydroperoxide reduction, which occurs 10^6 times faster than a fully deprotonated Sec. For this reason, the mere deprotonation of Sec to enhance its nucleophilicity does not suffice to explain GPxs reactivity with hydroperoxides.[5]

While the catalytic mechanism of GPxs with H_2O_2 is well understood, the way in which these enzymes deal with the peroxynitrite ($ONOO^-$) oxidant and its conjugate peroxynitrous acid (HOONO) remains elusive. Peroxynitrite is a strong oxidant and nitrant agent which is formed under biological conditions from the reaction of the nitroxide radical ($NO^{\bullet}$) with the superoxide anion ($O_2^{\bullet-}$).[6,7] The reaction between $O_2^{\bullet-}$ and $NO^{\bullet}$ is so fast to occur even in the presence of superoxide dismutase, i.e., the enzyme responsible for the conversion of $O_2^{\bullet-}$ to H_2O_2 and O_2.[6,8] Even if the product of the reaction is the peroxynitrite anion, $ONOO^-$, its pKa of 6.8 implies that, at biologically accessible values of pH, this oxidant is present as a mixture of peroxynitrite and peroxynitrous acid, with the predominant form depending on the local pH. Under most biological conditions, both species will be present in some percentage.[8]

Both oxidation[9] and nitration[10,11] reactions promoted by peroxynitrite can lead to cytotoxic effect, due to its capacity to modify biomolecules such as lipids, amino and nucleic acids.[6,12–15] Importantly, before the 90s, no enzymatic protection against peroxynitrite damage was recognized.[16] Only in that decade, after the discovery that the GPx-mimics ebselen (see Chapter 1) can act as a peroxynitrite scavenger,[17–19] the same "peroxynitrite reductase" activity was proposed and investigated for GPx.[20] Particularly, Sies and coworkers observed that both GPx1[20] and selenoprotein P can be implicated in the defense against peroxynitrite.[21] However, in the same period, it was also observed that GPx is inhibited by the presence of peroxynitrite in the absence of glutathione.[22–24] These results suggest that, in the reduction of peroxynitrite, a different oxidized enzymatic intermediate might be formed, i.e., different from the canonical selenenic acid (E-SeOH)[22] (Scheme 5.1), or the protective selenyl amide formed by intramolecular condensation of selenenic acid when the enzyme deals with other hydroperoxides.[4] (see Chapter 1). Indeed, these two species can be reintegrated in the canonical catalytic mechanism in the presence of glutathione, and thus does not explain GPx inactivation.[22] Additionally, at the beginning of the 2000s, Fu and

coworkers[25] observed that neither GPx1 knockout hepatocyte nor wild type cells were sensible to peroxynitrite induced apoptosis, thus proposing that GPx1 is not required by hepatocytes to cope with the peroxynitrite oxidant. In the same year, Sies and coworkers[26] observed that, even more strikingly, GPx1 knockout hepatocyte can be more resistant against peroxynitrite induced damage than wild type cells, suggesting an apoptosis inducing role of GPx in the presence of the peroxynitrite oxidant. To the best of our knowledge, a complete understanding of the topic is still to be reached, and this behavior of GPx1 (as well as similar behaviors of other antioxidant enzymes) has been reviewed as paradoxical.[27]

The potential energy surface (PES) of the catalytic mechanism of GPx as a peroxynitrite reductase has been previously investigated *in silico* by Morokuma and coworkers, employing a simplified cluster encompassing three out of the four essential amino acids which compose the enzyme catalytic tetrad.[1][28,29] In their investigation, the PES was studied by comparing two possible alternative mechanisms, i.e., one in which the peroxynitrite oxidizes GPx Sec to the canonical selenenic acid, and a second one in which the peroxynitrite acts as a nitrating agent, leading to a nitrated Sec intermediate.[28] However, in their study, the oxidation to selenenic acid was found to be preferred, thus leaving the problem of a plausible inactive intermediate open. .

While the reaction of thiols has been variously explored in the past years, far less investigations has been done with selenols.[16] Particularly, peroxynitrite is known to be able to oxidize thiols to disulfide,[16,30] with sulfenic acid as a plausible intermediate also in proteins,[16,30,31] in analogy to thiol chemistry with hydroperoxides. Importantly, even if peroxynitrous acid is relatively unstable in biological conditions, and without other targets to react with it undergoes a spontaneous degradation,[32] its reaction with thiols to produce sulfenic acid has been characterized to be faster than its degradation.[33,34] Additionally, peroxynitrite is known to be capable of nitrating thiols, leading to nitrothiols such as nitroglutathione (GS-NO$_2$),[35] or of nitrosylate thiols, leading to nitrosothiols such as nitrosoglutathione (GS-NO).[36] Particularly, the formation of radical species

---

[1] At the time of Morokuma *et al* investigation, the catalytic site of glutathione peroxidases was identified with a catalytic triad (Selenocysteine, Glutamine and Tryptophan) Only two years later, the importance of one additional residue, i.e., asparagine, was discovered.

seems to be excluded in the nitrosylation reaction[22,36] and a direct nucleophilic substitution mechanism was proposed. The best of our knowledge, no nitrosylation of Sec by peroxynitrite has ever been reported, and only very recently the nitrososelenocysteine (Sec-SeNO) species was isolated in a molecular cradle, thus opening the possibility to study its chemistry.[37]

In this Chapter, the reactivity of GPx with the peroxynitrite and peroxynitrous acid was investigated, focusing on the comparison between a possible oxidation pathway and a possible nitrosylation pathway. The nitration pathway, which was found less likely in the past by Morokuma and coworkers, was not investigated any further.

5.2 Computational Methods

All DFT calculations were done with Gaussian 16 program. For consistency with Chapter 3, and with previous literature on the topic[2,3] no changes to the level of theory were made. The details can be found in Chapter 1, Paragraph 1.2.

5.3 Results and discussion

The reactivity of ONOO⁻ and ONOOH with GPx was studied employing an active site cluster taken from a previous work by Bortoli *et al* based on molecular dynamics (MD) simulations of the selenoprotein GPx4[3], that comprises all conserved amino acids which are known to affect GPx catalysis, i.e. the catalytic tetrad: Sec46, Gln81, Trp136 and Asn137. In addition, also Phe138 and Gly47 are included in this model, and an extra Gly residue is used to mimic the peptide bond linking Gly47 to the down-stream residues (numeration refers to cytosolic rat GPx4).[4] The same set of amino acid was successfully used also in a previous work[4] to tackle GPx catalysis with H_2O_2 as substrate and is considered representative of all SecGPxs.[4] One water molecule is included in the calculations, since it is well-recognized to play a crucial role in GPx catalysis[3,4,38,39]. To investigate the interaction between GPx and peroxynitrite, four possible cases were investigated. Initially, the enzyme cluster was considered in its fully neutral form, i.e., with a protonated Sec selenol, and a

neutral Trp indole moiety. Secondly, we focused on the reactivity of the zwitterionic cluster, which shows a deprotonated Sec selenolate and a protonated indolium moiety on Trp. In both cases, the reactivities of ONOO⁻ and ONOOH were studied.

Two different hypotheses were considered: (i) GPx can follow the canonical oxidation mechanism, being oxidized by ONOO⁻/ONOOH to selenenic acid. This mechanism is well-documented and supported both experimentally and computationally for H_2O_2.[3,4,40] Alternatively, (ii) Sec can undergo a nitrosylation mechanism, resulting in the formation of the recently isolated Sec-SeNO species.[37] While this reaction has never been studied for Sec, there are experimental evidences that ONOO⁻/ONOOH can react with Cys residues leading to Cys-SNO, with the side-production of H_2O_2.[36,41] Thus, we wondered whether Sec might undergo a similar reaction, which would lead GPx to produce H_2O_2 as byproduct.

Firstly, the results obtained for the *neutral cluster* (points A, B and C) will be discussed. Then, the results starting directly from the zwitterionic active site will be commented (D and E). In all mechanistic schemes, only Sec and Trp will be shown since they directly take part in the reactions. All the other residues were included in the calculations but, for simplicity, they will not be represented.

(A)   Oxidation mechanism of Sec-GPx by ONOO⁻. (Scheme 5.2) Starting from the cluster above described, a ONOO⁻ unit was added instead of the canonical H_2O_2 substrate within the active site, postulating that the same binding site can interact with both H_2O_2 and ONOO⁻/ONOOH. A stable adduct was not localized on the potential energy surface (PES), because the anion is immediately deprotonated upon reaction with Sec-SeH. The stable adduct is thus between Sec-Se⁻ and ONOOH, as previously reported in a seminal computational study by Prabhakar *et al.*[28] This was expected, since Sec is a stronger acid than ONOOH. Then, the oxidation of Sec-Se⁻ was investigated as the direct nucleophilic attack of the Se atom to ONOOH, leading to O–O bond breaking and Se–OH bond formation, with the cleavage of NO_2^- from the substrate. This reaction proceeds via a low-energy transition state, located only 3.76 kcal mol⁻¹ above the initial adduct, and is strongly exergonic, leading to products which are 52.10 kcal mol⁻¹ more stable than the initial adduct.
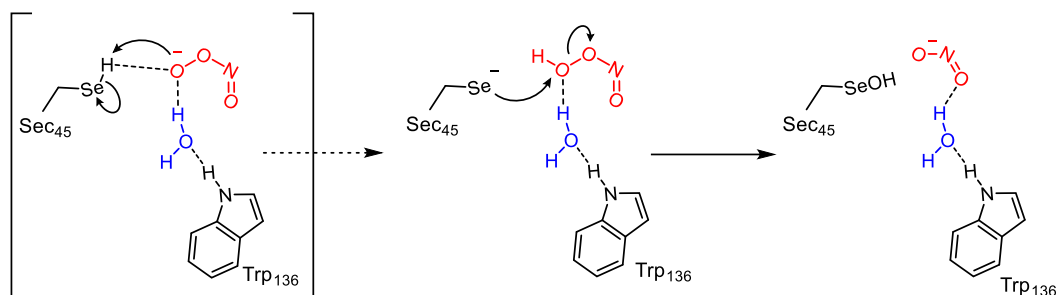
Scheme 5.2 Oxidation mechanism of Sec-GPx by ONOO$^-$. The first adduct shown in parentheses could not be optimized on the PES since the structure spontaneously evolves towards Sec-Se$^-$ and ONOOH.

(B)   *Oxidation mechanism of Sec-GPx by ONOOH.* (Scheme 5.3) Differently from (A), a stable adduct between the GPx cluster and ONOOH was optimized. Within this cluster, a suitable network of hydrogen bonds connects the selenol, ONOOH and the Trp-NH involving the water molecule. Thus, a proton-transfer–S_N2 mechanism close to the canonical one described for the peroxide reduction by GPx can be envisioned. (Scheme 5.1) Indeed, the selenol can shuttle its proton to the indole moiety of Trp via ONOOH and H_2O, with a rather modest activation energy of 16.29 kcal mol^{-1} and this leads to a destabilized zwitterionic catalytic pocket (12.65 kcal mol^{-1}). Since the proton is shuttled to a highly energetic indolium moiety, an almost barrierless back proton transfer from Trp to ONOOH with a concerted nucleophilic attack of Se to ONOOH can be envisioned, in close analogy to the dual-attack on the peroxide bond described for GPx[1,3] and other enzymes[2] working via a fast-reacting cysteine. However, a transition state for such process was not found. By analogy to GPx canonical catalysis, such process occurs with a negligible activation energy, as supported also by recent computational analyses on model molecular systems.[1] Anyway, the process is driven by the strong exergonicity of the process, which leads to a product which is 58.98 kcal mol^{-1} more stable than the initial adduct. This energetics is even more favorable than the one previously described by Prabhakar *et al*, likely because their cluster is smaller and much more simplified than ours (e.g., no amino acids backbone were included in the calculations).[28] Importantly, in their study, after the formation of the charge separated intermediate the system decays leading to the cleavage of the O–O bond with an activation energy lower than 2 kcal mol^{-1}. Thus, while in their case an appreciable activation energy was computed for the formation of selenenic acid,

both studies agree that the actual O–O bond cleavage occurs with a very low non-appreciable activation energy.
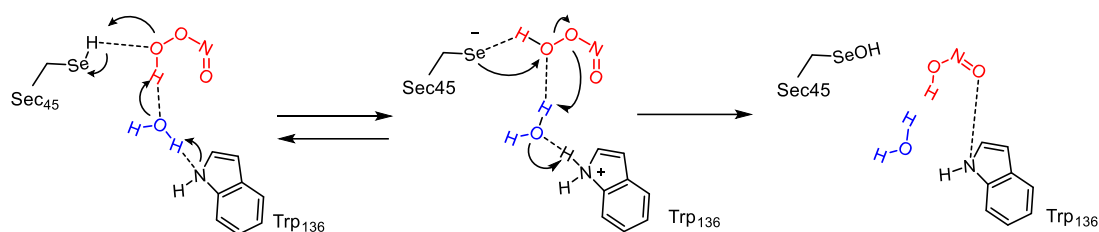
Scheme 5.3 Oxidation mechanism of Sec-GPx by ONOOH leading to selenenic acid and nitrous acid.

(C) *Nitrosylation mechanism of Sec-GPx by ONOOH.* (Scheme 5.4) Alternatively to what discussed in mechanism (B), we verified if, starting from a (slightly different) adduct between GPx and ONOOH, a nitrosylation mechanism might be feasible. In this adduct, the selenol, the water molecule and ONOOH are bridged together via hydrogen bonds, with Trp participating to a hydrogen bond with ONOOH. In a concerted mechanism, characterized by the proton transfer from Sec to ONOOH and by the nucleophilic attack of Se to the N atom of ONOOH, the peroxynitrous acid O–N bond can be cleaved with a modest activation energy of 12.12 kcal mol^{-1}. While Trp is not directly involved in the reaction, it remains coordinated to ONOOH. The cleavage of the N–O bond is overall exergonic by 17.12 kcal mol^{-1}. Thus, the reaction appears to be thermodynamically favored, even if it is significantly less favored than the oxidation.
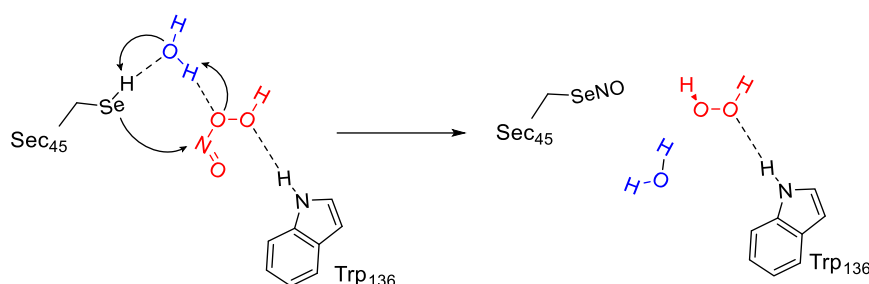
Scheme 5.4 Nitrosylation mechanism of Sec-GPx by ONOOH leading to Sec-SeNO and hydrogen peroxide.

(D) *Nitrosylation mechanism of Sec-GPx with ONOOH (zwitterionic cluster).* (Scheme 5.5) Alkylation kinetics and pK calculations indicate that GPxs always behaves as if being fully dissociated.[29,42,43] Thus, instead of starting from

the neutral, ground state, cluster, we tried to investigate also the reactivities of ONOO⁻/ONOOH as if the zwitterionic state found in mechanism (B) were the ground state enzyme. Quite interestingly, starting from the zwitterion from mechanism (B) and just rotating the hydroxy group of the peroxynitrous acid away from the selenolate, no stable adduct could be optimized. In contrast, the system spontaneously evolved towards the nitrosylated product. This result suggests that the peroxynitrous acid will nitrosylate GPx releasing H_2O_2 as soon as it reaches the zwitterionic active site. Since no initial reactant (adduct) was found, no precise description of the thermodynamics can be provided. Nevertheless, since the charge-separated state is roughly 12 kcal mol^{-1} destabilized with respect to the neutral cluster, by combining the data obtained in point (B) with those obtained in point (C), we can estimate this step to be exergonic by ca. 30 kcal mol^{-1}.
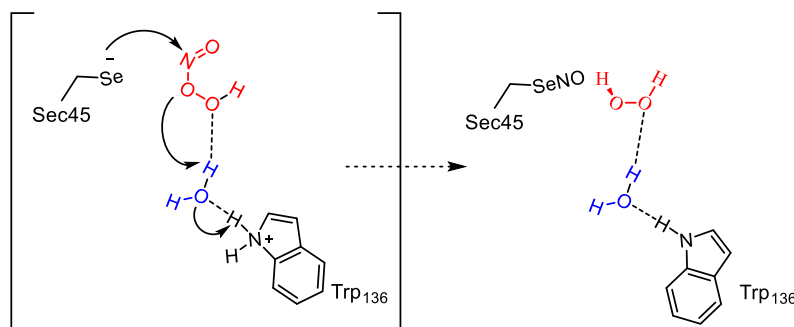
Scheme 5.5 Nitrosylation mechanism of zwitterionic Sec-GPx by ONOOH leading to Sec-SeNO and hydrogen peroxide. The first adduct represented between parentheses could not be optimized since the structure spontaneously evolve towards the nitrosylated product.

Most importantly, this result suggests that the nitrosylation may occur without any appreciable activation energy once the charge-separated intermediate is formed, similarly to what discussed in point (A) for the formation of selenenic acid. The two pathways might, thus, be competitive, depending on the orientation by which GPx and ONOOH interact. In any case, the formation of selenenic acid remains strongly favored from the thermodynamic point of view.

(E) *Nitrosylation mechanism of Sec-GPx with ONOO⁻ (zwitterionic cluster).* In analogy to what has been described in (D), starting from the zwitterionic cluster, we tried to optimize an adduct with ONOO⁻. Similarly to what previously described, the peroxynitrite anion is spontaneously protonated again, in this case taking back the proton from the indolium cation of Trp. This pathway is not

unexpected, since the proton on Trp is a high-energy situation and ONOO⁻ is a relatively weak base. Thus, aside from the arrangement of ONOOH within the active site, this situation is the same encountered in (A), with an active site consisting of ONOOH, the selenolate and the neutral Trp. As a consequence, the nitrosylation pathway (E) is an alternative to the oxidation to selenenic acid described in (A). However, in gas phase, all attempts to optimize a nitrosylated product, with the cleavage of HOO⁻ from the substrate failed. HOO⁻ seems to immediately attack the nitrogen atom of Sec-SeNO, leading back to the initial adduct. Further attempts to stabilize the nitrosylated product directly in condensed phase led to a structure which is 14.23 kcal mol⁻¹ less stable than the initial adduct, further suggesting that the reaction either cannot proceed or is strongly thermodynamically unfavored. This effect does not come completely unexpected, since the reaction releases HOO⁻ as a product, which is a powerful nucleophile.[44,45] Additionally, since H_2O_2 has a pKa of roughly 11.6, the HOO⁻ will be rapidly protonated essentially at any biological pH.[6,36] Since, in our model, no free water molecule except the catalytic one was included, the complete solvation and acid-base chemistry of HOO⁻ cannot be described. Even with these limitations, these results at least suggest that step (E) is intrinsically disfavored as compared to the other proposals.

5.4 Conclusions

In this Chapter, a perspective is offered over the possible reactivity of GPx with the peroxynitrite/peroxynitrous acid oxidant. By means of a cluster approach, including all the residues known to affect the catalysis of GPx, five different pathways were investigated to obtain insight into the possibly competitive oxidation of GPx Sec to selenenic acid Sec-SeOH or to nitrososelenocysteine Sec-SeNO. When GPx interacts with HOONO, we found that both outcomes are thermodynamically well-favored (by more than 15 kcal mol⁻¹). However, the formation of selenenic acid is favored by more than 40 kcal mol⁻¹ over the nitrosylation product.

The reactivity with the peroxynitrite anion is less clear. However, in this case, while the oxidation to selenenic acid remains strongly favored thermodynamically and can proceed with a low activation energy, the nitrosylation becomes strongly disfavored thermodynamically. In this case, explicit interactions with water

molecules might help stabilizing it, thus preventing the back attack of the hydroperoxide anion to the nitrosyl function. Additionally, while a low activation energy is computed for the oxidative pathway, in this step only Sec interacts with the oxidant, with the other residues acting more like spectators in the reaction. Thus, this step does not benefit from the double-attack mechanism responsible for the high efficiency of GPx catalysis, and is likely to occur with a chemistry more similar to that of a free Sec.

Unluckily, these results do not constitute a univocal picture over the chemistry of GPx with peroxynitrite. Nevertheless, given the paradoxical results experimentally obtained, this outcome was somewhat expected. In any case, they provide theoretical support to the possible formation of intermediates differing from the canonical selenenic acid and they prompt for further experimental investigations which, when combined with theoretical studies, can lead to a more representative description of the chemistry of GPx with the complex peroxynitrite oxidant. Enzymological studies as well as a mass-spectrometric investigation on the topic are currently being conducted by colleagues, with the hope of identifying the product(s) of the interaction between GPx and the peroxynitrite oxidant, and thus understanding its further evolution in biologically relevant conditions.

References

[1]   M. Dalla Tiezza, F. M. Bickelhaupt, L. Flohé, L. Orian, *Chempluschem* **2021**, *86*, 525–532.

[2]   M. Dalla Tiezza, F. M. Bickelhaupt, L. Flohé, M. Maiorino, F. Ursini, L. Orian, *Redox Biol.* **2020**, *34*, 101540.

[3]   M. Bortoli, M. Torsello, F. M. Bickelhaupt, L. Orian, *ChemPhysChem* **2017**, *18*, 2990–2998.

[4]   L. Orian, P. Mauri, A. Roveri, S. Toppo, L. Benazzi, V. Bosello-Travain, A. De Palma, M. Maiorino, G. Miotto, M. Zaccarin, A. Polimeno, L. Flohé, F. Ursini, *Free Radic. Biol. Med.* **2015**, *87*, 1–14.

[5]   L. Flohé, S. Toppo, L. Orian, *Free Radic. Biol. Med.* **2022**, *187*, 113–122.

[6]   R. Radi, *J. Biol. Chem.* **2013**, *288*, 26464–26472.

[7]   N. V. Blough, O. C. Zafiriou, *Inorg. Chem.* **1985**, *24*, 3502–3504.

[8]   G. Ferrer-Sueta, R. Radi, *ACS Chem. Biol.* **2009**, *4*, 161–177.

[9]   M. Exner, S. Herold, *Chem. Res. Toxicol.* **2000**, *13*, 287–293.

[10]   R. Radi, *Proc. Natl. Acad. Sci.* **2004**, *101*, 4003–4008.

[11]   B. Alvarez, H. Rubbo, M. Kirk, S. Barnes, B. A. Freeman, R. Radi, *Chem. Res. Toxicol.* **1996**, *9*, 390–396.

[12]   P. Pacher, J. S. Beckman, L. Liaudet, *Physiol. Rev.* **2007**, *87*, 315–424.

[13]   J. S. Beckman, J. P. Crow, *Biochem. Soc. Trans.* **1993**, *21*, 330–334.

[14]   K. Keyer, J. A. Imlay, *J. Biol. Chem.* **1997**, *272*, 27652–27659.

[15]   L. Castro, M. Rodriguez, R. Radi, *J. Biol. Chem.* **1994**, *269*, 29409–15.

[16]   B. Alvarez, R. Radi, *Amino Acids* **2003**, *25*, 295–311.

[17]   Hiroshi Masumoto, R. Kissner, W. H. Koppenol, H. Sies, *FEBS Lett.* **1996**, *398*, 179–182.

[18]   H. Sies, H. Masumoto, **1996**, pp. 229–246.

[19] K. BRIVIBA, I. ROUSSYN, V. S. SHAROV, H. SIES, *Biochem. J.* **1996**, *319*, 13–15.

[20] H. Sies, V. S. Sharov, L.-O. Klotz, K. Briviba, *J. Biol. Chem.* **1997**, *272*, 27812–27817.

[21] G. E. Arteel, V. Mostert, H. Oubrahim, K. Briviba, J. Abel, H. Sies, *Biol. Chem.* **1998**, *379*, 1201–5.

[22] S. Padmaja, G. L. Squadrito, W. A. Pryor, *Arch. Biochem. Biophys.* **1998**, *349*, 1–6.

[23] H. Sies, G. E. Arteel, *Free Radic. Biol. Med.* **2000**, *28*, 1451–1455.

[24] M. Asahi, J. Fujii, T. Takao, T. Kuzuya, M. Hori, Y. Shimonishi, N. Taniguchi, *J. Biol. Chem.* **1997**, *272*, 19152–19157.

[25] Y. FU, J. M. PORRES, X. G. LEI, *Biochem. J.* **2001**, *359*, 687–695.

[26] Y. Fu, H. Sies, X. G. Lei, *J. Biol. Chem.* **2001**, *276*, 43004–43009.

[27] X. G. Lei, J. H. Zhu, W. H. Cheng, Y. Bao, Y. S. Ho, A. R. Reddi, A. Holmgren, E. S. J. Arnér, *Physiol. Rev.* **2015**, *96*, 307–364.

[28] R. Prabhakar, K. Morokuma, D. G. Musaev, *Biochemistry* **2006**, *45*, 6967–6977.

[29] S. C. E. Tosatto, V. Bosello, F. Fogolari, P. Mauri, A. Roveri, S. Toppo, L. Flohé, F. Ursini, M. Maiorino, *Antioxidants Redox Signal.* **2008**, *10*, 1515–1525.

[30] L. Grossi, P. C. Montevecchi, S. Strazzari, *European J. Org. Chem.* **2001**, *2001*, 131–135.

[31] R. Bryk, P. Griffin, C. Nathan, *Nature* **2000**, *407*, 211–215.

[32] J. S. Beckman, T. W. Beckman, J. Chen, P. A. Marshall, B. A. Freeman, *Proc. Natl. Acad. Sci. U. S. A.* **1990**, *87*, 1620–4.

[33] R. Radi, *Proc. Natl. Acad. Sci. U. S. A.* **2018**, *115*, 5839–5848.

[34] R. Radi, J. S. Beckman, K. M. Bush, B. A. Freeman, *J. Biol. Chem.* **1991**, *266*, 4244–50.

[35]   M. Balazy, P. M. Kaminski, K. Mao, J. Tan, M. S. Wolin, *J. Biol. Chem.* **1998**, *273*, 32009–32015.

[36]   A. Van Der Vliet, P. A. Peter, P. S. Y. Wong, A. Bast, C. E. Cross, *J. Biol. Chem.* **1998**, *273*, 30255–30262.

[37]   R. Masuda, S. Kuwano, K. Goto, *J. Am. Chem. Soc.* **2023**, *145*, 14184–14189.

[38]   R. Prabhakar, T. Vreven, K. Morokuma, D. G. Musaev, *Biochemistry* **2005**, *44*, 11864–11871.

[39]   R. Prabhakar, T. Vreven, M. J. Frisch, K. Morokuma, D. G. Musaev, *J. Phys. Chem. B* **2006**, *110*, 13608–13613.

[40]   R. Masuda, R. Kimura, T. Karasaki, S. Sase, K. Goto, *J. Am. Chem. Soc.* **2021**, *143*, 6345–6350.

[41]   R. I. Viner, T. D. Williams, C. Schöneich, *Biochemistry* **1999**, *38*, 12408–12415.

[42]   L. Flohé, S. Toppo, L. Orian, *Free Radic. Biol. Med.* **2022**, *187*, 113–122.

[43]   M. Maiorino, K. D. Aumann, R. Brigelius-Flohe, F. Ursini, J. van den Heuvel, J. McCarthy, L. Flohé, *Biol. Chem. Hoppe. Seyler.* **1995**, *376*, 651–660.

[44]   T. Hansen, P. Vermeeren, F. M. Bickelhaupt, T. A. Hamlin, *Angew. Chemie Int. Ed.* **2021**, *60*, 20840–20848.

[45]   J. Clayden, N. Greeves, S. Warren, *Organic Chemistry*, Oxford University Press, Oxford, 2nd ed, 2012.

6 A Systematic Analysis of the Chalcogenoxide Elimination

6.1 Introduction

The *so-called* selenoxide elimination is a convenient reaction to easily introduce a C=C bond in an organic scaffold.[1] It requires a selenylating agent and a suitable oxidant to generate *in situ* the selenoxide moiety. Moreover, the actual C=C bond formation proceeds smoothly at room temperature or even below 0°C.[1] The reaction can be part of green synthetic protocols, based on selenylation–deselenylation catalytic cycles, in which hydrogen peroxide can be used as oxidant.[2–4] This elimination was serendipitously discovered by Jones, Mundy and Whitehouse in 1970,[5] and its scope was further analyzed by Sharpless *et al* and Reich *et al* in 1973.[6–9] The mechanism of the reaction is well recognized to be an E_i elimination, in which the selenoxide moiety abstracts one proton in β, leading to a selenenic acid and to the desired C=C bond formation.[5–7] (Scheme 6.1) Within the oxidizing conditions in which the reaction occurs, the selenenic acid usually undergoes further reactivity and is thus undetected (see Chapter 1).
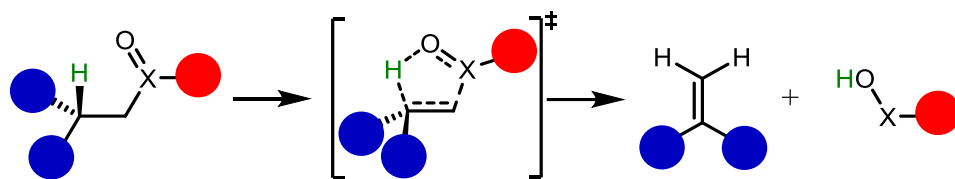
Scheme 6.1. General selenoxide (X=Se) or chalcogenoxide (X=S, Se, Te) elimination reaction; circles are organic groups or peptide/protein chains. The transition state for the reaction is represented between squared parentheses.

The same reaction for sulfoxides and telluroxides is known too,[10,11] but usually proceeds at higher temperatures. Indeed, while selenoxides are recognized to eliminate much faster than the analogous sulfoxides, telluroxides usually eliminate somewhat slower than analogous selenoxides,[12,13] an aspect which was recognized already by Sharpless in 1975.[14] To the best of our knowledge, this behavior was rationalized by formulating two hypotheses, i.e. i) due to the longer X=O bond in Te than in Se derivatives, the β-proton cannot be properly abstracted because of geometric constrains; ii) the higher tendency of telluroxides to form hydrates transforms Te=O in Te-OH, thus preventing the elimination. However, a unique conclusion was never reached.[12]

The same reactions for the highly oxidized systems (i.e., sulfones, selenones and tellurones) are much less investigated, even if all these systems formally have a chalcogen=oxygen bond which may promote elimination. In a combined experimental and theoretical study by Cubbage *et al*.[15], sulfones were demonstrated to eliminate via E_i mechanism only at very high temperatures (above 400°C). On the other hand, while selenones and tellurones might decompose above 100°C, to the best of our knowledge, their decomposition mechanism was never investigated.[1,16]

Chalcogenoxide eliminations occur also in biological chemistry.[17,18] In general, the chalcogenoxide elimination can alter the function of cysteine (Cys) and selenocysteine (Sec) containing proteins, such as albumin,[19] glyceraldehyde-3-phosphate dehydrogenase[20] and peroxiredoxins,[18] leading to potential toxic effects facilitating protein cross-linking, protein-protein aggregation, and protein aging due to the formation of dehydroalanine (DHA).[21] Moreover, in 2010, Cho *et al* proposed that in conditions of oxidative stress, the selenocysteine (Sec) of glutathione peroxidase (GPx) might undergo deselenylation via a selenoxide

elimination reaction of an unknown intermediate (likely a seleninic acid), leading to DHA residue. Orian *et al*[22] and, more recently, Masuda *et al*[23] proved that a bypass mechanism exists to prevent DHA formation in a fully functional enzyme and in a peptide mimic, based on the formation of a Se-N bond within the catalytic pocket. However, in the absence of a suitable partner for the formation of the Se-N bond, as it happens by disruption of the protein architecture after tryptic digestion,[22] DHA formation can still occur in highly oxidizing conditions. Moreover, while *in vivo* the protein architecture should protect selenocysteine deselenylation, in 2019, Reddy *et al*[24] observed that small-molecule inhibitors of the selenoenzyme thioredoxin reductase (TrxR) can bind to Sec leading to an oxidation–elimination mechanism, with consequent DHA formation. A similar mechanism for methylmercury toxified Sec and Cys was also theoretically proposed and investigated by some of us.[25] Thus, the interest in the sulfoxide/selenoxide elimination within thiol/selenoenzymes biochemistry remains alive.

Despite its role in organic and biological chemistry, the chalcogenoxide elimination reaction was investigated *in silico* by density functional theory (DFT) calculations only for very specific systems[26–31] and without a properly benchmarked level of theory. With this regard, Mcdougall *et al*[27] compared the results of the popular B3LYP density functional to highly-correlated *ab initio* methods for the investigation of selenoxide elimination, but no other density functionals were tested, nor B3LYP performance was investigated for sulfoxides or telluroxides elimination reactions. Thus, the aim of this Chapter is to fill some gaps in the understanding of the title reaction. Once assessed the most suitable DFT method(s) to computationally tackle the title reaction, also by evaluating the degree of error that comes with using a less accurate protocol, the scope is manifold: 1. To quantify and rationalize the effect of the chalcogen on the reaction and that of its oxidation state (OS) in bioinspired chalcogenoxide eliminations; 2. To provide explanation to why telluroxides eliminate somewhat slower than selenoxides, a question that, to the best of our knowledge, has remained open in the last forty years.

6.2 Computational Methods

All DFT calculations were done with the Amsterdam Density Functional (ADF) software.[32,33] The computational protocol and its benchmark are thoroughly described in the Appendix A. In this section, only the protocols employed within the Chapter will be described. For all DFT mechanistic calculations, geometries were optimized employing the OPBE functional[34–36] with the Slater type TZ2P basis set, combined with a small frozen core approximation to treat the core electrons. This basis set is of triple-ζ quality and is augmented with two sets of polarization functions on each atom. Scalar relativistic effects were included in all calculations within the zeroth-order regular approximation[37] (ZORA) as implemented in ADF. Energies have been refined as single points employing the meta-hybrid M06 density functional,[38] combined with an all-electron TZ2P basis set (TZ2P-ae). Thus, DFT energetics discussed along the Chapter are at ZORA-M06/TZ2P-ae // ZORA-OPBE/TZ2P level of theory, which will be labelled as M06 // OPBE. The nature of all stationary points was verified by frequency analysis on ZORA-OPBE/TZ2P optimized geometries: all minima display only positive frequencies, while transition states display only one imaginary frequency associated to the motion along the reaction coordinate from reactants to products. Only electronic energies are discussed along the Chapter, Gibbs free energies follow the same qualitative trend. (Appendix A, Table A6)

Highly correlated CCSD(T) energies were calculated by means of the DLPNO-CCSD(T) method,[39] as implemented in the Orca 4.2.1 package.[40,41] All-electron relativistic contracted basis set aug-cc-pVTZ-DK with Douglas−Kroll−Hess (DKH) scalar relativistic Hamiltonian was used for all atoms.[42,43] Geometries optimized with the OLYP functional[36,44] were used as a starting point for the calculation of highly-correlated energies. This level of theory is denoted as DLPNO-CCSD(T)/aug-cc-pVTZ-DK // ZORA-OLYP/TZ2P. Along the Chapter, it will be simply referred to as CCSD(T). Both the OPBE and OLYP functionals proved to well-reproduce organochalcogenides geometries in a previous benchmark study.[45] For the amino acid model, the conformation was chosen from a previously published paper by some of us[25] based on the most stable conformer for Cys as identified by Wilke *et al.*[46]

To obtain quantitative insight on bond energies, the activation strain analysis (ASA)[47,48] was performed as described in detail in Chapter 2.

While ASA was designed to investigate bimolecular reactions, it was extended to tackle also intramolecular reactions.[49,50] In this case, both the strain and the interaction terms can be expressed as differences with respect to an initial reference, usually the reactant of the reaction (Equation 6.1):

$$\Delta E(\zeta) = \Delta\Delta E_{strain}(\zeta) + \Delta\Delta E_{int}(\zeta) \qquad (6.1)$$

Conversely, when ASA is performed breaking a covalent bond, the bond dissociation energy (BDE) for such bond-breaking is related to the ASA terms by Equation 6.2:

$$-BDE = BFE = \Delta E_{strain} + \Delta E_{int} \qquad (6.2)$$

that is, the sum of strain and interaction is equal to the BDE taken with negative sign, i.e., to the bond formation energy (BFE).

Molecular structures were represented using CYLview.[51]

6.3 Results and Discussion
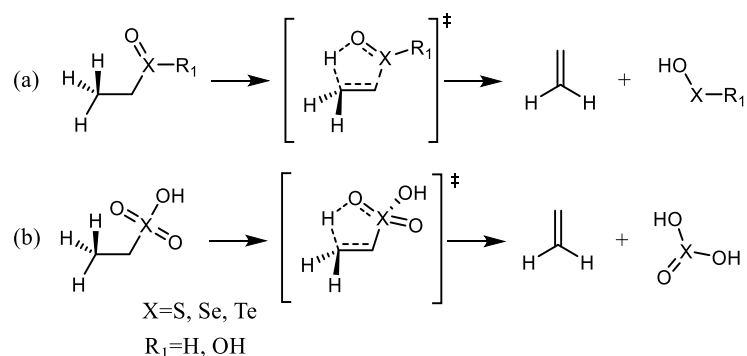
Scheme 6.2 General scheme of the elimination reactions in organochalcogenoxides (minimal models).

With the aim of obtaining seminal insight for a rigorous analysis of the chalcogenoxide elimination and for a clear and quantitative understanding of the effect of the chalcogen and of the OS on this reaction, a set of minimal models was investigated first, that is, the simplest compounds that can theoretically undergo the β-elimination process. (Scheme 6.2)

For the elimination process to occur, one β-proton must be preserved in all the models. Thus, in the simplest compounds, the chalcogenoxide moiety bears an ethyl substituent on. Keeping in mind the biological problem of selenocysteine deselenylation,[17] the R_1 substituent (Scheme 6.1 and 6.2a) was chosen to be either H, in the lowest OS (0) or OH in the intermediate OS (+2). These two states correspond to the oxidation state of *chalcogenenic* and *chalcogeninic* acids, respectively.[1] Since the real chalcogenenic acid does not have a formal chalcogen=oxygen bond, the tautomer was used to obtain theoretical insight and trends about the whole range of oxidation states. (Scheme 6.3)
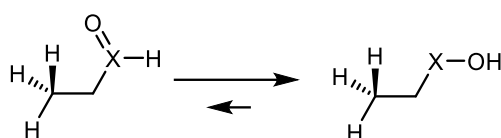
Scheme 6.3 Tautomeric equilibrium between a chalcogenoxide (left) and a chalcogenenic acid (right). The equilibrium is so shifted to the right that only the chalcogenenic acid is present in biological conditions (e.g., in the catalytic cycle of GPx).[52]

Notably, this system is also the simplest model for a general chalcogenoxide elimination as exploited in synthetic organic chemistry, where R_1 is usually an alkyl or aryl function. Lastly, the reaction represented in Scheme 6.2b proceeds from the highest oxidation state possible (+4) and is the model of a general *chalcogenonic* acid elimination. For the OSs 0 and +2, the reaction can proceed along two enantiomeric pathways due to the presence of the chalcogenoxide stereogenic center. Since the two pathways have the same activation energy, only one of them was investigated for all chalcogens and OSs.

Then, the elimination chemistry of the oxidized cysteine (Cys), Sec and tellurocysteine (Tec) was investigated. In this case, for the OS 0 and +2, two diastereoisomeric compounds can undergo elimination, because of the combination of the chalcogen (X=S, Se, Te) and the C_α stereogenic centers. Due to the

---

[1] Due to the different "languages" spoken between various branches of the organoselenium community, two different OS conventions are used along the thesis. In this Chapter, selenenic acid is considered to be in the OS 0, seleninic acid OS +2 and selenonic acid OS +4. This is in line with the convention of Reich and Hondal (*ACS Chem. Biol*. 2016, 11, 821−841). In Chapter 8, a different convention is used in which seleninic acid is in the OS +4 and selenonic in the OS +6, in agreement with the Back *et al* (*Angew. Chem. Int. Ed*. 2020,59, 4283 –4287).

biochemical importance of the substrates and for completeness, both pathways were investigated.

Lastly, a case of general interest in mechanistic organochalcogen chemistry is investigated, that is, understanding the origin of the inertia of telluroxides against elimination thus explaining why selenoxides eliminate faster than both the lighter and heavier analogues.

6.3.1 Minimal model elimination reactions

Table 6.1. Activation ($\Delta E^{\ddagger}$) and reaction (ΔE_r) energies (kcal mol^{-1}) for the β-elimination reaction of chalcogenoxides (OS 0), chalcogeninic acids (OS +2) and chalcogenonic acids (OS +4).[a]

	$\Delta E^{\ddagger}$			ΔE_r		
OS	S	Se	Te	S	Se	Te
0	31.22(31.36)	23.70(23.66)	21.42(21.89)	11.23(16.17)	1.16(1.71)	-3.09(-2.03)
+2	38.80(37.91)	29.95(28.42)	26.91(25.92)	26.80(31.10)	14.34(13.67)	8.27(7.88)
+4	57.52(58.93)	37.86(34.93)	30.84(27.65)	22.75(28.86)	-9.83(-12.99)	-24.29(-28.45)

[a]Electronic energies computed at CCSD(T), (M06 // OPBE.)

As described in Computational methods the reactants (R), transition states (TS) and products (P) of the title reaction were preliminarily optimized with OLYP and OPBE functionals, and accurate energetics have been obtained running single points with CCSD(T) and M06 functional, on OLYP and OPBE geometries respectively. The choice of the M06 // OPBE protocol is described in detail in Appendix A. Geometries and energies for the reaction depicted in Scheme 6.2 were computed for X=S, Se, Te and for R$_1$=H, OH, in order to encompass all chalcogens and to span all the relevant oxidation states. Since in a previous structural benchmark on organochalcogenides OLYP functional provided geometries in excellent agreement with crystallographic data,[45] OLYP optimized coordinates were used to perform highly-correlated single point energy calculations at CCSD(T) level of theory as described in Computational methods. The results of these calculations are shown in Table 6.1. In all reactions, at the transition state, the oxygen atom of the chalcogenoxide moiety abstracts the β-proton, leading to the concerted breaking of the C–X bond and to the formation of a C=C bond. (Figure 6.1)
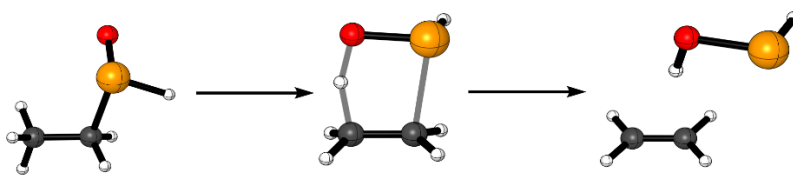
Figure 6.1 Representative reactant, transition state and product of a chalcogenoxide elimination (X=Se, OS=0); level of theory: ZORA-OPBE/TZ2P.

Focusing on the activation energies $\Delta E^{\ddagger}$, the elimination becomes kinetically more favored going from S to Se and to Te, for all the OSs under investigation. The lowering in activation energy is significantly larger going from S to Se, while it becomes less dramatic when moving from Se to Te, even if it remains relevant. Particularly, in the OS 0, while the activation energy is lowered of ca. 8 kcal mol^{-1} going from sulfoxide to selenoxide, the telluroxide has an activation energy 2 kcal mol^{-1} lower than the latter.

Conversely, changing the OS from 0 to +2 and +4 leads to an increase in the activation energy independently of the nature of the chalcogen. The effect is remarkable for S, for which between the OS 0 and +4 there is an increase in activation energy of over 20 kcal mol^{-1}, and far less remarkable for Te, with the telluronic acid having an activation energy ca. 9 kcal mol^{-1} higher than the telluroxide. Se displays an intermediate behavior, with an appreciable increase in activation energy upon increasing the OS of the chalcogen, but far from the dramatic behavior of the S analogs. In the OS +2, all systems display an activation energy 5-8 kcal mol^{-1} higher than the chalcogenoxide (OS 0). These results agree with the experimental behavior of chalcogenoxides and chalcogenones, that is, while the elimination reactions for sulfoxides, selenoxides and telluroxides are well-known, the analogous reactions for the highly oxidized systems proceed only at far higher temperatures or are not known to occur. Quite interestingly, these results suggest that the telluroxides should eliminate faster or as fast as selenoxides, in contrast to the experimental results. Thus, at least for these minimal models, it emerges that the geometrical features of the Te=O bond are not causing the experimentally observed kinetic inertia, since for all fully optimized systems the activation energy for the telluroxide elimination is lower than for the Se corresponding case. Further details are reported in Paragraph 6.3.4.

Similar trends were obtained for the reaction energies ΔE_r, which in general become more negative when going from S to Se and to Te, and more positive when increasing the OS. The only notable exception is an inversion in the expected trend when going from the OS +2 to the OS +4. In this case, while the activation energy increases, the reaction energy decreases, that is, the reaction becomes more favored. However, the high activation energy in the highest OS likely precludes the process anyway.

6.3.2 Cysteine, selenocysteine and tellurocysteine elimination reactions

Table 6.2 Activation ($\Delta E^{\ddagger}$) and reaction (ΔE_r) energies (kcal mol^{-1}) for the β-elimination reaction of chalcogenoxides (OS 0), chalcogeninic acids (OS +2) and chalcogenonic acids (OS +4).

	OS	Configuration	$\Delta E^{\ddagger}$	ΔE_r
Cys	0	RR	22.34	6.65
		RS	28.34	11.59
	+ 2	RR	30.27	22.76
		RS	32.51	23.70
	+ 4	R	52.73	18.87
Sec	0	RR	18.54	-2.86
		RS	20.81	-1.35
	+ 2	RR	21.36	7.17
		RS	25.85	9.44
	+ 4	R	30.10	-23.04
Tec	0	RR	17.81	-4.66
		RS	18.28	-4.20
	+ 2	RR	19.13	3.72
		RS	26.83	8.51
	+ 4	R	24.82	-35.32

In order to expand the scope of the investigation to more verisimilar systems, the problem of selenoproteins' deselenylation was investigated. (Table 6.2) It must be stressed that while for Cys all the OSs are available in a biological environment[9], because the oxidation to higher OSs (+2 and +4) has activation energies similar to the first oxidation[9,53] (0), selenium is somewhat more resistant towards overoxidation. While the oxidation to seleninic acid (OS +2) is possible, the oxidation to selenonic acid is three order of magnitude slower than the oxidation to the corresponding sulfonic acids.[9] For sake of completeness, however, the

elimination behavior of Cys, Sec and Tec was investigated spanning the same OSs of the minimal model i.e., 0, +2 and +4.

Firstly, it can be noticed that the amino acid model follows essentially the same trends described for the minimal model. M06 predicts a slightly lower activation energy for the elimination of Tec in the OS +4 than in OS +2. However, from the benchmark (Appendix A, Figure A2), the M06 density functional somewhat underestimates the activation energy of systems in the highest OS. Indeed, the M06-2X density functional (Appendix A, Table A4), which is the best performer in the OS +4, predicts the expected increase in activation energy increasing the OS. Thus, also for the amino acid model, the activation energy decreases increasing the size of the chalcogen (i.e. from S to Te), while it increases increasing the oxidation state of the chalcogen (i.e. from 0 to +4). The two diastereoisomers present moderately different activation energies, with the RS diastereoisomer systematically displaying the highest one. This is likely due to the different stability of the diastereoisomeric reactants. In fact, the diastereoisomer displaying the highest elimination barrier is also the more stable between the two, e.g.: in the OS 0, Cys (R,S) shows an activation energy ca. 6 kcal mol^{-1} higher than Cys (R,R), and the (R,S) diastereoisomer is ca. 5 kcal mol^{-1} more stable than the (R,R) one. Indeed, the energies of the two diastereoisomeric TSs are quite close (ca. 1 kcal mol^{-1} for Cys in the OS 0). While for the other OS and chalcogens the effect can be less remarkable, the higher activation energy for the (R,S) remains partly due to reactant stabilization. The absolute energies of reactants and transition states are reported in the Appendix A, Table A5.

Despite following identical trends as the minimal model, all the amino acids display significantly lower activation energies for the elimination process than the minimal model at the same level of theory (Table 6.1 and Table 6.2). Cys displays the strongest decrease, while Sec and Tec show a more modest but still appreciable lowering. This effect is more prominent along the RR pathway, but it is still appreciable even for the higher-barrier RS elimination. This behavior is likely due to the increased acidity of the β-proton (i.e., the acid α-proton with respect to the carboxyl moiety) which can be more properly abstracted by the chalcogenoxide moiety. Even so, it can be seen that while the chemical environment (i.e. RS/RR configuration, β-proton acidity, etc.) can tune the reaction, the overall behavior of

the process is rooted in the nature of the chalcogen, with sulfur displaying the highest and tellurium displaying the lowest activation energy, respectively. Importantly, also in this system, no selenium–tellurium inversion in the height of the barrier is revealed. Thus, also within a not oversimplified system, telluroxides should eliminate intrinsically faster than (or as fast as) selenoxides, and lead to more stable product as displayed by the reaction energies. The only exception is for the OS +2, RS pathway, for which a slightly higher activation energy for Te than for Se is predicted. The difference between the two activation energies is however less than 1 kcal mol^{-1} (M06 // OPBE) and thus is considered negligible. Overall, the amino acid systems and the minimal models behave alike.

6.3.3 Analysis of the trends

To the best of our knowledge, two main factors might concur to explain the increased reactivity of selenoxides over sulfoxides i.e., the increased basicity of the selenoxide oxygen and the lower strength of the Se–C bond, when compared to the S–C bond, which help in the proton abstraction and in the X–C bond breaking occurring along the reaction, respectively.[1,9] To quantify how the activation energy of the title reactions is related to the basicity of the chalcogenoxide and to the X–C bond strength, the $\Delta E^{\ddagger}$ computed for the minimal models were plotted against the electronic proton affinity (PA) of the substrate (i.e., the capacity of the chalcogenoxide to abstract the β-proton) and against the electronic bond dissociation energy (BDE) of the C–X (X=S, Se, Te) bond in different substrates (i.e., the ease by which the carbon–chalcogen bond breaks). It is interesting to verify if these simple explanations can be extended also to telluroxides and to the whole plethora of OSs under investigation, and not just to the S and Se chalcogenoxides more commonly discussed in the experimental literature. The results are shown in Figure 6.2.
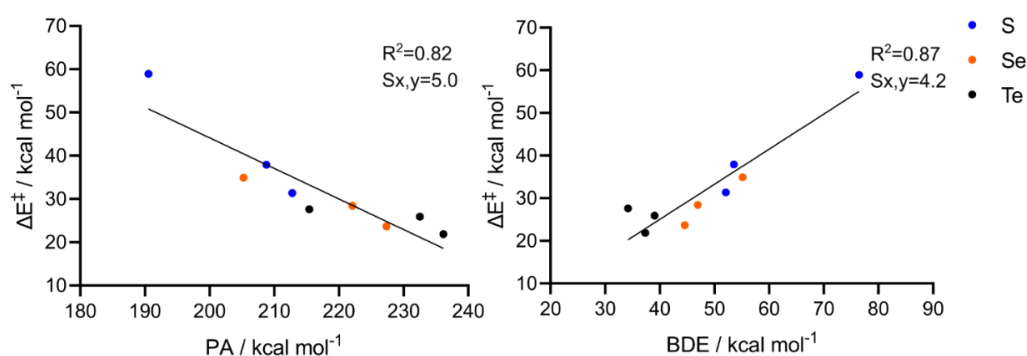
Figure 6.2 Linear correlation between activation energies and PA/BDE for the minimal model reactions (OS= 0, +2, +4). Statistical parameters (R^2 and standard deviation, Sy,x) are reported near the linear fit. Level of theory: M06 // OPBE.

For clarity, the systems are labelled by the chalcogen and oxidation states; thus, the sulfoxide is labelled S0, the sulfinic acid S2 and so on. Overall, both the basicity of the chalcogenoxide, which extracts the proton along the reaction, and the strength of the C–X bond, which undergoes bond-breaking along the reaction, nicely correlate with the elimination activation energy. Particularly, considering the S and Se subgroups, the PA decreases, and the BDE increases along the series OS 0, +2, +4, in line with the increase in activation energy. Conversely, for all OSs, the PA increases and the BDE decreases when going from S to Se, in agreement with the lower activation energy required by all selenoxides to undergo elimination. For Te, the PA still decreases with increasing OSs. However, for Te, the BDE does not display a clear trend when plotted against the activation energy.

Indeed, the PA trends correlate well with the charge density analysis of the chalcogenoxide bond, that is, the X=O acquires a more charge separated character as the size of the chalcogen increases, leading to a more prominent negatively charged oxygen atom (i.e., more basic) than in their lighter analogs. (Figure 6.3) Increasing the OS of the system leads to a more positively charged density on the chalcogen. Conversely, the charge density on the oxygen becomes less negative making the chalcogenoxide intrinsically less basic in high OSs despite the charge separated character of the bond. (Figure 6.3)
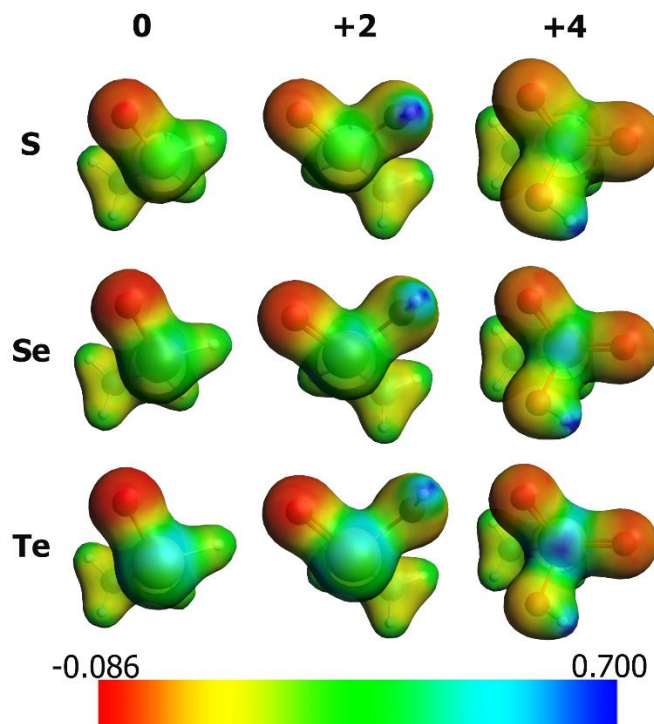
Figure 6.3 Molecular Electrostatic Potential (MEP) in a.u. for all the minimal model reactants. Columns are different OSs (0, +2, +4) while rows are different chalcogens (S, Se, Te). Areas in which the potential is more negative are of greater red intensity. Isodensity value: 0.04. *Level of theory*: M06 // OPBE. Hirshfeld partial charges on the oxygen atom can be found in the Appendix A, Table A8.

Table 6.3. Activation strain analysis (ASA) and energy decomposition analysis (EDA) of the X–C BDE (kcal mol^{-1}). Both fragments are unrestricted doublets. Level of theory: M06 // OPBE.

	BDE	BFE	ΔE_{strain}	ΔE_{int}
S0	52.06	-52.06	6.62	-58.68
Se0	44.57	-44.57	6.79	-51.36
Te0	37.32	-37.32	13.59	-50.91
S2	53.54	-53.54	7.90	-61.44
Se2	46.94	-46.94	8.59	-55.53
Te2	39.03	-39.03	15.70	-54.73
S4	76.45	-76.45	7.42	-83.87
Se4	55.13	-55.13	9.30	-64.43
Te4	34.16	-34.16	22.69	-56.85

To provide a quantitative discussion on the effect of the chalcogen and OSs on the BDE, ASA was performed on the BDEs previously shown, (Table 6.3) using as fragments the two radical (unrestricted doublets) products of the bond dissociation event. This can help to rationalize the poor correlation between BDE and activation energies of telluroxide elimination, which is also affected by the softness of the fragments, while the bond strength should be more clearly represented by the actual ΔE_{int} of the bond. Indeed, increasing the size of the chalcogen along the series S, Se and Te, the interaction energy of the C–X bond is weakened in agreement with the decrease in BDE. The situation is somewhat different for Te0, for which the BDE is lowered by an increase in ΔE_{strain}. However, also in this case, with respect to Se0, Te0 has a (slightly) lower ΔE_{int}, suggesting that telluroxides have an intrinsically weaker X–C bond, than selenoxides and sulfoxides. Conversely, increasing the OS along the series S0, S2 and S4, and Se0, Se2 and Se4, ΔE_{int} becomes more and more stabilizing, and the BDE becomes higher. The situation is, also in this case, somewhat different for Te, for which the BDE displays an alternation effect due to the interplay between ΔE_{strain} and ΔE_{int}. However, the Te–C bond in high OS remains intrinsically stronger as highlighted by a more negative ΔE_{int}. Thus, while the BDE for the series Te0, Te2 and Te4 poorly correlates with the activation energy of the elimination process, the increase (in absolute values) in ΔE_{int} of the Te–C bond along the series agrees with the increasing activation energy of the process, as it does for the other two chalcogens.

These results suggest indeed that both the chalcogenoxide basicity and the X–C bond strength (quantified as the BDE or, better, by the ΔE_{int}) are phenomenologically valid explanations for the differences in reactivities of different chalcogens and oxidation states in chalcogenoxide elimination reactions, and not just for S and Se in their lowest OS. However, no clear picture emerges about what factor actually controls the reactivity, if any, since the X=O basicity and the X–C bond strength appear to be somewhat intertwined. Thus, to better rationalize the trends in activation energy, a few model cases were analyzed within the framework of the Activation Strain Model. (Equation 6.1)
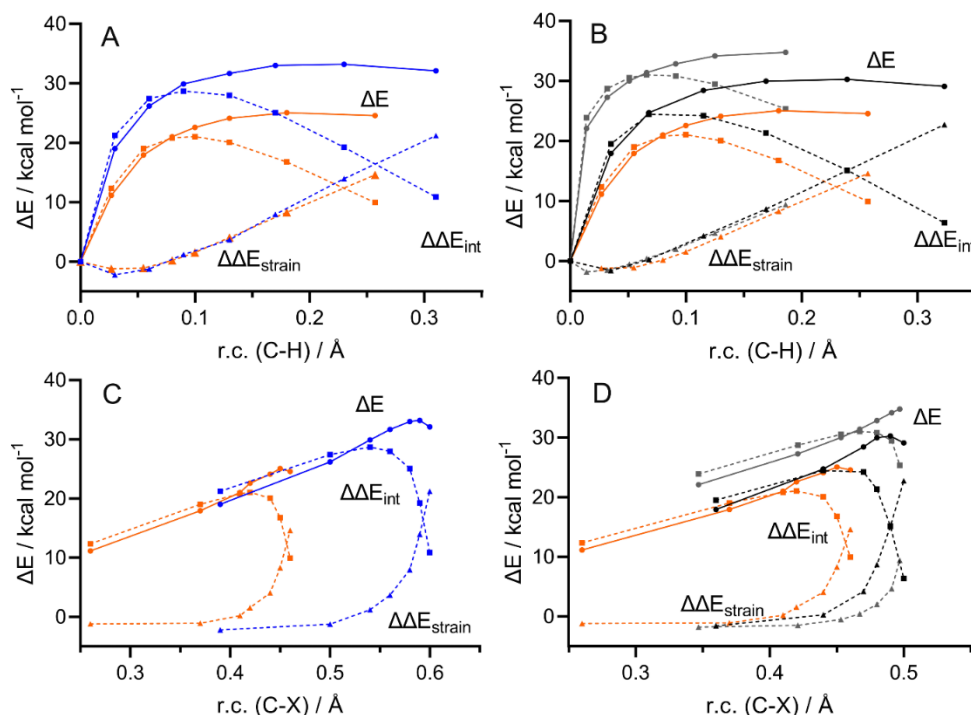
Figure 6.4 ASA along the reaction coordinate (r.c., C-H bond stretching (A, B) and C-X bond stretching (C, D)) for (A, C) the effect of the chalcogen, S0 (blue) vs Se0 (orange), and (B, D) the effect of the OS, Se0 (orange) vs Se2 (black) and Se4 (gray). Level of theory: M06 // OPBE. The final point is the TS as identified along the intrinsic reaction coordinate at OPBE level. The second-last point is at slightly higher energy for S0, Se0 and Se2 after M06 // OPBE single point. Solid lines are IRC energies, while dashed lines are strain (triangles dots) and interaction (squared dots) energies. The reference point (r.c. 0.0) is the final point of the IRC profile. Along the C-X r.c. the reference point (0, 0) is left out of the plot for clarity, and the focus is on the region in the surrounding of the TS.

Particularly, this approach was used to compare the reactivity of S0 to Se0, and of Se0 to Se2 and Se4, thus obtaining insight in the role of the chalcogen and of the OS, respectively. The system was fragmented in the ethyl radical and in the chalcogenoxide moiety, both considered as unrestricted radical fragments. (Figure 6.4)

The IRC profile was projected on two critical reaction coordinates (r.c.) i.e., the C–H and the X–C bond breaking. For *well-behaved* reactions, ASA along different r.c.s should provide similar or compatible results. However, chalcogenoxide eliminations appeared to have a somewhat pathological behavior likely due to different reasons: they are intramolecular reactions, thus making ASA *per se* more challenging; C–H and X–C bond breaking do not proceed simultaneously; the protophile and the leaving group of the elimination are the same function, thus their

role can be envisioned to be somewhat entangled. Indeed, while between the two r.c.s there are some similarities, the two analyses provide interesting different results.

Comparing the S0 to the Se0 curves along the C–H r.c., the whole reaction profile of the selenoxide is lower in energy with respect to the sulfoxide. Since the two $\Delta\Delta E_{strain}$ profiles are essentially superimposed, the lower reaction profile of Se0 is due to the less destabilizing $\Delta\Delta E_{int}$, that is to the less prominent decrease in ΔE_{int} when going from the reactant to the TS. In the end, the shape of the $\Delta\Delta E_{int}$ curve determines the reactivity. This term is likely due to the contribution of two concomitant main phenomena, the breaking of the X–C bond, and the formation of the O–H bond, with the first one being predominant in the early stages of the reaction, when the $\Delta\Delta E_{int}$ undergoes an abrupt increase despite a modest elongation of the C-H bond, and the second one being predominant later on, providing an extra stabilization which lowers the interaction leading to the observed single-maximum profile. Indeed, as previously discussed, both increased basicity of selenoxide and the lower strength of the Se–C bond, when compared to the S–C bond, have been used in the literature to explain the increased reactivity of selenoxides with respect to sulfoxides.[1,9] Both these aspects are captured by the shape of the interaction profile, and appear to contribute to the less destabilizing $\Delta\Delta E_{int}$, and, in the end, to a lower activation energy. A similar discussion can be made when comparing Se0 to Se2, for which a single-maximum profile is observed for $\Delta\Delta E_{int}$. In this case, not only Se0 has a less destabilizing $\Delta\Delta E_{int}$, but also a slightly lower $\Delta\Delta E_{strain}$. However, the interaction energy remains the main difference at the origin of the different reactivity.

Along the X–C r.c. the $\Delta\Delta E_{int}$ naturally has the same single-maximum shape. However, some details reveal a different picture. Particularly, the two $\Delta\Delta E_{strain}$ profiles are not anymore superimposed, neither for the effect of the chalcogen (bottom, left), nor for the effect of the OS (bottom, right), and the reactions with the highest barrier (i.e., S0, and Se2), display a later increase in the strain energy compared to Se0. Indeed, this is due to the fact that along this r.c. the two $\Delta\Delta E_{int}$ are initially almost superimposed (with S0 and Se2 displaying only a slightly more destabilizing interaction compared to Se0) and only in proximity of the TS, where the $\Delta\Delta E_{int}$ starts to decrease because of the O–H interaction, the two curves begin

to show strong differences. Indeed, Se0 $\Delta\Delta E_{int}$ starts to decrease earlier compared to S0 (left) and compared to Se2 (right). This aspect, which is not clearly captured along the C–H r.c., suggests that while the softer Se0–C bond might provide some advance over the stronger S0–C and Se2–C bond, the increased reactivity of selenoxides over sulfoxides and of the lowest OS over the intermediate OS is mostly due to the point along the r.c. at which the interaction between the protophile and the β-hydrogen becomes relevant.

A different argument can be made when the highest OS (Se4) is analyzed and compared to the two lower ones. Indeed, while along the C–H r.c. the same picture can be seen, with a single-maximum profile for the interaction energy, and a smooth increase in $\Delta\Delta E_{int}$ going from Se0 to Se2 and to Se4, in this case Se4 reach the TS earlier than Se2, despite having an even higher $\Delta\Delta E_{int}$ profile. Also in this case, the behavior of the reaction becomes clearer when it is observed along the X–C reaction coordinate: in this case, while the Se4 strain profile is the last one to undergo an increase in the proximity of the TS, its $\Delta\Delta E_{int}$ is significantly higher compared to Se0 and Se2, which, as previously discussed, display closer $\Delta\Delta E_{int}$ at similar r.c. values until the TS surrounding is reached. Thus, while the TS is still reached after the $\Delta\Delta E_{int}$ decreases because of the onset of the O–H interaction, in this case it is the overall highest $\Delta\Delta E_{int}$ profile that leads to the higher activation energy. Thus, for the highest OS, the energy required for X–C bond-breaking becomes determinant over the protophilicity of the chalcogenoxide itself.

Overall, this combined PA/BDE correlation and ASA investigation suggests that the simple explanations commonly found in the literature for S0 and Se0, can also be phenomenologically extended to the higher OSs (+2 and +4). It is clear from the $\Delta\Delta E_{int}$ profile, that the X–C bond breaking and O–H bond formation effects are intertwined. Both the basicity of the chalcogenoxide (quantified as the PA) and the strength of the X–C bond (quantified as the BDE or, even better, by the ΔE_{int}) correlate well with the whole plethora of reactions. However, ASA uncovered that there is an earlier onset of the protophile – β-proton interaction for selenoxides with respect to sulfoxides (at the same X–C bond breaking r.c.). This interaction is the main responsible for the lower activation energy of the selenoxide over the sulfoxide elimination. A similar behavior also characterizes the OS 0 with respect to the OS

+2, while for the OS +4 a stronger X–C bond significantly contributes to the heightening of the barrier.

6.3.4 Elimination of OS 0 phenyl- alkyl chalcogenoxides

Lastly, the methodological and theoretical knowledge obtained up to now was applied to investigate the elimination mechanism of phenyl alkyl chalcogenoxides and to shed some light on why many telluroxides appear to eliminate somewhat slower than the analogous selenoxides, in sharp contrast with the results of the calculations reported so far. Phenyl alkyl species have been chosen because they are employed as redox catalysts[28,54] and in organic synthesis as β-eliminating systems.[6,55] Phenyl ethyl sulfoxide, selenoxide and telluroxide (PhXEt) have been selected as model compounds since they are the smallest possible systems of this class that can theoretically undergo elimination. The elimination mechanism follows the same details previously explained, with a concerted transition state at which proton abstraction occurs along with the X–C bond breaking. (Scheme 6.4a)
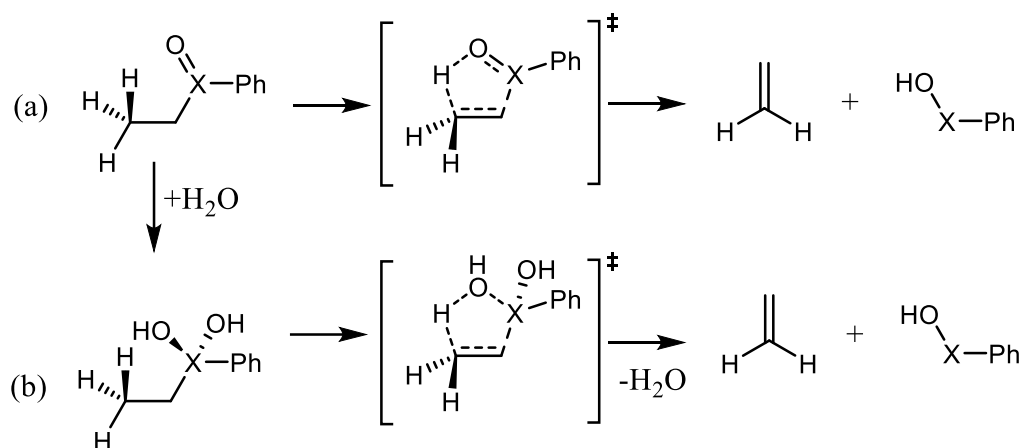
Scheme 6.4 Direct chalcogenoxide elimination mechanism of PhXEt (a) and hydration followed by dehydration elimination mechanism (b) as investigated in this study.

As expected, also in this case the sulfoxide displays the highest activation energy, with the selenoxide and telluroxide showing, much lower, similar activation energies, i.e., also for phenyl- ethyl- species no intrinsic inertia towards the elimination seems to characterize telluroxides. (Table 6.4)

Table 6.4 Activation energies (kcal mol^{-1}) relative to the direct elimination mechanism of PhXEt ($\Delta E_{elm}^{\ddagger}$), to the elimination mechanism of their hydrates ($\Delta E_{hyd,elm}^{\ddagger}$), and reaction energies^a for the hydrates formation (ΔE_r^{hyd}).

	$\Delta E_{elm}^{\ddagger}$	ΔE_r^{hyd}	$\Delta E_{hyd,elm}^{\ddagger}$
PhSEt	31.99	21.96	33.49
PhSeEt	25.22	-0.11	33.18
PhTeEt	23.52	-18.07	39.44

^{a}Electronic energies computed at M06 // OPBE level of theory. Gibbs free energies follow the same qualitative trends and are available in the Appendix A, Table A7.

In 1983, in their study on telluroxide elimination, Uemura *et al* realized that all their "telluroxides" were in fact characterized as the corresponding hydrates,[12] and hypothesized that the hydration might concur to slow down the reaction of telluroxides. Thus, the reaction energy for the addition of one water molecule to PhXEt was computed. Then, the capability of the hydrates to undergo an elimination process even after protonation of the X=O bond was investigated. (Scheme 6.4b and Figure 6.5)
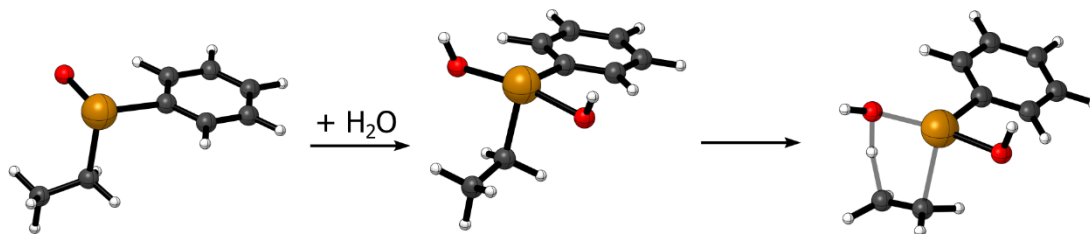
Figure 6.5 Representative phenyl- ethyl- chalcogenoxide, hydrate and transition state for the hydrate elimination (X=Te).

Interestingly, in agreement with the studies of Uemura *et al*, PhTeEt undergoes a more favorable hydration than both sulfoxides and selenoxides.[12] This is expected, because descending along a group in the periodic table, the elements can host more favorably hypervalent interactions,[9] and telluroxides have a more positive electrostatic potential around the chalcogen than selenoxides and sulfoxides. (Figure 6.3) Indeed, the stability of the hydrates smoothly increases along the series S, Se and Te. Unexpectedly, given the lack of the chalcogenoxide bond, all the hydrates can still undergo an elimination mechanism, with a transition state like the one of the conventional chalcogenoxide elimination (Scheme 6.4b and Figure 6.5) in which one of the -OH functions of the hydrate abstract the β-proton.

However, all these TSs are located on the PES at higher energies with respect to the correspondent chalcogenoxide elimination TSs, and all the activation energies are higher than the correspondent sulfoxide elimination, making the reaction much less favorable. (Table 6.4) Since the hydration process is much more favorable for Te than for the lighter chalcogens, it can be concluded that it is the primarily responsible factor behind the relatively slow telluroxide elimination in water-rich environment.

6.4 Conclusions

In this work, various aspects of the *so-called* chalcogenoxide eliminations were investigated *in silico*, with highly-correlated *ab initio* methods and properly benchmarked DFT protocols. The results of this study are manifold and can be summarized as follows:

1. DFT approaches and CCSD(T) provide the same qualitative conclusions about the behavior of the title reactions, that is, the activation energy of the process decreases increasing the size of the chalcogen (along the series S, Se and Te), with a sharp decrease from S to Se and a moderate decrease from Se to Te, and smoothly increases increasing the OS of the chalcogen (along the series 0, +2 and +4). This behavior is shared among systems of different complexity and is thus rooted in the property of the chalcogen itself.

2. For Sec, the OS 0 gives the most favorable (from the kinetic point of view) elimination. However, since in biological environment the OS 0 is represented by a selenenic acid and not by a chalcogenoxide (the tautomeric equilibrium is shifted to the chalcogenenic acid side), overoxidation to seleninic acid is confirmed to be necessary for the elimination process to occur. Overoxidation to selenonic acid, besides being slow, would lead to an even higher activation energy for the elimination, furtherly preventing the elimination from occurring. Conversely, Cys is known to be easily oxidized, even in biological media, to high OS (+2, +4) where the elimination is kinetically disfavored. However, oxidized disulfides might still be involved in a rich elimination chemistry as shown in previous studies.[18,20]

3. Both the chalcogenoxide basicity and the X – C bond strength correlate well with the computed activation energy of all chalcogens and all OSs. Activation Strain Analysis showed how these two effects are intertwined, at the same time providing insight into how selenoxides react faster than sulfoxides because of an anticipated interaction between the protophile and the β-proton.

4. Telluroxides are predicted to be the best eliminating systems even in the higher OSs. Thus, the known inertia of organotelluroxides towards elimination is not due to intrinsic geometric factors, but to their more favorable hydration process, which disrupts the Te–O double bond fundamental for an effective β-proton abstraction.

This investigation provides systematic insight into this fundamental organochalcogen reaction, encompassing simple models of theoretical interest as well as biological or synthetic compounds. In addition, the benchmarked level of theory can be used to quantitatively investigate the inhibition of selenoproteins by small-molecules and the elimination chemistry of oxidized dichalcogenides,[18,19] thus paving the route for a deeper mechanistic understanding of post-translational modifications in biological and toxicological chemistry, based on this fundamental organochalcogen reaction.

Appendix A

Extended benchmark for chalcogenoxide eliminations

For the benchmark, a total of five functionals (xc), i.e., two GGAs, OLYP[36,44,56] and OPBE;[34] one dispersion-corrected GGA, BLYP-D3(BJ);[36,44,56–60] one hybrid, B3LYP[61,62] and one meta-hybrid M06-2X[38,63], were preliminarily tested for the geometry optimization and energy calculations over the model minimal reactions discussed in Chapter 6 (Scheme A1).
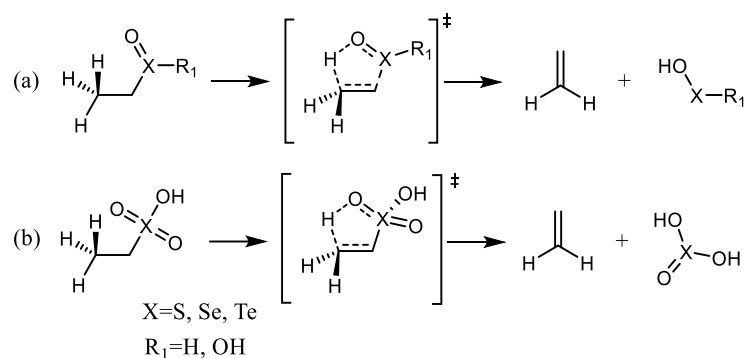
Scheme A1 General scheme of the elimination reactions in organochalcogenoxides (minimal models) used for benchmarking purposes.

 The Slater type TZ2P basis set was used for all calculations. This basis set is of triple-ζ quality and augmented with two sets of polarization functions on each atom. For the three GGA, the small frozen core approximation was used, while for the hybrid and the metahybrid, all-electron calculations were performed since frozen core approximation is not implemented in ADF for these functionals. The role of the basis set (TZP, TZ2P and QZ4P) and of frozen core approximation (no frozen core and small core approximation) was tested for the OPBE functional, by reoptimizing all the investigated geometries and computing activation and reaction energies (Table A1) Scalar relativistic effects were included in all calculations within the zeroth-order regular approximation[37] (ZORA) as implemented in ADF. This level of theory is denoted as ZORA-xc/TZ2P(-ae). Starting from the OPBE optimized geometries, single point energies have been computed with eighteen different density functionals i.e., ten GGAs (one dispersion-corrected GGA), two meta-GGAs, three hybrids and three meta-hybrids. In detail, BLYP,[44] BP86,[57,64]

HTBS,[65] PBE,[35] mPW,[66] PW91,[67] revPBE,[68] RPBE,[69] mPBE[70] were considered. In addition, the dispersion-corrected version of BP86 functional, BP86-D3(BJ), was also tested. TPSS[71,72] and SCAN[73] functionals were tested for the meta-GGAs category; PBE0,[74] OPBE0[34] and mPW1PW[66] were tested for the hybrid category (the popular B3LYP was already preliminary); M06,[38] M06-2X[38] and TPSSh[71] were tested for the meta-hybrid category. Frozen core (fc) approximation was not used, to allow for a rigorous comparison, since for hybrids and meta-hybrids fc is not available. All calculations are all-electron except when explicitly specified. Following this initial investigation, eighteen functionals were tested (M06-2X was included as the best performing preliminary functional, while the other four were excluded given their relatively poor performance) by running single-point energy calculations on ZORA-OPBE/TZ2P optimized geometries. All calculations were done without frozen core approximation to allow a rigorous comparison. The level of theory of these calculations is denoted as ZORA-xc/TZ2P-ae // ZORA-OPBE/TZ2P, and along the work it will be referred to as xc // OPBE.

All DFT calculations were compared against the DLPNO-CCSD(T) calculations, performed with the all-electron relativistic contracted basis set aug-cc-pVTZ-DK with Douglas−Kroll−Hess (DKH) scalar relativistic Hamiltonian. Single point DLPNO-CCSD(T) energy calculations were performed on OLYP optimized geometries, as described in paragraph 6.2.

Extended benchmark results

The performances of DFT in reproducing CCSD(T) trends were tested as described in the additional computational details. The activation and reaction energies obtained with DFT employing the five preliminary functionals were then compared to the CCSD(T) computed reference values. The results are shown in the Table A2, while the deviation from CCSD(T) results is represented in Figure A1. While all five functionals recover the trends discussed for CCSD(T), with the exception of the heightening of the activation energy going from Te (+2) to Te (+4) which is recovered only by OPBE and M06-2X, it can be clearly seen that the cheaper functionals (i.e. GGAs or the dispersion corrected GGA) underestimate the activation energy for the reaction of sulfoxides, selenoxides and telluroxides, with

BLYP-D3(BJ) providing the worst results, with errors larger than -15 kcal mol^{-1} in some cases. (Figure A1)

Figure A1. Deviation of the activation ($\Delta\Delta E^{\ddagger}$, A, C, E) and reaction ($\Delta\Delta E_r$, B, D, F) energies predicted at DFT (ZORA-xc/TZ2P) level of theory from CCSD(T) reference values. A negative value means that DFT underestimates the energy, while a positive value means that DFT overestimates the energy. Data are grouped on chalcogen basis: sulfur (A/B, blue), selenium (C/D, orange), tellurium (E/F, black). Bar filling is used to denote the OS: the lowest OS (0) is in solid color, the intermediate OS (+2) is dashed (thin lines), while the highest (+4) is dashed (thick lines).

For the other GGAs and B3LYP, the error generally increases going from S to Se, and from the lowest to the highest OS, with all the reactions in the OS +4 systematically displaying the strongest deviations from the CCSD(T) activation

energies. The situation is rather different for M06-2X activation energies, that agree almost perfectly with the highly-correlated single points. With this functional, no great error arises when going from the OS 0 to the OS +4, and the $\Delta E^{\ddagger}$ of reactions involving Se shows deviation only slightly larger than those involving S.

A somewhat different picture describes deviations in reaction energies. In this case, the performance of the functionals appears to be somewhat less systematic, with some changes with the chalcogen and with the OS. Particularly, OPBE functional seems to be the worst performer for reactions involving S, but is the best performer for reactions involving Se. On the other hand, while B3LYP appears to be the worst performer for Se and Te, it is the best performer for S, with OLYP and BLYP-D3(BJ) giving similar results. In this case, M06-2X neither excels nor completely fails, predicting reaction energies within ca. ±5 kcal mol^{-1} with respect to CCSD(T), and always with the correct qualitative trend.

Considering these results, OLYP and OPBE functionals, benchmarked and popularly used to study S_N2 reactions[34,75,76] (such as chalcogenide oxidations[77,78]) and E2 reactions,[79,80] do not perform equally well for the quantitative description of chalcogenoxide elimination activation energies, even if they can still be used with some caution to understand the trends in the energetics in analogous elimination reactions, since CCSD(T) trends in activation and reaction energies are properly recovered also with the cheapest GGA or dispersion corrected GGA functionals.

In this preliminary analysis, OPBE appears to be the best performing GGA (Figure A1). OPBE functional was already found to perform very well for geometry optimization of organochalcogenides.[45] Thus, starting from OPBE optimized geometries, 17 functionals were tested for single-point energy calculations as described. Activation and reaction energies computed at xc // OPBE level of theory clearly show that no cheap GGA functional can properly describe the title reactions. (Table A3) In contrast, the hybrid OPBE0, and the metrahybrid M06 and M06-2X provides good to excellent performances. (Figure A2)
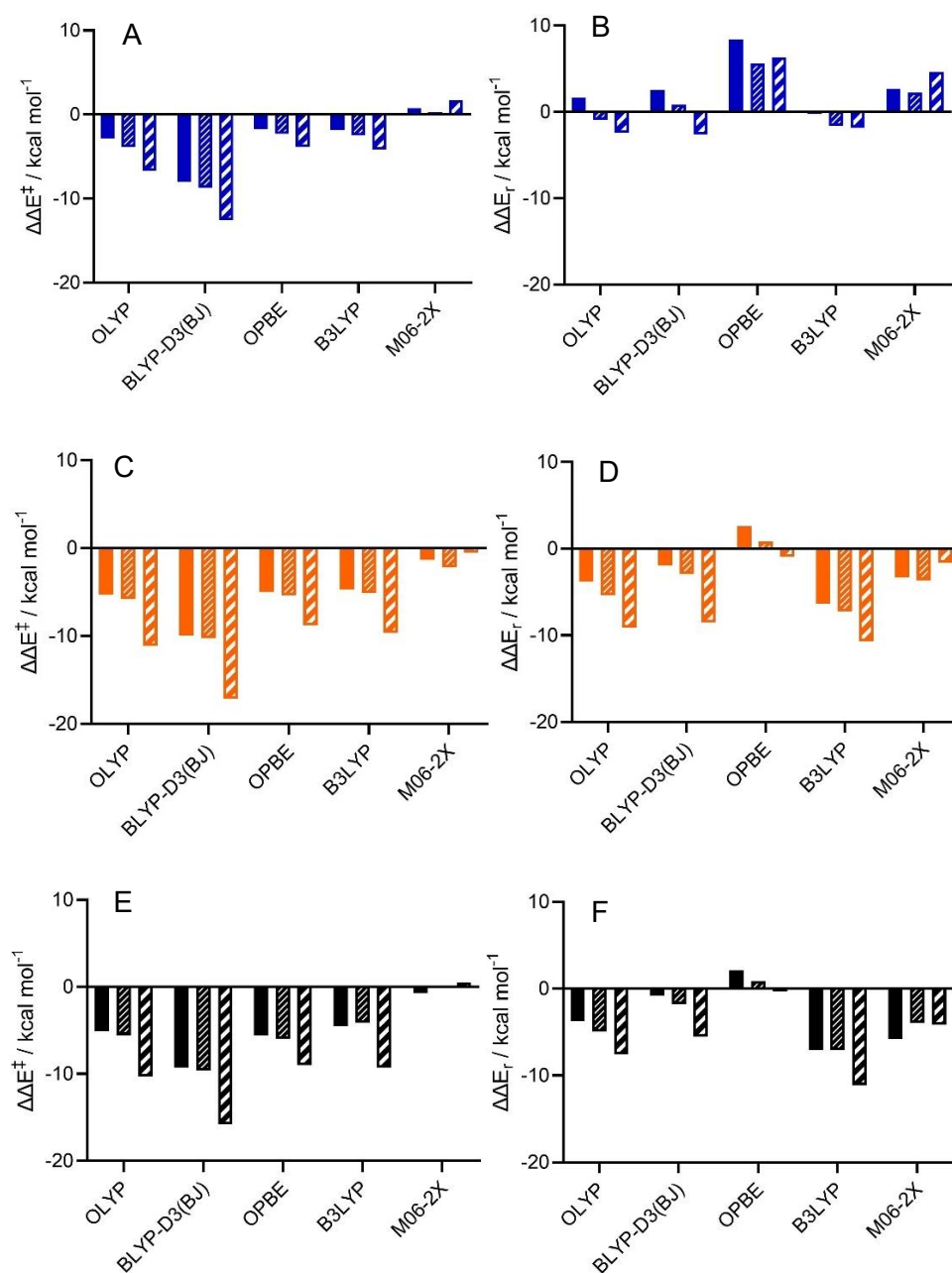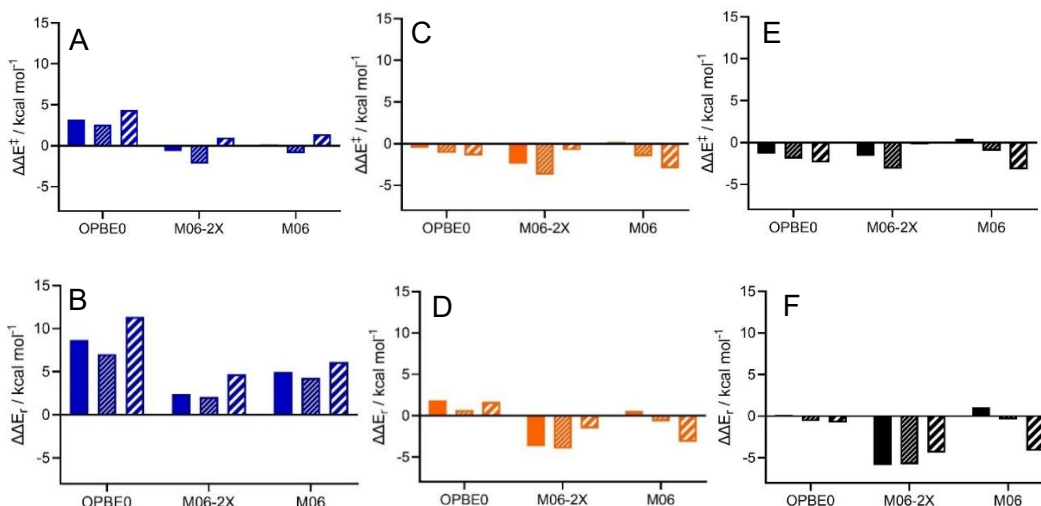
Figure A2 Deviation of the activation ($\Delta\Delta E^{\ddagger}$, A, C, E) and reaction ($\Delta\Delta E_r$, B, D, F) energies predicted at DFT (xc // OPBE) level of theory from CCSD(T) reference values. A negative value means that DFT underestimates the energy, while a positive value means that DFT overestimates the energy. Data are grouped on chalcogen basis: sulfur (A/B, blue), selenium (C/D, orange), tellurium (E/F, black). Bar filling is used to denote the OS: the lowest OS (0) is in solid color, the intermediate OS (+2) is dashed (thin lines), while the highest (+4) is dashed (thick lines).

Particularly, M06 // OPBE appears to be the best performing protocol for investigating reactions in the lowest oxidation state (OS 0) regardless of the chalcogen involved, while M06-2X // OPBE is the best approach to compute the activation energies in the highest OS (+4) for all chalcogens. OPBE0 // OPBE, on the other hand, gives a quite satisfying description of all Se reactions, with errors in reaction energies below 2.0 kcal mol^{-1} and errors in activation energies below 1.5 kcal mol^{-1} for all OSs.

Moreover, all three protocols predict activation and reaction energies that correlate very well against CCSD(T) ones, (Figure A3) with very similar R^2 values in the range 0.97-0.99 for both activation and reaction energies and mean absolute errors of ca. 2.00 kcal mol^{-1} or lower for activation energies and between 2 – 4 kcal mol^{-1} for reaction energies. Thus, in our opinion, all these three approaches can be employed to investigate the title reaction since the trends are qualitatively and quantitatively reproduced with the hybrid (OPBE0) as well as with the two meta-hybrids (M06 and M06-2X) functionals, and each of the three functionals outperforms the other two in a specific subset of reactions, with M06 being in average the best among the three.
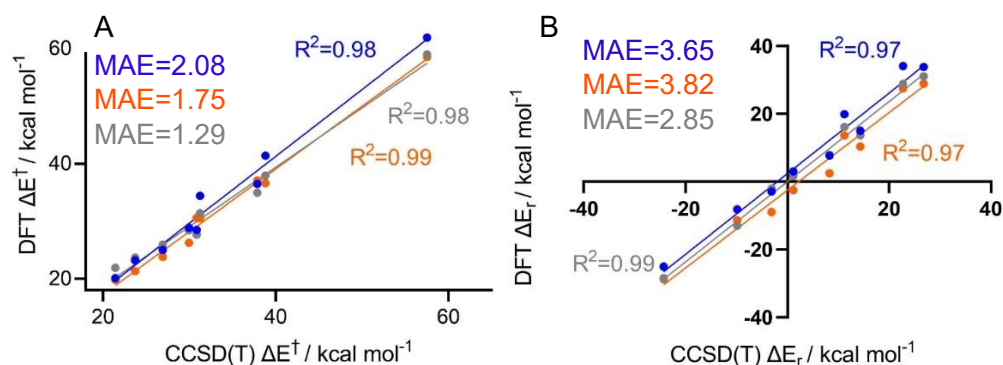
Figure A3 Correlation between xc // OPBE and CCSD(T) activation (A) and reaction energies (B). Blue dots: OPBE0 // OPBE; orange dots: M06-2X // OPBE; grey dots: M06 // OPBE. Statistical parameters (MAE: Mean Absolute Error, and R^2) are reported near the linear fit.

Along the Chapter, M06 // OPBE is employed as the main protocol.

Table A1 Activation and reaction electronic energies (kcal mol^{-1}) for the β-elimination reaction of chalcogenoxides (OS 0), chalcogeninic acids (OS +2) and chalcogenonic acids (OS +4). Level of theory: ZORA-OPBE/TZP-ae; TZ2P(-ae); QZ4P-ae.

basis	OS	S	Se	Te	S	Se	Te
	0	28.97	17.65	13.42	19.33	2.74	-5.37
TZP-ae	+2	35.91	23.28	18.15	31.89	13.91	4.48
	+4	53.00	27.66	20.71	28.96	-11.78	-27.20
			$\Delta E^{\ddagger}$			ΔE_r	
basis	OS	S	Se	Te	S	Se	Te
	0	29.42	18.85	16.14	19.70	4.14	-0.74
TZ2P-ae	+2	36.46	24.69	21.24	32.47	15.61	9.38
	+4	53.60	28.99	21.98	29.29	-10.79	-25.01
			$\Delta E^{\ddagger}$			ΔE_r	
basis	OS	S	Se	Te	S	Se	Te
TZ2P-sc	0	29.49	18.73	15.84	19.60	3.75	-0.94
	+2	36.50	24.59	20.96	32.41	15.16	9.17
	+4	53.71	29.05	21.86	29.08	-10.74	-24.64
			$\Delta E^{\ddagger}$			ΔE_r	
basis	OS	S	Se	Te	S	Se	Te
QZ4P-ae	0	30.77	19.17	16.66	21.28	4.16	0.00
	+2	37.66	24.91	21.77	33.73	15.31	10.00
	+4	54.58	29.14	22.32	30.01	-11.01	-24.74

Increasing the basis set from TZP to TZ2P leads to recovering 1-2 kcal mol^{-1} in activation energy and has a somewhat more relevant impact on reaction energies, which are affected in the $1 - 4$ kcal mol^{-1} range. Furtherly increasing the basis set to QZ4P leads to energetics which differs from those obtained with TZ2P of only fractions of kcal mol^{-1}. Moreover, the (small) frozen core approximation as applied

to TZ2P basis set does not seem to affect the energetics, with deviations from the TZ2P-ae are only a few fractions of kcal mol^{-1}. Thus, TZ2P basis set is deemed to be a reasonable compromise for the computation of chalcogenoxide elimination reactions, when small core approximation is available.

Table A2 Activation and reaction electronic energies (kcal mol^{-1}) for the for the β-elimination reaction of chalcogenoxides (minimal model) in OS 0, +2, +4. Level of theory: ZORA-xc/TZ2P(-ae)

xc	OS	ΔE‡			ΔE$_r$		
		S	Se	Te	S	Se	Te
OLYP	0	28.39	18.38	16.27	12.91	-2.63	-6.82
	2	34.97	24.13	21.38	25.89	8.95	3.30
	4	50.85	26.71	20.53	20.31	-18.91	-31.83
xc	OS	ΔE‡			ΔE$_r$		
		S	Se	Te	S	Se	Te
BLYP-D3(BJ)	0	23.22	13.75	12.16	13.77	-0.78	-3.87
	2	30.09	19.70	17.32	27.63	11.40	6.49
	4	44.95	20.70	15.07	20.17	-18.32	-29.82
xc	OS	ΔE‡			ΔE$_r$		
		S	Se	Te	S	Se	Te
OPBE	0	29.49	18.73	15.84	19.60	3.75	-0.94
	2	36.50	24.59	20.96	32.41	15.16	9.17
	4	53.71	29.05	21.86	29.08	-10.74	-24.64
xc	OS	ΔE‡			ΔE$_r$		
		S	Se	Te	S	Se	Te
B3LYP	0	29.36	19.00	16.88	11.00	-5.18	-10.12
	2	36.31	24.81	22.77	25.19	7.13	1.22
	4	53.38	28.23	21.58	20.91	-20.49	-35.39
xc	OS	ΔE‡			ΔE$_r$		
		S	Se	Te	S	Se	Te
M06-2X	0	31.99	22.36	20.71	13.92	-2.16	-8.87
	2	38.77	27.78	27.06	29.04	10.69	4.29
	4	59.24	37.36	31.34	27.37	-11.48	-28.48

Table A3. Activation and reaction electronic energies (kcal mol^{-1}) for the β-elimination reaction of chalcogenoxides (OS 0), chalcogeninic acids (OS +2) and chalcogenonic acids (OS +4). Level of theory: xc // OPBE.

xc	OS	ΔE‡				ΔE$_r$	
		S	Se	Te	S	Se	Te
BLYP	0	24.01	15.05	13.79	9.21	-5.51	-9.23
	+2	30.05	20.6	18.72	22.52	6.39	0.87
	+4	45.43	21.71	16.45	14.54	-24.50	-36.51

		ΔE‡				ΔE$_r$	
xc	OS	S	Se	Te	S	Se	Te
BP86	0	24.10	14.35	12.37	15.85	0.77	-3.50
	+2	30.87	20.14	17.39	29.29	12.69	6.72
	+4	47.17	22.69	16.45	23.10	-16.68	-29.74
		ΔE‡				ΔE$_r$	
xc	OS	S	Se	Te	S	Se	Te
HTBS	0	24.52	14.30	11.96	18.25	2.95	-1.61
	+2	31.50	20.11	16.97	31.42	14.71	8.57
	+4	47.97	23.29	16.78	26.39	-13.67	-27.07
		ΔE‡				ΔE$_r$	
xc	OS	S	Se	Te	S	Se	Te
PBE	0	24.85	14.87	12.69	18.71	3.49	-0.86
	+2	31.81	20.76	17.78	32.27	15.54	9.48
	+4	48.29	23.68	17.22	26.28	-13.62	-26.82
		ΔE‡				ΔE$_r$	
xc	OS	S	Se	Te	S	Se	Te
mPW	0	24.91	15.17	13.36	16.04	0.99	-3.12
	+2	31.60	20.94	18.28	29.39	12.85	7.04
	+4	47.84	23.36	17.23	23.21	-16.59	-29.41
		ΔE‡				ΔE$_r$	
xc	OS	S	Se	Te	S	Se	Te
PW91	0	24.65	14.62	12.48	18.75	3.44	-0.88
	+2	31.59	20.49	17.56	32.36	15.52	9.48
	+4	48.08	23.31	16.87	26.25	-13.91	-27.13
		ΔE‡				ΔE$_r$	
xc	OS	S	Se	Te	S	Se	Te
revPBE	0	25.85	16.42	14.60	14.40	-0.32	-4.35
	+2	32.31	22.12	19.59	27.43	11.34	5.67
	+4	48.25	24.45	18.57	21.28	-17.59	-30.05
		ΔE‡				ΔE$_r$	
xc	OS	S	Se	Te	S	Se	Te
RPBE	0	26.14	16.81	15.04	14.20	-0.45	-4.41
	+2	32.52	22.48	20.04	27.22	11.22	5.62
	+4	48.35	24.74	18.95	20.86	-17.76	-30.08
		ΔE‡				ΔE$_r$	
xc	OS	S	Se	Te	S	Se	Te
mPBE	0	25.20	15.40	13.34	17.49	2.43	-1.81
	+2	32.01	21.24	18.41	30.92	14.38	8.45
	+4	48.31	23.96	17.68	24.81	-14.75	-27.71
		ΔE‡				ΔE$_r$	
xc	OS	S	Se	Te	S	Se	Te
TPSS	0	26.29	16.96	15.53	16.01	1.56	-1.89
	+2	32.75	22.73	20.61	29.33	13.34	8.10
	+4	49.50	25.22	19.18	24.28	-14.58	-27.03
		ΔE‡				ΔE$_r$	
xc	OS	S	Se	Te	S	Se	Te
SCAN	0	28.89	18.30	15.77	22.22	6.15	1.40

xc	OS	ΔE‡				ΔE_r		
	+2	36.70	24.42	21.13	37.87	19.39	12.48
	+4	56.44	28.65	20.27	35.19	-8.54	-24.51
			ΔE‡				ΔE_r	
xc	OS	S	Se	Te	S	Se	Te
PBE0	0	31.00	20.14	17.39	19.15	2.37	-3.24
	+2	37.82	25.82	22.29	33.69	14.85	7.55
	+4	57.98	32.42	24.74	31.93	-10.44	-26.76
			ΔE‡				ΔE_r	
xc	OS	S	Se	Te	S	Se	Te
OPBE0	0	34.39	23.18	20.08	19.92	3.02	-2.93
	+2	41.37	28.84	25.00	33.84	15.04	7.67
	+4	61.88	36.47	28.47	34.11	-8.14	-25.06
			ΔE‡				ΔE_r	
xc	OS	S	Se	Te	S	Se	Te
mPW1PW	0	31.08	20.41	17.87	16.98	0.32	-5.11
	+2	37.73	25.98	22.71	31.34	12.66	5.53
	+4	57.60	32.16	24.75	27.47	-11.35	-28.68
			ΔE‡				ΔE_r	
xc	OS	S	Se	Te	S	Se	Te
M06-2X	0	30.57	21.31	19.81	13.66	-2.51	-8.95
	+2	36.60	26.23	23.76	28.88	10.38	2.51
	+4	58.52	37.07	30.59	27.47	-11.35	-28.68
			ΔE‡				ΔE_r	
xc	OS	S	Se	Te	S	Se	Te
M06	0	31.36	23.66	21.89	16.17	1.71	-2.03
	+2	37.91	28.42	25.92	31.10	13.67	7.88
	+4	58.93	34.93	27.65	28.86	-12.99	-28.45
			ΔE‡				ΔE_r	
xc	OS	S	Se	Te	S	Se	Te
TPSSh	0	28.65	18.80	17.15	16.33	1.14	-2.90
	+2	35.11	24.59	22.18	30.07	13.14	7.33
	+4	53.29	28.61	22.04	26.60	-13.39	-27.15
			ΔE‡				ΔE_r	
xc	OS	S	Se	Te	S	Se	Te
BP86-D3(BJ)	0	23.84	14.12	12.09	19.29	4.49	0.74
	+2	30.54	19.88	17.11	33.09	16.71	11.21
	+4	47.50	22.87	16.46	27.55	-12.14	-24.94

Table A4 Activation ($\Delta E^{\ddagger}$) and reaction (ΔE_r) energies (kcal mol^{-1}) for the β-elimination reaction of chalcogenoxides (OS 0), chalcogeninic acids (OS +2) and chalcogenonic acids (OS +4).[a]

	OS	Configuration	$\Delta E^{\ddagger}$	ΔE_r
Cys	0	RR	21.82 (22.34)	5.13 (6.65)
		RS	28.21 (28.34)	10.43 (11.59)
	+ 2	RR	28.97 (30.27)	20.92 (22.76)
		RS	31.54 (32.51)	22.03 (23.70)
	+ 4	R	52.51 (52.73)	17.59 (18.87)
Sec	0	RR	17.53 (18.54)	-6.05 (-2.86)
		RS	19.95 (20.81)	-4.33 (-1.35)
	+ 2	RR	19.96 (21.36)	4.17 (7.17)
		RS	24.96 (25.85)	6.85 (9.44)
	+ 4	R	32.52 (30.10)	-21.72 (-23.04)
Tec	0	RR	17.45 (17.81)	-10.61 (-4.66)
		RS	18.21 (18.28)	-9.83 (-4.20)
	+ 2	RR	19.00 (19.13)	-1.04 (3.72)
		RS	27.44 (26.83)	4.42 (8.51)
	+ 4	R	28.01 (24.82)	-35.58 (-35.32)

[a]Electronic energies computed at M06-2X // OPBE (M06 // OPBE) level of theory.

Table A5 Electronic energies (kcal mol^{-1}) for the cysteine, selenocysteine and tellurocysteine chalcogenoxide elimination in OS 0, +2, +4. Level of theory: M06 // OPBE.

		R	TS	P	DHA
Cys 0	RR	-2415.92	-2393.58	-515.03	-1894.24
	RS	-2420.86	-2392.52		
Sec 0	RR	-2387.41	-2368.87	-496.03	
	RS	-2388.92	-2368.11		
Tec 0	RR	-2365.99	-2348.18	-476.41	
	RS	-2366.45	-2348.17		
Cys 2	RR	-2642.94	-2612.67	-725.94	
	RS	-2643.88	-2611.37		
Sec 2	RR	-2610.93	-2589.57	-709.52	
	RS	-2613.20	-2587.35		
Tec 2	RR	-2596.19	-2577.06	-698.23	
	RS	-2574.15	-2574.15		
Cys 4	R	-2866.97	-2814.24	-953.86	
Sec 4	R	-2790.65	-2760.55	-919.45	
Tec 4	R	-2768.99	-2744.17	-910.07	

Table A6 Activation and reaction Gibbs free energies (kcal mol^{-1}) for the minimal model reactions. Level of theory: M06 // OPBE.

	$\Delta G^{\ddagger}$			ΔGr		
OS	S	Se	Te	S	Se	Te
0	28.27	21.31	19.92	2.88	-10.81	-14.07
+2	35.09	26.34	24.86	18.01	1.67	-2.91
+4	53.54	31.29	25.41	13.19	-27.33	-41.00

Table A7 Activation Gibbs free energies (kcal mol^{-1}) relative to the direct elimination mechanism of PhXEt ($\Delta G^{\ddagger}_{elm}$), to the elimination mechanism of their hydrates ($\Delta G^{\ddagger}_{hyd,elm}$), and reaction energies for the hydrates formation (ΔG^{hyd}_{r}). Level of theory: M06 // OPBE.

	$\Delta G^{\ddagger}_{elm}$	ΔG^{hyd}_{r}	$\Delta G^{\ddagger}_{hyd,elm}$
PhSEt	28.42	33.51	29.57
PhSeEt	20.74	10.69	30.15
PhTeEt	19.33	-8.36	35.65

Table A8 Hirshfeld partial charges (a.u.) on the X = O oxygen atom of chalcogenoxides in different oxidation states.

	S	Se	Te
0	-0.373	-0.428	-0.471
2	-0.349	-0.400	-0.452
4	-0.294	-0.347	-0.398

References

[1] J. Młochowski, R. Lisiak, H. Wójtowicz-Młochowska, in *PATAI'S Chem. Funct. Groups*, John Wiley & Sons, Ltd, Chichester, UK, **2011**.

[2] D. M. Freudendahl, S. Santoro, S. A. Shahzad, C. Santi, T. Wirth, *Angew. Chemie - Int. Ed.* **2009**, *48*, 8409–8411.

[3] S. Santoro, J. B. Azeredo, V. Nascimento, L. Sancineto, A. L. Braga, C. Santi, *RSC Adv.* **2014**, *4*, 31521–31535.

[4] L. Yu, H. Li, X. Zhang, J. Ye, J. Liu, Q. Xu, M. Lautens, *Org. Lett.* **2014**, *16*, 1346–1349.

[5] D. N. Jones, D. Mundy, R. D. Whitehouse, *J. Chem. Soc. D Chem. Commun.* **1970**, 86–87.

[6] K. B. Sharpless, R. F. Lauer, A. Y. Teranishi, *J. Am. Chem. Soc.* **1973**, *95*, 6137–6139.

[7] K. B. Sharpless, M. W. Young, R. F. Lauer, *Tetrahedron Lett.* **1973**, *14*, 1979–1982.

[8] H. J. Reich, I. L. Reich, J. M. Renga, *J. Am. Chem. Soc.* **1973**, *95*, 5813–5815.

[9] H. J. Reich, R. J. Hondal, *ACS Chem. Biol.* **2016**, *11*, 821–841.

[10] C. A. Kingsbury, D. J. Cram, *J. Am. Chem. Soc.* **1960**, *82*, 1810–1819.

[11] D. W. Emerson, A. P. Craig, I. W. Potts, *J. Org. Chem.* **1967**, *32*, 102–105.

[12] S. Uemura, S. Fukuzawa, *J. Am. Chem. Soc.* **1983**, *105*, 2748–2752.

[13] C. M. Gatley, L. M. Muller, M. A. Lang, E. E. Alberto, M. R. Detty, *Molecules* **2015**, *20*, 9616–9639.

[14] K. . Sharpless, K. M. Gordon, R. F. Lauer, D. W. Patrick, S. P. Singer, M. W. Young, *Chem. Scr.* **1975**, *8A*, 9.

[15] J. W. Cubbage, B. W. Vos, W. S. Jenks, *J. Am. Chem. Soc.* **2000**, *122*, 4968–4971.

[16]   H. Lee, M. P. Cava, *J. Chem. Soc. Chem. Commun.* **1981**, 277.

[17]   L. Orian, L. Flohé, *Antioxidants* **2021**, *10*, 1–22.

[18]   J. Jeong, Y. Kim, J. Kyung Seong, K. J. Lee, *Proteomics* **2012**, *12*, 1452–1462.

[19]   R. Bar-Or, L. T. Rael, D. Bar-Or, *Rapid Commun. Mass Spectrom.* **2008**, *22*, 711–716.

[20]   J. Jeong, Y. Jung, S. Na, J. Jeong, E. Lee, M.-S. Kim, S. Choi, D.-H. Shin, E. Paek, H.-Y. Lee, K.-J. Lee, *Mol. Cell. Proteomics* **2011**, *10*, M110.000513.

[21]   Z. Wang, B. Lyons, R. J. W. Truscott, K. L. Schey, *Aging Cell* **2014**, *13*, 226–234.

[22]   L. Orian, P. Mauri, A. Roveri, S. Toppo, L. Benazzi, V. Bosello-Travain, A. De Palma, M. Maiorino, G. Miotto, M. Zaccarin, A. Polimeno, L. Flohé, F. Ursini, *Free Radic. Biol. Med.* **2015**, *87*, 1–14.

[23]   R. Masuda, R. Kimura, T. Karasaki, S. Sase, K. Goto, *J. Am. Chem. Soc.* **2021**, *143*, 6345–6350.

[24]   K. M. Reddy, G. Mugesh, *Chem. - A Eur. J.* **2019**, *25*, 8875–8883.

[25]   P. A. Nogara, A. Madabeni, M. Bortoli, J. B. Teixeira Rocha, L. Orian, *Chem. Res. Toxicol.* **2021**, *34*, 1655–1663.

[26]   C. A. Bayse, B. D. Allison, *J. Mol. Model.* **2007**, *13*, 47–53.

[27]   P. E. Macdougall, N. A. Smith, C. H. Schiesser, *Tetrahedron* **2008**, *64*, 2824–2831.

[28]   G. Ribaudo, M. Bellanda, I. Menegazzo, L. P. Wolters, M. Bortoli, G. Ferrer-Sueta, G. Zagotto, L. Orian, *Chem. - A Eur. J.* **2017**, *23*, 2405–2422.

[29]   G. Ribaudo, M. Bortoli, A. Ongaro, E. Oselladore, A. Gianoncelli, G. Zagotto, L. Orian, *RSC Adv.* **2020**, *10*, 18583–18593.

[30]   N. Kondo, H. Fueno, H. Fujimoto, M. Makino, H. Nakaoka, I. Aoki, S. Uemura, *J. Org. Chem.* **1994**, *59*, 5254–5263.

[31] G. Ribaudo, M. Bortoli, E. Oselladore, A. Ongaro, A. Gianoncelli, G. Zagotto, L. Orian, *Molecules* **2021**, *26*, 2770.

[32] G. te Velde, F. M. Bickelhaupt, E. J. Baerends, C. Fonseca Guerra, S. J. A. van Gisbergen, J. G. Snijders, T. Ziegler, *J. Comput. Chem.* **2001**, *22*, 931–967.

[33] **N.d.**

[34] M. Swart, A. W. Ehlers, K. Lammertsma *, *Mol. Phys.* **2004**, *102*, 2467–2474.

[35] J. P. Perdew, K. Burke, M. Ernzerhof, *Phys. Rev. Lett.* **1996**, *77*, 3865–3868.

[36] N. C. Handy, A. J. Cohen, *Mol. Phys.* **2001**, *99*, 403–412.

[37] E. Van Lenthe, E. J. Baerends, J. G. Snijders, *J. Chem. Phys.* **1994**, *101*, 9783–9792.

[38] Y. Zhao, D. G. Truhlar, *Theor. Chem. Acc.* **2008**, *120*, 215–241.

[39] D. G. Liakos, Y. Guo, F. Neese, *J. Phys. Chem. A* **2020**, *124*, 90–100.

[40] F. Neese, *Wiley Interdiscip. Rev. Comput. Mol. Sci.* **2018**, *8*, DOI 10.1002/wcms.1327.

[41] F. Neese, *WIREs Comput. Mol. Sci.* **2012**, *2*, 73–78.

[42] F. Neese, A. Wolf, T. Fleig, M. Reiher, B. A. Hess, *J. Chem. Phys.* **2005**, *122*, 204107.

[43] D. A. Pantazis, F. Neese, *Wiley Interdiscip. Rev. Comput. Mol. Sci.* **2014**, *4*, 363–374.

[44] C. Lee, W. Yang, R. G. Parr, *Phys. Rev. B* **1988**, *37*, 785–789.

[45] F. Zaccaria, L. P. Wolters, C. Fonseca Guerra, L. Orian, *J. Comput. Chem.* **2016**, *37*, 1672–1680.

[46] J. J. Wilke, M. C. Lind, H. F. Schaefer III, A. G. Csaszar, W. D. Allen, *J. Chem. Theory Comput.* **2009**, 1511–1523.

[47] F. M. Bickelhaupt, K. N. Houk, *Angew. Chemie - Int. Ed.* **2017**, *56*, 10070–10086.

[48] L. P. Wolters, F. M. Bickelhaupt, *Wiley Interdiscip. Rev. Comput. Mol. Sci.* **2015**, *5*, 324–343.

[49] I. Fernández, F. M. Bickelhaupt, F. P. Cossío, *Chem. - A Eur. J.* **2012**, *18*, 12395–12403.

[50] E. D. Sosa Carrizo, F. M. Bickelhaupt, I. Fernández, *Chem. - A Eur. J.* **2015**, *21*, 14362–14369.

[51] Legault, C. Y. CYLview1.0b; Universit de Sherbrooke: Sherbrooke, QC, Canada, 2020. http://www.cylview.org

[52] L. Flohé, S. Toppo, L. Orian, *Free Radic. Biol. Med.* **2022**, *187*, 113–122.

[53] L. A. H. Van Bergen, G. Roos, F. De Proft, *J. Phys. Chem. A* **2014**, *118*, 6078–6084.

[54] V. Nascimento, E. E. Alberto, D. W. Tondo, D. Dambrowski, M. R. Detty, F. Nome, A. L. Braga, *J. Am. Chem. Soc.* **2012**, *134*, 138–141.

[55] Y. Nishibayashi, N. Komatsu, K. Ohe, S. Uemura, *J. Chem. Soc. Perkin Trans. 1* **1993**, 1133.

[56] B. G. Johnson, P. M. W. Gill, J. A. Pople, *J. Chem. Phys.* **1993**, *98*, 5612–5626.

[57] A. D. Becke, *Phys. Rev. A* **1988**, *38*, 3098–3100.

[58] A. D. Becke, E. R. Johnson, *J. Chem. Phys.* **2005**, *123*, 154101.

[59] S. Grimme, *Wiley Interdiscip. Rev. Comput. Mol. Sci.* **2011**, *1*, 211–228.

[60] E. R. Johnson, I. D. Mackie, G. A. DiLabio, *J. Phys. Org. Chem.* **2009**, *22*, 1127–1135.

[61] A. D. Becke, *J. Chem. Phys.* **1993**, *98*, 5648–5652.

[62] P. J. Stephens, F. J. Devlin, C. F. Chabalowski, M. J. Frisch, *J. Phys. Chem.* **1994**, *98*, 11623–11627.

[63]   Y. Zhao, D. G. Truhlar, *J. Chem. Phys.* **2006**, *125*, 194101.

[64]   J. P. Perdew, W. Yue, *Phys. Rev. B* **1986**, *33*, 8800–8802.

[65]   P. Haas, F. Tran, P. Blaha, K. Schwarz, *Phys. Rev. B* **2011**, *83*, 205117.

[66]   C. Adamo, V. Barone, *J. Chem. Phys.* **1998**, *108*, 664–675.

[67]   J. P. Perdew, J. A. Chevary, S. H. Vosko, K. A. Jackson, M. R. Pederson, D. J. Singh, C. Fiolhais, *Phys. Rev. B* **1992**, *46*, 6671–6687.

[68]   Y. Zhang, W. Yang, *Phys. Rev. Lett.* **1998**, *80*, 890–890.

[69]   B. Hammer, L. B. Hansen, J. K. Nørskov, *Phys. Rev. B* **1999**, *59*, 7413–7421.

[70]   C. Adamo, V. Barone, *J. Chem. Phys.* **2002**, *116*, 5933–5940.

[71]   V. N. Staroverov, G. E. Scuseria, J. Tao, J. P. Perdew, *J. Chem. Phys.* **2003**, *119*, 12129–12137.

[72]   J. Tao, J. P. Perdew, V. N. Staroverov, G. E. Scuseria, *Phys. Rev. Lett.* **2003**, *91*, 146401.

[73]   J. Sun, A. Ruzsinszky, J. P. Perdew, *Phys. Rev. Lett.* **2015**, *115*, 036402.

[74]   C. Adamo, V. Barone, *J. Chem. Phys.* **1999**, *110*, 6158–6170.

[75]   T. A. Hamlin, M. Swart, F. M. Bickelhaupt, *ChemPhysChem* **2018**, *19*, 1315–1330.

[76]   A. P. Bento, M. Solà, F. M. Bickelhaupt, *J. Comput. Chem.* **2005**, *26*, 1497–1504.

[77]   M. Bortoli, M. Bruschi, M. Swart, L. Orian, *New J. Chem.* **2020**, *44*, 6724–6731.

[78]   M. Bortoli, F. Zaccaria, M. D. Tiezza, M. Bruschi, C. F. Guerra, F. Matthias Bickelhaupt, L. Orian, *Phys. Chem. Chem. Phys.* **2018**, *20*, 20874–20885.

[79]   L. P. Wolters, Y. Ren, F. M. Bickelhaupt, *ChemistryOpen* **2014**, *3*, 29–36.

[80]   P. Vermeeren, T. Hansen, P. Jansen, M. Swart, T. A. Hamlin, F. M. Bickelhaupt, *Chem. - A Eur. J.* **2020**, *26*, 15538–15548.

# 7 Reduction of Chalcogenoxides by Thiols: The Key Intermediates

adapted from

A. Madabeni, L. Orian

Int. J. Mol. Sci. 2023, 24(9), 7754

7.1 Introduction

Since the 60s,[1] sulfoxides have been well-known for their capacity of acting as mild oxidizing agents. Selenoxides can engage in a similar, but faster, redox chemistry, and can easily oxidize thiols to disulfides at room temperature.[2–5] (Scheme 7.1)
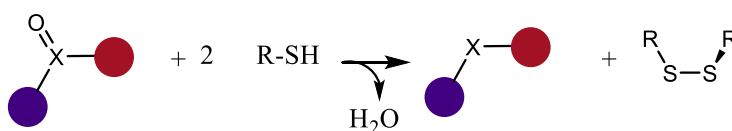
Scheme 7.1 General reaction for the reduction of a chalcogenoxide (X = S, Se) to a chalcogenide, with concomitant oxidation of two equivalents of thiol to disulfide.

Attempts to exploit this reactivity in a glutathione peroxidase (GPx) - like catalytic cycle[6,7] have been pursued and, in these cases, the oxidation of the selenide to selenoxide is usually rate determining, while the reduction from selenoxide to selenide is, as above stated, fast.[8,9] However, selenoxides are more likely to act as pro-oxidants species rather than as intermediates in GPx-like cycles.[10] Particularly,

Iwaoka and co-workers showed that soluble selenoxides can be used to induce fast and complete disulfide formation in proteins having multiple free reduced thiols.[4,9]

In addition to the synthetic value of the reaction, sulfoxides and selenoxides can be produced *in-vivo* by the oxidation of critical methionine (Met) and selenomethionine (SeMet) residues to methionine sulfoxide (MetO) and selenomethionine selenoxide (SeMetO), respectively. These oxidized amino acids are then reduced back either by free thiols or by enzymatic processes. Particularly, the reduction of SeMetO has been repeatedly shown to proceed in a fast and spontaneous way at room temperature in the presence of low molecular mass thiols such as glutathione.[2,3] Conversely, MetO requires its own reducing enzyme, i.e. Methionine Sulfoxide Reductase (Msr).[11]

Msrs are antioxidant repair enzymes which catalyze the reaction shown in Scheme 7.1. Two structurally different classes of enzymes constitute the Msrs family, MsrA and MsrB, specific for the S and R epimers of MetO, respectively, which are generated by the oxidation of the prochiral sulfur nucleus. While MsrAs display some variability, with enzymes working *via* one, two, or even three reactive Cys residues, MsrBs usually employ one or two cysteines (Cys) to reduce MetO to Met, namely a catalytic Cys (CysA) and a recycling Cys (CysB). Interestingly, some members of both classes naturally evolved to employ one catalytic selenocysteine (Sec) instead of CysA.[12] In mammals, this is the case of one of the three known MsrB enzymes, i.e., MsrB1, in which Sec95 (numeration refers to Mus Musculus MsrB1) acts as the catalytic CysA. (Figure 7.1)
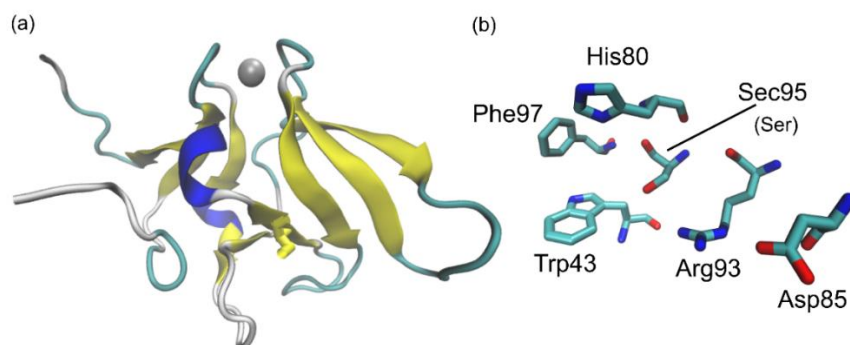

Figure 7.1 (A) Crystal structure of human MsrB1 (PDB: #3MAO) with Sec95 (mutated to Ser95) represented in licorice; and (B) close-up on the residues surrounding Sec95, which are known to play a role in Msr catalysis.[12]

As verified for other selenoenzymes[13] (e.g. GPx4),[14] site-directed mutagenesis proved that the presence of Sec instead of Cys in the active site of human MsrBs provides a kinetic advantage in MetO reduction.[12,15]

Despite possessing diverse structural features, MsrA and MsrB are postulated to reduce MetO employing similar reaction pathways, even if different residues might be involved in the stabilization of the transition states and intermediates.[12,16–18] First, CysA attacks the sulfur atom of the sulfoxide, while one proton is dislocated from a catalytic pocket residue to the oxygen atom of the sulfoxide moiety. This leads to the formation of a thiosulfurane.[19] This first step is analogous to the one postulated for the reduction of sulfoxides by free thiols. Similarly, in the reduction of selenoxides, such as SeMetO, the formation of a selenurane is invoked.[3] (Scheme 7.2)
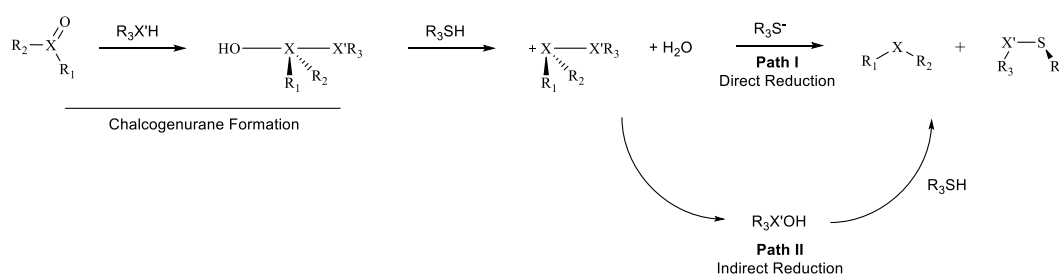
Scheme 7.2 Schematic mechanism for the reduction of chalcogenoxides to chalcogenides. Chalcogenurane (X=S, Se) formation in the first step of sulfoxides and selenoxides reaction with thiols and further direct (path I) or indirect (path II) reduction of the chalconium intermediate to sulfide and disulfide, or to sulfenic acid and sulfide respectively. In our study, R_1, R_2, R_3 = CH_3.

Then, the chalcogenurane undergoes O–X bond breaking, with formation of a chalconium cation.[16,20] In MsrA, a suitably activated water molecule was found to act as nucleophile, converting the catalytic CysA (Sec95) to its sulfenic (selenenic) acid form and leading to the reduced methionine.[16] The sulfenic/selenenic acid is then reduced by condensation with a resolving Cys to a disulfide/selenyl sulfide bond, which is ultimately further reduced by the thioredoxin system to release the ground state Msr enzyme.[12] The formation of a sulfenic acid (RX'OH in Scheme 7.2) was assessed via X-ray crystallography, mass spectrometry and by trapping experiments.[16,21] Conversely, to the best of our knowledge, no evidence has been so far reported on the formation of this intermediate when the reaction occurs with free thiols, suggesting a direct reduction in which the nucleophilic thiolate attacks

the sulfurane/sulfonium cation. However, since sulfenic acids can undergo rapid condensation to disulfides, their involvement in the reaction cannot be completely ruled out.[20] Interestingly, previous computational investigation of the Msr catalytic cycle showed that the formation of sulfenic acid (Scheme 7.2, path II) is kinetically disfavored with respect to the direct reduction of the chalconium cation (Scheme 7.2, path I), even if both processes have a biologically accessible activation energy[19] and might occur in parallel. In fact, the direct reduction was postulated also in the biological literature before the experimental detection of sulfenic acid was reported.[11] The similarities between the reduction mechanism of sulfoxides by free thiols and the catalytic mechanism of Msrs should not come unexpected, since the plausible mechanism for the enzyme was partly built upon previous small-molecules mechanistic knowledge.[11,22]

Within this Chapter, Density Functional Theory (DFT) calculations are employed to investigate the mechanism of reduction of selenoxides, revisiting *in silico* also some known aspects of the reduction mechanism of sulfoxides. Simple molecular models are employed to draw general conclusions about the title reaction and gain insight on the role of the chalcogen. In fact, intrigued by the natural occurrence of Sec in selenoprotein MsrB1, one of the few human selenoproteins with a known function, we aim at the exploration of the role of Se also when a selenol acts as a reducing agent instead of a thiol. Particular attention will be given to the preliminary sulfurane and selenurane formation, which is a key reactive step shared by both the enzymatic and the molecular mechanism. While our small model clearly cannot capture all of the structural complexity of Msr, the intrinsic trends for the effect of the chalcogen can be expected to be qualitatively transferable also in an enzymatic context, as reported for GPx and proteins with *peroxidatic* cysteines/selenocysteines.[23–25] For the other steps of the reduction mechanism (i.e. following the chalcogenurane formation) a more cautious comparison with the enzyme will be done, since the molecular and the enzymatic pathways might at least partially diverge.

7.2 Computational Methods

All Density Functional Theory (DFT) calculations were carried out using ADF2019.[26,27] For geometry optimization of all minima and transition states, BLYP density functional was employed, combined with the Grimme D3 dispersion correction and the Becke-Johnson Damping.[28–32] The TZ2P basis set (triple-ζ with two sets of polarization functions on each atoms) with the small frozen core approximation was used in all calculations. Scalar relativistic effects were included at the zeroth-order relativistic approximation (ZORA), as implemented in ADF.[33] This level of theory, i.e. ZORA-BLYP-D3(BJ)/TZ2P, was found adequate for the structural description of organochalcogenides. To ascertain the nature of each optimized geometry, frequency calculations were performed in gas phase at the same level of theory. All minima displayed only positive frequencies, while transition states displayed only one imaginary frequency associated to the nuclear motion along the reaction coordinate. Additionally, for selected transition states (TS), the minimum energy path connecting the TS to the two closest minima was obtained via an Intrinsic Reaction Coordinate (IRC) procedure as implemented in the ADF software.[35]

To increase the accuracy of the energy description, single-points calculations were performed using M06 functional combined to all-electron TZ2P basis set,[36] in accord with the benchmark provided in Chapter 6. The effect of implicit solvation was included with M06 functional using the COSMO model of solvation as implemented in ADF.[43] Water was chosen as the solvent, to account for the effect of a strongly polar environment, which is the most likely to affect significantly the energetics. All energetics discussed in the main text were thus computed at the COSMO-ZORA-M06/TZ2P-ae // ZORA-BLYP-D3(BJ)/TZ2P. For simplicity, this level of theory is from now on labelled as COSMO-M06 // BLYP-D3(BJ).

To provide a deeper insight into the effect of the chalcogen (S vs Se) on the chalcogenoxide and on the chalcogenol, the Activation Strain Model (ASM) of chemical reactivity was applied to step 1 in Scheme 7.2 employing the program pyfrag 2019.[44] (see Chapter 2)

Since both ASM and EDA can be rigorously applied only to gas phase electronic energies, M06 // BLYP-D3(BJ) calculations were employed, i.e., results

obtained without COSMO solvation model. Further details are given in Paragraph 7.3.3. For sake of clarity, only electronic energies are discussed in the main text. Since the interesting comparison is between structurally analogous reactions, entropy corrections are expected to leave the relative trends unaffected. Indeed, Gibbs free activation and reaction energies for the key mechanistic step followed essentially analogous trends for the effect of the chalcogen on the chalcogenoxide and on the chalcogenol (DMSO vs DMSeO + CH_3SH and DMSO+ CH_3SH vs DMSO + CH_3SeH respectively, Appendix B, Table B1)

7.3 Results and Discussion

To investigate the title reaction, a minimal model was employed consisting in the reduction of dimethyl sulfoxide (DMSO) and dimethyl selenoxide (DMSeO) by two methyl thiols (CH_3SH). Moreover, to probe the role of Sec95 in MsrB1, the same reaction was investigated with one methyl selenol (CH_3SeH) and one CH_3SH. The reaction with two CH_3SeH was not investigated, since, to the best of our knowledge, no Msr selenoprotein possesses two active Sec residues. Moreover, the selenol was considered to react as first with the chalcogenoxide, to form the chalcogenurane in Scheme 7.2.

7.3.1 Mechanistic details

As modelled in this Chapter, the mechanism can be described as three progressive steps, i.e., (a) chalcogenurane formation; (b) chalconium cation formation (or chalcogenurane disruption); and lastly (c) sulfide or selenide release. (Scheme 7.3) This pathway closely resembles the one investigated by Balta *et al* which was limited to DMSO and methyl thiols.[20] Differently, two water molecules are employed to mediate the proton transfer from $CH_3X'H$ to the chalcogenoxide oxygen as previously done by Bayse for the reduction of seleninic acid.[49]

Representative structures along the mechanism in gas phase are displayed in Figure 7.2. Starting from a reactant complex (RC1), the first step passes through a TS in which the two chalcogens X and X' come close, and in a concerted fashion the proton of $CH_3X'H$ is shuttled through the two water molecules to the
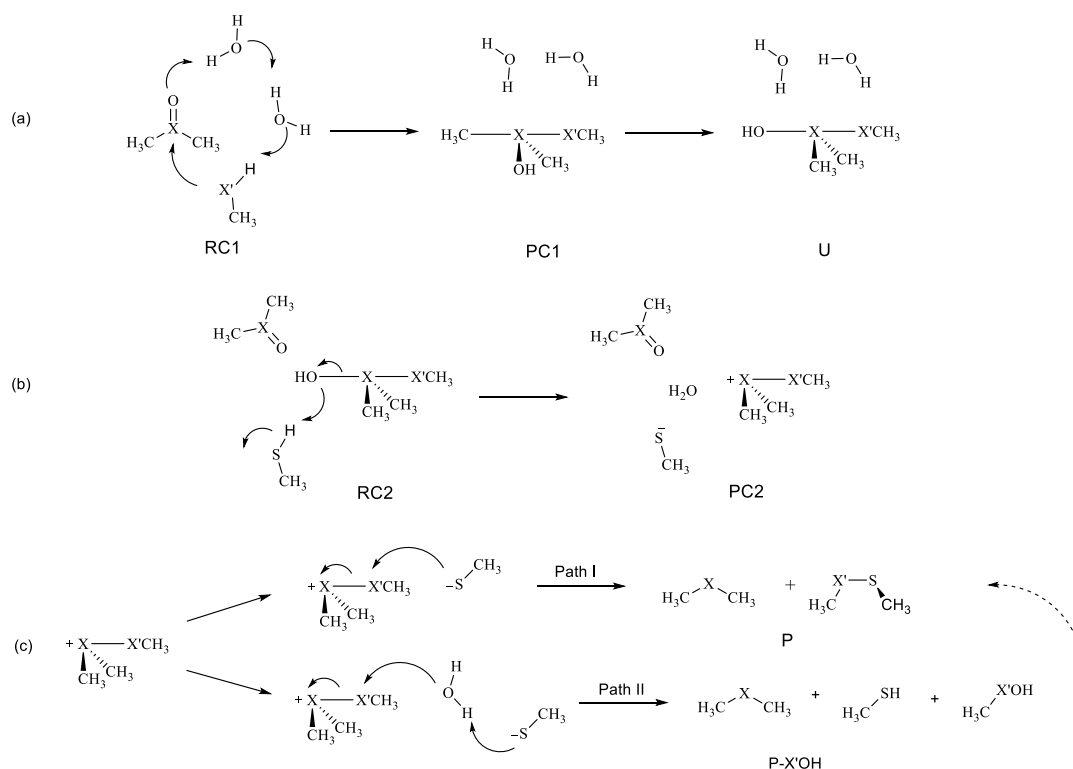
Scheme 7.3 All reaction mechanisms investigated in this Chapter. (a) Chalcogenurane (U) formation; (b) Chalcogenurane disruption and chalconium cation formation (PC2); (c) Chalcogenide (P) release either via a direct mechanism (path I) or indirect mechanism (path II) passing through a sulfenic or selenenic acid (P-X'OH). The condensation of sulfenic acid (dashed arrow) to the final products P was not investigated.
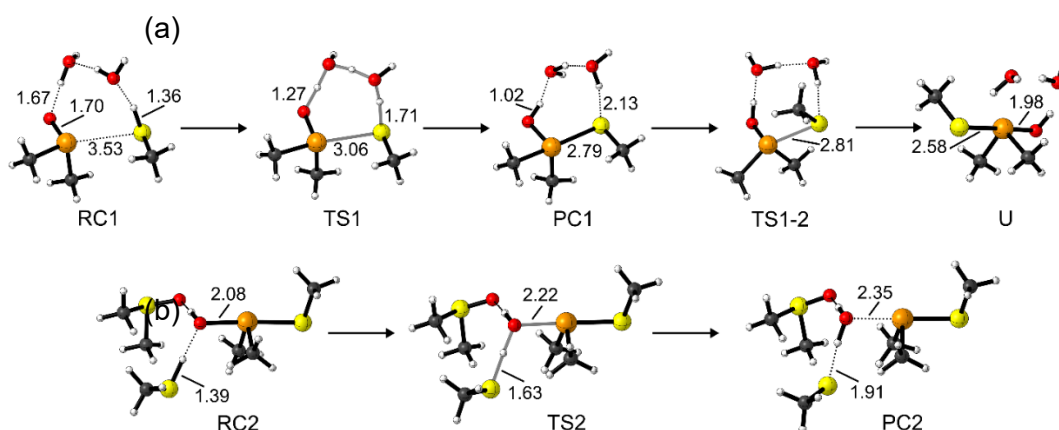

Figure 7.2 Representative structures along the reduction mechanism of DMSeO by CH$_3$SH. (a) selenurane (U) formation; (b) selenurane (U) disruption and selenonium cation (PC2) formation. Interatomic distances (in Å) that undergo relevant changes along the reaction are indicated. Level of theory: ZORA-BLYP-D3(BJ)/TZ2P.

chalcogenoxide moiety (TS1). A product complex (PC1) is formed, in which the central chalcogen is surrounded by an OH group, the chalcogenolate CH$_3$X', and the A subsequent isomerization (TS1-2) leads to the canonical chalcogenurane U with a linear O–X–X' bond.

The O–X bond breaking is modelled starting from an adduct between the second CH$_3$SH and U (RC2). The O–X bond of U is then cleaved by a proton transfer from CH$_3$SH (TS2), leading to an adduct between methyl thiolate, water and the chalconium cation (PC2). To stabilize the released water molecule, a second DMSO was employed in RC2, TS2 and PC2, as previously done by Balta *et al.*[20] While this choice may seem rather arbitrary, the bulk solvent can be expected to take on the same role when the reaction occurs in solution; similarly, specific hydrogen bond acceptor residues can act as DMSO when the reaction occurs in the protein environment.[19] As shown in Scheme 7.3, the chalconium cation can then be reduced to chalcogenide by either a direct or indirect pathway. In gas phase, both reactions proceed without any appreciable activation energy at our level of theory. This can be expected, since the reaction involves two charged reactants – thus, the charge recombination occurs spontaneously leading either to sulfenic/selenenic or directly to the dichalcogenide and to the sulfide/selenide. Further details about this step will be discussed later on in Paragraph 7.3.4.

7.3.2 Energetics and role of the chalcogen

The reaction profiles for the steps described in 3.1 were computed for X, X' = S, Se, in order to provide a comprehensive insight into the reduction of sulfoxides, selenoxides, and into the role of Sec vs Cys. (Figure 7.3) First, DMSO reduction will be compared to DMSeO reaction when CH$_3$SH is the only reducing agent, (Figure 7.3a blue vs Figure 7.3b, red.); then, the features of the potential energy surface (PES) when CH$_3$SeH is involved will be discussed (Figure 7.3a turquoise and 7.3b orange).

The first step of the reaction is characterized by the highest activation energy of the whole mechanism, i.e., 21.81 kcal mol^{-1} for DMSO + CH$_3$SH, and 19.58 for DMSeO + CH$_3$SH. Interestingly, after the proton is transferred from the thiol to the chalcogenoxide, DMSeO forms a much more stable adduct with the thiolate than
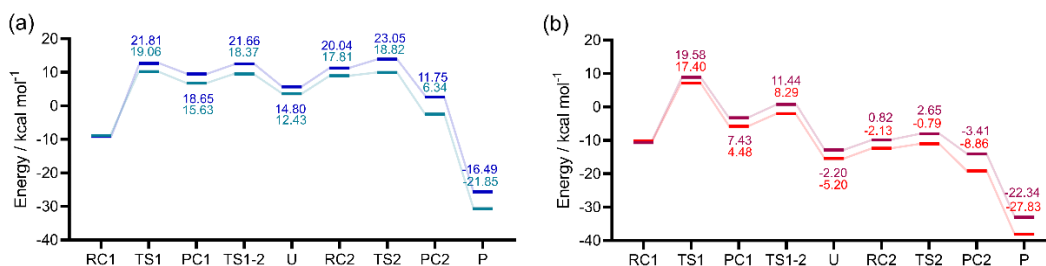
Figure 7.3 Reaction profiles (kcal mol⁻¹). (a) Comparison between the reduction of DMSO by CH₃SH (blue) and CH₃SeH (turquoise); (b) Comparison between the reduction of DMSeO by CH₃SH (dark red) and CH₃SeH (orange). Activation and reaction energies with respect to RC1 are shown on the profile. Level of theory: COSMO-M06 // BLYP-D3(BJ).

DMSO (PC1). Then, a low energy isomerization transition state connects PC1 to the canonical chalcogenurane with a linear O–X–S arrangement. The difference in stability between DMSO and DMSeO PC1 is mirrored by the stability of U, which is ca. 18 kcal mol⁻¹ more stable for DMSeO (-12.88 kcal mol⁻¹ with respect to the free reactants, and almost iso-energetic to the corresponding RC1) than for DMSO (lying +5.67 kcal mol⁻¹ with respect to the free reactants and almost 15 kcal mol⁻¹ higher than the corresponding RC1). The difference in stability of the two adducts/chalcogenuranes is not surprising, since Se forms more easily hypervalent species than S,[13,37] and it appears to be the most striking difference in the two mechanistic profiles.

Considering the chalcogenurane disruption through TS2, DMSO and DMSeO display a very similar activation energy with respect to closest adduct RC2 (2.65 kcal mol⁻¹ vs 1.83 kcal mol⁻¹, respectively). However, TS2 is located way higher on the PES for DMSO than for DMSeO; since it lies even higher than TS1, i.e., 23.05 kcal mol⁻¹ above RC1. For DMSO, the chalcogenurane formation and disruption proceed with an overall barrier of ca. 23 kcal mol⁻¹. Conversely, for DMSeO, U formation and disruption proceed with an overall barrier corresponding only to the formation of U, i.e. 19.58 kcal mol⁻¹. In both cases, however, the chalcogenurane formation appears to be a key step, contributing mostly or totally to the activation energy required for the chalcogenoxide reduction and gives a peculiar shape to the PES.

In a somewhat unexpected contrast with these data, kinetic analysis for the reduction of SeMetO showed that U disruption might be slower than U formation.[3]

However, SeMetO is present in solution partly as a cyclic intramolecular selenurane[50]; thus, its reduction mechanism will likely differ from the one of DMSeO. This aspect for sure needs future attention, but it is beyond the scope of the current investigation.

Lastly, the fully reduced chalcogenide is released after the thiolate attacks the chalconium cation. The process appears to be energetically well-favored for both DMSO and DMSeO but is almost 8 kcal mol^{-1} more favored for the latter (or ca. 6 kcal mol^{-1} more favored with respect to the respective RC1). This is in line with the well-known relative instability of selenoxides with respect to sulfoxides. These results comply well with the faster reduction of selenoxides with respect to sulfoxides. Indeed, while sulfoxides require long times (hours) to induce disulfide formation, or mildly high temperature, selenoxides induce disulfide formation within minutes or even seconds at room temperature.[3,5,9]

The same discussion holds true when CH$_3$SeH acts as the reducing agent instead of CH$_3$SH. Indeed, minimal changes in the overall mechanism are predicted from our DFT calculations. (Figure 7.3a turquoise and 7.3b orange) However, as expected, CH$_3$SeH lowers the activation energy for U formation (e.g., while DMSO+CH$_3$SH has an activation energy leading to PC1 of 21.81 kcal mol^{-1}, the same step for DMSO+CH$_3$SeH has an activation energy of 19.06 kcal mol^{-1}). Also, the downstream reaction steps (i.e., isomerization and PC2 formation) proceed with slightly lower activation energy when CH$_3$SeH acts as the chalcogenol, leading in the very end to more stable products. However, compared to U formation, the other activation energies remain way lower. In any case, both these aspects can contribute to the advantage of Sec over Cys in MrsB selenoenzyme since they are intrinsic in the properties of either the chalcogenol itself or of the products.

7.3.3 Insight from activation strain analysis

Selenoxides react faster than sulfoxides,[5,13,51] and selenols engage in a faster reactivity with chalcogenoxides than the lighter thiols as deduced from Msr enzymatic studies.[12,15] While our calculations reproduced and rationalized these observations, to reach a deeper understanding of these effects, DFT energy data must be translated into chemically meaningful concepts. Thus, in the spirit of *give us*

insight and numbers,[52] the ASA/EDA approach was employed as described in the Chapter 2. ASA and EDA can be rigorously applied only to gas phase calculations; luckily, the effect of the chalcogen on our reactions is qualitatively the same both in gas phase and in water. Thus, a discussion of gas phase results can be done and general insight can be obtained with confidence. ASA/EDA plot are displayed in Figure 7.4. Particularly, the first step of the reaction was investigated in detail, i.e., the proton transfer from the chalcogenol to the chalcogenoxide, with the concerted formation of the X–X' chalcogen bond of PC2. This step has the highest barrier in all the four mechanisms.
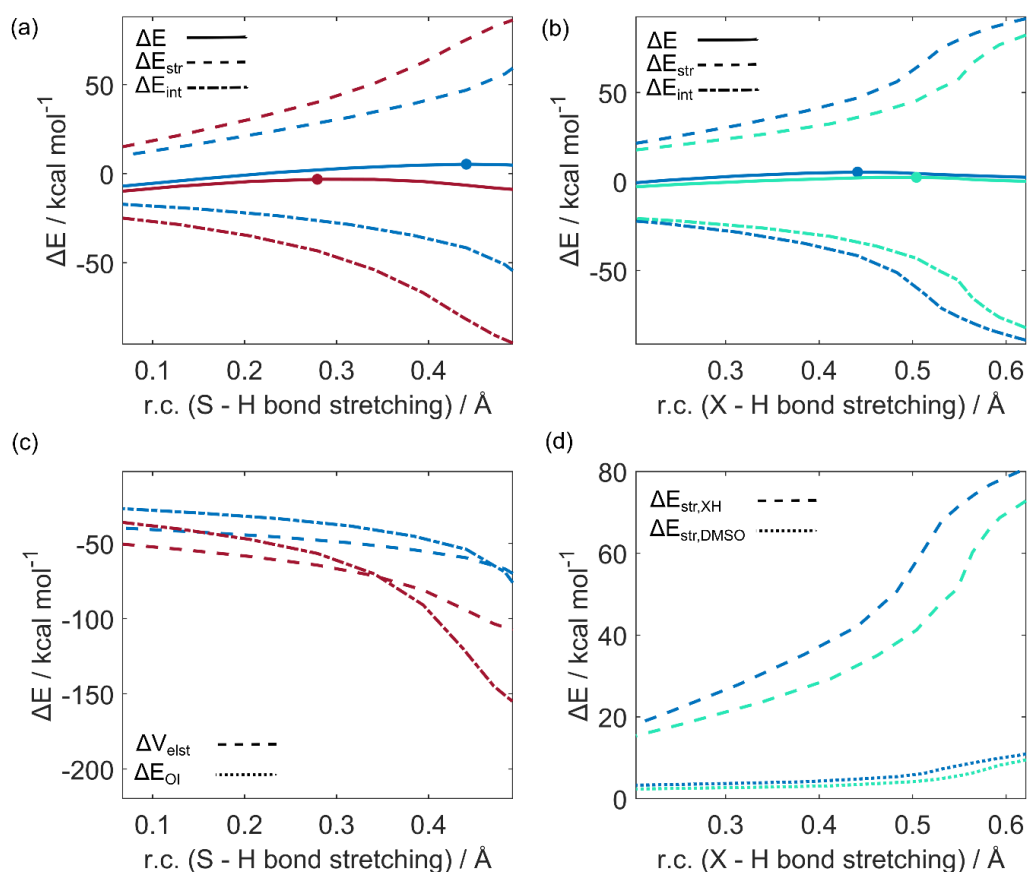

Figure 7.4 Activation Strain Analysis and Energy Decomposition Analysis for three representative reactions, i.e., DMSO+CH$_3$SH (dark blue); DMSeO+CH$_3$SH (dark red); DMSO+CH$_3$SeH (turquoise). (a) ASA showing the role of the chalcogen in the chalcogenoxide (DMSO vs DMSeO); (b) ASA showing the role of the chalcogen in the chalcogenol, CH$_3$SH vs CH$_3$SeH; (c) EDA showing the role of the chalcogen in the chalcogenoxide (stabilizing components only, Pauli repulsion can be found in Appendix B, Figure B1); (d) Strain decomposition analysis showing the role of the chalcogen in the chalcogenol.

Our systems were partitioned into two reactant-like fragments: one fragment consists in the chalcogenoxide moiety, and the other is composed by the chalcogenol and two water molecules. Focusing on the role of the chalcogen, DMSO+CH$_3$SH reaction was compared to DMSeO+CH$_3$SH to understand the difference between the sulfoxide and the selenoxide; then, DMSO+CH$_3$SH reaction was compared to DMSO+CH$_3$SeH to understand the role of the chalcogenol. The energy profiles were projected onto the critical X'–H bond stretching, which undergoes a well-defined change along the reaction.

The comparison between the $\Delta E(\xi)$ profiles for DMSO+CH$_3$SH and DMSeO+CH$_3$SH (Figure 7.4a) clearly shows that DMSeO displays an earlier TS than DMSO (r.c. ca 0.3 and 0.45 Å respectively), and this leads to a higher activation energy when the former is involved. ASA highlights that this is due to a more stabilizing $\Delta E_{int}(\xi)$ along the whole r.c. for DMSeO, but particularly in the surroundings of the TSs. EDA (Figure 7.4c) pinpoints how both a stronger electrostatic and orbital interaction between the two fragments is responsible for the more stabilizing $\Delta E_{int}(\xi)$ of DMSeO. Indeed, both $\Delta V_{elst}(\xi)$ and $\Delta E_{OI}(\xi)$ are more stabilizing for DMSeO than for DMSO. While, in magnitude, $\Delta V_{elst}(\xi)$ appears to play a slightly more significant role in the beginning of the reaction, $\Delta E_{OI}(\xi)$ soon becomes more and more determinant as the S–H bond is broken and X–X' bond is formed. Thus, both factors contribute to some extent to the enhanced reactivity of DMSeO, and no attempt to identify a unique predominant factor is pursued.

The larger $\Delta V_{elst}(\xi)$ term for DMSeO is interpreted as a consequence of the more charge separated Se–O bond, when compared to the S–O bond, which leads to a more negative potential on the oxygen atom and to a higher positive potential on the chalcogen nucleus of DMSeO,[13,37] as already highlighted in Chapter 6. This results in a combined stronger electrostatic interaction with the proton transferred from water, as well as with the nucleophilic thiolate. Finally, the more stabilizing $\Delta E_{OI}(\xi)$ is ascribed to the low-lying LUMO of DMSeO when compared to DMSO, which can more easily interact with the HOMO of CH$_3$SH. (Figure 7.5) Thus, DMSeO takes part to the reaction as the electrophile, and the thiol / thiolate as the nucleophile, resulting in a 1,2 nucleophilic addition reaction.
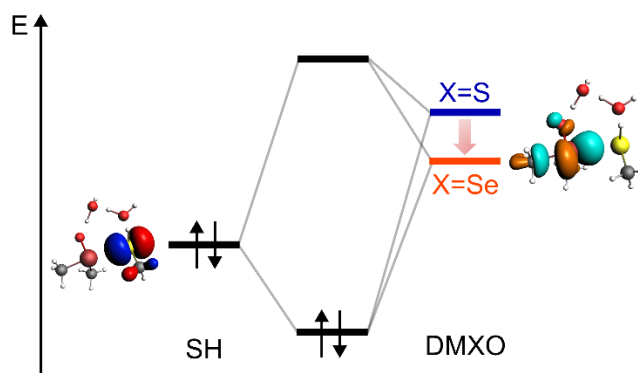
Figure 7.5 Schematic qualitative Molecular Orbital diagram for the orbital interaction between the HOMO of CH$_3$SH (on the left) and the LUMO of DMXO (on the right). The lower energy of DMSeO LUMO is emphasized with an arrow pointing downward. The calculated Kohn-Sham molecular orbitals for DMSeO+SH fragments are represented on the side of the diagram (isodensity value 0.05; r.c. = 0.341).

Conversely, the comparison of the ASA plots for DMSO+CH$_3$SH and DMSO+CH$_3$SeH (Figure 7.4b) shows a quite different picture. Particularly, while the $\Delta E(\xi)$ profile is always stabilized when CH$_3$SeH acts as the nucleophile as compared to CH$_3$SH, CH$_3$SeH reaches the transition state later along the r.c. Despite this, DMSO+CH$_3$SeH reaction is characterized by a significantly lower $\Delta E_{str}(\xi)$ profile, which is ultimately responsible for the faster reactivity of selenols as compared to thiols. Since the chalcogenoxide is the same in the two reactions, it is reasonable to assume this effect to be directly related to the ease by which X'–H distorts. However, to provide a quantitative discussion, the overall $\Delta E_{str}(\xi)$ was furtherly decomposed into the separate contributions of the two fragments (Figure 7.4d). As expected, DMSO gives a minimal (and very similar for the two reactions) contribution to the overall $\Delta E_{str}(\xi)$; conversely, X'–H bond breaking provides the determinant contribution to $\Delta E_{str}(\xi)$, with CH$_3$SeH undergoing a less destabilizing distortion than CH$_3$SH. This physico-chemical mechanism is, indeed, quite general, and was explored in detail by Dalla Tiezza *et al* in model systems of GPx,[25] and complies with the well-known increased acidity of the heavier chalcogenols as compared to the lighter ones.

Overall, the effect of the chalcogen on the chalcogenoxide is electrophilic in nature; conversely, CH$_3$SeH is a better nucleophile because it undergoes an easier heterolytic dissociation, shuttling the proton to the chalcogenoxide and nucleophilically binding it.

7.3.4 Direct vs indirect reduction

As last goal, a more exhaustive discussion about the final step of the reduction mechanism is presented (Scheme 7.3, part 3). As previously anticipated, all the attempts to optimize transition state structures in gas phase for both processes (i.e. direct and indirect, path I and II respectively in Scheme 7.3) failed, likely because the negatively charged thiolate and the positively charged chalcogenonium cation spontaneously recombine.[1] Thus, to provide a quantitative discussion, an analysis was carried out by optimizing the geometries in the presence of the solvation field, i.e., at COSMO-ZORA-BLYP-D3(BJ)/TZ2P. Then, single-points in solvent were done using the M06 functional combined to TZ2P-ae basis set in order to have energy values consistent with the rest of the points along the mechanism.

Interestingly, no transition state was located for the direct pathway. Even in the presence of the solvent field, the thiolate and the chalconium cation recombined without any appreciable activation energy at our level of theory when starting from a linear X–X'–S arrangement. Balta et al[20] located a low energy TS for the reduction of DMSO. But it is worth to notice that in their case, the process was modelled with a non-linear S–S–S arrangement, which is expected to disfavor an S_N2-like process. Since the transition state they reported was already low in energy ($\Delta E^{\ddagger}$ ca. 2 kcal mol^{-1}), we confidently believe that with a linear arrangement the process should be almost instantaneous also at their level of theory. Conversely, water activation by the thiolate, which leads to the formal OH$^-$ attack to the chalcogenurane appears to be an activated process. (Figure 7.5).

The activation energy of the process is modulated by both the chalcogen on the chalcogenoxide and by the chalcogen on CH$_3$X'H, with a larger influence of the latter. Indeed, changing the chalcogen from DMSO to DMSeO affects $\Delta E^{\ddagger}_{indir}$ by roughly 3 kcal mol^{-1}. Conversely, changing the chalcogen on CH$_3$X'H leads to a $\Delta\Delta E^{\ddagger}$ of more than 7 kcal mol^{-1} at our level of theory. (Table 7.1)

---

[1] The same result (i.e., barrierless process) was reproduced also by optimizing the system in gas phase with M06 functional directly.
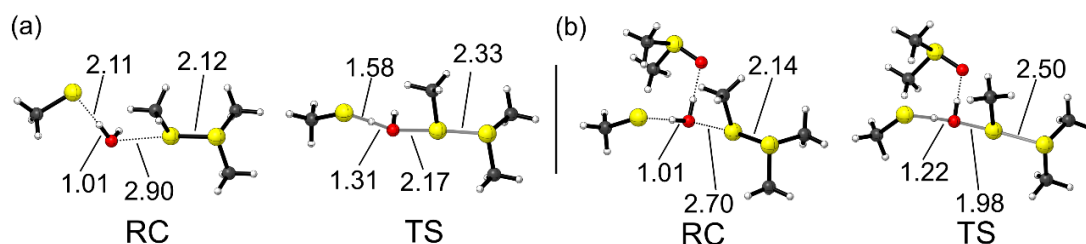
Figure 7.5 Representative structures for the indirect reduction mechanism of DMSO. (a) without an extra DMSO stabilizing H_2O; (b) with an extra DMSO stabilizing H_2O. Interatomic distances (in Å) that undergo relevant changes along the reaction are indicated. Level of theory: COSMO-ZORA-BLYP-D3(BJ)/TZ2P.

Table 7.1 Activation and reaction energies[1] (kcal mol^{-1}) for the direct and indirect evolution of the chalconium cation towards disulfide / selenyl sulfide or sulfenic / selenenic acid respectively.[2]

	$\Delta E^{\ddagger}_{dir}$	$\Delta E_{r,dir}$	$\Delta E^{\ddagger}_{indir}$	$\Delta E_{r,indir}$
DMSO + CH_3SH	-	-25.62	14.48(12.75)[3]	0.46
DMSeO + CH_3SH	-	-33.02	17.80	-6.94
DMSO + CH_3SeH	-	-30.68	6.94	-5.39
DMSeO + CH_3SeH	-	-38.03	9.98	-12.79

[1]$\Delta E^{\ddagger}$ are computed with respect to the closest minimum (i.e., a reactant complex like structure), while ΔE_r are computed with respect to the free reactants (DMXO, $CH_3X'H$ and H_2O). [2]$\Delta E^{\ddagger}_{indir}$ is computed at COSMO-M06 // COSMO-BLYP-D3(BJ) as explained in the discussion. [3]Between parenthesis, indirect transition state with one extra DMSO coordinating H_2O. Level of theory COSMO-M06 // COSMO-BLYP-D3(BJ).

Particularly, while changing X from S to Se on the chalcogenoxide leads to an increase in the activation energy required to break the X–X' bond, changing S with Se on $CH_3X'H$ leads to a sharp decrease in the activation energy. This is not completely unexpected, since X' acts as the central atom in the S_N2-like process. (reaction 3 in Scheme 7.3) Thus, the more electrophilic central Se nucleus is expected to provide a kinetic advantage in the reaction (see Chapter 5). Nevertheless, in all cases under investigation, indirect reductions involving Se are energetically more favored than the correspondent ones with S, but are all less favored then the correspondent direct reduction. Thus, for reactions occurring in solution, the direct reduction appears to be both kinetically and thermodynamically favored, regardless of the chalcogens. Although tempting, the discussion cannot be safely translated into the enzymatic context: indeed, the formation of a sulfenic acid has been confidently assessed at least in some Msrs proteins.[16,21] Thus, it is possible

that geometric constraints within the enzyme architecture somewhat suppress the direct reduction and that water activation by other residues promotes sulfenic acid formation.[53,54] Instead, in our model, which more accurately describes the reduction in solution, only the thiolate can activate H_2O. In any case, also in this step, Sec95 could provide an advantage over Cys95 since Se would participate in the selenenic acid formation as the central atom of the S_N2 process as above described.

7.4 Conclusions

In this Chapter, the molecular mechanism for the reduction of DMSO and DMSeO to sulfide and selenide was investigated when two equivalents of methyl thiol or a mixed methyl selenol - methyl thiol system acts as reductants. While the reduction of DMSO by methyl thiols was already studied in the past,[1,20] little attention was devoted to the reactions in which other chalcogens act as oxidizing or reducing agents. DMSeO was identified as a better oxidizing agent mainly because the selenurane, which is a key intermediate in the reaction, is more stable and is formed more easily than the analogous sulfurane. Activation Strain Analysis pinpointed that this is related to the stronger electrophilic nature of DMSeO when compared to DMSO, due to a reinforced orbital and electrostatic interaction.

Selenium provides a kinetic advantage also when it acts as the reducing selenol. In this case, the increased acidity of the selenol provides the decisive contribution to the reaction, since the Se–H bond is broken more easily than S–H, analogously to what found for the mechanism of GPx and related molecular models.[23,25] Overall, these results provide a comprehensive theoretical, physico-chemical look on the title reaction that complements the available experimental literature.

The system here investigated properly describes the reaction as it occurs in solution. However, the effect of the chalcogenol can be at least qualitatively used to interpret the kinetic competence of the human selenoenzyme MsrB1, in which a selenocysteine is present as catalytic residue. To the best of our knowledge, this is the first time that the kinetic advantage of Sec over Cys in MsrB catalysis is tackled *in silico*, providing a preliminary theoretical rationale to the experimental data.

Importantly, this outcome is another puzzle piece in the redox biology topic on the role of selenium rather than sulfur, which is still an open problem.[13]

Future investigations focusing on the role of Sec in MsrB catalysis in more realistic enzymatic models are expected to provide a more complete insight into one of the few selenoenzymes with known function, especially when comparison with molecular model mechanisms, such as those provided in this Chapter, are available as starting ground.

Appendix B

Table B1 Activation and reaction[1] Gibbs free energies (kcal mol^{-1}) for the reactions DMSO+SH, DMSeO+SH and DMSO+SeH (see main text). Level of theory: COSMO-M06 // BLYP-D3(BJ).[2]

	$\Delta G^{\ddagger}_{TS1}$	ΔG_{PC1}	$\Delta G^{\ddagger}_{TS1-2}$	ΔG_U	$\Delta G^{\ddagger}_{TS2}$[3]	ΔG_{PC2}	ΔG_r
DMSO+CH$_3$SH	21.65	21.70	24.72	17.45	1.28 (26.80)	-6.79	-22.50
DMSeO+ CH$_3$SH	18.76	11.53	15.82	0.77	2.74(8.48)	-0.25	-29.04
DMSO+ CH$_3$SeH	19.87	19.15	22.12	16.12	-0.67(22.42)	-10.81	-27.25

[1]Activation energies and energies of PC and U are relatives to the *relative* RC. The reaction Gibbs free energy is relative to the free reactants. [2]The contribution of solvation is taken into account at the M06 level, while thermodynamics corrections are taken into account at the BLYP-D3(BJ) level of theory.[3] The energy in parenthesis is with respect to RC1.
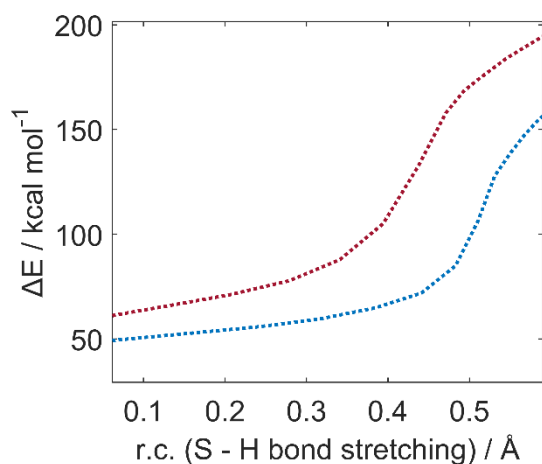

Figure B1 Pauli Repulsion plot for DMSO+SH (blue) vs DMSeO+SH (dark red).

References

[1]   T. J. Wallace, *J. Am. Chem. oc.* **1964**, *86*, 2018–2021.

[2]   A. Assmann, K. Briviba, H. Sies, *Arch. Biochem. Biophys.* **1998**, *349*, 201–203.

[3]   L. Carroll, D. I. Pattison, S. Fu, C. H. Schiesser, M. J. Davies, C. L. Hawkins, *Redox Biol.* **2017**, *12*, 872–882.

[4]   M. Iwaoka, T. Takahashi, S. Tomoda, *Heteroat. Chem.* **2001**, *12*, 293–299.

[5]   F. Ogura, H. Yamaguchi, T. Otsubo, H. Tanaka, *Bull. Chem. Soc. Jpn.* **1982**, *55*, 641–642.

[6]   L. Flohé, S. Toppo, L. Orian, *Free Radic. Biol. Med.* **2022**, *187*, 113–122.

[7]   S. Toppo, L. Flohé, F. Ursini, S. Vanin, M. Maiorino, *Biochim. Biophys. Acta - Gen. Subj.* **2009**, *1790*, 1486–1500.

[8]   V. Nascimento, E. E. Alberto, D. W. Tondo, D. Dambrowski, M. R. Detty, F. Nome, A. L. Braga, *J. Am. Chem. Soc.* **2012**, *134*, 138–141.

[9]   K. Arai, K. Dedachi, M. Iwaoka, *Chem. - A Eur. J.* **2011**, *17*, 481–485.

[10]   L. Orian, S. Toppo, *Free Radic. Biol. Med.* **2014**, *66*, 65–74.

[11]   W. T. Lowther, N. Brot, H. Weissbach, B. W. Matthews, *Biochemistry* **2000**, *39*, 13307–13312.

[12]   L. Tarrago, A. Kaya, H.-Y. Kim, B. Manta, B.-C. Lee, V. N. Gladyshev, *Free Radic. Biol. Med.* **2022**, *191*, 228–240.

[13]   H. J. Reich, R. J. Hondal, *ACS Chem. Biol.* **2016**, *11*, 821–841.

[14]   M. Maiorino, K. D. Aumann, R. Brigelius-Flohe, F. Ursini, J. van den Heuvel, J. McCarthy, L. Flohé, *Biol. Chem. Hoppe. Seyler.* **1995**, *376*, 651–660.

[15]   H. Y. Kim, V. N. Gladyshev, *PLoS Biol.* **2005**, *3*, 1–10.

[16]   J. C. Lim, Z. You, G. Kim, R. L. Levine, *Proc. Natl. Acad. Sci. U. S. A.* **2011**, *108*, 10472–10477.

[17]   F. M. Ranaivoson, M. Antoine, B. Kauffmann, S. Boschi-Muller, A. Aubry, G. Branlant, F. Favier, *J. Mol. Biol.* **2008**, *377*, 268–280.

[18]   B. Kauffmann, A. Aubry, F. Favier, *Biochim. Biophys. Acta - Proteins Proteomics* **2005**, *1703*, 249–260.

[19]   J. J. Robinet, H. M. Dokainish, D. J. Paterson, J. W. Gauld, *J. Phys. Chem. B* **2011**, *115*, 9202–9212.

[20]   B. Balta, G. Monard, M. F. Ruiz-López, M. Antoine, A. Gand, S. Boschi-Muller, G. Branlant, *J. Phys. Chem. A* **2006**, *110*, 7628–7636.

[21]   S. Boschi-Muller, S. Azza, S. Sanglier-Cianferani, F. Talfournier, A. Van

Dorsselear, G. Branlant, *J. Biol. Chem.* **2000**, *275*, 35908–35913.

[22] W. T. Lowther, N. Brot, H. Weissbach, J. F. Honek, B. W. Matthews, *Proc. Natl. Acad. Sci. U. S. A.* **2000**, *97*, 6463–6468.

[23] M. Bortoli, M. Torsello, F. M. Bickelhaupt, L. Orian, *ChemPhysChem* **2017**, *18*, 2990–2998.

[24] M. Dalla Tiezza, F. M. Bickelhaupt, L. Flohé, M. Maiorino, F. Ursini, L. Orian, *Redox Biol.* **2020**, *34*, 101540.

[25] M. Dalla Tiezza, F. M. Bickelhaupt, L. Flohé, L. Orian, *Chempluschem* **2021**, *86*, 525–532.

[26] G. te Velde, F. M. Bickelhaupt, E. J. Baerends, C. Fonseca Guerra, S. J. A. van Gisbergen, J. G. Snijders, T. Ziegler, *J. Comput. Chem.* **2001**, *22*, 931–967.

[27] ADF2019, SCM, Theoretical Chemistry, Vrije Universiteit, Amsterdam, The netherlands, https://www.scm.com

[28] C. Lee, W. Yang, R. G. Parr, *Phys. Rev. B* **1988**, *37*, 785–789.

[29] A. D. Becke, E. R. Johnson, *J. Chem. Phys.* **2005**, *123*, 154101.

[30] E. R. Johnson, I. D. Mackie, G. A. DiLabio, *J. Phys. Org. Chem.* **2009**, *22*, 1127–1135.

[31] S. Grimme, *J. Comput. Chem.* **2004**, *25*, 1463–1473.

[32] A. D. Becke, *Phys. Rev. A* **1988**, *38*, 3098–3100.

[33] E. Van Lenthe, E. J. Baerends, J. G. Snijders, *J. Chem. Phys.* **1994**, *101*, 9783–9792.

[34] F. Zaccaria, L. P. Wolters, C. Fonseca Guerra, L. Orian, *J. Comput. Chem.* **2016**, *37*, 1672–1680.

[35] L. Deng, T. Ziegler, *Int. J. Quantum Chem.* **1994**, *52*, 731–765.

[36] Y. Zhao, D. G. Truhlar, *Theor. Chem. Acc.* **2008**, *120*, 215–241.

[37] A. Madabeni, S. Zucchelli, P. A. Nogara, J. B. T. Rocha, L. Orian, *J. Org. Chem.* **2022**, *87*, 11766–11775.

[38] A. P. Bento, M. Solà, F. M. Bickelhaupt, *J. Chem. Theory Comput.* **2010**, *6*, 1445–1445.

[39] L. de Azevedo Santos, T. C. Ramalho, T. A. Hamlin, F. M. Bickelhaupt, *J. Comput. Chem.* **2021**, *42*, 688–698.

[40] F. Neese, *Wiley Interdiscip. Rev. Comput. Mol. Sci.* **2018**, *8*, DOI 10.1002/wcms.1327.

[41] F. Neese, *WIREs Comput. Mol. Sci.* **2012**, *2*, 73–78.

[42] D. G. Liakos, Y. Guo, F. Neese, *J. Phys. Chem. A* **2020**, *124*, 90–100.

[43] C. C. Pye, T. Ziegler, *Theor. Chem. Acc.* **1999**, *101*, 396–408.

[44] X. Sun, T. M. Soini, J. Poater, T. A. Hamlin, F. M. Bickelhaupt, *J. Comput. Chem.* **2019**, *40*, 2227–2233.

[45] T. Ziegler, A. Rauk, *Inorg. Chem.* **1979**, *18*, 1558–1565.

[46] K. Morokuma, *Acc. Chem. Res.* **1977**, *10*, 294–300.

[47] F. M. Bickelhaupt, E. J. Baerends, in *Rev. Comput. Chem.*, **2007**, pp. 1–86.

[48] F. M. Bickelhaupt, K. N. Houk, *Angew. Chemie - Int. Ed.* **2017**, *56*, 10070–10086.

[49] C. A. Bayse, *J. Phys. Chem. A* **2007**, *111*, 9070–9075.

[50] J. A. Ritchey, B. M. Davis, P. A. Pleban, C. A. Bayse, *Org. Biomol. Chem.* **2005**, *3*, 4337–4342.

[51] M. Iwaoka, S. Tomoda, *Chem. Lett.* **2000**, *29*, 1400–1401.

[52] F. Neese, M. Atanasov, G. Bistoni, D. Maganas, S. Ye, *J. Am. Chem. Soc.* **2019**, 141, 2814-2824.

[53] H. M. Dokainish, J. W. Gauld, *Biochemistry* **2013**, *52*, 1814–1827.

[54] S. Boschi-Muller, *Antioxidants* **2018**, *7*, DOI 10.3390/antiox7100131.

# 8 Role of Selenium Oxidation State in Organoselenium-Catalyzed Reactions

8.1 Introduction

Organoselenides are recognized as effective oxygen-transfer catalysts[1] in epoxidation/dihydroxylation reactions,[2–5] sulfoxidation[6], aldehyde[7] and amine oxidations[8,9], with H_2O_2 as final oxidant. For reactions catalyzed by phenyl seleninic acids **1** or their respective precursors (e.g., diphenyl diselenides **2**), until recently phenyl peroxyseleninic acids **3** were deemed as the only plausible active catalytic intermediates.
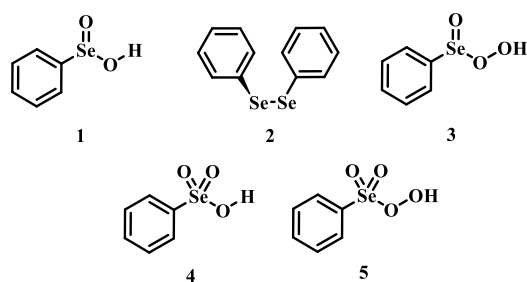
Scheme 8.1 Organoselenides employed as catalysts or precatalysts for selenium mediated oxygen-transfer reactions and postulated plausible active oxidants.

Their first hypothetical participation in oxidation reactions dates back to the early days of organoselenium chemistry, when the oxidation of seleninic to peroxyseleninic acid was postulated to rationalize the autocatalytic behavior of selenide oxidation.[10] (see Chapter 1) Later on, their participation in various organic substrate oxidations was proposed[2,6,11] and it consolidated in the past fifty

years.[1,12] In 2020, Back and coworkers[4] reported for the first time evidence of the involvement of the high oxidation state intermediate selenonic **4** and peroxyselenonic acid **5** in the selenium mediated epoxidation of cyclooctene. This observation, while thought-provoking, was later found to be not completely general. Indeed, in 2021, Tanini and coworkers provided evidence for the involvement of the "conventional" peroxyseleninic acid **2** in another selenium catalyzed oxygen-transfer reaction i.e., the on-water oxidation of aniline to nitrobenzene.[9] (Scheme 8.2)
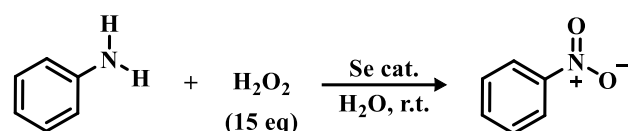
Scheme 8.2 On-water selenium catalyzed oxidation of aniline to nitrobenzene at room temperature (r.t.).

In the work by Tanini *et al*, Se(VI) selenonic acid **4** was recovered in the water after complete oxidation of the substrate, but was found inactive towards further catalytic activity if not reduced back to Se(IV) seleninic acid **1**. Conversely, in the selenium mediated epoxidation of alkenes, selenonic acid was found to be more active than seleninic acid itself.[4] Puzzled by these apparently conflicting results, we chose to investigate more carefully the mechanistic details of the aniline oxidation reaction, with particular attention to the H_2O_2 activation by phenylseleninic acid, which should be a key reactive step common to all reactions catalyzed by **1** or **2**.

Despite the long-standing experimental experience in the field, to the best of our knowledge no detailed theoretical mechanistic investigation has ever been carried out on catalytic oxygen-transfer reactions mediated by organoselenides. Only a previous report discussed peroxyseleninic acid **3** formation starting from the parent diphenyl diselenide **2**, addressing the autocatalytic decomposition of H_2O_2.[13] Indeed, while much theoretical mechanistic efforts were devoted in the past twenty years to the elucidation of glutathione-peroxidase like catalytic potential of organoselenides,[14,15] other catalytic reactions, such as the one explored in this work, remained somewhat unexplored *in silico*. This Chapter aims at filling this gap.

8.2 Computational Methods

All calculations were performed in line with the benchmarked protocol of Chapter 6. Thus, all energies were computed at M06 // OPBE level of theory, which proved to be in average the best approach to tackle the organochalcogen reactions previously explored. Additionally, M06 is found to be one of the best functionals to reproduce the activation energies of S_N2 reactions,[16] like many reactive steps described in the following are. Thermodynamic corrections were computed by means of standard statistical thermodynamics methods, at 1 atm and 298.15 K, at the lower level of theory (with OPBE functional). The effect of implicit solvation was included at the higher level of theory (with the M06 functional), employing the COSMO model of solvation as implemented in ADF,[17,18] with water as solvent. All COSMO parameters (dielectric constant, atomic radii, and empirical scaling function) have been used as per default in ADF. The Activation Strain Model of chemical reactivity and the Energetic Span Model have been applied as described in Chapter 2.

8.3 Results and discussion

Bearing in mind the inactive nature of selenonic acid **4** in the selenium mediated oxidation of aniline to nitrobenzene, when compared to seleninic acid **1**, we first screened thorough DFT calculations the potential energy surface (PES) for the complete catalytic mechanism from the fully reduced (aniline) to the fully oxidized substrate (nitrobenzene). Both seleninic and selenonic acids were theoretically investigated as possible catalysts, for a straight comparison of two PESs and to gain insight into the role of Se oxidation state in the catalytic mechanism. This process can be described by three consecutive catalytic cycles. (Figure 8.1d) The most stable Gibbs free energy profile is represented in Figure 8.1a. In the beginning, the key mechanistic features of the process as deduced by DFT calculations will be described.
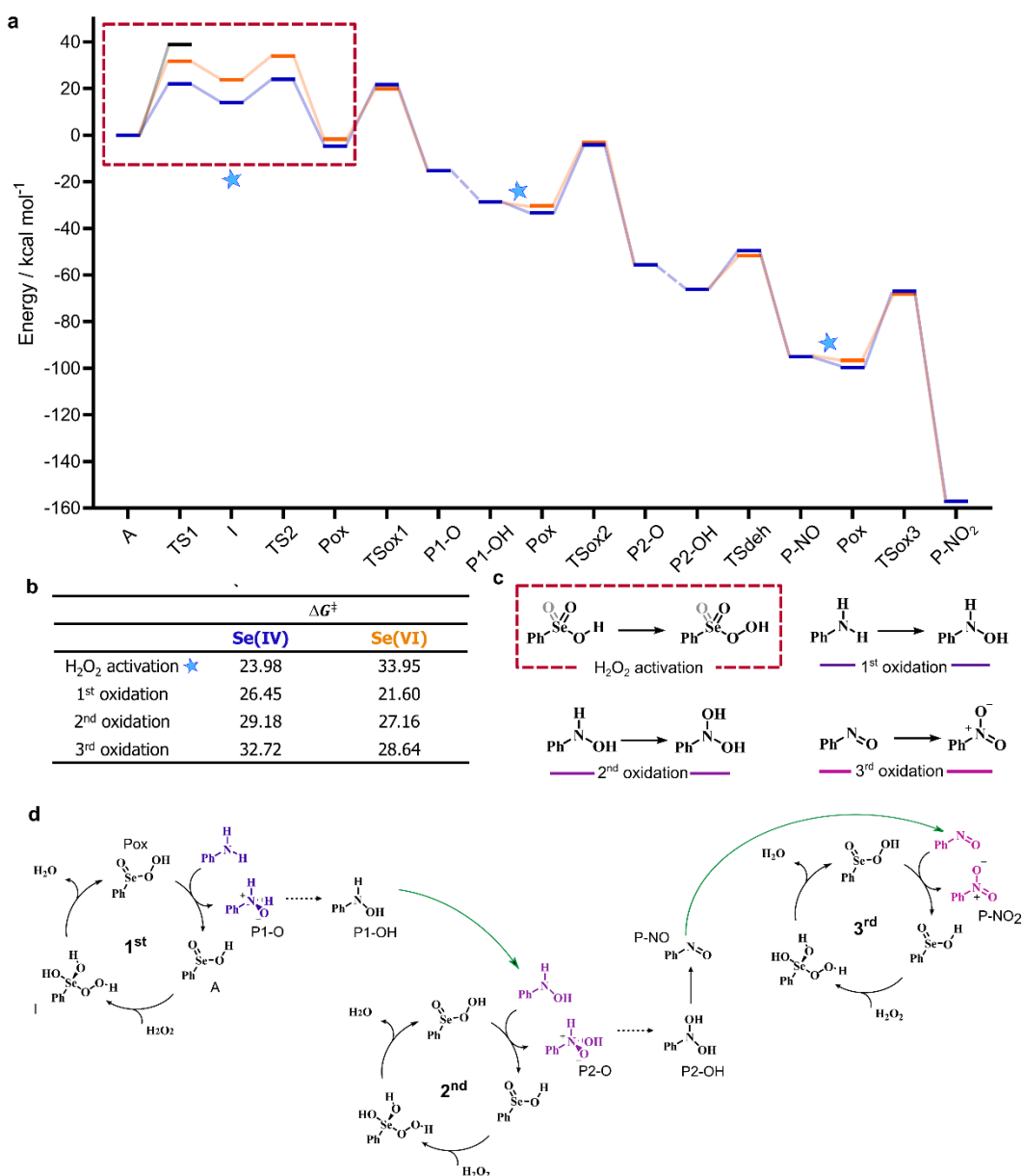
Figure 8.1 (a) Gibbs free energy profile (kcal mol^{-1}) for the oxidation of aniline to nitrobenzene: Se(IV) mediated process (blue); Se(VI) mediated process (orange). All energies are with respect to the free seleninic/selenonic acid and H_2O_2. The black line is the direct aniline oxidation to aniline N-oxide by H_2O_2 (i.e., the uncatalyzed process). Level of theory: COSMO-M06 // OPBE. Lines are intended as a guide to the eye only. Only the first H_2O_2 activation step is represented (within a dashed red box); the subsequent analogous steps are omitted, and their position is indicated by a star. Dashed lines are acid/base processes occurring without or with very low activation energies. (b) Activation energies (kcal mol^{-1}) for the key steps of the mechanism. (c) Schematic representation of the H_2O_2 activation process and of the three consecutive oxidative steps. (d) Catalytic cycles for the description of the overall oxidation to nitrobenzene. Only Se(IV) species are represented. Analogous Se(VI) species have one additional Se–O formal double bond. Dashed steps occur with a low to non-appreciable activation energy and corresponds to dashed lines in **1a.** Green arrows represent the products which exits from one cycle to enter the next one. The substrate oxidation step is represented in purple.

8.3.1 Description of the whole mechanism

Analogous pathways for the Se catalyzed conversion of aniline to nitrobenzene were found regardless of the oxidation state of the Se nucleus i.e., for both seleninic and selenonic acid. In both cases, the acid (A, **1** or **4**) reacts first with H_2O_2 to produce the correspondent peroxyacid (Pox, **3** or **5**). Three consecutive catalytic cycles progressively lead to the oxidation of aniline to the correspondent mono hydroxyl amine (P1-OH), dihydroxyl amine (P2-OH) and lastly to nitrobenzene (P-NO$_2$). In each cycle, the peracid generated by H_2O_2 activation (Figure 8.1c) reacts with the substrate in a S_N2 fashion, producing the relative N-oxide products (P1-O and P2-O) and the correspondent seleninic or selenonic acid. In the acidic conditions in which the reaction takes place, the primary N-oxide is easily protonated by either **1** or **4** on the O position, and then easily deprotonated on the N position, leading to the mono hydroxyl amine and dihydroxyl amine (P1-OH and P2-OH). For aniline N-oxide (P1-O) the process was found to proceed without any appreciable activation energy, while for aniline hydroxylamine N-oxide (P2-O) the process occurs with a low activation energy of less than 2 kcal mol^{-1}.

Before the 3rd catalytic cycle, P2-OH undergoes an acid catalyzed dehydration reaction to nitrosobenzene (P-NO), in which either **1** or **4** acts as amphoteric acid/base catalysts with an overall activation energy of 16.64 and 14.43 kcal mol^{-1} respectively. Lastly, in the final oxidative cycle, P-NO is oxidized to the final species, nitrobenzene (P-NO$_2$). The potentially competitive direct oxidation of P2-OH to the correspondent N-oxide followed by dehydration to P-NO$_2$ was found to be less favored kinetically with respect the dehydration to P-NO, even if it has a lower activation energy with respect to the oxidation of P-NO to P-NO$_2$. (Appendix C, Table C1) Thus, Se-catalyzed dehydration to P-NO was deemed more likely. Additionally, the formation of P-NO was confirmed in previous Se-catalyzed oxidations of aniline, and it is likely the key intermediate in the formation of azoxy benzene, one of the side products of the reaction.[9]

In the mechanistic hypothesis followed in this Chapter, which closely matches the one made by Back *et al*,[4] the H_2O_2 activation step is independent on the nature of the substrate. Other H_2O_2 activation mechanisms (all independent on the nature of the substrate) were found to be kinetically less favored (*vide infra*). The favored process proceeds stepwise through the formation of a peroxyselenurane (I), which

can then undergo a non-redox dehydration to the correspondent peroxyacid (Pox). The direct participation of this peroxyselenurane in the oxidation of the substrate was excluded on the basis of the activation energy of the process e.g., for Se(IV), aniline oxidation to P1-O occurs with an activation energy of ca. 45 kcal mol^{-1} and of ca. 26 kcal mol^{-1} when the peroxyselenurane (**I**), and the peroxyacid (Pox) act as the oxidant, respectively. (Appendix C, Table C2)

Following H$_2$O$_2$ activation, the three oxidations occur with increasing activation energies, regardless of the oxidation state of the catalyst. That is, oxidation of aniline has the lowest activation energy (Figure 8.1b, 1st oxidation) and oxidation of P-NO the highest (Figure 8.1b, 3rd oxidation). Intuitively, since the amine acts as the nucleophile in the reaction, each increase in N oxidation state reduces the nucleophilicity of the substrate due to the electron-withdrawing nature of each new binding oxygen group. Indeed, the Hirshfeld partial charge[19,20] on N increases from –0.212 to –0.088 and to –0.003 going from aniline to P1-OH to P-NO, thus highlighting a reduced nucleophilicity of the oxidized intermediates. Similarly, the barrier for the three acid-catalyzed processes increases i.e., while the isomerization of P1-O proceeds without any appreciable activation energy, and the conversion of P2-O to P2-OH has a low activation energy of less than 2 kcal mol^{-1} when seleninic acid **1** acts as the acid catalyst, the dehydration of P2-OH to P-NO has an activation energy of 14–16 kcal mol^{-1}. Thus, excluding the two previous almost barrierless acid catalyzed processes, for both oxidation states, this step has the lowest appreciable barrier of the overall mechanism by 10 kcal mol^{-1} or more.

Overall, the whole process from aniline to nitrobenzene is strongly exergonic by more than 150 kcal mol^{-1}. All the reaction steps of the mechanism are exergonic or almost isergonic, apart from the H$_2$O$_2$ addition to **1** or **4**, leading to the formation of the intermediate peroxyselenurane (**I**) which is destabilized with respect to the correspondent acid. In contrast, the reaction energy for each sequential oxidation becomes more and more negative along the pathway, starting from a ΔG_r of -28.65 kcal mol^{-1} for the oxidation of aniline to P1-OH and reaching a ΔG_r of -62.05 for the final oxidation of P-NO to P-NO$_2$.

8.3.2 Comparison between Se(IV) and Se(VI) catalytic cycles

Figure 8.1 provides the overall representation of the energy profile leading to the conversion of aniline to P-NO$_2$, in which a clear comparison between the performances of Se(IV) and Se(VI) species can be made.

In H$_2$O$_2$ activation process (from A to Pox), Se(IV) seleninic acid **1** appears to be the best reactant. Indeed, not only the formation of the peroxyseleninic acid **3** is slightly more favored thermodynamically as compared to the same process for Se(IV) i.e., the conversion of **4** to **5**, (ΔG_r of -4.69 and -1.67 kcal mol^{-1} respectively), but the overall process occurs on a much lower energy surface. While the formation of the peroxyselenurane (I) is endergonic for both selenium oxidation states, the dehydration then occurs with a relatively low activation energy. Both H$_2$O$_2$ addition (TS1), and the peroxyselenurane (I) dehydration (TS2) transition states are located much lower on the PES when the substrate of the reaction is seleninic acid **1**, as compared to selenonic acid **4**. Particularly, the selenurane (I) itself is much more stable for Se(IV) than for Se(VI), being located on the PES respectively at 13.92 and 23.82 kcal mol^{-1}. This energy difference is roughly conserved also in TS1 and TS2 i.e., in the transition states for the H$_2$O$_2$ addition and dehydration processes. Thus, overall, the peroxyacid Pox formation occurs with an activation energy 10 kcal mol^{-1} lower for seleninic acid than for selenonic acid, making the former much more privileged energetically in H$_2$O$_2$ activation. (Figure 8.1b) Conversely, Se(VI) appears to consistently perform better in each of the following reaction steps, i.e., the three substrate oxidations and the Se-catalyzed dehydration of P2-OH to P-NO. Focusing on the three substrate oxidations, activation energies for Se(VI) mediated processes are 2–5 kcal mol^{-1} lower than correspondent Se(IV) mediated processes. Thus, peroxyselenonic acid **5** is a better oxidant from the kinetic point of view than peroxyseleninic acid **3**. Part of this activation energy lowering is clearly due to the lower stability of peroxyselenonic with respect to selenonic acid (as compared to the peroxyseleninic with respect to seleninic acid) assessed on the basis of their ΔG_r, as previously mentioned. Thus, while Se(VI) appears to be the best oxidant for the reactions under investigation, Se(IV) appears to be the best species in the H$_2$O$_2$ activation process, with a much higher energy gap between the two PESs in this latter case.

8.3.3 Theoretical comparison of the catalytic performance

While the analysis of the PESs already provides valuable insight into the catalytic potential of Se(IV) and Se(VI) species, a much more quantitative index of their catalytic potential is represented by the calculated turnover frequency (TOF) of each catalytic cycle, when the two different catalysts i.e., seleninic and selenonic acid, are employed.

This quantity is directly related to an experimentally accessible parameter, and accounts for *all* steps of each cycle at once in the evaluation of the performance of the catalyst. Within the Energetic Span Model proposed by the Kozuch and Shaik, it is possible, starting from the energy landscape constructed with quantum mechanics calculations, to obtain a well-defined TOF value.[21–23] Additionally, this procedure allows to gain insight into the states which mostly (or totally) determine the value of the TOF, i.e. the TOF determining transition state (TDTS) and the TOF determining intermediate (TDI). (See Chapter 2, Paragraph 2.3).
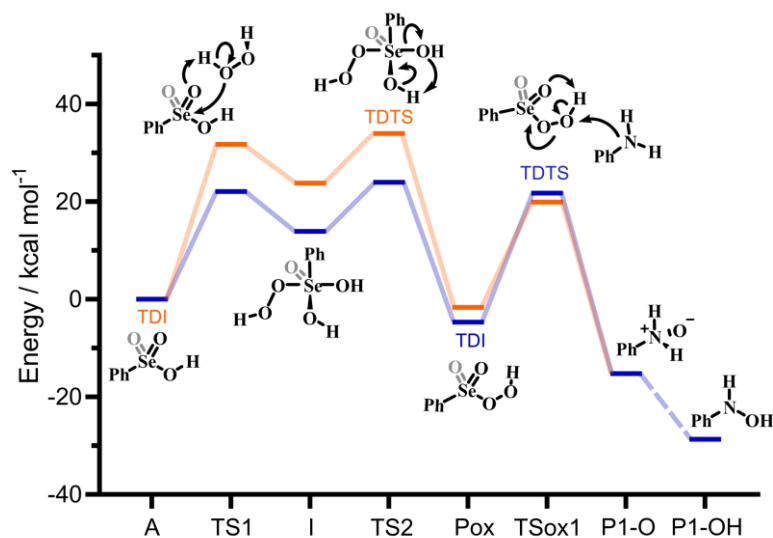

Figure 8.2 Gibbs free energy profile, intermediates, transition states, and calculated TDI and TDTS for the 1st catalytic cycle: Se(IV) mediated process (blue); Se(VI) mediated process (orange). Lines are intended as a guide to the eye only. Grey portions on the Lewis structures represent the additional Se=O bond which is present only in Se(VI) structures.

In Figure 8.2, a representative close-up of the first catalytic cycle is illustrated; the TDI and the TDTS are shown for both Se(IV) and Se(VI) catalyzed processes. The two downhill cycles bear close similarity until Pox, differing only in the substrate oxidations. Notably, the TDI and TDTS positions do not change in the

other two cycles. For the Se(VI) catalyzed processes, the TDI/TDTS are always identified within the H_2O_2 activation step corresponding respectively to the selenonic acid and to the Se(VI) peroxyseleurane dehydration (A and TS2 in Figure 8.2). For all three Se(VI) catalyzed oxidations, this step has the overall highest transition state–minimum energy difference i.e., the energetic span of the cycle.

Conversely, for the Se(IV) catalyzed processes, the TDI/TDTS couple is always identified within the substrate oxidation step, corresponding respectively to the peroxyacid and to the S_N2 oxygen-transfer transition state (Pox and TSox in Figure 8.2) In the two downhill cycles, as previously outlined, this couple remains the TDI/TDTS, but since the three oxidations appear to have progressively increasing activation energies (Figure 8.1b) the energetic span of Se(IV) cycles increases along the overall mechanism, with the first cycle having the lowest and the last having the highest span, always corresponding to the substrate oxidation activation energy.

To verify how these mechanistic differences affect the overall process, the six TOFs for the three Se(IV)/Se(VI) catalyzed oxidations were computed, and their ratio was evaluated (Table 8.1) to quantify the different performance of Se(VI) and Se(IV) catalysis.

Table 8.1 TOF ratio between Se(VI) and Se(IV) catalyzed oxidations for each catalytic cycle. Level of theory: COSMO-M06 // OPBE.

	$\dfrac{TOF^{Se(VI)}}{TOF^{Se(IV)}}$
1st Cycle	$3 \ 10^{-6}$
2nd Cycle	$3 \ 10^{-4}$
3rd Cycle	$1 \ 10^{-1}$

From these results, it emerges that the differences between Se(VI) and Se(IV) as catalysts go attenuating along the overall mechanism, with the greatest difference in the first cycle (highest TOF ratio) and the smallest difference in the last cycle (lowest TOF ratio). This result comes from the different nature of the TDI/TDTS couple when Se(VI) selenonic and Se(IV) seleninic acids are the catalysts, as above described. Indeed, since for Se(VI) the TDI and the TDTS remains the same in the three cycles, and corresponds to the same energetic span, all three Se(VI) catalyzed processes have the same TOF. Conversely, since the activation energy of the three

substrate oxidations increases along the mechanism, and this activation energy matches to the energetic span of Se(IV) catalyzed processes, their TOF becomes lower along the overall conversion from aniline to nitrobenzene, thus narrowing down the TOF ratio from ca. 10^{-6} to ca. 10^{-1}. Most importantly, the data reported in Table 8.1 clearly reveal that Se(IV) is always a better catalyst for aniline oxidation than the correspondent Se(VI) species, since in all cases the TOF ratio is smaller than 1 by at least one order of magnitude. These results further corroborate the privileged role of seleninic acid **1** in the organoselenium catalyzed oxidation of aniline to nitrobenzene, that is, peroxyseleninic acid **3** appears to be a much better oxygen-transfer *catalyst* than peroxyselenonic acid **5**, even if the latter is in principle a better oxidizing agent (Figure 8.1b).

8.3.4 Insight into Se(IV) to Se(VI) interconversion

While the data above discussed highlight the privileged role of the Se(IV) oxidation state in the reaction under investigation, one could argue that Se(IV) seleninic acid cannot catalyze the three reactions simply because it is rapidly oxidized to Se(VI) selenonic acid in the conditions in which the reaction takes place. According to Table 8.1, this conversion would result in a catalyst inactivation.
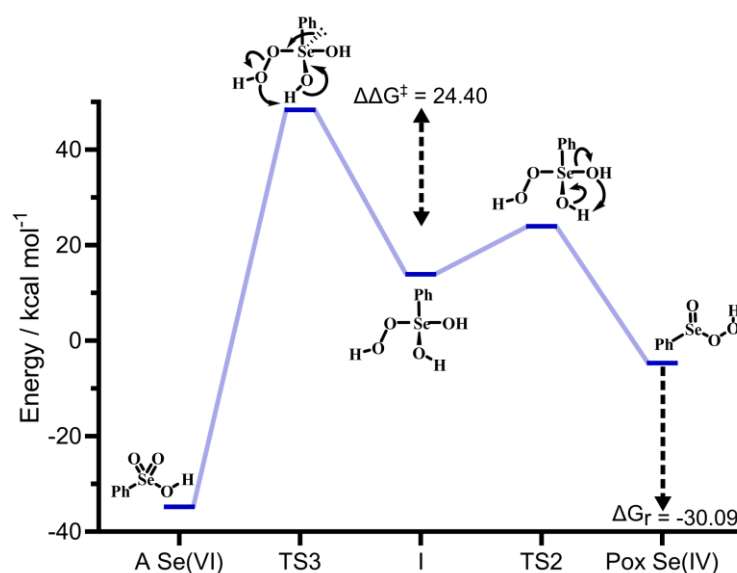

Figure 8.3 Gibbs free energy profile (kcal mol^{-1}) and relative structures for the interconversion of peroxyseleninic acid (Pox) to selenonic acid (A). All energies are relative to seleninic acid and H_2O_2.

However, we followed this hypothesis, since Back and coworkers reported the fast formation of Se(VI) species when diphenyl diselenide is treated with H_2O_2[4] and Tanini and coworkers observed the formation of Se(VI) selenonic acid in the water recovered after the complete oxidation of aniline to nitrobenzene.[9] Guided by the inspiring work of Back *et al*, we first probed the mechanistic hypothesis that the peroxyselenurane (I) on the Se(IV) PES acts as the key intermediate in the interconversion. Indeed, it was previously postulated that while a non-redox dehydration would lead to peroxyacid, as previously described, an alternative redox dehydration should lead to selenonic acid. (Scheme 8.2a) Unfortunately, while such interconversion is strongly favored thermodynamically, it proved to be quite troublesome kinetically. (Figure 8.3)

Particularly, with respect to peroxyseleninic acid (Pox in Figure 8.3), the formation of selenonic acid (A in Figure 8.3) is exergonic by ca. 30 kcal mol^{-1}. As previously mentioned, the peroxyselenurane (I) is destabilized by ca. 13 kcal mol^{-1} with respect to seleninic acid and its non-redox dehydration to peroxyseleninic acids occurs thorough a low-lying transition state (TS2). Conversely, its redox dehydration to selenonic acid goes through a transition state TS3 located way higher on the PES, so that the process is kinetically disfavored by ca. 24.40 kcal mol^{-1} over the correspondent non-redox dehydration. Thus, while the peroxyselenurane is a key intermediate in H_2O_2 activation, it does not seem to be involved in the interconversion between Se(IV) and Se(VI).

Intrigued by this result, we explored a couple of alternative plausible mechanisms. To the best of our knowledge, the question of the formation of selenonic acid was firstly tentatively addressed by Syper and coworkers in 1987,[24] who invoked a peroxo transition state / intermediate already envisioned by Sharpless and Hori in 1978.[2] (Scheme 8.2b) A transition state for the formation such peroxo intermediate was found to have an activation energy of 52.52 kcal mol^{-1} with respect to peroxyseleninic acid, not much lower than the redox-dehydration, which has an overall activation energy of 53.07 kcal mol^{-1} with respect to peroxyseleninic acid. Thus, these two processes were deemed equally unlikely to occur. Further evolution of the peroxo intermediate to selenonic acid was not investigated, because the barrier for its formation was prohibitively high.
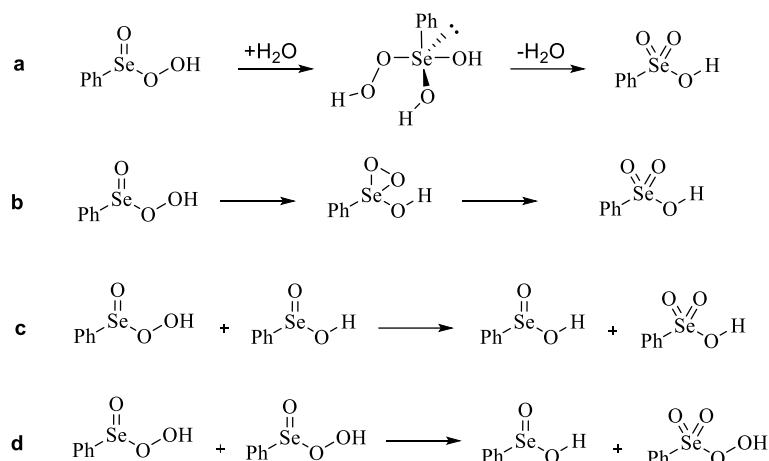
Scheme 8.2 Plausible pathways for Se(IV) to Se(VI) interconversion. (a) Redox dehydration of peroxyselenurane. (b) Syper hypothesis, through a peroxo transition state/intermediate. (c) Direct oxidation of seleninic acid by peroxyseleninic acid. (d) Dismutation of peroxyseleninic acid to seleninic and peroxyselenonic acid.

Since the active role of peroxyseleninic acid in the autocatalytic oxidation of organoselenides was observed in the past,[13] we checked whether a similar "autocatalytic" oxidation might operate also in this case. (Scheme 8.2c) Such process, in which one equivalent of peroxyseleninic acid **3** oxidizes some residual seleninic acid **1** to selenonic acid **4**, while being reduced back to seleninic acid, occurs with an activation energy of 37.50 kcal mol^{-1}, way more accessible than the two previous proposed mechanisms, but still significantly higher than the H_2O_2 activation process of seleninic acid, which has an overall barrier of 23.98 kcal mol^{-1} (Figure 8.1b) Thus, such process does not appear to be autocatalytic in nature. Most importantly, since all mechanistic proposals in Scheme 8.2 a-c have an activation energy higher than each of the three substrate oxidations by peroxyseleninic acid (Figure 8.1b), we conclude that no conversion to selenonic acid should occur as long as there is some substrate left to undergo catalytic oxidation. This result is consistent with the hypothesis by Tanini *et al* that selenonic acid forms by overoxidation of the catalyst after all aniline and derivatives have been fully oxidized to the final product.

Lastly, we checked whether peroxyseleninic acid **3** might undergo a self-oxidation reaction directly to peroxyselenonic acid **5**, thus bypassing the high activation energy required by selenonic acid in H_2O_2 activation. Selenonic acid would be finally produced from the oxidation of the organic substrate, which is a favored process. (Figure 8.1b) However, also this self-oxidation occurs with a rather
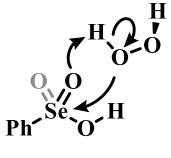
high activation energy of 39.77 kcal mol^{-1}, higher than the previously described oxidation to selenonic acid and of its further reaction with H_2O_2. Thus, also this process is not expected to take place in presence of aniline and its intermediates towards nitrobenzene.

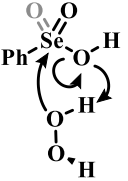### 8.3.5 Alternative H_2O_2 activation mechanisms

The computational analysis carried out so far has highlighted how it is unlikely for the peroxyselenurane (I) to be involved in the interconversion from Se(IV) to Se(VI) species. However, we propose that it has a pivotal role in the H_2O_2 activation process since, among the probed mechanistic pathways from the acids to the correspondents peroxyacids, the stepwise process going through the peroxyselenurane has the lowest activation energy. (Table 8.2)

Table 8.2 Activation energies (kcal mol^{-1}) for three different H_2O_2 activation mechanisms. Schematic transition states of the processes are showed below.[a]
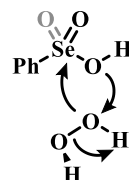
	$\Delta G^{\ddagger}$	
	Se(IV)	Se(VI)
a	22.06[b]	31.75[b]
b	36.88	48.19
c	61.95	73.96

a   b   c

[a]Grey portions of the Lewis structures represents the additional Se=O bond present in Se(VI) structures only. [b]The H_2O_2 addition process sketched in **a** is represented for comparison with **b** and **c**, with its relative activation energy. The overall barrier towards peroxyseleninic / peroxyselenonic acid is slightly higher, corresponding to dehydration of the selenurane (I). However, it remains much lower than both process **b** and **c**. (See Figure 8.1b and relative discussion).

Both investigated concerted processes (Table 8.2, b and c) have a higher activation energy than the correspondent H_2O_2 addition step (Table 8.2, a) and than the overall stepwise H_2O_2 activation process. (Figure 8.1b) Particularly, the previously proposed concerted mechanism,[13] in which one proton of H_2O_2 is transferred to the –OH group of the acids **1** or **4** (Table 8.2 b) has an activation energy already more

than 10 kcal mol^{-1} higher than H$_2$O$_2$ addition, in which the proton of H$_2$O$_2$ is transferred to the correspondent Se=O bond moiety. (Table 8.2, a) A concerted mechanism corresponding to an "O insertion" within the Se–OH bond of seleninic and selenonic acids, thus turning the –OH function into the –OOH function (Table 8.2 c) displays an even higher, unfeasible activation energy. These results suggest that the formation of the peroxyselenurane intermediate (I), while not directly involved in the Se(IV) to Se(VI) conversion (Figure 8.2) and not directly responsible for aniline oxidation (Appendix C, Table C2), is pivotal in the actual conversion between the acid and the peroxyacid species. Interestingly, also for the two concerted (unlikely) mechanisms, Se(IV) appears to be consistently more reactive, a results further corroborating our previous conclusions about H$_2$O$_2$ activation by seleninic and selenonic acids, and suggesting that the relative inertia of Se(VI) in activating H$_2$O$_2$ might be intrinsic in its high oxidation state.

8.3.6 Insight from activation strain analysis

To provide a quantitative discussion on the effect of the oxidation state on the two key reactive steps of the oxygen-transfer mechanism i.e., the H$_2$O$_2$ activation step and the S$_N$2-like oxidation of the aniline, ASA and EDA were performed on representative reactions. Particularly, the addition of H$_2$O$_2$ to seleninic and selenonic acid and oxidation of aniline to aniline-N-oxide by peroxyseleninic and peroxyselenonic acid were compared. First, the effect of the oxidation state on the H$_2$O$_2$ activation will be discussed, (Figure 8.4a, b) then the oxidative potential of the two peroxyacids will be analyzed. (Figure 8.4c–e)

The ASA for the H$_2$O$_2$ addition step is represented in Figure 8.4a. All energies were plotted at consistent values of O–H bond breaking. This reaction coordinate undergoes a well-defined variation along the reaction since the proton is transferred from H$_2$O$_2$ to the Se=O bond of seleninic and selenonic acid. Analogous conclusions can be drawn by analysis of the complementary reaction coordinate i.e., the H–O bond formation in the peroxyselenurane (I). (Appendix C, Figure C2) It can be seen how, from the beginning of the reaction to the TS, which occurs roughly at the same value of r.c. for the two reactions (at ca. 0.35 Å) the ΔE_{int} for both OS is superimposed, suggesting that both seleninic and selenonic acids interact similarly
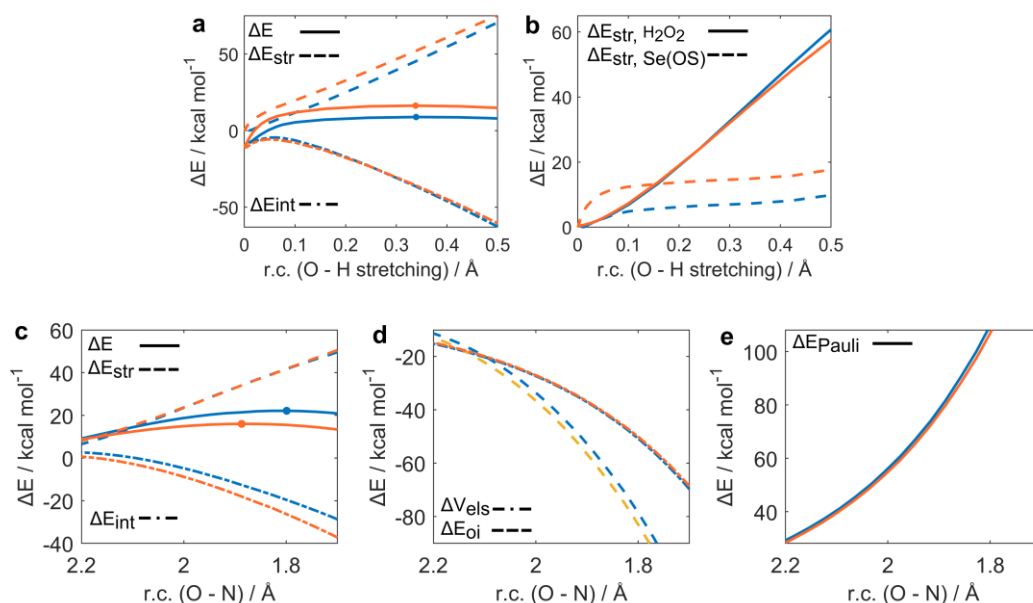
Figure 8.4 Activation strain and energy decomposition analysis of (**a, b**) H_2O_2 addition to seleninic (blue) and selenonic (orange) acids and (**c–e**) of aniline oxidation to aniline N-oxide (P1-O) by peroxyseleninic (blue) and peroxyselenonic (orange) acids.

with H_2O_2. Conversely, seleninic acid has a consistently lower ΔE_{str}, which appears to be the main player in its reduced activation energy in H_2O_2 addition.

The strain energy was then decomposed into the contribution of each fragment i.e., a $\Delta E_{str,H_2O_2}$ accounting for H_2O_2 deformation only, and $\Delta E_{str,Se(OS)}$ associated to seleninic/selenonic acid deformation alone. (Figure 8.4b) What can be inferred is that the higher strain, and thus the higher activation energy predicted for H_2O_2 addition to Se(VI), is due exclusively to the higher $\Delta E_{str,Se(VI)}$ when compared to $\Delta E_{str,Se(IV)}$. Indeed, seleninic acid has a lower $\Delta E_{str,Se(OS)}$ along the whole r.c., when compared to selenonic acid. We interpreted this result as an effect of the different "saturation" of the two Se nuclei in the two OSs. Indeed, selenonic acid has four groups in the surrounding of Se (a phenyl group, two oxygens and one hydroxyl group), while seleninic has only three groups (one Se=O less than selenonic acid): thus, the distortion required to collocate the new OOH group around Se is intuitively larger for the former than for the latter, as reflected by its higher ΔE_{str}.

Conversely, in the actual oxygen-transfer step, peroxyselenonic acid acts as the best oxidant. To analyze this step, ASA was plotted along the O–N distance, which

undergoes a well-defined change along the reaction. Analogous conclusions can be drawn by investigating the complementary reaction coordinate i.e., O–O bond breaking. (Appendix C, Figure C2) ASA (Figure 8.4c) reveals how for the two reactions, similar values of ΔE_{str} occur at consistent points of r.c. Conversely, the ΔE_{int} value alone accounts for the trend in activation energy, being systematically more stabilizing for Se(VI) than for Se(IV), and thus correlating with the lower ΔE of the former. To understand what factors are responsible for this effect, ΔE_{int} was partitioned according to EDA. (Figure 8.4d,e) The main factor responsible for the lower ΔE_{int} of Se(VI) is ΔE_{OI}, which is consistently more stabilizing for peroxyselenonic acid.

An Energy Decomposition Analysis – Natural Orbitals for Chemical Valence (EDA-NOCV) calculation was performed to characterize the orbital interaction between the two reactants. (Figure 8.5) Within the EDA-NOCV approach, ΔE_{OI} can be further decomposed into contributions associated to NOCV. For each NOCV pair, a deformation density can be visualized, associated with a certain charge transfer degree from one fragment to the other. (Chapter 2, Paragraph 2.2)
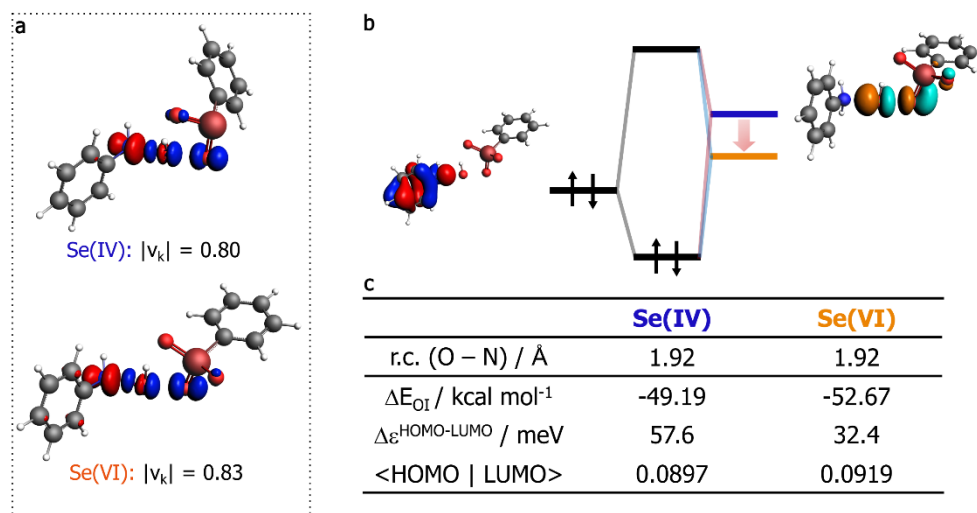

	Se(IV)	Se(VI)
r.c. (O − N) / Å	1.92	1.92
ΔE_{OI} / kcal mol^{-1}	-49.19	-52.67
$\Delta\varepsilon^{HOMO-LUMO}$ / meV	57.6	32.4
<HOMO | LUMO>	0.0897	0.0919

Figure 8.5 Analysis at consistent geometries, r.c. (O–N)=1.92 A. **a** Deformation density associated to the NOCVs with the largest eigenvalue (ν_k). Red areas are associated to charge depletion, while blue lobes are associated to charge accumulation. **b.** Schematic representation of the HOMO(aniline)–LUMO (peroxyacid) orbital interaction and KS-MO for Se(VI), isodensity value: 0.03). **c.** ΔE_{OI}, HOMO(aniline)–LUMO (peroxyacid) energy gap ($\Delta\varepsilon^{HOMO-LUMO}$) and HOMO (aniline)–LUMO (peroxyacid) orbital overlap (<HOMO \| LUMO>).

The deformation density associated to the NOCV with the greater eigenvalue (i.e., to the greatest charge transfer between the two fragments), is represented in Figure 8.5a.[1] It appears that that for both Se(IV) and Se(VI) the strongest orbital interaction leads to a charge depletion from the nitrogen lone pair, and to charge accumulation on the oxygen atom of the peroxy bond directly bonded to Se. This representation is also consistent with the S_N2-like nature of the reaction, in which aniline acts as the nucleophile and the peroxyacid as the electrophile. Additionally, the absolute value of the eigenvalue associated to the NOCV of Se(VI) reaction is greater than for Se(IV), being equal to 0.83 and 0.80, respectively, thus unveiling a higher charge-transfer character for the former. Since the nucleophile is the same, this can be associated to the better electron-accepting properties of the peroxyacid in the highest OS. In fact, the couple of canonical KS-MO mainly associated to this charge-transfer interaction can be identified with the HOMO-LUMO couple, in which the HOMO of the nucleophile (mostly the nitrogen lone pair) interacts with the LUMO of the electrophile. The peroxyacid of Se(VI) has a lower LUMO that better matches to the energy of aniline's HOMO. Additionally, the LUMO is slightly more polarized toward the terminal oxygen in Se(VI) than in Se(IV), thus also allowing for a better orbital overlap with the HOMO of aniline. Overall, both these aspects increase the orbital interaction, rationalizing the better performance of peroxyselenonic acid in the substrate oxidation step, if it is indeed produced in the reaction mixture.

Nevertheless, it is important to stress once again that these two opposite effects lead to a TOF which remains consistently in favor of the Se(IV) oxidation state. Thus, in the context of a catalytic mechanism, the less favorable orbital matching of peroxyseleninic acid with H_2O_2 is favorably counterbalanced by the lower distortion associated to its H_2O_2 activation step, which makes Se(IV) reaction pathway overall more productive.

---

[1] This deformation density is also associated to the couple of NOCV giving the largest contribution to ΔE_{OI} in the EDA-NOCV partitioning scheme. However, since the meta-hybrid correction (which is positive, i.e., destabilizing) to the orbital interaction cannot be partitioned any further in ADF, we chose to not report the EDA-NOCV partitioned energies, since their sum would not add up to the total ΔE_{OI}.

8.4 Conclusions

In this work, an extensive theoretical mechanistic investigation has been carried out on the on-water organoselenium catalyzed oxidation of aniline to nitrobenzene using H_2O_2 as final oxidant, with particular attention to the H_2O_2 activation step. An accurate analysis of the PES, carried out in the framework of the energetic span model, showed how the Se(VI) selenonic acid catalyst has a lower catalytic performance (evaluated on the basis of calculated TOFs) in all three catalytic cycles progressively oxidizing aniline to nitrobenzene, highlighting the privileged role of Se(IV) seleninic acid species in the title oxygen-transfer reaction.

Additionally, our analysis pinpointed how peroxyselenonic acid **5** is indeed a stronger oxidant (at least from the kinetic point of view) as compared to peroxyseleninic acid **3**, since all three substrate oxidations occurs with a lower activation energy. Thus, if peroxyselenonic acid **5** is indeed produced, a faster reactivity is envisioned. Conversely, selenonic acid **4** performs worse than seleninic acid **1** in H_2O_2 activation, thus rationalizing its poor catalytic performances. Through ASA, we interpreted the sluggish H_2O_2 activation by selenonic acid as an effect of the higher distortion associated to this step when compared to the analogous one for seleninic acid. Conversely, the enhanced nucleophilicity of peroxyselenonic acid was associated to its reinforced orbital interaction, mainly granted by its low-lying LUMO.

Lastly, the conversion of seleninic to selenonic acid in oxidizing conditions was found to proceed with a higher activation energy than the three substrate oxidations by peroxyseleninic acid. Thus, the formation of the Se(VI) species is expected to occur only when the substrate is fully converted to nitrobenzene and thus its oxidation by peroxyseleninic acid is not competitive anymore. The implication of the acid-base chemistry of selenenic acid in the conversion from Se(IV) to Se(VI) are currently being investigated, but preliminary results shows that also when the oxidation occurs starting from the seleninic acid conjugate-base, H_2O_2 activation to peroxyseleninic acid remains kinetically preferred over the overoxidation to Se(VI). Nevertheless, also this pathway might be involved in the production of Se(VI) after

all substrate has been catalytically oxidized, and this hypothesis is being explored in further detail.

This work provides a detailed mechanistic picture on the catalytic oxygen-transfer behavior of the popular organoselenium catalysts derived from the commercial diphenyl diselenide, shading light on the physico-chemical role of the oxidation state in their catalytic performances, spanning from the H_2O_2 activation to their oxidative potential toward the organic substrate. Additionally, to the best of our knowledge, this is the first comprehensive theoretical attempt to rationalize the oxygen-transfer catalytic cycles of seleninic acid and derivatives, providing theoretical complementary basis to the existing experimental knowledge and tackling the general problem of identifying the active and inactive intermediates in organoselenium catalyzed reactions.

Appendix C

Table C1 Activation energies (kcal mol^{-1}) for the direct oxidation of P2-OH to the correspondent N-oxide and competitive selenium-catalyzed dehydration to P-NO.

	P2-OH to N-oxide	P-OH2 to P-NO
Se(IV)	28.67	16.64
Se(VI)	26.74	14.43

Table C2 Activation energies^a (kcal mol^{-1}) for the direct peroxyselenurane (I) oxidation of aniline to aniline N-oxide.

	$\Delta G^{\ddagger}$	$\Delta G^{\ddagger\prime}$
Se(IV)	44.91	58.83
Se(VI)	31.55	55.47

^{a} $\Delta G^{\ddagger}$ is computed with respect to the peroxyselenurane (I), while $\Delta G^{\ddagger\prime}$ with respect to the free seleninic and selenonic acids (considering that I is destabilized with respect to the free reactants).
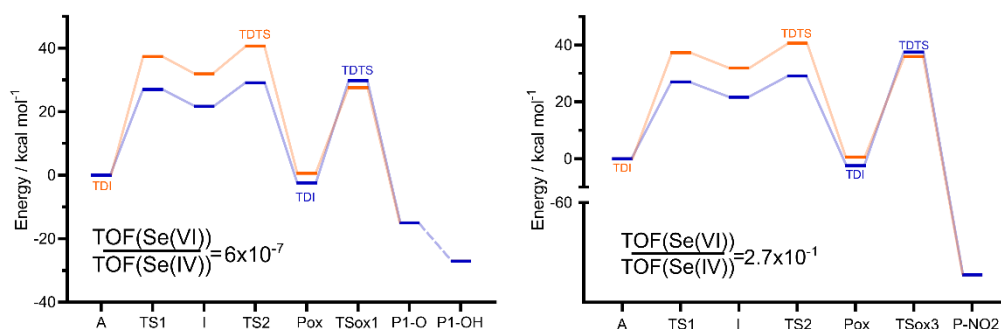

Figure C1 Gibbs free energy profile, and calculated TDI and TDTS for the 1st and 3rd catalytic cycle and relative TOF ratio: Se(IV) mediated process (blue); Se(VI) mediated process (orange). Level of theory: OPBE0 // OPBE.

To gain further confidence in the result, the energy profile for the first and third catalytic cycle was recomputed employing OPBE0 rather than M06 density functional, always starting from OPBE optimized geometries. From data reported in Appendix A, OPBE0 appears to be the best scoring functional when the subset of selenium reactions is considered. Nevertheless, qualitatively analogous results are obtained: Se(VI) performs the best in the actual substrate oxidation, but it poorly activates H$_2$O$_2$. These two counterbalancing effects leads to a TOF which favors

Se(IV) over Se(VI) catalysis. The same results were obtained, also, with the pure GGA functional OPBE employed for all geometry optimizations.
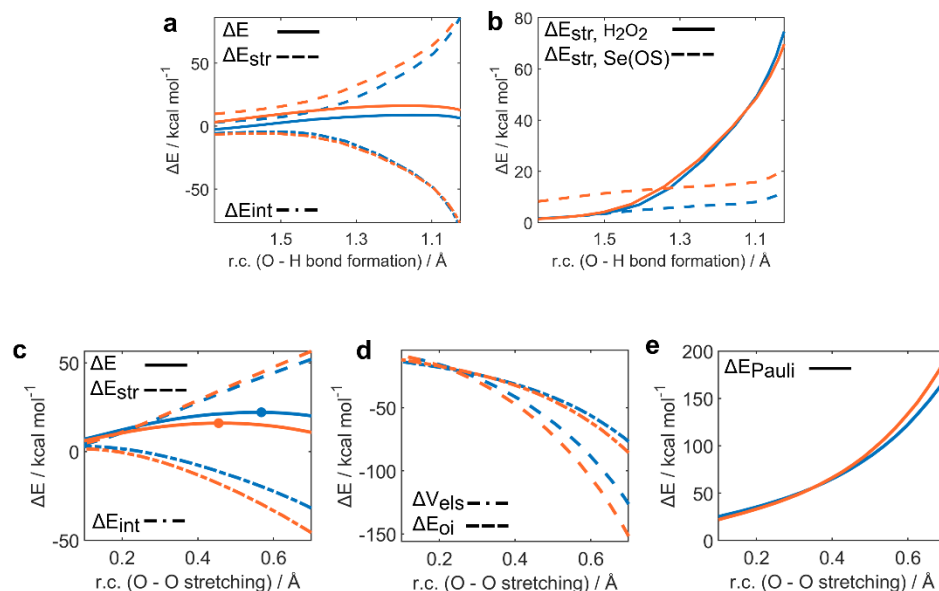

Figure C2 Activation strain and energy decomposition analysis of (**a, b**) H_2O_2 addition to seleninic (blue) and selenonic (orange) acids and (**c–e**) of aniline oxidation to aniline N-oxide (P1-O) by peroxyseleninic (blue) and peroxyselenonic (orange) acids, along the complementary reaction coordinates (r.c.) to Figure 8.4

References

[1]   A. J. Pacuła-Miszewska, L. Sancineto, *Oxygen-Transfer Reactions Catalyzed by Organoselenium Compounds*, INC, **2022**.

[2]   T. Hori, K. B. Sharpless, *J. Org. Chem.* **1978**, *43*, 1689–1697.

[3]   S. Santoro, C. Santi, M. Sabatini, L. Testaferri, M. Tiecco, *Adv. Synth. Catal.* **2008**, *350*, 2881–2884.

[4]   K. N. Sands, E. Mendoza Rengifo, G. N. George, I. J. Pickering, B. S. Gelfand, T. G. Back, *Angew. Chemie - Int. Ed.* **2020**, *59*, 4283–4287.

[5]   G. J. Ten Brink, B. C. M. Fernandes, M. C. A. Van Vliet, I. W. C. E. Arends, R. A. Sheldon, *J. Chem. Soc. Perkin 1* **2001**, 224–228.

[6]   H. J. REICH, F. CHOW, S. L. PEAKE, *Synthesis (Stuttg).* **1978**, *1978*, 299–301.

[7]   K. H. Tan, W. Xu, S. Stefka, D. E. Demco, T. Kharandiuk, V. Ivasiv, R. Nebesnyi, V. S. Petrovskii, I. I. Potemkin, A. Pich, *Angew. Chemie - Int. Ed.* **2019**, *58*, 9791–9796.

[8]   D. Zhao, M. Johansson, J. E. Bäckvall, *European J. Org. Chem.* **2007**, 4431–4436.

[9]   D. Tanini, C. Dalia, A. Capperucci, *Green Chem.* **2021**, *23*, 5680–5686.

[10]   H. J. Reich, I. L. Reich, J. M. Renga, *J. Am. Chem. Soc.* **1973**, *95*, 5813–5815.

[11]   P. A. Grieco, Y. Yokoyama, S. Gilman, M. Nishizawa, *J. Org. Chem.* **1977**, *42*, 2034–2036.

[12]   D. M. Freudendahl, S. Santoro, S. A. Shahzad, C. Santi, T. Wirth, *Angew. Chemie - Int. Ed.* **2009**, *48*, 8409–8411.

[13]   G. Ribaudo, M. Bellanda, I. Menegazzo, L. P. Wolters, M. Bortoli, G. Ferrer-Sueta, G. Zagotto, L. Orian, *Chem. - A Eur. J.* **2017**, *23*, 2405–2422.

[14]   C. A. Bayse, K. N. Ortwine, *Eur. J. Inorg. Chem.* **2013**, 3680–3688.

[15]   L. Orian, L. Flohé, *Antioxidants* **2021**, *10*, 1–22.

[16]   A. P. Bento, M. Solà, F. M. Bickelhaupt, *J. Chem. Theory Comput.* **2010**, *6*, 1445–1445.

[17]   A. Klamt, G. Schüürmann, *J. Chem. Soc. Perkin Trans. 2* **1993**, 799–805.

[18]   C. C. Pye, T. Ziegler, *Theor. Chem. Acc.* **1999**, *101*, 396–408.

[19]   F. L. Hirshfeld, *Theor. Chim. Acta* **1977**, *44*, 129–138.

[20]   C. Fonseca Guerra, J.-W. Handgraaf, E. J. Baerends, F. M. Bickelhaupt, *J. Comput. Chem.* **2004**, *25*, 189–210.

[21]   S. Kozuch, S. Shaik, *J. Am. Chem. Soc.* **2006**, *128*, 3355–3365.

[22]   S. Kozuch, S. Shaik, *Acc. Chem. Res.* **2011**, *44*, 101–110.

[23]   D. Garay-Ruiz, C. Bo, *ACS Catal.* **2020**, *10*, 12627–12635.

[24]   L. Syper, J. Młochowski, *Tetrahedron* **1987**, *43*, 207–213.

9 Conclusions

9.1 Summary

In the past fifty years, organoselenium chemistry proved to be a valuable tool to introduce new functional groups and modify the structure of chemical scaffolds. Indeed, it is so valuable that evolution somewhat preserved selenium usage up to mammals in at least 25 selenoproteins, in which this heavy chalcogen must provide some advantages over the lighter sulfur.

In this Thesis, various applications of organoselenium chemistry in biological and organic chemistry have been investigated *in silico*, to obtain a mechanistic understanding of selenium mediated or promoted processes. The main computational approach employed is the Density Functional Theory, also combined to the Activation Strain Model of chemical reactivity and a matching Energy Decomposition scheme. It can sometimes come naturally to think of computational chemistry as an easy science: doesn't the computer do most of the work? Doesn't the computational chemist take little to no risk? It may seem so. However, as F. Jensen highlighted in the preface to its book[1]*: computers don't solve problems, people do.* Thus, what problems were tackled in this Thesis, aided by the computers?

In Chapters 3 to 5, the focus was on biological implications of organoselenium chemistry. Particularly, in Chapter 3, the reaction of ebselen with protein targets (i.e., the SARS-CoV-2 Main Protease, and Inositol Monophosphatase), was modelled for the first time highlighting the importance of the Se–N bond as well as the weakness of the Se–S bond, which characterizes ebselen metabolites. It was possible to observe that, if ebselen reaches the target with the Se–N bond already

---

[1] Introduction to Computational Chemistry, Third Edition, John Wiley & Sons, 2017.

broken, its binding to the target cysteine is less favored thermodynamically. Thus, the formation of a Se–S bond with unspecific cysteines (i.e., different from the target Cys) was identified as a troublesome problem in the ebselen biochemistry.

Conversely, the important role of the Se–S bond in a thioredoxin reductase specific probe (RX1) has been explored in Chapter 4, to obtain a representative description of RX1 chemistry in the thiol rich biological environment. The design factors at the core of RX1 development have been explored theoretically to complement the available experimental data and provide mechanistic evidence in support of RX1 functioning. Particularly, the importance of thiol exchange reactions and of the restoration of the closed-ring form of the probe as a protective mechanism against the unspecific release of the fluorogenic cargo were pinpointed. Both these factors explain the resistance of RX1 against reactivity with monothiols.

Lastly, in Chapter 5 awareness has been raised about the possible unconventional interaction of glutathione peroxidase with the peroxynitrite oxidant, i.e., via N–O bond breaking and consequent selenocysteine nitrosylation. While it could not be assessed with certainty whether this reaction operates in the enzyme, since the conventional peroxide bond breaking was found to be way more favored thermodynamically, both processes appear to occur with negligible activation energies when the oxidant reaches the charge–separated state of the enzyme. Nevertheless, these observations stimulated the interest of biochemical collaborators and prompted them to investigate the problem in further detail: this is, in our humble opinion, a valuable result.

In Chapters 6 to 8, the organic chemistry of selenium has been explored in a more fundamental way, focusing on the intimate mechanistic path of selected reactions. These Chapters, focusing on more fundamental and model systems, were also employed to obtain general insight in the reactive properties of organoselenides. In Chapter 6, a comprehensive mechanistic investigation of the chalcogenoxide elimination reaction has been performed, observing how high oxidation states disfavor the reaction, while heavy chalcogens facilitate it. Importantly, the proton-acceptor capacity of the chalcogenoxide moiety was identified as the determinant factor tuning the reactivity in the activation strain model framework, especially in the low oxidation states of the chalcogen nucleus. Additionally, the inertia of telluroxides towards elimination has been rationalized in the light of a detrimental

hydration side reaction, which protonates the chalcogenoxide moiety reducing its basicity.

Then, the reduction mechanism of sulfoxides and selenoxides by thiols and selenols has been thoroughly explored in Chapter 7, to pinpoint the role of the chalcogen on both the oxidant and the reductant in the reaction. Beside corroborating the experimental bulk of evidence in favor of the beneficial role of selenium on both species in speeding up the reaction, we precisely quantified the origin of the enhanced nucleophilicity of selenols and electrophilicity of selenoxides with the activation strain model of chemical reactivity.

Lastly, in Chapter 8 an extensive mechanistic investigation has been conducted on the organoselenium-catalyzed oxidation of aniline to nitrobenzene to rationalize the reactive events which lead to hydrogen peroxide activation by organoselenides and, lastly, to the effective oxidation of organic substrates. The role of the chalcogen oxidation state, Se(IV) or Se(VI), recently debated in the community, has been assessed and density functional theory calculations rule in favor of a Se(IV) catalyzed process. Not only these results complement the available experimental knowledge, but they provide a closer look to reactions which, to the best of our knowledge, have never been explored *in silico*, and for which experimental mechanistic evidence is scarce or still controversial.

9.2 Outlook: where do we go from here?

Due to the vastness of the field, along this dissertation some questions were left unanswered. Particularly, in Chapter 3 and in Chapter 5, only a molecular (i.e., cluster) study to enzyme reactivity has been undertaken. In both Chapters, the importance of the substrate arrangement within the target protein has been highlighted. To properly account for the substrate dynamics and rearrangement within target proteins, hybrid computational methods should be used. Indeed, due to the size of biomolecular systems, the ideal approach is represented by the combination of an accurate quantum mechanical (QM) description of the reactive site, to a more fast but rough classical description of the surrounding environment, carried out at the molecular mechanics (MM) level. A QM/MM Hamiltonian can be

used to run molecular dynamics simulations (QM/MM MD), which account for the dynamical processes accompanying bond breaking and formation events, thus allowing for a more comprehensive description of biomolecular reactions. Such protocols are currently being investigated in our group as well as their application to some of the biomolecular reactions discussed in this Thesis.

Additionally, in Chapter 4 and 7, biological thiols have been modelled in an oversimplified manner (i.e., as methyl or ethyl thiols). In future investigations, the chemical complexity of these systems will be extended, thus enabling the description of different biological thiols, whose chemistry is not only made more complicated by the variety of the peptide structures (e.g., free Cys vs GSH vs thiol containing proteins), but also by their conformational flexibility. Also in this case, a QM/MM MD approach can help in shading light over their complex biomolecular behavior. This approach is expected to allow to reach a finer description of organoselenides (such as ebselen and RX1) interaction with the reactive biological thiols. Indeed, at the level of approximation applied in this Thesis, an answer about the selectivity of these systems towards different thiols cannot be provided. Conversely, at a more fundamental and molecular level, the investigation undertaken in Chapter 4 for the TrxR1 specific probe RX1 is currently being extended to other chemical scaffolds, to verify how changes to the probe structure affect its reactivity with thiols and selenols.

A final important question which remained unanswered in this Thesis is the extent of generality of the conclusions reached in Chapter 8: in which oxidation state is the active organoselenium catalyst in oxygen-transfer reactions? While our analysis was limited to a single overall reaction, the investigation is currently being extended to other organoselenium-catalyzed oxygen-transfers (e.g., epoxidation reactions), with the aim of obtaining more general insight into the topic. A unifying mechanism might not exist, since the catalytic performance of organoselenides is expected to be influenced by the solvent, substrate, and reaction conditions. Nevertheless, other organoselenium catalyzed reaction mechanisms can be tackled computationally for insightful comparison aiming at a comprehensive mechanistic picture of selenium catalyzed oxygen-transfer reactions.

9.3 Concluding remarks

Beside all the chapter-specific conclusions above mentioned, the main product of this Thesis is the bulk of mechanistic information obtained either as the principal end (e.g., Chapter 8), or as the intermediate step in understanding the behavior of a reaction through theoretical methods (e.g., Chapter 6). For this reason, it is always wise to remind that a reaction mechanism can never be proven to be correct, and thus the *burden of disproof*[2] is on everyone choosing to delve into reaction mechanisms, either experimentally or theoretically. Indeed, to propose a reasonable reaction mechanism some creativity is required, but Chemistry's imagination sometimes exceeds that of the most imaginative chemist: and even when a mechanism explains all *available* evidence, new experiments might reveal blind corners in the mechanistic picture so far proposed.

However, reaction mechanisms are endowed with one adamant virtue: to allow chemists to talk precisely about chemistry. In this context, physical organic chemistry showed that through a mechanistic understanding of chemical reactivity, reactions can be shaped to will. Mechanisms are, in fact, *models* themselves: and their usefulness should be valued over their truth. Thus, even if organoselenium chemistry is already a well-developed, solid field, this dissertation has hopefully provided some useful mechanisms to put aspects of this chemical area on an even more firm ground, which can sustain the construction of new chemistry. Time will tell if this ground is stable for good, or if it will rearrange under the scientific pressure of new mechanistic hypotheses, experimental evidence, and ideas. Should this event occur, it will be an opportunity to explore in even more detail the properties of the *element of the moon*: from theory, to experiment, back to theory, and so forth…

Up to then, though, I hope to have explored these themes to the current best.

---

[2] Susannah L. Scott, *ACS Catal.* **2019**, *9*, 5, 4706–4708.

List of Abbreviations

Activation Strain Model (ASM)

Activation Strain Analysis (ASA)

Addition-Elimination (A-E)

Bimolecular Nucleophilic Substitution (S_N2)

Cysteine (Cys)

Density Functional Theory (DFT)

Energy Decomposition Analysis (EDA)

Energetic Span Model (ESM)

Glutathione peroxidase (GPx)

Glutathione (GSH)

Iodothyronine Deiodinase (DIO)

Methionine Sulfoxide Reductase (Msr)

Natural Orbitals for Chemical Valence (NOCV)

Oxidation state (OS)

Potential Energy Surface (PES)

Reaction Coordinate (r.c.)

Selenophosphate Synthetase (SPS)

Selenocysteine (Sec)

Tellurocysteine (Tec)

Thioredoxin (Trx)

Thioredoxin Reductase (TrxR)

Three-centers Intermediate (TCI)

TOF Determining Intermediate (TDI)

TOF Determining Transition State (TDTS)

Turnover Frequency (TOF)

List of Publications

(1) Madabeni, A.; Dalla Tiezza, M.; Omage, F. B.; Nogara, P. A.; Bortoli, M.; Rocha, J. B. T.; Orian, L. Chalcogen–Mercury Bond Formation and Disruption in Model Rabenstein's Reactions: A Computational Analysis. *J. Comput. Chem.* **2020**, *41* (23), 2045–2054.

(2) Bortoli, M.; Madabeni, A.; Nogara, P.; Omage, F.; Ribaudo, G.; Zeppilli, D.; Rocha, J.; Orian, L. Chalcogen-Nitrogen Bond: Insights Into a Key Chemical Motif. *Catalysts*, **2020**, *11* (114), 7589.

(3) Madabeni, A.; Nogara, P. A.; Bortoli, M.; Rocha, J. B. T.; Orian, L. Effect of Methylmercury Binding on the Peroxide-Reducing Potential of Cysteine and Selenocysteine. *Inorg. Chem.* **2021**, *60* (7), 4646–4656.

(4) Nogara, P. A.; Madabeni, A.; Bortoli, M.; Teixeira Rocha, J. B.; Orian, L. Methylmercury Can Facilitate the Formation of Dehydroalanine in Selenoenzymes: Insight from DFT Molecular Modeling. *Chem. Res. Toxicol.* **2021**, *34* (6), 1655–1663.

(5) Madabeni, A.; Nogara, P. A.; Omage, F. B.; Rocha, J. B. T.; Orian, L. Mechanistic Insight into SARS-CoV-2 Mpro Inhibition by Organoselenides: The Ebselen Case Study. *Appl. Sci.* **2021**, *11* (14), 6291.

(6) Masuda, R.; Kuwano, S.; Sase, S.; Bortoli, M.; Madabeni, A.; Orian, L.; Goto, K.Model Study on the Catalytic Cycle of Glutathione Peroxidase Utilizing Selenocysteine-Containing Tripeptides: Elucidation of the Protective Bypass Mechanism Involving Selenocysteine Selenenic Acids, *Bull. Chem. Soc. Jpn.* **2022***, 95,* 1360-1379.

(7) Madabeni, A.; Zucchelli, S.; Nogara, P.A.; Rocha, J. B. T.; Orian, L.; In the Chalcogenoxide Elimination Panorama: Systematic Insight into a Key Reaction. *J. Org. Chem.* **2022**, *87*, 17, 11766–11775.

(8) Ribaudo, G; Madabeni, A; Nogara, P.A.; Pavan, C.; Bortoli, M.; Rocha, J. B. T.; Orian, L.; The Potential of Ebselen Against Bipolar Disorder: a Perspective on the Interaction with Inositol Monophosphatase. *Curr. Org. Chem.* **2022,** *26*, 1503-1511.

(9) Zeppilli, D.; Ribaudo, G.; Pompermaier, N.; Madabeni, A.; Bortoli, M; Orian, L. Radical Scavenging Potential of Ginkgolides and Bilobalide: Insight from Molecular Modelling. *Antioxidants* **2023**, *12*(2), 525.

(10) Nogara, P.A.; Oliveira, C.S.; Madabeni, A.; Bortoli, M.; Rocha, J.B.T.; Orian, L.; Thiol modifier effects of diphenyl diselenides: insight from experiment and DFT calculations. *New J. Chem.*, **2023**, *47*, 5796-5803.

(11) Omage, F.B.; Madabeni, A.; Resende, A.T.; Nogara, P.A.; Bortoli, M.; dos Santos Rosa, A.; dos Santos Ferreira, V.N.; Rocha, J.B.T.; Dias Miranda, M.; Orian, L.; Diphenyl Diselenide and SARS-CoV-2: in silico Exploration of the Mechanisms of Inhibition of Main Protease (M[pro]) and Papain-like Protease (PL[pro]). *J. Chem. Inf. Model.*, **2023**, *63(7)*, 2226-2239.

(12) Madabeni, A.; Orian, L. The Key Role of Chalcogenurane Intermediates in the Reduction Mechanism of Sulfoxides and Selenoxides by Thiols Explored In Silico. *Int. J. Mol. Sci*. **2023,** 24(9), 7754.